Terms and Conditions of Use of Digitised Theses from Trinity College Library Dublin

Copyright statement

All material supplied by Trinity College Library is protected by copyright (under the Copyright and Related Rights Act, 2000 as amended) and other relevant Intellectual Property Rights. By accessing and using a Digitised Thesis from Trinity College Library you acknowledge that all Intellectual Property Rights in any Works supplied are the sole and exclusive property of the copyright and/or other IPR holder. Specific copyright holders may not be explicitly identified. Use of materials from other sources within a thesis should not be construed as a claim over them.

A non-exclusive, non-transferable licence is hereby granted to those using or reproducing, in whole or in part, the material for valid purposes, providing the copyright owners are acknowledged using the normal conventions. Where specific permission to use material is required, this is identified and such permission must be sought from the copyright holder or agency cited.

Liability statement

By using a Digitised Thesis, I accept that Trinity College Dublin bears no legal responsibility for the accuracy, legality or comprehensiveness of materials contained within the thesis, and that Trinity College Dublin accepts no liability for indirect, consequential, or incidental, damages or losses arising from use of the thesis for whatever reason. Information located in a thesis may be subject to specific use constraints, details of which may not be explicitly described. It is the responsibility of potential and actual users to be aware of such constraints and to abide by them. By making use of material from a digitised thesis, you accept these copyright and disclaimer provisions. Where it is brought to the attention of Trinity College Library that there may be a breach of copyright or other restraint, it is the policy to withdraw or take down access to a thesis while the issue is being resolved.

Access Agreement

By using a Digitised Thesis from Trinity College Library you are bound by the following Terms & Conditions. Please read them carefully.

I have read and I understand the following statement: All material supplied via a Digitised Thesis from Trinity College Library is protected by copyright and other intellectual property rights, and duplication or sale of all or part of any of a thesis is not permitted, except that material may be duplicated by you for your research use or for educational purposes in electronic or print form providing the copyright owners are acknowledged using the normal conventions. You must obtain permission for any other use. Electronic or print copies may not be offered, whether for sale or otherwise to anyone. This copy has been supplied on the understanding that it is copyright material and that no quotation from the thesis may be published without proper acknowledgement.

Pharmaceutical cocrystals:
A contribution to fundamental studies addressing solubility, dissolution, formation and characterisation

A dissertation submitted
for the degree of
Doctor of Philosophy
at the
School of Pharmacy & Pharmaceutical Sciences
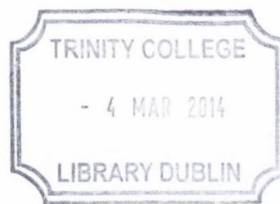University of Dublin, Trinity College
Ireland

presented by
Christine Grossjohann

September 2013

TRINITY COLLEGE DUBLIN | THE UNIVERSITY OF DUBLIN
COLÁISTE NA TRÍONÓIDE, BAILE ÁTHA CLIATH

Supervisor: Professor Anne Marie Healy
                           School of Pharmacy & Pharmaceutical Sciences
                           Trinity College Dublin
                           Dublin, Ireland

Co-supervisors: Assistant Professor Lidia Tajber
                           School of Pharmacy & Pharmaceutical Sciences
                           Trinity College Dublin
                           Dublin, Ireland

                           Emeritus Professor Owen I. Corrigan
                           School of Pharmacy & Pharmaceutical Sciences
                           Trinity College Dublin
                           Dublin, Ireland

Examiners: Professor Sitaram P. Velaga
                           Department of Health Sciences
                           Luleå University of Technology
                           Luleå, Sweden

                           Assistant Professor John F. Gilmer
                           School of Pharmacy & Pharmaceutical Sciences
                           Trinity College Dublin
                           Dublin, Ireland

Declaration

I declare that this thesis has not been submitted as an exercise for a degree at this or any other university and it is entirely my own work, except where duly acknowledged.

I agree to deposit this thesis in the University's open access institutional repository or allow the library to do so on my behalf, subject to Irish Copyright Legislation and Trinity College Library conditions of use and acknowledgement.

Christine Grossjohann

Table of contents

Chapter 5: Solubility and dissolution behaviour of sulfadimidine:aromatic carboxlic acid cocrystals

Chapter 6: General discussion

Acknowledgements

I would like to acknowledge all past and present members of the pharmaceutics research lab for having the pleasure to work with you. I thank you all for welcoming me so nicely when I joined the group and for introducing and advising me in all the lab work. I always liked the international atmosphere in our group and I'm happy that I found in some of you great friends. Thank you all for making my time in Ireland so enjoyable: Krzysztof, Ines, Evelyn, Stefano, Frederic, Vincent Caron, Ahmad, Shadeed, Vincent Curtin, Joanne, Anita, Maria, Bo and Youness. And to those who just started their PhD, good luck with everything: Claire, Naila and Kieran.

My warmest thanks go to Stephy, Maria, Svenja, Joanne, Johanna and Ines. You are great friends. I thank you for being there for me and for encouraging me in the last months, each of you in your own wonderful way. My special thanks go to Johanna for supporting me, for listening and cheering me up in times when I struggled and when I was assailed by doubts, especially at the beginning of the PhD. And I thank you for all the fun we had together with Stephy, Ines, Leonie, Simona and Jessi.

Last, I would like to thank my family, my parents and my two sisters with special thanks to my mum and my sister Eva-Maria. You supported me always and you believed in me when I did not believe in myself. I'm deeply grateful and happy to have you.

Presentations and publications

Poster presentations

Grossjohann, C., Tajber, L., Corrigan, O.I., Healy, A.M.. Co-crystal engineering of sulfadimidine/4-aminosalicylic acid by co-grinding in the solid state. 9th International Workshop on Crystal Growth of Organic Materials (CGOM), August 2010, Singapore, Singapore.

Grossjohann, C., Tajber, L., Corrigan, O.I., Healy, A.M., Characterisation of sulfadimidine and 4-aminosalicylic acid composite systems produced by grinding and spray drying. The Academy of Pharmaceutical Sciences, APS Pharmsci, August/September 2011, Nottingham, United Kingdom.

Grossjohann, C., Tajber, L., Corrigan, O.I., Healy, A.M., Co-grinding and co-spray drying: alternative approaches to the formation of cocrystals. 8th World Meeting on Pharmaceutics, Biopharmaceutics and Pharmaceutical Technology (PBP), March 2012, Istanbul, Turkey.

Grossjohann, C., Tajber, L., Corrigan, O.I., Healy, A.M., Physicochemical properties, solubility and dissolution of a cocrystal composed of two amphoteric components. 10th International Workshop on Crystal Growth of Organic Materials (CGOM), June 2012, Limerick, Ireland.

Grossjohann, C., Paluch, K.J., McCabe, T., Tajber, L., Corrigan, O.I., Healy, A.M.. Investigating the potential for reaction crystallisation on spray drying sulfadimidine with aromatic carboxylic acids. American Association of Pharmaceutical Scientists (AAPS) Annual Meeting & Exposition October 2012, Chicago, Illinois, USA.

Publications

Grossjohann, C., Eccles, K.S., Maguire, A.R., Lawrence, S.E., Tajber, L., Corrigan, O.I., Healy, A.M., 2012. Characterisation, Solubility and Intrinsic Dissolution Behaviour of Benzamide:Dibenzyl Sulfoxide Cocrystal, Int. J. Pharm. 422, 24-32.

Abbreviations and symbols

4-ASA	4-aminosalicylic acid
ANOVA	analysis of variance
API	active pharmaceutical ingredient
arb. unit	arbitrary unit
ATR	attenuated total reflection
BA	benzoic acid
BAM	benzamide
BCS	Biopharmaceutics Classification System
BP	British Pharmacopoeia
CC	cocrystal
CCR	cooling crystallisation
CPMAS	cross polarisation – magic angle spinning
CSD	Cambridge Structural Database
C_{tr}	transition concentration
DBSO	dibenzyl sulfoxide
DMSO	dimethyl sulfoxide
DSC	differentcial scanning calorimetry
EA	elemental analysis
EDXA	energy-dispersive X-ray analysis
EtOH	ethanol
$^\wedge$exo	exothermic direction
FTIR	fourier transform infra-red
HCl	hydrochloric acid
HPLC	high performance liquid chromatography
ICH	International Conference on Harmonisation
IDR	intrinsic dissolution rate
IR	infra-red
IT	inlet temperature
K_{11}	complexation constant of a 1:1 molar complex
K_a	acid dissociation constant
K_{app}	apparent constant
K_{sp}	solubility product
LAM	liquid-assisted milling

LOD	limit of detectin
LOQ	limit of quantification
Me_2CO	acetone
MeCN	acetonitrile
MeOH	methanol
NA	nicotinic acid
NaOH	sodium hydroxide
NMR	nuclear magnetic resonance
OT	outlet temperature
PA	pyridine-2-carboxylic acid
PCA	pyrazine-2-carboxylic acid
Ph. Eur.	European Pharmacopoeia
pK_a	negative decadic logarithm of K_a
PM	physical mixture
PVDF	polyvinylidene difluoride
PVP	polyvinylpyrrolidone
PXRD	powder X-ray diffraction
R^2	regression coefficient
R	gas constant
RH	relative humidity
SA	salicylic acid
SC-XRD	single crytsal X-ray diffraction
SD	sulfadimidine
SEM	scanning electron microscopy
SEV	solvent evaporation
Si_3N_4	silicon nitride
SPD	spray drying
ssNMR	solid state nuclear magnetic resonance
T	temperature
T_1	spin-lattice relaxation time constant
T_{exo}	exothermic onset temperature
T_g	glass transition
TGA	thermogravimetric analysis
T_m	melting temperature

UATR	universal attenuated total reflection
USP	United States Pharmacopoeia
ZnSe	zink selenide
ΔH_f	enthalpy of fusion
cpm	counts per minute
dm/dt	change of mass per unit time
rpm	revolutions per minute
t	time
wt.	weight
2θ	2 theta (diffraction angle)

Summary

This thesis has focused on the study of pharmaceutical cocrystals. The investigations have addressed the solubility, dissolution and stability of cocrystals as well as the evaluation of selected production techniques, in order to contribute to an overall understanding of these solid state forms.

Extensive evaluation of known cocrystals such as the benzamide:dibenzyl sulfoxide cocrystal and three sulfadimidine:aromatic carboxylic acid (benzoic acid, salicylic acid, 4-aminosalicylic acid) cocrystals as well as newly synthesised cocrystals are presented in this work. Nicotinic acid and pyrazine-2-carboxylic acid have been introduced as potential new cocrystal formers with sulfadimidine. Several techniques such as X-ray diffraction, thermal analyses, infra-red spectroscopy, nuclear magnetic resonance spectroscopy, scanning electron microscopy, energy-dispersive X-ray analysis, high performance liquid chromatography, dynamic vapour sorption analysis and appropriate statistical tests have been used for analysing the properties of cocrystal studied and interpreting the results.

The aqueous solubility and stability behaviour as well as dissolution from powder compacts by the intrinsic dissolution method have been examined for the benzamide:dibenzyl sulfoxide cocrystal and four sulfadimidine:aromatic carboxylic acid cocrystals.

The validity of recently introduced models to describe and predict cocrystal solubility and stability has been demonstrated. For the first time a model to predict the pH-dependent solubility and stability of a cocrystal composed of two amphoteric components has been presented. By means of the four different sulfadimidine cocrystals it was shown that the cocrystal solubility is complex to control, in particular when pH influences play a role. No correlation between cocrystal solubility, coformer solubility and cocrystal lattice energies could be established. Generally, the study elucidated that the solubility advantage achived by means of the cocrystal has a negative impact on its stability, associated with precipitation of the less soluble component (drug). Additionally, if the cocrystal reveals a large coformer to drug solubility difference, in the order of > 75 (in terms of molar solubilities), no advantage in the dissolution rate is observed. In the case of stable cocrystals, it was found that the dissolution rate is improved when the cocrystal solubility is improved and when the coformer to drug solubility ratio is small. However, a major issue is that most pharmaceutical cocrystals with high solubility are unstable in water. It remains to be clarified what impact this

instability has on the dissolution rate. It is assumed that the coformer to drug solubility ratio plays a role.

The formation of sulfadimidine:aromatic carboxylic acid cocrystals has been investigated using techniques such as milling and spray drying. Moreover, spray drying has been compared to common crystallisation techniques such as liquid-assisted milling, solvent evaporation and cooling crystallisation. It was found, and presented here for the first time, that the sulfadimidine:4-aminosalicylic acid 1:1 form I cocrystal can be generated by a solid-based technique using liquid-assisted milling. Two new cocrystals were discovered: (1) A polymorphic form (form II) of the sulfadimidine:4-aminosalicylic acid 1:1 cocrystal. It was observed that the crystal structure of form II is unusually complex, with structure elucidation results indicating that two polymorphs are intergrown in one crystal structure, the exact nature of which still remains to be clarified. (2) The sulfadimidine:nicotinic acid 1:1 cocrystal.

Spray drying was found to be a successful alternative in the formation of cocrystals compared to other common crystallisation methods such as liquid-assisted milling, solvent evaporation and cooling crystallisation. However, it has been observed that during processing a mass loss of one of the starting components can occur and consequently affect the purity, attributable to the presence of unreacted crystalline or amorphous component (s).

The generated sulfadimidine:aromatic carboxylic acid cocrystals were also investigated for stability when exposed to different humidities from 0-90% RH at 25 °C (by dynamic vapour sorption). It was shown that all cocrystals investigated in the current work are physically stable and are classified as non-hygroscopic or slightly hygroscopic.

Thus cocrystals can provide an opportunity for biopharmaceutical property adjustment of the API in tandem with good physically stability in the solid state.

Origin and scope of the thesis

In recent years, cocrystal formation as a crystal engineering approach has gained an increased interest in the field of pharmaceutical sciences, as it has been shown to offer a tool for tailoring drug physicochemical properties with the potential for improving physical stability and biopharmaceutical parameters, in particular for active pharmaceutical ingredients (APIs) with non-ionisable properties and poor aqueous solubility. As the cocrystal approach presents a relatively new class of pharmaceutical materials, a fundamental understanding of cocrystal characteristics is required in order to ensure maximum benefit arises from them in drug development.

Studies on cocrystals cover various topics such as developing methods to efficiently synthesise and isolate them for the purpose of crystal structure determination, screening of suitable cocrystal formers for a specific API, investigation and characterisation of the properties in the solid state and in solution as well as polymorphism in cocrystals.

Initially, most studies have been focused on the formation, screening and structure determination of cocrystals, as for example in the work of Caira (1992) and Caira et al., (1995) who demonstrated, in some of the early studies on cocrystals, the generation of sulfonamide:aromatic carboxylic acid cocrystals, and Eccles et al. (2010), who more recently reported on the formation of sulfoxide cocrystals, such as the benzamide:dibenzyl sulfoxide 1:1 cocrystal. However, relatively few studies are found in the literature which address biopharmaceutical aspects of cocrystals, such as dissolution characteristics (Childs et al., 2004; Jung et al., 2010; Lee et al., 2011; Rahman et al., 2012). Rodríguez-Hornedo and co-workers have developed theoretical models in order to predict solubility and solution stability of cocrystals (Nehm et al., 2006; Good and Rodríguez-Hornedo, 2009; Reddy et al., 2009; Good and Rodríguez-Hornedo, 2010). Due to the limited numbers of cocrystals on which these models are based, more studies using different types of pharmaceutical cocrystals are required in order to draw accurate conclusions.

In the production of cocrystals, solution-based methods, especially solvent evaporation and slurry conversion (Caira, 1992; Zhang et al., 2007; Shattock et al., 2008) are commonly used. Likewise, solid-based approaches such as dry and liquid-assisted grinding are popular, as they have shown to be viable, providing a faster processing method than common solution-based techniques and have also been found to be useful in screening for polymorphic cocrystal forms (Etter et al., 1993; Caira et al., 1995; Kuroda et al., 2002; Trask et al., 2004; Friščić et al., 2006; Braga et al., 2006; Chadwick et al., 2007). As a novel approach in the formation of cocrystals, spray drying

has been proposed by Alhalaweh and Velaga (2010). These researchers have discussed the fact that spray drying provides a suitable scale-up technique for the generation of cocrystals, but that further investigations are necessary.

The overall scope of this thesis was to obtain further fundamental understanding of cocrystals in terms of solubility, dissolution and stability behaviour, formation and consequently identification, in order to evaluate their pharmaceutical use.

These interests were addressed by focusing on the following specific objectives:

(1) Investigations of the solubility and dissolution behaviour of the benzamide:dibenzyl sulfoxide 1:1 cocrystal.

(2) Investigations of the solubility and dissolution of different sulfadimidine:aromatic carboxylic acid cocrystals and the impact of the acid coformer on their solubility and dissolution behaviour.

(3) Examination of co-grinding and co-spray drying as alternative techniques to solvent evaporation in the formation of the sulfadimidine:4-aminosalicylic acid cocrystal.

(4) Investigations of the potential of spray drying as a cocrystal formation technique compared to other common crystallisation methods using sulfadimidine and different aromatic carboxylic acids as coformers.

1.1 Pharmaceutical solids

1.1.1 Importance and development

Most active pharmaceutical ingredients (APIs) are available as solid oral dosage forms such as tablets, capsules or powders as they provide a number of convenient properties. They are simple and economical to manufacture, stable (as dry materials), facilitate accurate dosing, they are easy to administer and are patient-friendly.

However, the drug development of solid forms provide a number of challenges to address such as both biopharmaceutical and manufacturing parameters, which are largely dependent on the physicochemical properties of the API in its solid state. These properties significantly influence the performance of the final product.

As part of the early development of a potentially new drug form, it is therefore essential to characterise and evaluate the solid state properties and to generate a thorough understanding of the material's stability under various conditions (Niazi, 2006). The information obtained through these studies provides the basis for defining and selecting the optimal form of the API for inclusion in marketed dosage forms.

An overview of relevant parameters that are addressed in the early stage of drug development is illustrated in Figure 1.1. As these parameters impact on each other, the major challenge is to find a compromise for selection of the best API solid state form.
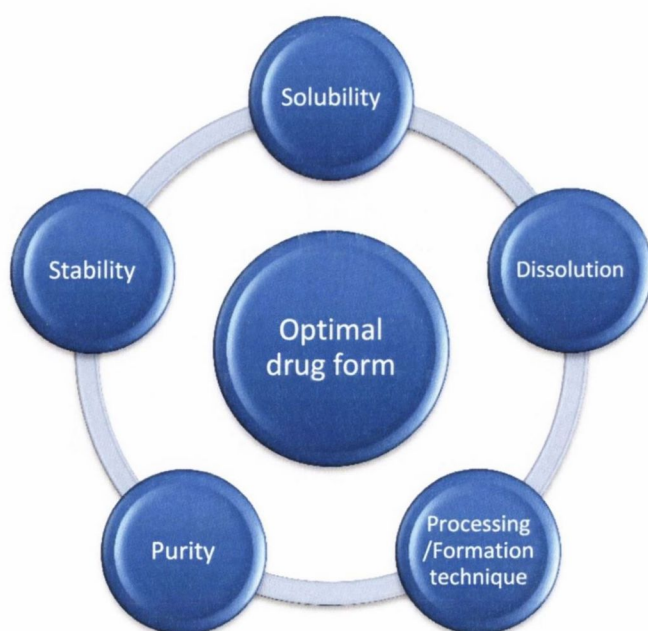
Figure 1.1: Important parameters which need to be investigated in formulation studies.

1.1.2 Forms, properties and formulation strategies

Solid drug forms are classified into two major groups (Figure 1.2). They can either be crystalline or amorphous, based on the order of molecular packing. In contrast to amorphous materials, which exhibit a disordered state (Figure 1.3), in crystalline materials the atoms, ions or molecules are arranged in an order manner and in periodic units. Their unique arrangement can be described by a three dimensional network, the crystal lattice. The smallest component (unit) that is repeated in the crystal lattice to form the whole network is called the unit cell. These characteristics allow the molecular structure of a crystal to be determined. Crystalline materials can be polymorphic, which means that solids containing APIs of the same chemical structure can exist in two or more crystal forms that have different arrangements and/or conformations of the molecules.
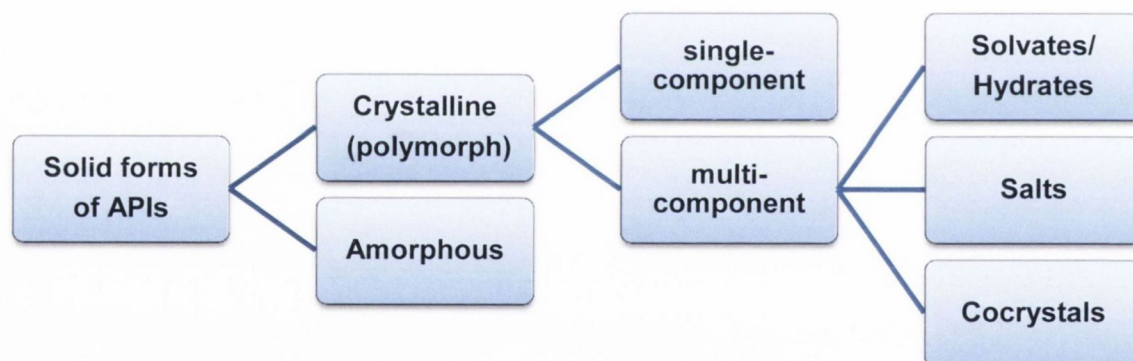
Figure 1.2: Classification of solid forms of APIs based on structure and composition (Sekhon, 2009).
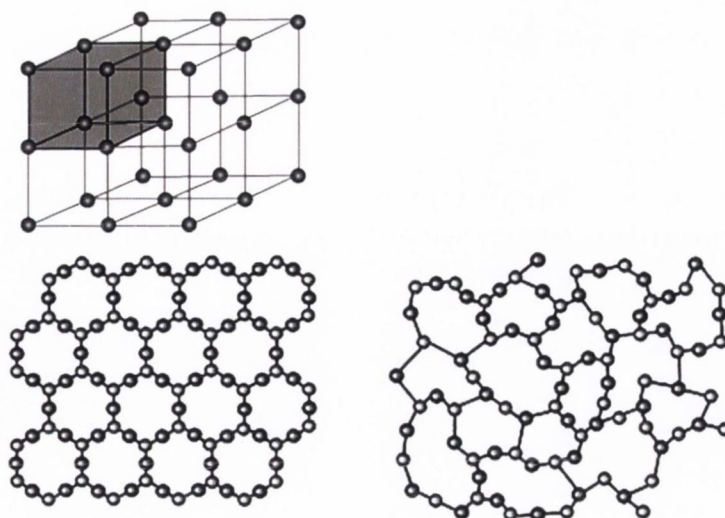
Figure 1.3: The structural difference between the crystalline and the amorphous state. Left: crystalline (with illustration of crystal lattice and unit cell), right: amorphous (Ashkenazi and Eliaz, 2008).

The type of molecular arrangement within the solid has a fundamental impact on the physiochemical behaviour of the particular API. For example, crystalline drug forms may reveal good physical stability but limited aqueous solubility which may be altered in the case of polymorphic forms. Amorphous forms are highly energetic forms which show benefits relative to their crystalline counterparts in terms of solubility and dissolution, but are thermodynamically unstable.

Generally, a particular solid form can be transferred into another, for example as a result of a certain chemical reaction, processing method or due to a solution-mediated process, consequently leading to changes of the solid state properties. This may be favoured or not in terms of improvement to the physicochemical or biopharmaceutical properties of the API and a careful investigation (characterisation) is required to have control and understanding of these matters.

Poor aqueous solubility of drugs is a general concern in pharmaceutical drug formulation of solid dosage forms as this has an influence on the absorption and thus on bioavailability. Most poorly water soluble drugs have weakly acidic or weakly basic properties and usually require high doses in order to reach therapeutic concentrations after oral administration. It is estimated that more than 40% of the newly discovered drugs have poor aqueous solubility or are practically insoluble (defined according to International Pharmacopoeias) (Sharma et al., 2009).

A guidance to improve the efficiency of drug development with respect to the prediction of bioavailability has been introduced by the Biopharmaceutics Classification System (BCS) (Amidon et al., 1995). It is a framework, which classifies drug substances based on their aqueous solubility and intestinal permeability (Table 1.1). The system also takes into account dissolution properties or dissolution rate, a further major factor that controls the absorption of an orally administered drug and hence its bioavailability.

Dissolution was first described by Noyes and Whitney (1897) and was later extended by Nernst and Brunner (Nernst, 1904; Brunner, 1904) who have demonstrated that the dissolution rate is affected by three main factors, the solubility, the diffusion coefficient and the surface area of the dissolving body, based on the following equation:

$$\frac{dm}{dt} = \frac{DA\,(C_s - C)}{h} \tag{1.1}$$

where dm/dt is the dissolution rate (referring to a mass change per unit time), D and A are the diffusion coefficient and the surface area of the dissolving solid, respectively, C_s is the equilibrium solubility of the solid in the dissolution medium, C is the concentration of the solid at time t in the bulk medium and h is the thickness of the diffusion boundary through which the dissolved solid diffuses.

Table 1.1: Biopharmaceutics classification system.

BCS Class	Solubility	Permeability
1	High	High
2	Low	High
3	High	Low
4	Low	Low

In particular, for poorly water soluble drugs such as BCS Class 2 and Class 4, oral absorption and thus bioavailability can be limited by the dissolution rate.

According to Skinner and Kanfer (1992) the main physicochemical aspects relevant to drug absorption are the intrinsic dissolution rate (IDR) and the solubility. Dissolution

rate determination, based on the intrinsic dissolution method, is a common and standardised practice that is used for characterisation of solid drugs in formulation studies (BP Appendix XII B (5), 2009; Ph. Eur. Method 2.9.29, 2009; USP 32-NF 27, 2009). A detailed description of the method is presented in Chapter 2. In later studies it has been demonstrated that the IDR is useful for determining the solubility BCS class of drugs and thus to predict the bioavailability of solid drugs (Yu et al., 2004). The authors suggest, as the IDR measurement refers to a rate and not to equilibrium, there is a better correlation to predict the oral absorption *in vivo* than solubility.

The improvement of drug aqueous solubility and dissolution rate and thereby the oral bioavailability is one of the most challenging tasks in drug formulation. Several strategies have been applied to improve the physicochemical properties of solid APIs by means of multi-component solid forms such as hydrates/solvates, salts and cocrystals (Figure 1.2).

The most common current approach to solid form manipulation is salt formation (Berge et al., 1977; Bighley et al., 1995; Stahl and Wermuth, 2002). It is estimated that more than 50% of the drugs on the market are available as salt forms. However, a major issue with salt formation is that the approach is limited to APIs which have suitable ionisable properties. The success of salt formation and salt stability depends largely upon the relative strength of the acid or base, where it is reported that a pK_a difference of ≥ 2 units (between the acid and base) is required to form a salt (Hippel, 1962; Bighley et al., 1995). In addition, there are other problems that have been encountered with salts such as increased formation of hydrates and polymorphs resulting in greater variability of the drug's physicochemical properties, reduced dissolution rate and solubility of hydrochloride salts in gastric fluid and corrosiveness of some salts resulting in processing problems such as in tableting (Stahl and Wermuth, 2002).

In contrast to salt formation, the approach of cocrystal formation is applicable to a broader range of APIs and offers the possibility for non-ionisable, ionisable, acidic, basic and amphoteric APIs to form cocrystals. Cocrystals are long known multi-component structures (a comprehensive overview of the history and chemistry of cocrystals before the year 2000 can be found in the report of Stahly, 2009), but are relatively unexplored. Their use in drug formulation has emerged as an interesting complementary strategy to salt formation for improving the physicochemical properties of APIs, primarily those that cannot form salts due to the presence of non-ionisable properties and which would therefore fall into BCS Class 2 and 4.

At the present time, no pharmaceutical cocrystal has yet been approved for sale.

1.2 Cocrystals as formulation strategy

1.2.1 Definition of cocrystals

The answer to the question of what is a cocrystal has caused some debate in the scientific literature and is still controversial, in particular when it comes to distinguishing a cocrystal from other multi-component systems such as solvates/hydrates and salts. Probably the most suitable definition of a cocrystal is a combination of the currently available suggestions, where a cocrystal can be defined as a crystalline complex of two or more different molecules, which are solids at ambient conditions and which are mainly held together by non-covalent bonds such as hydrogen bonds in the same crystal lattice (Aakeröy and Salmon, 2005; Jones et al. 2006; Vishweshwar et al. 2006; Childs and Hardcastle, 2007; Stahly, 2007).

If one of the components is liquid at room temperature then the complex would be considered as a solvate. If there is a proton transfer between the components and thus the presence of an ionic bond, the complex would be designated as a salt.

However, as illustrated in Figure 1.4, the possible classes of multi-component solid forms overlap between hydrates/solvates, salts and cocrystals and it is therefore difficult to clearly distinguish them from each other. The debate will thus continue.
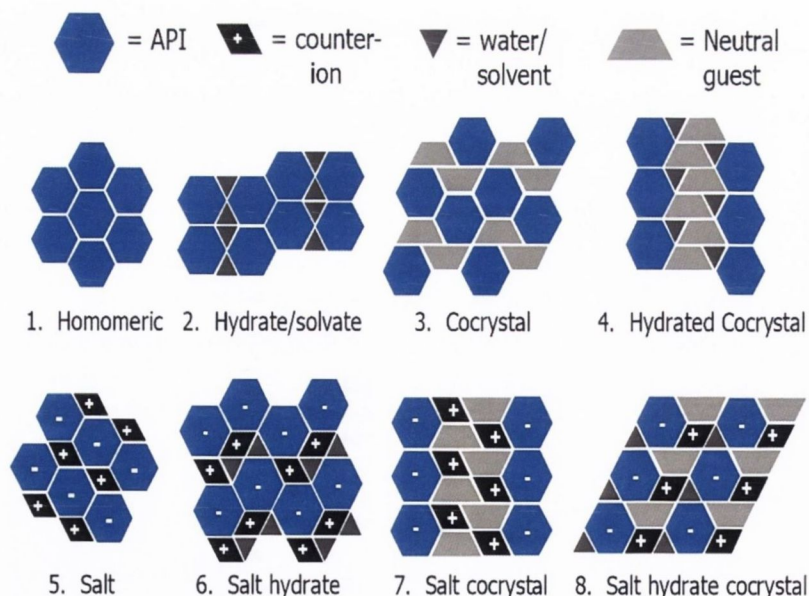
Figure 1.4: Classes of multi-component crystals (Childs, 2009).

8

1.2.2 Design of cocrystals

The design of cocrystals is also described as crystal engineering (detailed information about crystal engineering has been reported by Hippel et al., 1962) and involves a strategic selection of the cocrystal components. Based on the observation that hydrogen bonds are the main molecular interactions in a cocrystal, once an API has been selected, screening of a suitable coformer (usually a pharmaceutically acceptable excipient) with the ability to form hydrogen-bonds is performed. The objective is to identify hydrogen bonding motifs which are stable and which can be used to predict cocrystal formation within a family of related structures (Blagden et al., 2007). This procedure is also known as screening for supramolecular synthons. The term "supramolecular synthon" is defined as a structural unit which can be formed and/or assembled by known conceivable synthetic operations involving intermolecular interactions and has been introduced by Desiraju (1995). Etter and co-workers (1990) have described different hydrogen bonding rules which can be used as models in the screening of functional group preferences for hydrogen bonding formation (Etter, 1990 and 1991). Frequently, searching for synthons in existing crystal structures, which have been desposited in the Cambridge Structural Database (CSD), is of support (Vishweshwar et al., 2005).

Up to now, a large number of potential functional groups for cocrystal formation is known, where the carboxylic acid group is probably one of the most studied as it forms hydrogen bonds with a variety of amine functionalities that are present in many API molecules. A few examples of cocrystals which interact via a carboxylic acid and an amino group are the sulfadimidine:acetylsalicylic acid 1:1 and the sulfadimidine:4-aminosalicylic acid 1:1 cocrystals (Caira, 1992), the gabapentin:oxalic acid 1:1 cocrystal (Wenger and Bernstein, 2008) and the carbamazepine:succinic acid 2:1 cocrystal (Childs and Rodríguez-Hornedo, 2008). Several cocrystal production methods have been reported, such as solvent evaporation, slurrying, grinding, sublimation, melting, sonication or spray drying, but the mechanisms behind some of these processes are not fully understood (Aaerköy et al., 2003; Zawarotko, 2005; Blagden et al., 2007; Alhalaweh and Velaga, 2010).

Up to now, there are no general rules which enable predictions of successful cocrystal formation as several factors such as pK_a values of the functional group, conformational flexibility of the molecules, solubility of the components (in the case of solution-based formation methods) and the type of method used to prepare cocrystals play a fundamental role in cocrystal formation (Blagden et al., 2007; Issa et al., 2009).

1.2.3 Cocrystal phase diagrams

Important tools in understanding and predicting cocrystal formation from solution are phase diagrams such as ternary phase diagrams. They are used to visualise solution and solid phase compositions based on thermodynamic considerations (Wouters and Quéré, 2012). The practical procedure of constructing phase diagrams involves the determination of both the solution phase (solubility) and the solid phase which remains after the solution has reached equilibrium. Preferred methods to analyse the solubility and the solid composition are High Performance Liquid chromatography (HPLC) and powder X-ray diffraction (PXRD), respectively.

An important parameter which controls cocrystal formation in solution and which is relevant when selecting cocrystal components is the solubility of the individual components in a given solvent (Chiarella et al., 2007). If the solubilities are similar it is expected that the components dissolve congruently (i.e. that the components dissolve in the same stoichiometric ratio as they exist in the solid phase) and the resulting cocrystal would be termed as congruently saturating. If the components have very different solubilities, they will be considered as incongruently dissolving (i.e. that the components dissolve in a different stoichiometric ratio than present in the solid phase) and the resulting cocrystal is termed incongruently saturating (Chiarella et al., 2007; Good and Rodríguez-Hornedo, 2009). Chiarella et al. (2007) have shown that cocrystal formation is more likely to be successful when the cocrystal components have similar solubilities, however this will limit the number of potential cocrystal formers for the purpose of solution crystallisation. The construction of ternary phase diagrams can help to predict cocrystal formation for both congruently and incongruently saturating systems, as cocrystallisation pathways can be deduced.

There are two types of ternary phase diagrams which are of practical importance: the phase solubility diagram (PSD) and the triangular phase diagram (TPD) (Childs and Rodríguez-Hornedo, 2008). The phase solubility diagram (PSD) shows the solution concentrations at equilibrium with solid phases and is useful to study solution complexation (Zughul and Badwan, 1997), while the triangular phase diagram (TPD) shows the total composition of the system, the solid phases and liquid phases at equilibrium.

The more complex one to construct and to read is the triangular phase diagram which is further explained in the following.

Figure 1.5 presents triangular phase diagrams in the case when the component concentrations are similar (congruently saturating) (left) and when the component concentrations are very different (incongruently saturating) (right).
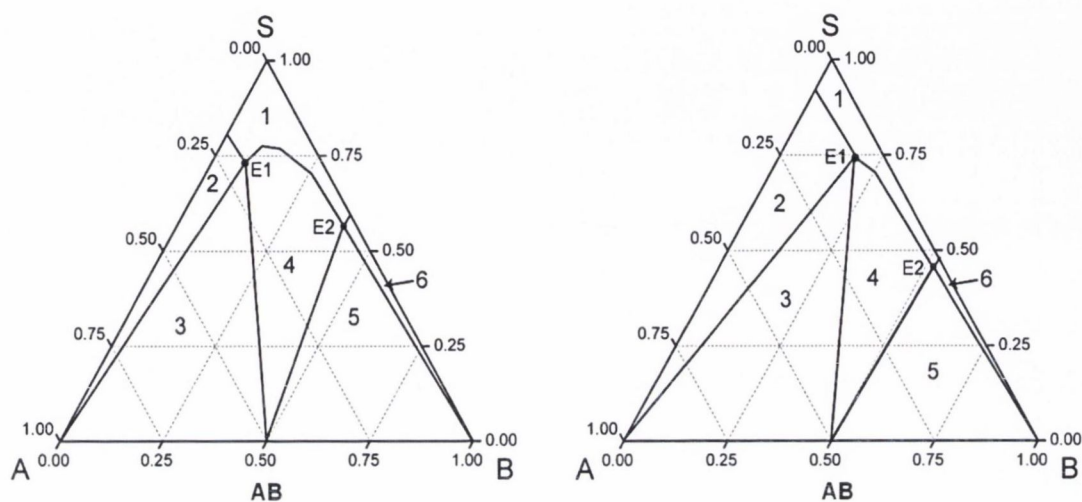
Figure 1.5: Schematic triangular phase diagram (TPD) (Rager and Hilfiker, 2009) of component A and B which form the AB (1:1) cocrystal in solvent (S) when the solubilities of A and B are similar (left) and when the solubilities of A is much lower than that of B. Scales are in mole fraction. (The different regions, 1-6, depicted in the phase diagrams are explained in the text below).

Each apex of the triangle represents 100% of the individual component (solid A, B and solvent S), while the side of the triangle opposite the apex represents 0% of the component at the apex. A typical triangular phase diagram of a cocrystal has six different regions. Region 1 presents a homogenous liquid phase, where both components A and B are dissolved in the solvent S. In region 2, solid A is in equilibrium with the liquid phase. In region 3, solid A and cocrystal AB are in equilibrium with the liquid phase. In region 4, the cocrystal AB is in equilibrium with the liquid phase. In region 5, solid B and cocrystal AB are in equilibrium with the solvent and in region 6, solid B is in equilibrium with the solvent. The points E1 and E2 are the eutectic points, also called invariant points. At these points, the liquid phase is in equilibrium with a fixed concentration of solid A and cocrystal (at point E1) and solid B and cocrystal (at point E2). The solution composition between these two points is

favourable for cocrystal formation (Good et al., 2011) and indicates the pathway for crystallisation of pure cocrystal phase in a given solvent.

The construction of such phase diagrams can be quite time-consuming as it has to be determined separately for each solvent.

A relatively new approach to facilitate the construction of triangular phase diagrams has been presented by Ainouz et al. (2009) based on data measured by discontinuous isoperibolic thermal analysis (DITA), a calorimetric method. It is a solvent independent method and enables extrapolations to be made from one data set to other solvents.

1.2.4 Identification and characterisation of cocrystals

An overview of the typical techniques which are used to determine the specific physical and chemical properties of both, crystalline and amorphous solid state forms and the information provided by each technique is presented Table 1.2.

Interpretation of results generated by these techniques is however not always straightforward, especially in differentiating between a salt and a cocrystal i.e. in determining whether proton transfer from an acid to a base has occurred or not (Stahly, 2007). Although cocrystal formation can, in some instances, be readily apparent due to a colour change of the material compared to the individual components (e.g. the acetaminophen:2,4-pyridine dicarboxylic acid cocrystal is red, while its components are white solids, Sander et al., 2010), a combination of techniques is generally most reliable in verifying cocrystal formation. Single crystal X-ray diffraction together with solid state NMR and FTIR spectroscopy have been found to be the most suitable to distinguish between a cocrystal and a salt (Schultheiss and Newman, 2009).

Single crystal X-ray diffraction (SC-XRD) is the preferred technique in order to identify the crystal structure and packing patterns of crystalline and polymorphic forms. Knowledge about how the molecules are packed together is important as this can influence the solid state properties significantly (Wouters and Quéré, 2012). However, the growth of a single crystal of sufficient size, as is required to make use of the technique, can be a very challenging and tedious task, in particular in the case of multi-component crystalline forms. Single crystals for X-ray structure analysis should practically be perfect in size and shape (around 0.1-0.3 mm in all three dimensions) and require specific conditions to grow where the type of solvent, the temperature, the time and the technique can have considerable impact on the result (Laudise, 1970; Chetina, 2012).

Since many crystalline solids cannot be prepared as single crystals or are only available as crystalline powders, powder X-ray diffraction (PXRD) has become an advanced alternative tool for crystal structure determination (Harris and Cheung, 2004).

One of the first examples where a crystal structure was solved from powder data for a cocrystal (a three molecular component cocrystal composed of racemic bis-β-naphtol, benzoquinone and anthracene) that had been prepared by grinding was reported by Cheung et al. (2003). Recently, Lapidus and co-workers have compared powder and single crystal techniques based on ten cocrystals and they found that high resolution powder diffraction is a reliable technique for solving crystal structures (Lapidus et al., 2010).

Table 1.2: Characterisation techniques of solid forms.

Technique	Information derived
X-ray diffraction analysis 1) Powder X-ray diffraction (PXRD)	Detection of crystalline and amorphous phase, polymorph detection, crystal structure determination
2) Single crystal X-ray diffraction (SC-XRD)	Crystal structure determination
Differential Scanning Calorimetry (DSC)	Detection of melting point (T_m), glass transition (T_g), crystallisation, solid form transformation, decomposition, residual solvent content
Thermogravimetric analysis (TGA)	Mass loss due to solvent loss, sublimation, evaporation, decomposition
Fourier transform - infra-red (FTIR) spectroscopy	Molecular structure information, detection of molecular interactions
Nuclear magnetic resonance (NMR) spectroscopy 1) Liquid	Molecular structure information, stoichiometry
2) Solid state	Molecular conformations and interactions, polymorph identification
Elemental analysis (EA)	Elemental composition % (w/w), stoichiometry
Scanning Electron Microscopy (SEM)	Morphology
Energy-dispersive X-ray analysis (EDXA) in conjunction with SEM	Elemental mapping (qualitative and quantitative analysis)
Dynamic Vapour Sorption (DVS)	Hygroscopicity
High Performance Liquid chromatography (HPLC)	Chemical content, purity

1.2.5 Polymorphism in cocrystals

Screening for polymorphic forms is of particular importance since polymorphs can exhibit different physical and chemical properties such as different stabilities (polymorph conversion), melting points and solubilities which can influence the dissolution rate and thus the bioavailability. Polymorphs are therefore an interesting additional possibility to modify the physicochemical properties of APIs.

An example of polymorph formation depending on the formation method used has been reported for cocrystals of caffeine and glutaric acid (Trask et al., 2004). While solvent evaporation from a mixture of chloroform and methanol resulted in the formation of two cocrystal polymorphs (A and B), liquid-assisted grinding of caffeine and glutaric acid using small amounts of cyclohexane gave only cocrystal form A and pure polymorphic form B was obtained by adding chloroform to the dry mixture prior to grinding. It was also shown that the two forms differed in their stability when exposed to different humidities, where the less stable form (polymorph A) converted to the more stable form (polymorph B).

The chlorzoxazone:2,4-dihydroxybenzoic acid 1:1 cocrystal is another example showing polymorphism (Childs and Hardcastle, 2007). By means of solvent evaporation, form I could be crystallised from tetrahydrofuran and form II from ethyl acetate. When dry grinding was used, only form II could be generated, while liquid-assisted grinding of form I resulted in the formation of the more stable form II.

These findings show the importance of the production method in the formation and discovery of cocrystal polymorphs.

1.2.6 Case studies of cocrystals

The following few examples demonstrate how cocrystal formation can modify and improve the physicochemical properties and how cocrystals can be formed by strategic design.

Itraconazole cocrystals: Itraconazole is an antifungal drug which has very poor aqueous solubility in the crystalline form. To achieve good oral bioavailability, it is available in the amorphous form (as Sporanox®). Remenar et al. (2003) have shown, based on three itraconazole cocrystals composed of succinic acid, $_L$-malic acid and $_L$-tartaric acid that the solubility of crystalline itraconazole can be improved when formulating as a cocrystal. The (dynamic) solubility was determined in 0.1 N HCl solutions at 25 °C for over 500 minutes. The solubility profiles of the cocrystals

revealed 4- to 20-fold higher drug concentrations compared to pure itraconazole and the concentrations were maintained for up to 8 hours. The dissolution rate of the itraconazole:$_L$-malic acid cocrystal was found to be comparable with that of amorphous itraconazole (Sporanox®). Due to the crystalline nature of the cocrystal, it is anticipated that the solid state stability is improved compared to the amorphous form.

Glutaric acid cocrystals: Trask et al. (2005) have shown based on the caffeine:glutaric acid 2:1 cocrystal prepared by liquid-assisted grinding, that the cocrystal revealed superior physical stability under conditions of up to 98% RH at 20 °C over a time period of seven weeks compared to pure anhydrous caffeine. Additional slurry experiments in water at ambient conditions over 2 days confirmed the cocrystal stability since no phase transformation was observed. McNamara et al. (2006) have presented a study of a glutaric acid cocrystal containing the low water-soluble non-ionisable 2-[4-(4-chloro-2-fluorophenoxy) phenyl] pyrimidine -4-carboxamide, a sodium channel blocker. Intrinsic dissolution studies in water at 37 °C over 90 minutes revealed that the cocrystal showed a significant improvement in dissolution rate of approximately 18 times compared to the parent drug. The cocrystal was also shown to improve the bioavailability (based on a study with dogs) by three times in comparison to the drug on its own.

Carbamazepine cocrystals: Carbamazepine is an antiepileptic drug which is known to exist in four polymorphic forms. It reveals poor aqueous solubility and requires a high dose in order to achieve a therapeutic concentration (>100 mg/day). Based on seven different carbamazepine cocrystals, Good and Rodríguez-Hornedo (2009) reported 2 to 152 times greater aqueous solubility than the solubility of the stable carbamazepine dihydrate form. Extensive studies on solution stability were performed which have shown that the solubility can be tailored by selecting a coformer with appropriate solubility. Coformers which exhibited relatively low aqueous solubility resulted in stable carbamazepine cocrystals, whereas cocrystals containing coformers with relatively high aqueous solubility showed conversion to carbamazepine dihydrate after slurrying in water. The investigation of solution stability of drug forms is in general an important parameter since the solid drug form, when in contact with the body fluid, may convert and result in precipitation of the more stable form. In the case of cocrystals, which are multi-component systems it is possible that after dissolving one of the

components will precipitate, which will have a significant impact on the actual bioavailability. A study based on twenty carbamazepine cocrystals with eighteen different carboxylic acid coformers prepared from water has shown that only seven were stable, while the others showed conversion to the parent drug after slurrying in water for 20–48 hours (Childs et al., 2008). The construction of ternary phase solubility diagrams has been useful to indicate the thermodynamic stability regions of the carbamazepine cocrystals (Childs et al., 2008).

In a study by Hickey et al. (2007) the carbamazepine:saccharin 1:1 cocrystal was compared to the marketed form of carbamazepine (Tegretol®). It was shown that the chemical and physical stability of the cocrystal was comparable to the available marketed form. The stability study was performed at elevated temperature (5, 40 and 60 °C at ambient humidity) and at elevated RH conditions (25 °C/60% RH and 40 °C/75% RH) over 2 months. The results demonstrated that both, the cocrystal and pure carbamazepine, did not degrade at the elevated temperatures, but showed similar degradation profiles under the elevated RH conditions. Oral bioavailability studies of the cocrystal in dogs have shown that the cocrystal formulation exhibited higher plasma levels (AUC and C_{max}) than Tegretol®.

The compaction and compression properties of the carbamazepine:saccharin 1:1 cocrystal and pure carbamazepine have been investigated by Rahman et al. (2012). The study was performed by compressing powder at nine different compression force. The compacts were evaluated for thickness, diameter, weight, hardness and the radial tensile strength was calculated. The results showed that the cocrystal is better compressible and compacts of cocrystal have a higher tensile strength at any compression pressure than compacts of carbamazepine.

Paracetamol cocrystals: A study by Karki et al. (2009) based on four paracetamol cocrystals has shown that cocrystals improve the mechanical properties such as compressability and tensile strength. The study of compression properties revealed for all four cocrystals a better tablet formation ability than free paracetamol, polymorph I. While paracetamol, polymorph I could not be compressed into a tablet without the observation of capping, the four cocrystals formed readily tablets. The best tensile strength was found for the paracetamol:theophylline 1:1 cocrystal.

AMG 517 cocrystals: AMG 517 is a development lead candidate of Amgen for the treatment of chronic pain. The drug reveals solubility limited absorption and is unstable at low pH. A study by Stanton and Bak (2008) investigated cocrystal formation of AMG 517 with ten commercially available acids. The solubility was measured in fasted state simulated intestinal fluid (FaSSIF). Six of the tested cocrystals showed a transient solubility advantage (for 1–2 hours) when compared to the pure drug. After that time, the solubility decreased significantly as a result of conversion to the free base hydrate of AMG 517. However, it was suggested that the enhanced apparent solubility is high enough to give increased drug exposure in pharmacokinetic studies. Moreover, most of the cocrystals showed good solid state stability under conditions of 75% RH and 40 °C. No phase changes based on PXRD experiments were observed. Eight of nine AMG 517 cocrystals were classified as non-hygroscopic, while one was slightly hygroscopic. In the study it was also observed that in 78% of the cases the melting point of the cocrystal correlated with the melting point of the coformer. It was therefore suggested that it is possible to modify the melting point of an API by selecting of the cocrystal former melting point (high values are usually preferred for achieving better thermal stability with respect to material processing).

Sulfoxide cocrystals: A study by Kumar et al. (2002) investigated complex formation of the sulfoxide trans-1,4-dithiane-1,4-dioxide with some mono and dicarboxylic acids. They have shown that stable cocrystals can be formed, interacting by hydrogen bond formation between the carboxylic acid and sulfoxide moiety. Steiner (2001) realised in a CSD analysis that the preference of hydrogen bond formation between a carboxylic acid and a sulfoxide group within molecules occurs with a probability of 75% indicating that there is great potential to predict cocrystal formation between these two functional groups. In later studies performed by Eccles et al. (2010) it was demonstrated that the sulfoxide moiety not only interacts well with carboxylic acids; there is also preference for hydrogen bonding formation with amino functional groups, a common functionality in numerous APIs. Seven cocrystals were successfully formed by solvent evaporation and by solid state grinding. Salt formation was excluded due to the very poorly basic properties of sulfoxide.

Sulfonamide cocrystals: Caira and co-workers have reported extensively on interactions between the sulfonamide functional group and the carboxylic acid group. The sulfonamide functional group is present in a number of antibiotics, but also in some diuretics (of the thiazide type) and some antidiabetic drugs (of the sulfonylurea type). Based on the antibiotic sulfadimidine as a model compound, Caira (1991, 1992) has demonstrated complex formation (at that time the term cocrystal was not defined) with different aromatic carboxylic acids coformers in what were some of the first studies on cocrystal formation. The author reported on the formation of six sulfadimidine aromatic carboxylic acid (2- and 4- aminobenzoic, 4-aminosalicylic, acetylsalicylic, p-chlorobenzoic and o-phthalic acid) cocrystals produced by solvent evaporation. In a later study based on sulfadimidine with benzoic, 2-aminobenzoic, salicylic, acetylsalicylic, p-chlorobenzoic and o-phthalic acid as coformers it was shown that cocrystals can be formed by solid state grinding (Caira et al., 1995). The hydrogen bonding preferences were found to be the same in all sulfadimidine cocrystals involving the sulfonamide functionality and the carboxylic acid group.

Sulfadimidine is a known sulfonamide antibiotic (folic acid inhibitor) used against a wide variety of infectious diseases particularly those affecting the respiratory, gastrointestinal and urogenital tract in humans and in veterinary medicine (Prescott and Baggot, 1988). The study of cocrystal formation using two APIs such as sulfadimidine and 4-aminosalicylic acid (also an antibiotic with the same pharmacological mechanism of action as sulfadimidine and primarily used in the treatment of tuberculosis (O'Donnell et al., 1992; Bailey et al., 2008)) and sulfadimidine and acetylsalicylic acid (known as aspirin, an API with analgesic, anti-inflammatory and antipyretic effect) was suggested to be therapeutically useful, as the drug combination may exhibit a synergistic effect requiring (normally) sub-therapeutic amounts to be administered (Caira, 1992).

In another study by Bettineti et al. (1997) it was demonstrated that sulfadimidine forms a cocrystal with trimethoprim (also an antibiotic); the cocrystal being prepared by solution crystallisation. In contrast, when sulfamethoxazole, a structurally related sulfonamide, and trimethoprim are used, a salt is formed (Nakai et al., 1984). The difference in outcome depending on which sulfa compound was used was attributed to the stronger acidic property of sulfamethoxazole compared to sulfadimidine. The study demonstrated that the acid strength is a determining factor as to whether a salt or a cocrystal is formed. Later investigations showed that the sulfonamide,

sulfamethoxypyridazine can form a cocrystal with trimethoprim when crystallised from methanol but forms a salt hydrate when crystallised from water (Bettineti et al., 2000). The interactions between the two components were similar involving the same functional groups, whereas the cocrystal showed two hydrogen bonds while the salt showed one hydrogen bond and one ionic interaction (proton transfer). The study elucidated that careful characterisation is required to distinguish between cocrystal and salt formation.

1.2.7 Perspective

Due to the structural diversity, cocrystal formation offers a broad scope with the ability to fine-tune the physicochemical properties of known and new APIs and to discover new forms. Further research is essential in order to finally implement cocrystal manufacturing and use on a commercial scale.

Chapter 2:

Characterisation, solubility and intrinsic dissolution behaviour of the benzamide:dibenzyl sulfoxide cocrystal

2.1 Introduction

It has been previously shown that the sulfoxide (S=O) functionality, common in a significant number of APIs, is a potent hydrogen bonding acceptor and forms cocrystals in association with a wide variety of amino (NH) functional groups (Eccles et al., 2010). The benzamide:dibenzyl sulfoxide (BAM:DBSO) 1:1 cocrystal is a representative example of this class. Dibenzyl sulfoxide acts as a hydrogen bond acceptor due to the polar sulfoxide moiety (Eccles et al., 2010) while being poorly water soluble, as is the case for a wide range of APIs. BAM is a hydrogen bond donor with higher aqueous solubility in comparison to DBSO (O'Neil et al., 2006). Therefore, BAM represents a model coformer of the cocrystal.

Some cocrystals have previously been reported to result in improved bioavailability of poorly soluble APIs as a result of improved dissolution rate (McNamara et al., 2006; Hickey et al., 2007; Jung et al., 2010). Determination of the solubility of complexes was reported by Higuchi as early as in the 1950s (Higuchi and Connors, 1965). Rodríguez-Hornedo and co-workers have recently developed new theoretical models in order to predict solubility and solution stability of cocrystals (Nehm et al., 2006; Good and Rodríguez-Hornedo, 2009; Reddy L.S. et al., 2009; Good and Rodríguez-Hornedo, 2010). It was found that the solubility of cocrystals is dependent on the coformer concentration in the appropriate solvent (Good and Rodríguez-Hornedo, 2009). Therefore, it is important to measure concentrations of both compounds when undertaking the solubility experiment. Solubility is a relevant parameter that has to be investigated for each cocrystal system since true equilibrium solubility might be difficult to measure due to solid state transformation in solution (Good and Rodríguez-Hornedo, 2009). Such solution-mediated transformations to the thermodynamically more stable state should result in a change in the dissolution rate and therefore it is important to control/measure these processes. However, solid state changes are not the sole rate-determining factors. Surface area, particle size distribution of the drug, fluid dynamics and the experimental apparatus can complicate the interpretation of dissolution results (Good and Rodríguez-Hornedo, 2009).

Intrinsic dissolution tests have been reported for numerous single component pharmaceutical materials (Higuchi et al., 1965; O'Connor and Corrigan, 2001; Mauger et al., 2003; Yu et al., 2004; Avdeef and Tsinman, 2008) whereas little literature is found for cocrystals (Childs et al., 2004; Jung et al., 2010; Lee et al., 2011; Rahman et al., 2012). The intrinsic dissolution rate is based on measurements of powder compacts

of known surface area under conditions of controlled hydrodynamics (Healy et al., 2002) and is described as particle-size independent (Wood et al., 1965; Hendriksen and Williams, 1991). Since the surface area does not change over time, the dissolution rate depends on the solubility of the solute, hydrodynamics and diffusion coefficient in the dissolution medium (Wood et al., 1965; Hendriksen and Williams, 1991).

This report investigates solid state characteristics, solubility and dissolution behaviour of the benzamide:dibenzyl sulfoxide cocrystal in comparison to its pure compounds and an equimolar physical mixture.

2.2 Materials and Methods

2.2.1 Materials

Dibenzyl sulfoxide (DBSO) was synthesised as described by Kuliev et al. (1984), using dibenzyl sulfide which was purchased from Sigma-Aldrich (Ireland). The synthesis was performed by Kevin Eccles (Department of Chemistry, Analytical and Biological Chemistry Research Facility, University College Cork, Cork, Ireland). Benzamide (BAM) was obtained from Sigma-Aldrich (Ireland). (Details of physical and chemical properties of DBSO and BAM can be found in Appendix 5, Table A.5.1) Acetonitrile, HPLC grade, was purchased from Fisher Scientific (Ireland). Water, analytical and HPLC grade, was prepared from an Elix 3 connected to a Synergy UV system (Millipore, UK).

2.2.2 Methods

2.2.2.1 Preparation of the cocrystal

The benzamide:dibenzyl sulfoxide (BAM:DBSO) 1:1 cocrystal was synthesised by Kevin Eccles (Department of Chemistry, Analytical and Biological Chemistry Research Facility, University College Cork, Cork, Ireland). Therefore, an ethyl acetate solution (5 ml) of benzamide (60 mg, 0.50 mmol) was added to a slurried mixture of dibenzyl sulfoxide (115 mg, 0.50 mmol) in ethyl acetate (5 ml) with stirring. After dissolution of dibenzyl sulfoxide the solution was filtered and the filtrate was allowed to stand until crystals have formed. The crystals were then analysed by single crystal X-ray diffraction, as reported by Eccles et al. (2010). The structure has been deposited in the Cambridge Crystallographic Data Centre, reference number is CCDC 782027. Crystallographic cif files and supplementary data are available at http://pubs.acs.org.

2.2.2.2 Powder X-ray diffraction (PXRD)

Powder X-ray analysis was performed using a Miniflex II Rigaku diffractometer with Ni-filtered Cu Kα radiation (λ = 1.54 Å). The tube voltage and tube current used were 30 kV and 15 mA, respectively. The samples were scanned over a 2 theta range of 5° to 40° with a step size of 0.05° per second (Tajber et al., 2009). The program Mercury 2.3 (Mercury CSD 2.0, 2008) was used for calculation of X-ray powder patterns on the basis of the single crystal structure established by Eccles et al. (2010).

2.2.2.3 Thermal analysis

2.2.2.3.1 Differential scanning calorimetry (DSC)

Differential scanning calorimetry was performed using a Mettler Toledo DSC 821^e instrument under nitrogen purge. Sample powders were placed in aluminium pans, sealed, pierced to provide three vent holes and heated at a rate of 10 °C/min in the temperature range of 25 to 250 °C (Tajber et al., 2005). Calibration of the instrument was carried out using indium as standard. The DSC system was controlled by Mettler Toledo STARe software (version 6.10) working on a Windows NT operating system. Temperatures of melting and crystallisation events refer to onset temperatures. Presented values are the average of 3 results.

2.2.2.3.2 Thermogravimetric analysis (TGA)

Thermogravimetric analysis was performed using a Mettler TG 50 module. Samples were placed into open aluminium pans (5-12 mg) and analysed at a constant heating rate of 10 °C/min under nitrogen purge (Tajber et al., 2005). The instrument was controlled by Mettler Toledo STARe software (version 6.10) working on a Windows NT operating system.

2.2.2.4 Attenuated total reflection - Fourier transform infra-red (ATR-FTIR) spectroscopy

Infrared spectra were recorded on a PerkinElmer Spectrum 1 FT-IR Spectrometer equipped with a UATR and a diamond/ZnSe crystal accessory. Each spectrum was scanned in the range of 650-4000 cm^{-1} with a resolution of 4 cm^{-1} and a minimum of six scans were collected and averaged in order to gain good quality spectra. Data were evaluated using Spectrum v5.0.1. software.

2.2.2.5 Solubility studies

2.2.2.5.1 Equilibrium, phase solubility and dynamic solubility

The solubilities of pure compounds and the cocrystal were determined using a 24-hour shake flask method (used previously for many compounds) (Wermuth, 2008). Therefore, an excess of solid (approximately 2–3 times the amount expected to achieve saturation solubility) was added to 10 ml of water in glass ampoules, which were then heat sealed. To measure complexation between compounds, known amounts of BAM of increasing concentration (= initial BAM concentration) were dissolved in 10 ml of water in glass ampoules. Then excess of solid DBSO or cocrystal was added to each ampoule and the ampoules were heat sealed. The ampoules were placed horizontally in a thermostated waterbath at 37 °C and shaken at 100 cpm for 12 and 24 hours and also at 48 and 72 hours for dynamic solubility studies. After the appropriate time, the ampoules were opened, the supernatant withdrawn and filtered through 0.45 µm membrane filters (PVDF - Cronus®). Concentrations of the components in the supernatant were determined by HPLC. The term "apparent solubility" is used to denote the solubility of systems where complexation occurs and "true" equilibrium solubility is therefore difficult to measure. The solid materials, remaining in the ampoule after 12 and 24 hours of solubility studies were kept, dried at 40 °C and examined for phase transformation by PXRD and DSC. The experiments were performed in triplicate.

2.2.2.5.2 Transition concentration (C_{tr}) measurement

The transition concentration or invariant point was determined using a previously reported method (Good and Rodríguez-Hornedo, 2009). This was achieved by adding excess DBSO to a slightly undersaturated aqueous BAM solution and by adding excess cocrystal to a presaturated aqueous DBSO solution. The suspensions were stirred over 24 hours at 37 °C. After 24 hours supernatants were withdrawn, filtered through 0.45 µm membrane filters (PVDF - Cronus®) and quantified by HPLC. C_{tr} values are expressed as the average established from these two experimental approaches (Good and Rodríguez-Hornedo, 2009). The solid phases were characterised by PXRD and DSC. The experiments were performed in triplicate.

2.2.2.6 Intrinsic dissolution study

The intrinsic dissolution rate (IDR) of solid materials was determined using constant surface area disks. These disks were prepared by compressing powder into compacts using a Perkin Elmer hydraulic press. Therefore, 300 mg of each solid was weighed and compressed in a 13 mm punch and die set at a pressure of 8 tonnes for 1.5 min. The compacts were coated using paraffin wax, leaving only the surface under investigation free for dissolution (Nicklasson et al., 1981; Healy et al., 2002) and affixed horizontally to the base of the dissolution vessel using adhesive tape. The stationary disc method was used in preference to the rotating disc method (Wood's apparatus). It was previously observed that, while the Wood apparatus is suitable for studying the dissolution of single component systems, it is less suited to multicomponent systems, with a greater tendency for disintegration and thus disruption of the constant surface area, than with the stationary disc method, which was previously used successfully for two component systems (Healy and Corrigan, 1992; Healy and Corrigan, 1996). The dissolution studies were carried out in 900 ml of vacuum filtered and degassed water at 37 °C in a paddle apparatus (Varian/Vankel; Apparatus 2, Ph. Eur.) at a rotation speed of 100 rpm. Aliquots of 5 ml were withdrawn (with replacement) at appropriate time intervals, filtered through 0.45 μm filters (PVDF - Cronus®) and analysed for sample concentration by HPLC. The study, performed in triplicate, was terminated after 90 minutes. The intrinsic dissolution rate (IDR) was determined from the slope of the dissolution time profiles. Initial and limiting rates were determined within the first five minutes and between sixty and ninety minutes, respectively. The disks were recovered, dried at ambient temperatures and then analysed by ATR-FTIR and SEM/EDX for surface changes.

2.2.2.7 High Performance Liquid Chromatography (HPLC)

The HPLC method was developed by Nuala Maguire (Department of Chemistry, Analytical and Biological Chemistry Research Facility and School of Pharmacy, University College Cork, Cork, Ireland). Concentrations of DBSO and BAM in solutions were determined using a Shimadzu HPLC Class VP series with a LC-10AT VP pump, SIL-10AD VP autosampler and SCL-10VP system controller. The mobile phase was vacuum filtered through a 0.45 μm membrane filter (Gelman Supor-450). Separation was performed on a Luna C18 column (250 mm length, diameter 4.6 mm, particle size 5 μm) at a UV detection wavelength of 254 nm with an injection volume of

10 µl. The mobile phase consisted of acetonitrile/water 60/40 (v/v). The elution was carried out isocratically at ambient temperatures with a flow rate of 1 ml/min. For peak evaluation Class-VP 6.10 software was used.

2.2.2.8 Energy-Dispersive X-ray (EDX) analysis and Scanning Electron Microscopy (SEM)

In order to determine the elemental composition on compact surfaces, EDX analysis was performed using a Tescan Mira Variable Pressure Field Emission Scanning Electron Microscope (Czech Republic), operating at a resolution of 3 nm at 30 kV and equipped with an Oxford Inca energy-dispersive microprobe and a backscattered electron detector. Powder compacts were glued onto aluminium stubs using carbon cement, dried for 24 hours at ambient temperatures and coated with carbon under vacuum prior to analysis. X-ray spectra were evaluated quantitatively on the basis of the carbon peak. Furthermore, surface images at various magnifications were performed by SEM using a Zeiss Supra Variable Pressure Field Emission Scanning Electron Microscope (Germany) at a resolution of 1.5 nm at 15 kV equipped with a secondary electron detector. Powder compacts were glued onto aluminium stubs using carbon cement, dried for 24 hours at ambient temperatures and sputter-coated with gold under vacuum prior to analysis.

2.2.2.9 Statistical analysis

2.2.2.9.1 Two sample t-test

Microsoft® Excel data analysis software was used to determine statistical significance. The two sample t-test was used to compare the means and standard deviations of two independent samples at a significance level of $\alpha=0.05$.

2.2.2.9.2 ANOVA

Origin Lab® data analysis software was used to determine statistical significance using one-way ANOVA at a significance level of $\alpha=0.05$.

2.2.2.9.3 Linear regression

Linear regression analysis was performed using the method of least squares by Microsoft® Excel software. The adequacy of the fit was assessed from the regression coefficient (R^2).

2.3 Results and Discussion

2.3.1 Solid state properties

The powder X-ray diffraction pattern of the 1:1 BAM:DBSO cocrystal is shown in Figure 2.1. This revealed a characteristic diffraction pattern, which differed from those of the two individual components (DBSO and BAM) and the equimolar physical mixture. The DSC thermogram in Figure 2.2 confirmed the presence of the cocrystal and indicated a sharp endothermic melting event with an onset temperature of around 115.68 ± 0.33 °C (with a heat of fusion, $\Delta H_f = 159.32 \pm 4.82$ J/g). In contrast BAM and DBSO, showed melting onsets at around 126.90 ± 0.31 °C ($\Delta H_f = 188.05 \pm 3.79$ J/g) and 134.23 ± 0.53 °C ($\Delta H_f = 131.90 \pm 1.24$ J/g), respectively.
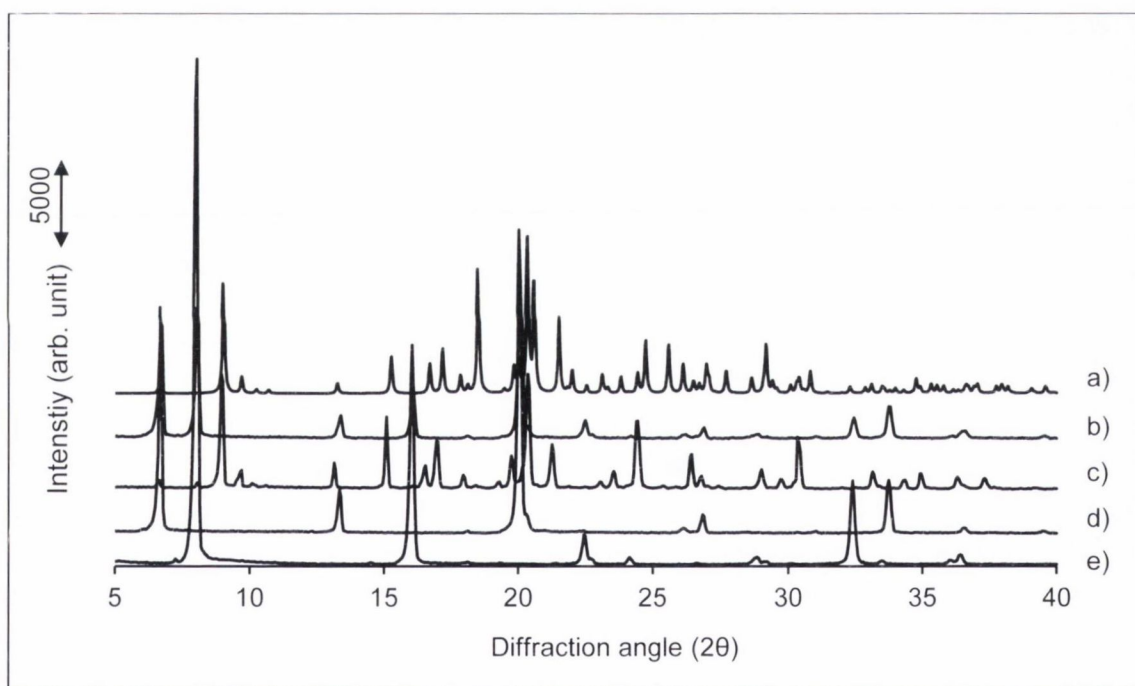
Figure 2.1: PXRD patterns of a) 1:1 BAM:DBSO cocrystal calculated based on single crystal data, b) BAM:DBSO (1:1) physical mixture, c) 1:1 BAM:DBSO cocrystal, d) pure DBSO and e) pure BAM.
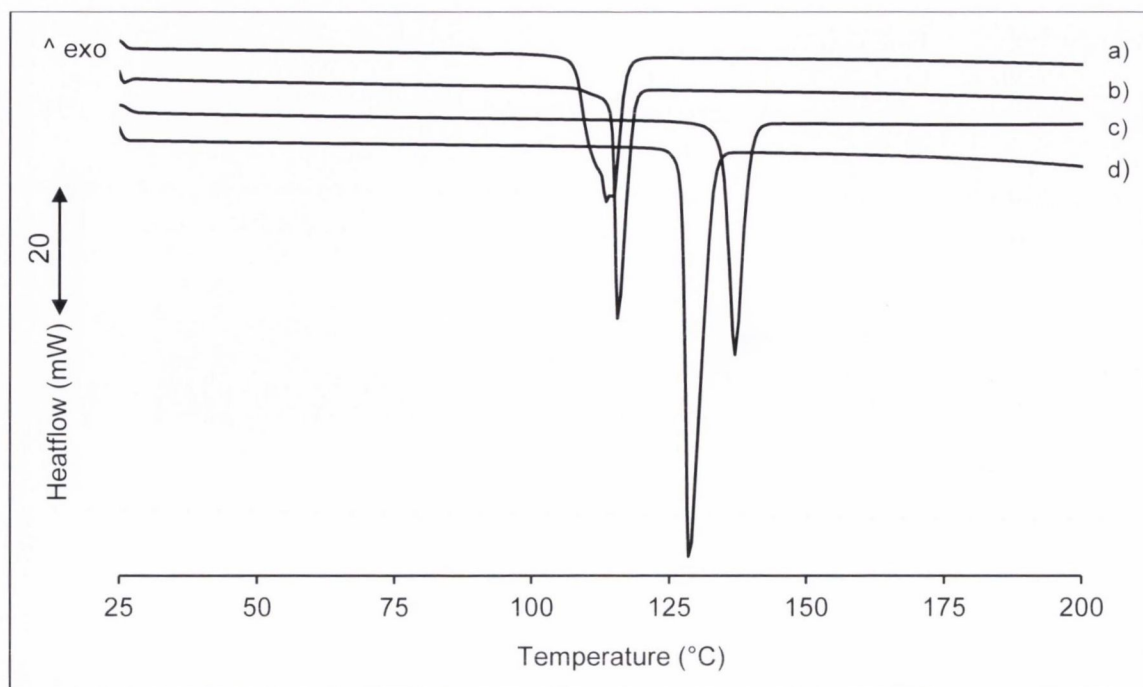
Figure 2.2: DSC thermograms of a) BAM:DBSO (1:1) physical mixture, b) 1:1 BAM:DBSO cocrystal, c) pure DBSO and d) pure BAM.

ATR-FTIR revealed evidence of significant intermolecular interactions based on two characteristic shifts towards lower frequencies. As shown in Figure 2.3, the symmetric NH stretching band of BAM is shifted from 3173 cm^{-1} to 3140 cm^{-1} and the S=O functional group from 1032 cm^{-1} to 1013 cm^{-1}. These shifts were not observed for the physical mixture.

The reason for these shifts of IR bands was explained based on the single crystal X-ray diffraction data previously reported for the 1:1 BAM:DBSO cocrystal which showed that molecular association between BAM and DBSO occurs through hydrogen bonding (Eccles et al., 2010). Generation of the theoretical PXRD diffractogram from the single crystal data (Figure 2.1a) showed consistency with the experimental PXRD pattern of the cocrystal (Figure 2.1c).
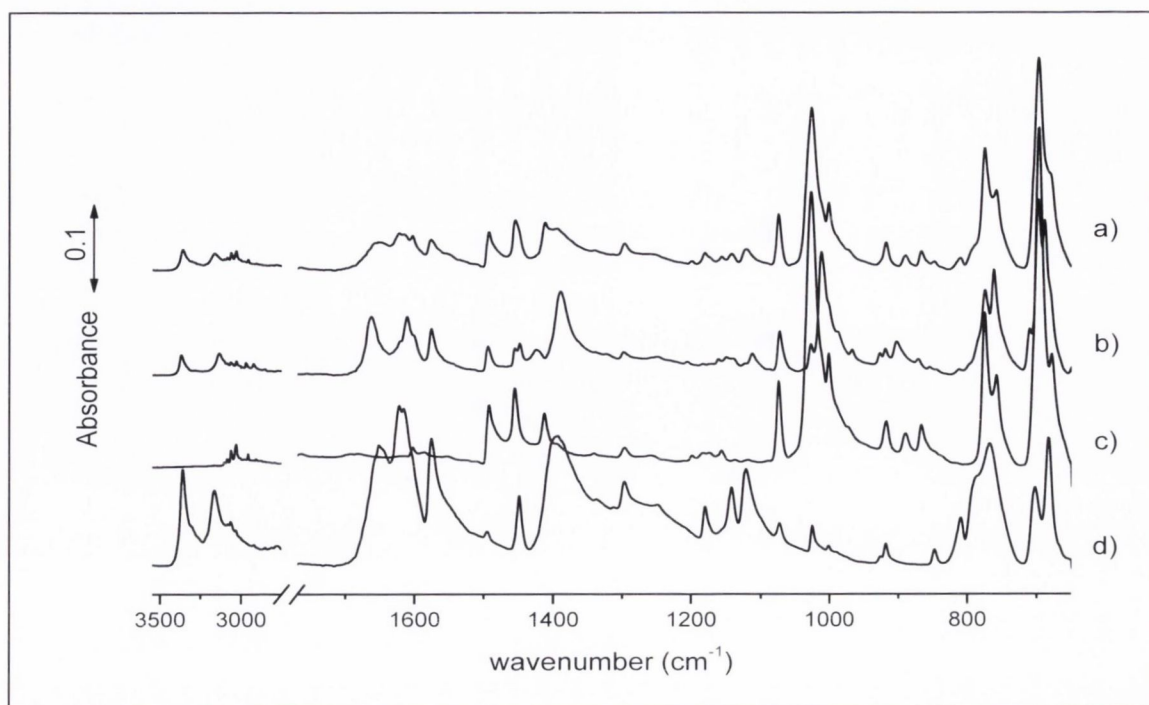
Figure 2.3: FTIR spectra of a) BAM:DBSO (1:1) physical mixture, b) 1:1 BAM:DBSO cocrystal, c) pure DBSO and d) pure BAM.

2.3.2 Solubility study

The solubilities for BAM and DBSO in water at 37 °C were found to be 13.10 ± 0.20 mg/ml ($108.14 \times 10^{-3} \pm 1.67 \times 10^{-3}$ mmol/ml) and 0.33 ± 0.01 mg/ml ($1.43 \times 10^{-3} \pm 0.03 \times 10^{-3}$ mmol/ml), respectively (Table 2.1). The apparent solubility (based on 24 hours equilibrium) of the cocrystal in water at 37 °C was determined by measuring DBSO and BAM concentrations and values of 3.07 ± 0.18 mg/ml ($25.37 \times 10^{-3} \pm 1.48 \times 10^{-3}$ mmol/ml) for BAM and 0.27 ± 0.01 mg/ml ($1.18 \times 10^{-3} \pm 0.04 \times 10^{-3}$ mmol/ml) for DBSO were obtained (Table 2.1). These results show that the apparent solubilities of the cocrystal components were decreased in comparison to the solubilities of the pure compounds.

Table 2.1: Solubility/apparent solubility of pure compounds, co-mixed and cocrystallised BAM and DBSO.

Substance	Description	Solubility (mg/ml)	Solubility (mmol/ml)
BAM	pure material	13.10 ± 0.20	$108.14 \times 10^{-3} \pm 1.67 \times 10^{-3}$
	physical mixture	9.40 ± 0.16	$77.60 \times 10^{-3} \pm 1.36 \times 10^{-3}$
	cocrystal	3.07 ± 0.18	$25.37 \times 10^{-3} \pm 1.48 \times 10^{-3}$
DBSO	pure material	0.33 ± 0.01	$1.43 \times 10^{-3} \pm 0.03 \times 10^{-3}$
	physical mixture	0.32 ± 0.00	$1.41 \times 10^{-3} \pm 0.01 \times 10^{-3}$
	cocrystal	0.27 ± 0.01	$1.18 \times 10^{-3} \pm 0.04 \times 10^{-3}$

The apparent solubilities of DBSO and cocrystal were measured as a function of coformer (BAM) concentration in order to determine solution complexation. Investigation of solution interactions revealed that the apparent solubility of DBSO initially increased with increasing concentration of BAM, when DBSO was the excess phase, due to soluble complex formation between the two compounds (Figure 2.4). The solubility profile of DBSO with increasing BAM concentration can be described as a Type B phase-solubility diagram (Higuchi and Connors, 1965). When the concentration of BAM was initially ≥ 3 mg/ml the solubility limit of the complex formed was exceeded and uncomplexed DBSO in solution did not change significantly, as shown by the plateau in Figure 2.4. In this context, the increase in the apparent DBSO solubility i.e. the amount of DBSO that enters into soluble complex formation was determined (Higuchi and Connors, 1965). A nearly two-fold increase of the apparent DBSO solubility in the presence of BAM, in comparison to DBSO solubility in water alone, was observed.
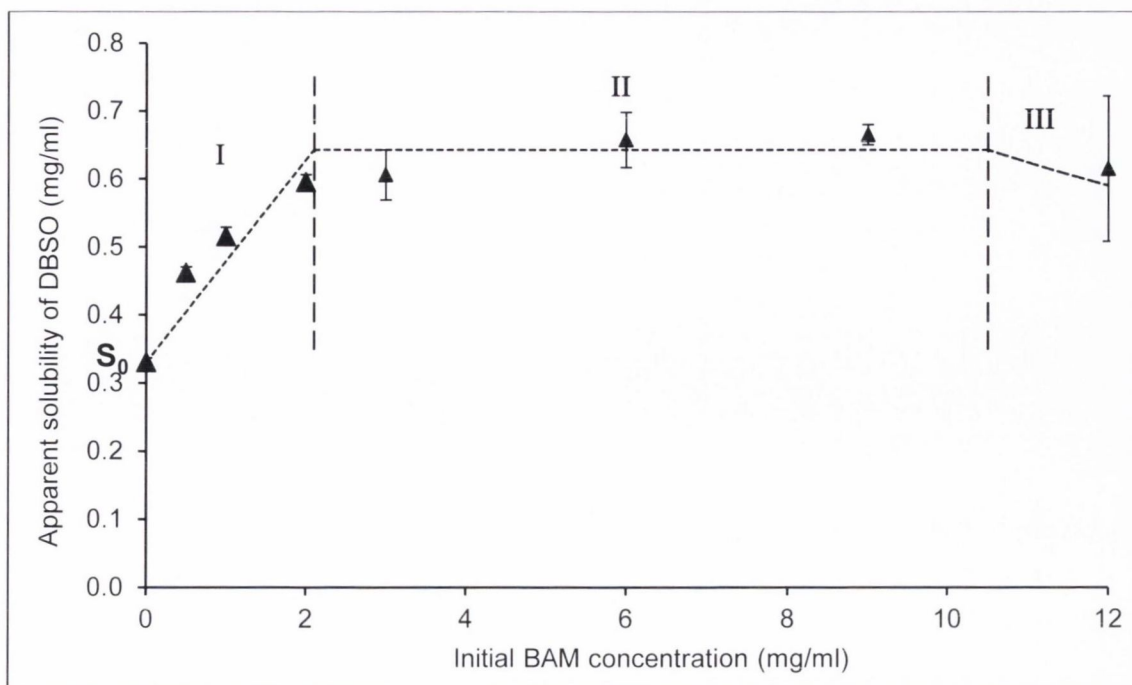
Figure 2.4: Profile of the apparent solubility of DBSO (mg/ml) as a function of BAM concentration measured after 24 hours. S_o is the DBSO concentration in absence of BAM. The dashed lines confirm the behaviour of a Type B phase solubility diagram illustrating region I (solution complexation), II (conversion to complex and precipitation) and III (decreased solubility of precipitated complex with increasing BAM in solution).

Precipitation of the complex was apparent on PXRD analysis of the solid residue which indicated the presence of two phases, cocrystal and DBSO. When the initial BAM concentration was 12 mg/ml, and therefore close to its aqueous solubility, nearly all solid DBSO was consumed leading to depletion of DBSO, followed by complex precipitation induced by supersaturation of the solution. The precipitated solid phase was cocrystal contaminated with DBSO (Figure 2.5).

Furthermore, a significant decrease in the apparent DBSO solubility after 24 hours in comparison to 12 hours was observed at 12 mg/ml BAM in solution. PXRD analysis of the remaining solid material revealed that this decrease in solubility reflected cocrystal formation and subsequent precipitation, since the diffraction pattern of the solid residue is superimposable on that of the cocrystal re-crystallised from ethyl acetate (Figure 2.5).
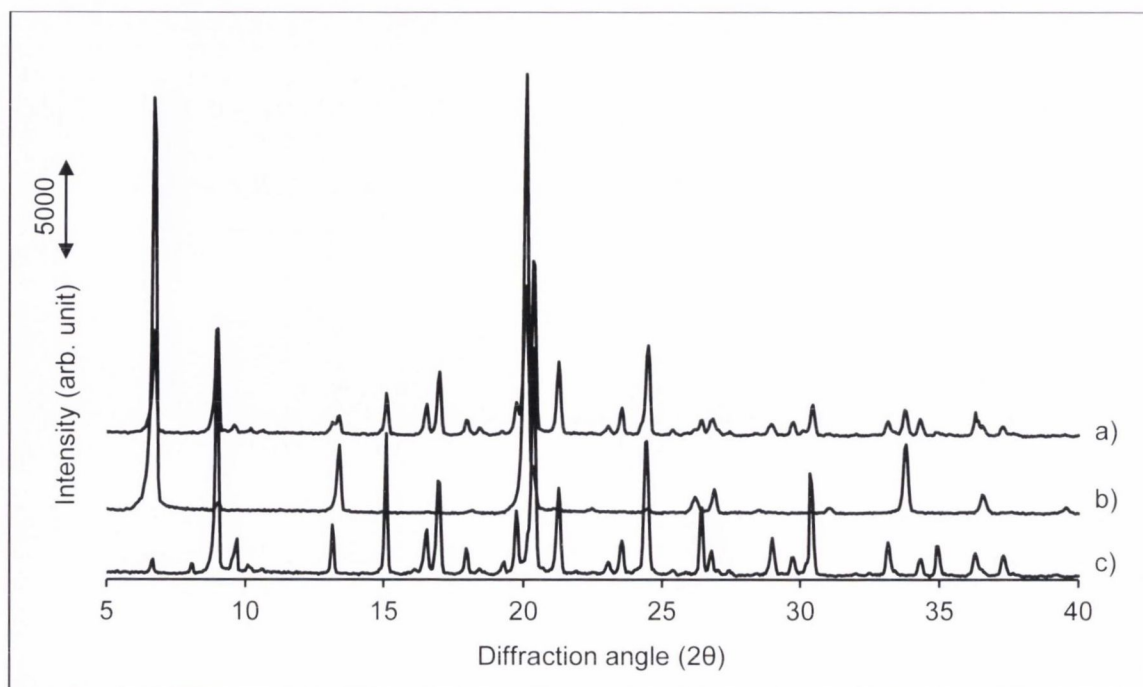
Figure 2.5: PXRD patterns of a) remaining solid (12mg/ml BAM added) after 24 hours solubility study, b) remaining solid (12mg/ml BAM added) after 12 hours solubility study, c) 1:1 BAM:DBSO cocrystal.

The increase in the apparent solubility of DBSO in the presence of BAM can be expressed by a complex formation (or stability) constant (Higuchi and Connors, 1965). For 1:1 soluble complexes, this constant is given by equation 2.1:

$$K_{11} = \frac{[AB]}{[A][B]} \tag{2.1}$$

where [A] and [B] are the (molar) concentrations of each component at equilibrium. Thus the increase in solubility may be quantified (equation 2.2):

$$[A]_T = \frac{K_{11}[A]_0[B]_T}{1 + K_{11}[A]_0} + [A]_0 \tag{2.2}$$

where $[A]_T$ is the total concentration of dissolved A, $[A]_0$ is the equilibrium solubility of A in the absence of B and $[B]_T$ is the total added concentration of B. Assuming that compound A and B are DBSO and BAM, respectively, a plot of the total concentration of DBSO in solution against the total concentration of BAM in solution enables the stability constant, K_{11}, to be determined from the slope of the line using equation 2.3

32

(Higuchi and Connors, 1965) (equivalent to data shown in Figure 2.4, best fit 0-2 mg/ml).

$$K_{11} = \frac{slope}{[A]_0(1-slope)} \tag{2.3}$$

Assuming the formation of a single soluble complex, a value of $K_{11} = 55.67 \pm 2.92$ M^{-1} was calculated (Table 2.2).

Table 2.2: Estimated constants calculated from solubility data.

Calculation of parameter based on	Determined parameter	Result	Regression coefficient
API solubility as a function of ligand	K_{11}	55.67 ± 2.92 M^{-1}	0.83
Cocrystal solubility as a function of ligand	K_{sp} K_{11}	$3.90\times10^{-5} \pm 0.36\times10^{-5}$ M^2 30.53 ± 2.54 M^{-1}	0.95
Transition concentration	K_{sp}	$10.50\times10^{-5} \pm 0.01\times10^{-5}$ M^2	—

In studies where the cocrystal was the excess phase, a different solubility profile was observed. Although the apparent DBSO solubility increased initially with increasing BAM concentration, a significant continuous decrease in DBSO concentration associated with precipitation of the cocrystal, confirmed by PXRD and DSC (Appendix 1, Figure A.1.1 and A.1.2), as the sole remaining solid phase was observed at initial BAM concentrations of ≥ 6 mg/ml BAM (Figure 2.6). The data suggests that the soluble complex reached a solubility limit when the initial BAM concentration was > 3 mg/ml BAM (Figure 2.6).
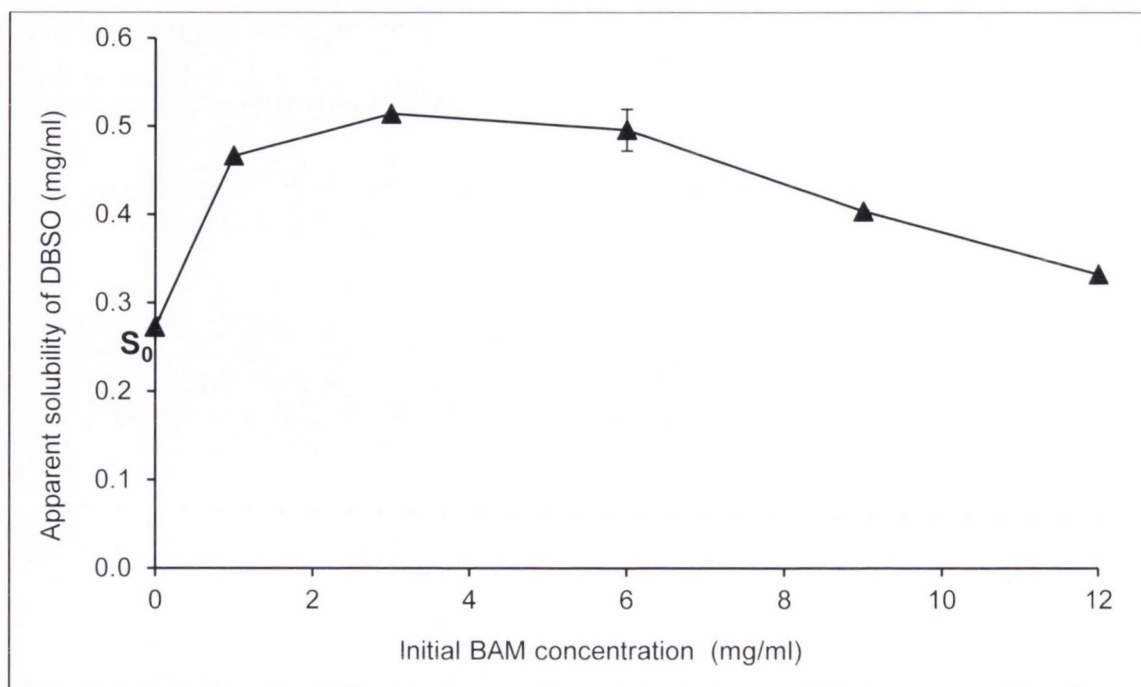
Figure 2.6: Solubility profile of DBSO after 24 hours where cocrystal is the excess phase in dependency of BAM. S_o represents the DBSO concentration in the absence of BAM.

A dynamic solubility profile, obtained on a sample containing initially 6 mg/ml BAM and excess of the cocrystal, is shown in Figure 2.7. It is evident that, after 24 hours a maximum apparent DBSO solubility was reached followed by a significant decrease in DBSO concentration. Analysis of the solid residue for the $\geq$ 24 hours time points indicated the presence of only the cocrystal phase. Thus the decrease in DBSO concentration was associated with cocrystal precipitation.
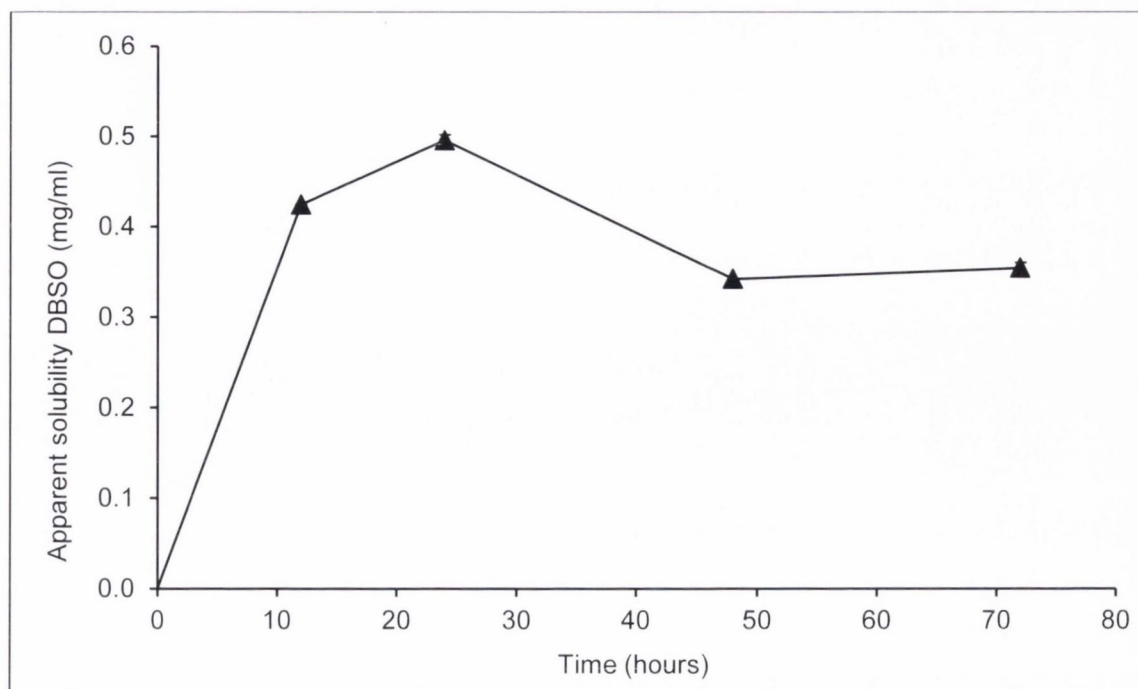
Figure 2.7: Dynamic solubility profile of DBSO from cocrystal in presence of 6 mg/ml BAM over 72 hours.

To describe the solubility of binary cocrystals considering the equilibrium between cocrystal and cocrystal components in solution, equations have been developed by Nehm et al. (2006). Complex formation in solution of a 1:1 stoichiometric cocrystal is described by two constants (Nehm et al., 2006); firstly the cocrystal solubility product, K_{sp} (equation 2.4), which reflects the strength of cocrystal solid state interactions of component A and component B relative to interactions with the solvent, where [A] and [B] are the molar concentrations of each cocrystal component at equilibrium, and the superscripts, α and β, refer to the stoichiometric number of molecules of A and B in the complex (Nehm et al., 2006) and secondly the binding constant for a 1:1 complex formed in solution, K_{11}, as described by equation 2.5 or 2.1.

$$K_{sp} = [A]^{\alpha}[B]^{\beta} \tag{2.4}$$

$$K_{11} = \frac{[AB]}{[A][B]} = \frac{[AB]}{K_{sp}} \tag{2.5}$$

Equation 2.4 elucidates that the cocrystal solubility (represented by the solubility product, K_{sp}) is dependent on both components. Consequently, increasing amounts of one of the components will result in a decrease of the other component. Thus, the observed decrease in the apparent DBSO concentration with increasing BAM concentration as shown in Figure 2.6 can be explained by the solubility product of the cocrystal.

Combining equations 2.4 and 2.5 leads to equation 2.6 (Nehm et al., 2006), where cocrystal solubility can be expressed in terms of the total ligand concentration $[B]_T$:

$$[A]_T = \frac{K_{sp}}{[B]_T} + K_{11}K_{sp} \tag{2.6}$$

Therefore a plot of $[A]_T$ versus $1/[B]_T$ enables K_{sp} and K_{11} to be determined from the slope and the intercept, provided that no higher order complexes are formed in solution (Nehm et al., 2006). For the 1:1 BAM:DBSO cocrystal, a solubility product of $K_{sp} = 3.90 \times 10^{-5} \pm 0.36 \times 10^{-5}$ M^2 (a graphical representation is shown in Figure 2.8 by the curved line) and a solution complexation constant of $K_{11} = 30.53 \pm 2.54$ M^{-1} were estimated (Table 2.2). The K_{11} in this case was quite high compared to previously reported values for cocrystals (Nehm et al., 2006) (Table 2.2) as a result of the compound's low solubility (K_{11} is inversely related to K_{sp}). Strong solute-solute interactions in water at 37 °C are expected, which is reflected in the high stability of the complex in solution (Good and Rodríguez-Hornedo, 2009).

In order to control crystallisation of cocrystals in solution, predict phase transformations and therefore determine the thermodynamic stability of individual cocrystal systems, another parameter, the so-called transition concentration or eutectic concentration, C_{tr}, at which two phases (cocrystal-drug or cocrystal-coformer) coexist in equilibrium with the solution was shown to be relevant (Good and Rodríguez-Hornedo, 2009). In particular of importance is the cocrystal-drug transition concentration since the drug is often the less soluble component compared to the coformer. The transition concentration can also be used to determine the cocrystal solubility or more specifically the solubility product. In particular for incongruently saturating cocrystals, which are thermodynamically unstable and thus equilibrium solubility is difficult to measure, the transition concentration was found to be a good estimate of the cocrystal solubility (Good and Rodríguez-Hornedo, 2009).

Based on the solubility obtained for the 1:1 BAM:DBSO cocrystal, the molar ratio of BAM to DBSO in solution was found to be 1:0.05 indicating that the system is incongruently saturating. This was graphically further elucidated. As shown in Figure 2.8 the dashed line represents stoichiometric concentrations of cocrystal components assuming that the 1:1 BAM:DBSO cocrystal is congruently saturating, and its intersection with the cocrystal equilibrium curve indicates the theoretical maximum drug concentration attributed to cocrystal solubility (Good and Rodríguez-Hornedo, 2009). In the case of incongruently saturating cocrystals this intersection lies above the solubility of the pure drug (Good and Rodríguez-Hornedo, 2009) as confirmed for the BAM:DBSO cocrystal and implies that the cocrystal should be more soluble than the drug. This theoretical increase in DBSO solubility was calculated to be approximately 4-fold for the BAM:DBSO cocrystal compared to the solubility of pure DBSO.
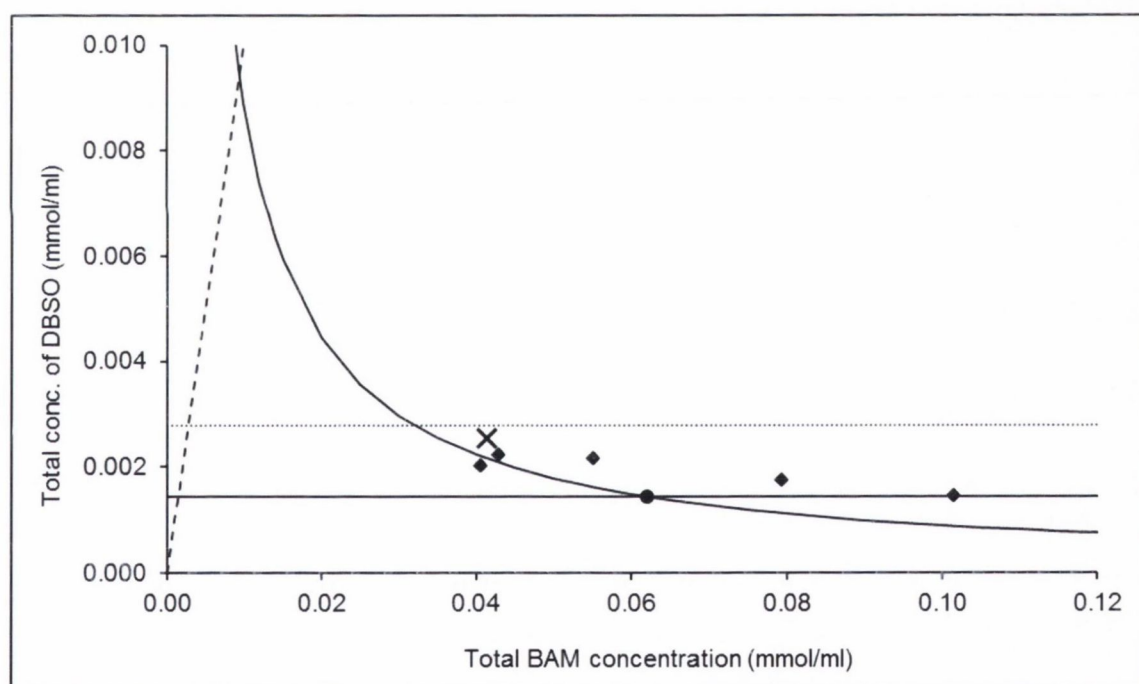
Figure 2.8: Phase solubility diagram of 1:1 BAM:DBSO cocrystal (CC). The horizontal line marks the solubility of pure DBSO, the curved line represents the cocrystal solubility curve determined by equation 2.4, the dotted line represents the solubility limit of complex as determined from the plot presented in Figure 2.4, the filled diamonds mark the experimental cocrystal solubility values (BAM dependent), the dashed line represents stoichiometric concentrations of cocrystal components that dissolution could follow in ideal case, the filled circle symbolizes the transition concentration (DBSO/CC) and the cross illustrates the experimental obtained transition concentration (DBSO/CC).

The determination of the transition concentration (C_{tr}) revealed values of $41.37 \times 10^{-3} \pm 1.20 \times 10^{-3}$ mmol/ml for BAM and $2.54 \times 10^{-3} \pm 0.10 \times 10^{-3}$ mmol/ml for DBSO at the eutectic composition of cocrystal/DBSO (confirmed by PXRD and DSC analysis – shown in Appendix 1, Figure A.1.3 and A.1.4) and is presented in Figure 2.8 (cross symbol). From these concentrations, a cocrystal solubility product with a value of $10.50 \times 10^{-5} \pm 0.01 \times 10^{-5}$ M^2 (Table 2.2) was calculated and the molar ratio of BAM:DBSO at C_{tr} of 1:0.06 was found, which is similar to the molar BAM:DBSO solubility ratio measured for the pure cocrystal. A comparison of the K_{sp} values obtained from transition concentrations and calculated from equilibrium cocrystal solubility revealed that the former is a two-fold higher (Table 2.2). The difference in K_{sp} values can be explained by solution complexation as solubility products based on transition concentrations do not account for solution complexation of cocrystal components (Good and Rodríguez-Hornedo, 2009).

As illustrated in Figure 2.8, the DBSO transition concentration was shifted towards the DBSO solubility induced by solution complexation (dotted line, Figure 2.8). It can be concluded that the solubility (represented by the solubility product) based on transition concentrations will be overestimated for the 1:1 BAM:DBSO cocrystal.

2.3.3 Ternary phase diagram

A three-component phase diagram (triangular phase diagram) of the benzamide:dibenzyl sulfoxide cocrystal in water at 37 °C was constructed, based on methods previously described (Ainouz et al., 2009; Chiarella et al., 2007; Nehm et al., 2006), and is shown in Figure 2.9. The cocrystal solution equilibrium is described by

$$K_{app} = X_A^{\alpha} * X_B^{\beta} \qquad (2.7)$$

where K_{app} is the apparent constant and X_A^{α} and X_B^{β} are the molar fractions of the API and coformer in stoichiometric ratio, respectively (Ainouz et al., 2009). Plotting X_A versus $1/X_B$ allows K_{app} to be calculated from the slope of the line and K_{app} is therefore regarded as equivalent to K_{sp} (see equation 2.4) determined from the component concentrations as previously described.
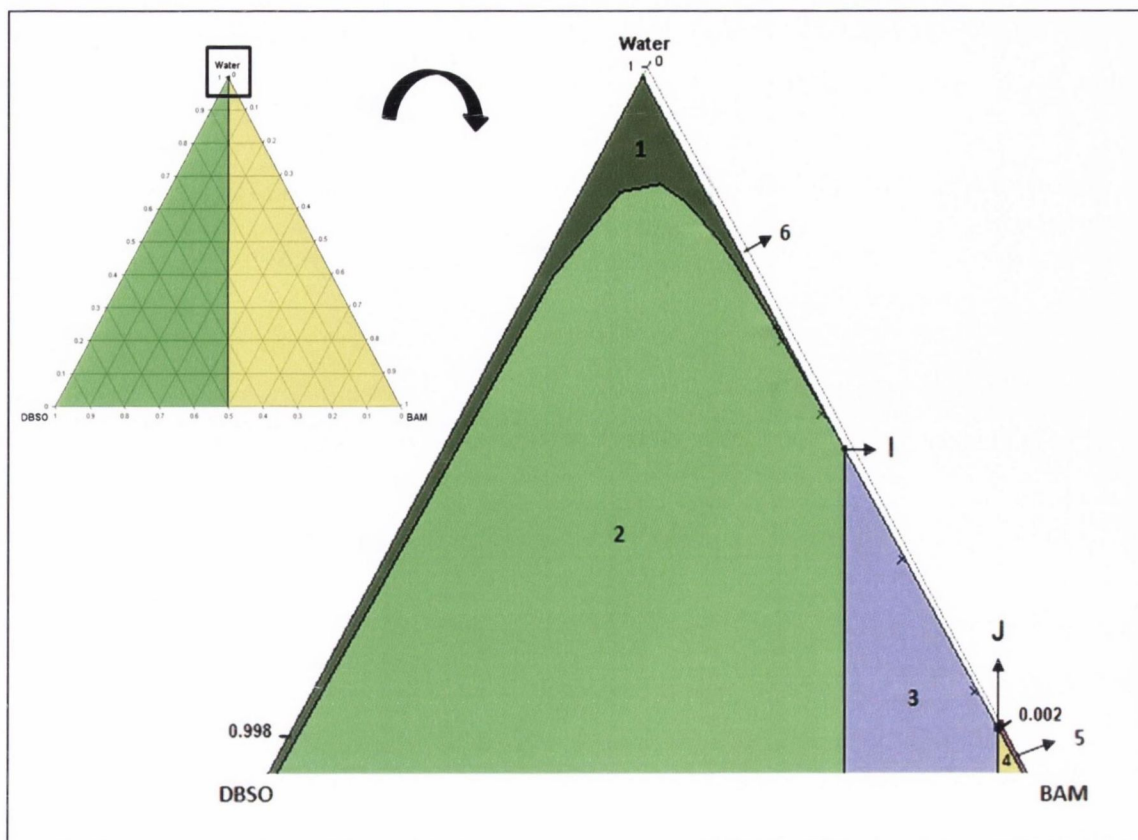
Figure 2.9: Zoom and downscaled view of ternary phase diagram of 1:1 BAM:DBSO cocrystal in water at 37 °C (in mole fractions).

Figure 2.10 illustrates the X_A versus $1/X_B$ relationship for 1:1 BAM:DBSO cocrystal leading to a K_{app} of 1.38×10^{-8}. This value was then used to model the cocrystal equilibrium line as seen in Figure 2.9.
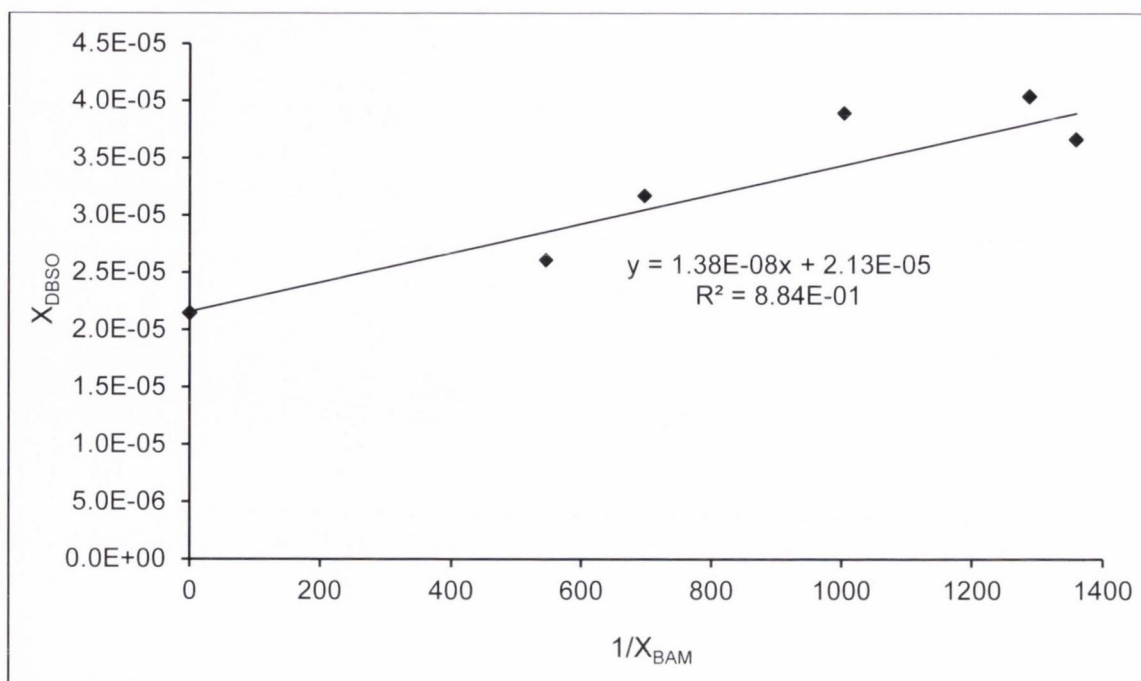
Figure 2.10: DBSO in equilibrium with cocrystal as a function of the inverse total BAM concentration at 37 °C (in molar fractions).

The DBSO-liquid equilibrium line and BAM-liquid equilibrium line, respectively, are illustrated based on the molar fractions of the respective binary solubilities (Figure 2.9). The numbers (1–6) describe the region of the appropriate stable solid phase(s) and the black lines illustrate the solid-liquid equilibrium curves. The curved line displays the solid-liquid equilibrium of the cocrystal (CC) and the points, labelled by a cross (x), are experimental data points. The following solid phases were found to be stable in the marked zones: pure DBSO in zone 1, DBSO and cocrystal in zone 2, cocrystal in zone 3, BAM and cocrystal in zone 4 and pure BAM in zone 5, respectively. Zone 6 is the undersaturated solution phase where all three compounds are present and point I and J symbolise the eutectic mixtures of DBSO/CC and BAM/CC, respectively.

The asymmetric shape of the different zones is consistent with the incongruent solubility behaviour of the 1:1 BAM:DBSO cocrystal since the homogenous liquid phase (zone 6) and cocrystal phase (zone 3) are very small and shifted to the right of the diagram (Ainouz et al., 2009). Even though the solubilities of BAM and DBSO in water are low and zone 3 very asymmetric, it is still possible to isolate the cocrystal from water, consistent with the experimental observations.

From these results, showing incongruent apparent solubility of the 1:1 BAM:DBSO cocrystal in water at 37 °C, it is expected that BAM and DBSO from the cocrystal will dissolve incongruently.

2.3.4 Dissolution rate studies

Intrinsic dissolution profiles from compacts of the 1:1 BAM:DBSO cocrystal and an equimolar physical mixture of DBSO and BAM as well as the pure compounds in water at 37 °C are shown in Figure 2.11. BAM dissolved much more rapidly than DBSO, consistent with the solubility differences. BAM dissolution from the equimolar physical mix was initially more rapid than from the cocrystal and both profiles were nonlinear, the rates declining over time. Based on the initial dissolution rate, pure BAM dissolved approximately 7 times faster than when physically mixed with DBSO and approximately 12 times faster than BAM from the cocrystal. Furthermore the dissolution rates of BAM from the cocrystal and the physical mixture appeared to converge (Table 2.3, limiting rate). In contrast, DBSO profiles were linear and gave similar intrinsic dissolution rates ($R^2 > 0.96$) in all cases (Table 2.3).
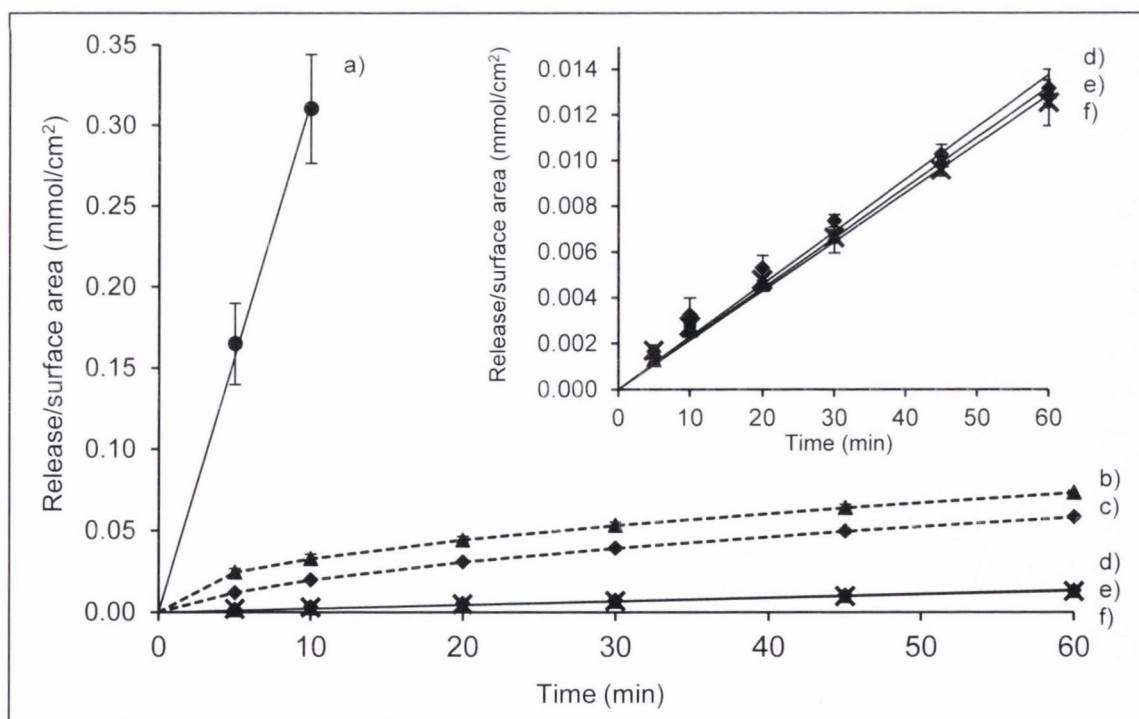

Figure 2.11: Dissolution profiles of a) BAM, b) BAM from a physical mixture, c) BAM from the cocrystal, d) DBSO from a physical mixture, e) DBSO from the cocrystal and f) DBSO. The dashed line refers to the square-root of time fit. The inset shows a zoomed view of the dissolution profiles of d), e) and f).

Table 2.3: Dissolution rates (mmol/min/cm^2) of pure BAM and pure, co-mixed and cocrystallised DBSO.

Substance	Description	IDR (mmol/min/cm^2)
BAM	pure material	$39.50\times10^{-3} \pm 6.83\times10^{-3}$ [a] $8.75\times10^{-3} \pm 0.15\times10^{-3}$ [b]
	physical mixture	$5.74\times10^{-3} \pm 0.64\times10^{-3}$ [a]* $5.65\times10^{-4} \pm 0.08\times10^{-4}$ [b]*
	cocrystal	$3.19\times10^{-3} \pm 0.09\times10^{-3}$ [a]* $4.91\times10^{-4} \pm 0.27\times10^{-4}$ [b]*
DBSO	pure material	$2.11\times10^{-4} \pm 0.27\times10^{-4}$
	physical mixture	$2.18\times10^{-4} \pm 0.05\times10^{-4}$ **
	cocrystal	$2.17\times10^{-4} \pm 0.09\times10^{-4}$ **

a) initial dissolution rate b) limiting dissolution rate

* significantly different ($p < 0.05$) to pure BAM and to cocrystal or physical mixture

** not significantly different ($p > 0.05$) to pure DBSO and to cocrystal or physical mixture

The dissolution from the physical mix compact was qualitatively consistent with that expected for dissolving polyphase mixtures (Higuchi et al., 1965) when the more soluble component dissolves more rapidly from the surface of a compact, leaving a porous layer of the less soluble component behind.

Energy-dispersive X-ray (EDX) analysis was used to determine the elemental composition of the sample surfaces and revealed that the surface of the cocrystal and the equimolar physical mixture contained a similar amount of sulfur after the 90 min dissolution experiments. The same was observed before dissolution, however, the sulfur content was significantly lower compared to that after dissolution (Table 2.4). Furthermore, both samples after dissolution showed sulfur contents which were nearly equal to that detected for pure DBSO disks. The percentage of sulfur is calculated relative to the amount of carbon and thus, the sulfur content is expected to be lower when both organic components, BAM and DBSO, are present at the surface, as is the case prior to dissolution. The faster dissolution of the more soluble BAM leaving the less soluble DBSO at the surface results in higher sulfur content on the surface of the disk, as confirmed by the EDX results (Table 2.4). The absence of BAM at the disk surface of the physical mixture and the cocrystal after dissolution was also verified by ATR-FTIR analysis (Appendix 1, Figure A.1.5).

Additionally, backscattered electronic images displayed differences in the surface structure between the cocrystal and physical mixture (Figure 2.12). The physical mixture showed an inhomogeneous compact surface with randomly positioned voids in the surface after dissolution, attributed to the dissolution of BAM. In contrast, the cocrystal displayed a rather homogenous surface and after dissolution an ordered surface structure, presumed to be as a result of BAM release (Figure 2.12 a–d). These results were consistent with the SEM images using a secondary electron detector and a 5 to 50 times higher magnification (Figure 2.12 e–h).

Table 2.4: Sulfur content found on the compact surface, before and after dissolution, by energy-dispersive X-ray (EDX) analysis.

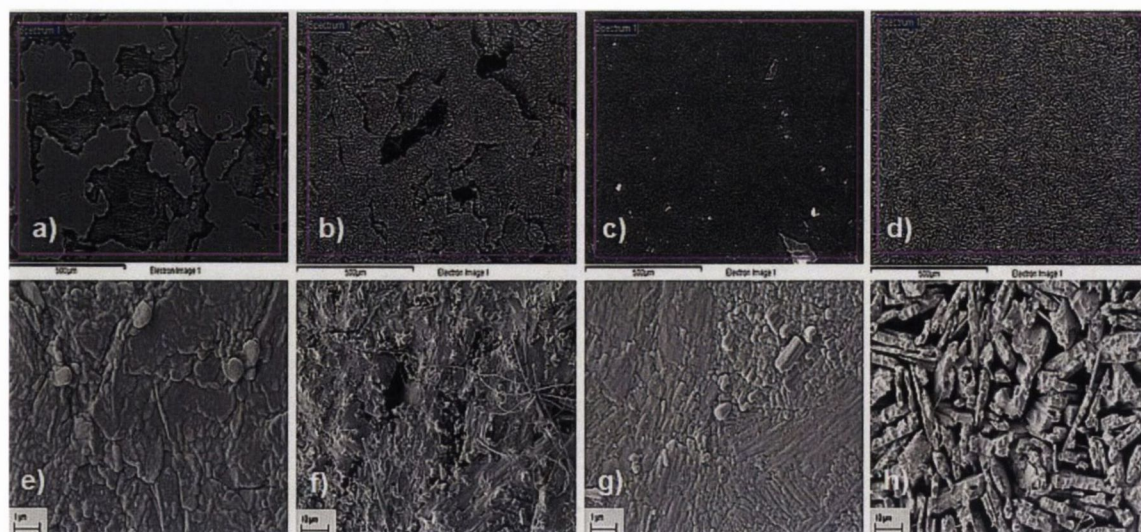| Sample	Sulfur content (%, wt.)
DBSO	
a) before dissolution	14.21 ± 0.11
b) after dissolution	13.70 ± 0.37
Physical mixture	
a) before dissolution	10.30 ± 0.01
b) after dissolution	13.30 ± 0.26
Cocrystal	
a) before dissolution	10.20 ± 0.09
b) after dissolution	13.21 ± 0.25

Figure 2.12: Backscattered electron images of solid compacts of a) BAM:DBSO (1:1) physical mixture before dissolution, b) BAM:DBSO (1:1) physical mixture after dissolution, c) 1:1 BAM:DBSO cocrystal before dissolution and d) 1:1 BAM:DBSO cocrystal after dissolution and secondary electron images of e) BAM:DBSO (1:1) physical mixture before dissolution, f) BAM:DBSO (1:1) physical mixture after dissolution, g) 1:1 BAM:DBSO cocrystal before dissolution and h) 1:1 BAM:DBSO cocrystal after dissolution.

Calculated dissolution rates for polyphase mixtures under steady state conditions require that the solubilities of A and B do not differ by more than a factor of about 100 for the case of a compact thickness of the order of millimetres (Higuchi, 1967). Since the solubility ratio of BAM/DBSO (in mmol/ml) is large with a value of approximately 75, and the more soluble BAM is present with a lower weight fraction (34 %), it was expected that the steady state assumptions were not applicable (Higuchi et al., 1965) and consequently, solute release for the more soluble component is better described as from an inert matrix system (Higuchi, 1967), where the more soluble component dissolves through a matrix of the less soluble component. The BAM release was found to be diffusion controlled and directly proportional to the square root of time ($R^2 > 0.99$) (Higuchi 1963) (Figure 2.11).

From these dissolution results it can be concluded that the dissolution of the less soluble DBSO, either when physically mixed or in the cocrystallised form is not enhanced. The solubility and dissolution of BAM is found to be controlled by, and suppressed in the presence of, DBSO.

2.4 Conclusions

Solubility studies on the 1:1 BAM:DBSO cocrystal have demonstrated that the solubility of the cocrystal is a function of the coformer, BAM concentration in water and decreases with increasing BAM concentration. The cocrystal solubility involved solution complexation which resulted in an increase of the solubility of the poorly water soluble DBSO compared to DBSO alone. A relatively high complexation constant, indicative for strong solute-solute interactions was determined. Phase-solubility studies of DBSO as a function of BAM have confirmed the presence of solution complexation and could be described by a Type B phase-solubility diagram.

Cocrystal solubility estimation based on transition concentrations was found to be inaccurate by overestimating the solubility as a result of solution complexation. A graphical presentation has elucidated these findings by a shift of the transition concentration (C_{tr}) towards higher DBSO concentrations in the cocrystal phase diagram. Moreover, it was found that the 1:1 BAM:DBSO cocrystal is incongruently saturating and thus thermodynamically unstable which was evidenced by the asymmetric phase behaviour of the ternary phase diagram.

Investigation of the intrinsic dissolution rate confirmed, as expected from the solubility tests, that BAM and DBSO dissolved incongruently. The dissolution of the cocrystal was not enhanced in comparison to an equimolar physical mixture and the pure components.

The coformer compound, BAM, dissolved initially faster when mixed than when cocrystallised with DBSO, which is assumed to be due to stronger solid state attractive forces between the amino and sulfoxide group in the form of hydrogen bonds on the surface of the compact for the cocrystal. However, for both forms, cocrystal and physical mixture, it was found that the surface of the compacts contained only DBSO after dissolution.

Based on dissolution models for compressed physical mixtures, it was apparent that steady-state conditions were not reached in the dissolution experiment as a result of the large solubility difference between BAM and DBSO in water. Furthermore, it could be demonstrated that DBSO controls and retards dissolution of BAM and becomes the phase remaining at the surface independent of the initial solid state form.

Consequently, the more soluble BAM is not a suitable cocrystal component to improve the dissolution of the poorly soluble DBSO. Complexation may be a factor that can have a different impact on solubility and dissolution and is therefore important to

measure. To optimise solubility and dissolution of the API from a cocrystal a compromise between solid state, solute-solute and solute-solution stability needs to be found.

Chapter 3:

Sulfadimidine and 4-aminosalicylic acid produced by co-grinding and co-spray drying

3. 1 Introduction

Several production methods have been reported for a number of cocrystals with different coformers (Childs et al., 2004; Trask et al., 2005; Wenger and Bernstein, 2008; Padrela et al., 2009; Lu and Rohani, 2009; Alhalaweh and Velaga, 2010). Next to the common industrial crystallisation techniques such as solvent evaporation and cooling crystallisation, grinding techniques in dry and liquid-assisted forms have also been used successfully in the formation of cocrystals (Etter et al., 1993; Caira et al., 1995; Kuroda et al., 2002; Trask et al., 2004; Friščić et al., 2006; Braga et al., 2006; Chadwick et al., 2007). One of the main advantages of grinding compared to the solvent evaporation method is that products can be obtained in a short time of processing (Caira et al., 1995; Trask et al., 2005; Wenger and Bernstein, 2008). Variable grinding times are usually selected, with many cocrystals being found to form in less than one hour, sometimes in only a few minutes (Caira et al., 1995; Trask and Jones, 2005a). Grinding also provides higher yields with often favourable small particle size. Moreover, for a number of cases, solid state grinding appeared to be more efficient in cocrystal formation compared to solution crystallisation (Lynch et al., 1991; Trask and Jones, 2005b). A modified grinding method which has been used to generate cocrystals is liquid-assisted grinding, where a small quantity of solvent is added to the solid prior to processing. This method has been shown to enhance the kinetics of grinding cocrystallisation, resulting in a higher yield, higher crystallinity of the product and providing the possibility of controlling polymorph formation by selection of the grinding liquid (Trask et al., 2004; Trask et al., 2005; Friščić et al., 2006).

As a novel approach in the formation of cocrystals, spray drying, a well established scale-up technique has been proposed by Alhalaweh and Velaga (2010). The authors found that in contrast to slurry or reaction crystallisation methods pure cocrystals can be formed by spray drying. The mechanism is not fully understood but it is suggested that cocrystal formation by spray drying could be kinetically controlled and/or mediated by the amorphous state (Alhalaweh and Velaga, 2010). Cocrystal formation induced by an amorphous phase has also been reported using solid state grinding (Jayasankar et al., 2006). More studies on cocrystal formation via spray drying might lead to a better understanding and may draw further conclusions for scale-up processing.

In one of the early works on cocrystals, Caira (1992) reported on the formation of a solid molecular complex (at that time the term "cocrystal" was not defined) composed of one molecule of sulfadimidine (SD) and one molecule of 4-aminosalicylic acid (4-

ASA) by the solvent evaporation method. As other methods in the formation of the SD:4-ASA cocrystal have not been reported, one of the main objectives in this study was to investigate cocrystal formation between SD and 4-ASA by solid state grinding, in the form of dry and liquid-assisted milling and by spray drying.

In the previous Chapter, the solubility and dissolution behaviour of a cocrystal composed of a non-ionic, low water-soluble model API, DBSO, was demonstrated. SD and 4-ASA are APIs used in the treatment of bacterial diseases. They show poor aqueous solubility and both have amphoteric properties (more details about the components have been described in Chapter 1 and further in Appendix 5, Table A.5.1). For some cocrystals composed of ionisable components the solubility has been described and predicted by the use of mathematical models (Bethune et al., 2009). So far, no example has been shown for the case of a cocrystal composed of two amphoteric components. Therefore, the second main objective was to examine the solubility and dissolution behaviour of the amphoteric SD:4-ASA 1:1 cocrystal.

3. 2 Materials and Methods

3.2.1 Materials

Sulfadimidine (SD) and 4-aminosalicylic acid (4-ASA) were purchased from Sigma-Aldrich (Ireland). Ethanol was supplied from Corcoran Chemicals (Ireland). Methanol, HPLC grade, was purchased from Fisher Scientific (Ireland), potassium hydrogen phosphate was obtained from Sigma-Aldrich (Ireland) and phosphoric acid from Merck (Germany). Polyvinylpyrrolidone (PVP 10) was purchased from Sigma-Aldrich (Ireland). Water, analytical and HPLC grade, was prepared from an Elix 3 connected to a Synergy UV system (Millipore, UK). All other chemicals purchased from commercial suppliers were of analytical grade.

3.2.2 Methods

3.2.2.1 Milling (dry and liquid-assisted)

Dry and liquid-assisted co-milling was carried out for different molar ratios of SD:4-ASA (1:2, 1:1, 2:1) in a Retsch PM100 planetary ball mill (Germany) using three stainless steel balls in each milling jar (50 ml). A maximum of 2.5 g of sample mass was used. In the case of liquid-assisted milling, five drops of ethanol were added to the solid mix prior to milling using a 3.5 ml disposable transfer pipette (Fisher Scientific). The milling was carried out at room temperature for 15, 30 and 45 minutes at a rotation

speed of 400 rpm. For the milling time of 45 minutes, the milling process was stopped after 30 minutes for 10 minutes in order to avoid high temperature in the jar and thus the risk of melting/decomposition of the compounds.

3.2.2.2 Spray drying (SPD)

Spray drying was performed using a Büchi B-290 Mini Spray Dryer connected to a compressor (HaughTM SD 45EZ ASY) operating in the open-mode. Solution concentrations of 1 % (w/v) of SD:4-ASA in 1:2, 1:1 and 2:1 molar ratio were prepared using ethanol. The solutions were delivered to a 2-fluid atomization nozzle using a peristaltic pump at a pump speed of 30 % (9–10 ml/min) and the aspirator was operated at 100%. The flowmeter for the standard 2-fluid nozzle was set at 4 cm which is equivalent to 473 Normlitres per hour (Nl/h) of gas flow in normal conditions (p=1013.25 mbar and T=273.15 K) (Büchi Labortechnik, 93001). The inlet temperature was fixed at 78 °C and the appropriate outlet temperature varied between 50–57 °C.

3.2.2.3 Powder X-ray diffraction (PXRD)

as described in Chapter 2

3.2.2.4 Thermal analysis

as described in Chapter 2

3.2.2.5 Elemental analysis (EA)

The analysis was performed by Ann Connolly (School of Chemistry & Chemical Biology, University College Dublin, Dublin, Ireland). Elemental analysis was carried out using an Exeter Analytical CE440 CHN analyser. The molar amount of carbon as carbon dioxide, nitrogen, as nitrogen oxide and hydrogen as water, was determined by oxidation of the sample (n=3, around 10 mg) and the thermal conductivity analysis of obtained gases and water vapour.

3.2.2.6 Attenuated Total Reflection - Fourier Transform Infra-red (ATR-FTIR) Spectroscopy

as described in Chapter 2

3.2.2.7 Solid state Nuclear Magnetic Resonance (ssNMR) spectroscopy

The analysis was performed by Panagiotis Manesiotis (Pharmaceutical and Molecular Biotechnology Research Centre, Waterford Institute of Technology, Waterford, Ireland). All measurements were performed using a broadband 3.2 mm solid state NMR probe and a 400 MHz JEOL ECX400 spectrometer. Sample were prepared by packing an adequate amount of each sample, as received, into 3.2 mm Silicon nitride (Si_3N_4) solid state NMR rotors. The sample spinning rate was set to 10 kHz. ^{13}C NMR spectra (100 scans) were recorded using the CPMAS (Cross Polarisation – Magic Angle Spinning) pulse sequence. Prior to each spectrum, the corresponding T_1 constant (spin-lattice relaxation) was measured using the saturation recovery pulse sequence.

3.2.2.8 Solubility studies

3.2.2.8.1 Equilibrium/Apparent solubility

The solubility was determined using a 24-hour (for SD) and 1-hour (for 4-ASA) shake flask method (used previously for many compounds) (Wermuth, 2008). Therefore, an excess of solid (approximately 2–3 times the amount expected to achieve saturation solubility) was added to 10 ml of water in glass ampoules, which were then heat sealed and placed horizontally in a thermostated waterbath at 37 °C and shaken at 100 cpm. The supernatant was filtered using 0.45 µm membrane filters (PVDF - Cronus®) and analysed for sample concentration by HPLC. The remaining solid phase was characterised by PXRD. The experiments were performed in triplicate. The equilibration time in the case of 4-ASA was selected based on previously reported work by Forbes et al. (1995) which showed that due to degradation of 4-ASA in solution, an equilibration time of 1 hour is appropriate to measure its apparent solubility ("apparent" is attributed to the non-equilibrium conditions).

3.2.2.8.2 Phase-solubility studies

In order to examine complexation between the compounds, excess (approximately 2–3 times the amount expected to achieve saturation solubility) of solid SD was added to 10 ml aqueous solution aliquots containing different concentrations (0.00065–0.02 M) of 4-ASA in glass ampoules, which were heat sealed. The ampoules were placed horizontally in a thermostated waterbath at 37 °C and shaken at 100 cpm for 1 hour. The supernatant was filtered using 0.45 µm membrane filters (PVDF - Cronus®) and

analysed for sample concentration by HPLC. The remaining solid phase was characterised by PXRD. The study was performed in triplicate.

3.2.2.8.3 Transition concentration (C_{tr}) measurement

The cocrystal transition concentration (C_{tr}) was determined as described by Good and Rodríguez-Hornedo (2009). Therefore, excess cocrystal was added to a presaturated aqueous SD solution and the suspension was stirred for 1 hour at 37 °C. After 1 hour, an aliquot of the solid residue was withdrawn and analysed by PXRD for phase identification. When the solid phase indicated a mixed phase composed of cocrystal and SD, the supernatant was withdrawn, filtered through 0.45 µm membrane filters (PVDF - Cronus®) and component concentrations were analysed by HPLC. The pH of the supernatant was also measured. The experiments were performed in triplicate.

3.2.2.8.4 pH-dependent solubility

The cocrystal solubility was determined at different pH values by the addition of small volumes of 1M HCl and 1M NaOH using the shake-flask method under conditions as described above. Solid phases and solution concentrations were analysed after 1 hour equilibration and the pH was measured. The solid was characterised by PXRD and the concentration of the supernatant was analysed by HPLC after filtration through 0.45 µm membrane filters (PVDF - Cronus®). The experiments were performed in triplicate.

3.2.2.8.5 Dynamic solubility studies

Dynamic solubilities were determined in a jacketed glass vessel (50 ml) connected to a pump and a waterbath, sitting on a magnetic stirrer. Excess amount of solid was added to 30 ml of solvent (water and/or 0.1% (w/v) PVP solution) and the solution was stirred at a temperature of 37 °C for up to 1 hour. Samples of 2 ml were withdrawn at appropriate intervals, filtered through 0.45 µm membrane filters (PVDF - Cronus®) and analysed for sample content by HPLC. At each time point an aliquot of the solid phase was withdrawn, dried at ambient temperature and examined by PXRD. The experiments were performed in triplicate.

3.2.2.9 Intrinsic dissolution studies

The studies were performed as described in Chapter 2. The compacts were compressed at a pressure of 8 tonnes for 20 seconds up to 1.5 minutes depending on the type of

sample and to ensure no capping (details are attached in Appendix 2, Table A.2.1). The study was performed in triplicate for a maximum time of 60 minutes. The compacts were recovered, dried under nitrogen purge and the surface was analysed by PXRD, ATR-FTIR and SEM.

3.2.2.10 Viscosity measurement

Viscosity of a 0.1% (w/v) aqueous PVP solution and water was determined at 37 °C using a Vibro viscometer SV-10 (A & D Co. Ltd., Japan). The liquids were transferred to the provided cup and the sensor plates were immersed as required for the measurement. The instrument was calibrated using water. The measurement was performed in triplicate.

3.2.2.11 High Performance Liquid Chromatography (HPLC)

Concentrations of SD and 4-ASA in solutions were determined using a Shimadzu HPLC Class VP series with a LC-10AT VP pump, SIL-10AD VP autosampler and SCL-10VP system controller. The mobile phase was vacuum filtered through a 0.45 μm membrane filter (Gelman Supor-450). Separation was performed on a Phenomenex Inertsil ODS (3) C18 column (150 mm length, diameter 4.6 mm, particle size 5 μm) at a UV detection wavelength of 260 nm with an injection volume of 10 μL. The mobile phase consisted of methanol/buffer pH 6.5 40/60 (v/v). The buffer was prepared from a 50 mM potassium hydrogen phosphate solution adjusted to pH 6.5 with 100 mM phosphoric acid. The elution was carried out isocratically at ambient temperature with a flow rate of 1 ml/min. For peak evaluation Class-VP 6.10 software was used. The calibration curves were linear for both components between 0.5–100 μg/ml ($R^2 > 0.998$). Based on the ICH guidelines (ICH, 1996), for SD the calculated LOD was 0.6 μg/ml and the LOQ was 1.8 μg/ml. For 4-ASA the LOD was 1.3 μg/ml and the LOQ was 4.2 μg/ml.

3.2.2.12 Scanning electron microscopy (SEM)

Surface images of powder compacts before and after intrinsic dissolution studies were performed at various magnifications by SEM using a Zeiss Supra Variable Pressure Field Emission Scanning Electron Microscope (Germany) equipped with a secondary electron detector at a resolution of 1.5 nm at 15 kV. Powder compacts were glued onto aluminium stubs and sputter-coated with gold under vacuum prior to analysis.

3.2.2.13 Stability studies

3.2.2.13.1 Dynamic Vapor Sorption (DVS)

The analysis was performed by Krzysztof Paluch (School of Pharmacy & Pharmaceutical Sciences, Trinity College Dublin, Dublin, Ireland). Vapour sorption experiments were carried out on a DVS Advantage-1 automated gravimetric vapour sorption analyser (Surface Measurement Systems Ltd., London, UK). The DVS-1 measures the uptake and loss of water vapour gravimetrically with a mass resolution of ± 0.1 µg. The temperature was maintained at 25.0 ± 0.1 °C. A mass of around 10 mg of powder was loaded into a sample basket and placed into the system. The sample was analysed from 0% to 90% RH in 10% steps and the same for desorption. The sample was equilibrated at each of relative humidity (RH) conditions until constant mass (dm/dt ≤ 0.002 mg/min for at least 10 min) was reached. The reference sample mass (m_0) for each experiment was recorded at 0% RH. The RH isotherms were calculated from the complete sorption and desorption profiles. The solid phase after sorption and desorption was characterised by PXRD for solid state changes. The experiment was performed in triplicate.

3.2.2.13.2 Long-term stability test

Solid state stability of the bulk material was carried out using an Amebis Test System (Amebis, Ireland) under conditions of 60 ± 5% RH at 25 ± 5 °C. The samples were placed in Amebis humidity devices at 60% RH and stored in an oven at 25 °C. The test conditions were monitored using the Amebis Control Software. Samples were assayed in duplicate after 1, 2, 6 and 12 months using PXRD, DSC, FTIR and HPLC.

3.2.2.14 Liquid-state Nuclear Magnetic Resonance (NMR) spectroscopy

The analysis was performed by John O'Brien (School of Chemistry, Trinity College Dublin, Dublin, Ireland). A Bruker Avance 400 NMR with 4-nucleus (^{1}H, ^{13}C, ^{31}P and ^{19}F) probe was used for NMR studies. Deuterated DMSO-D6 was used to prepare the samples. Sample concentrations were in the range of 5–20 mg/ml. Spectrometer frequency was 400 MHz with an acquisition time of 2 seconds. The number of scans was appropriate to gain good quality spectra. Standard Pulse Sequence supplied by Bruker was used for ^{1}H, ^{13}C and 2-dimensional experiments. Details of the results can be found in the Appendix 2, Figure A.2.15 and Table A.2.2.

3.2.2.15 Crystallisation from solution

SD (1 mmol) and 4-ASA (1.1 mmol) were dissolved in 20 ml of hot ethanol (and acetone). The solution was covered with an aluminium foil in which a syringe needle (0.3x12mm, Sterican®) was inserted and left for slow evaporation of the solvent while maintaining the elevated temperature of the solution using an oil bath (set temperature of oil bath was around 70 °C).

3.2.2.16 Powder X-ray diffraction for structure determination

The analysis was performed by Liana Vella-Zarb (Department of Chemistry, Durham University, Durham, UK). X-ray powder diffraction patterns were recorded at room temperature on a Bruker D8 ADVANCE high-resolution laboratory X-ray powder diffractometer using Cu-Kα_1 radiation from a primary Ge(111)-Johansson-type monochromator and a Våntec position-sensitive detector (PSD) in Debye-Scherrer geometry. Data collection spanned over 20 hours, covering a range of 2° to 65° along 2θ in steps of 0.008° with a 6° opening of the PSD. The sample (crystals obtained by solvent evaporation, see 3.2.2.15) was spun during measurement to ensure better particle statistics. Structure determination and refinement of powder data were carried out using the programs TOPAS 4.1 (Bruker AXS, 2007) and DASH 4.2 (David, 2006) Indexing was carried out via the singular value decomposition method as implemented within TOPAS (Coelho, 2003) resulting in an orthorhombic unit cell. This was later confirmed by Rietveld refinement of the solved structure (Rietveld, 1969). The peak profile and precise lattice parameters were determined by Le Bail fits (Le Bail et al., 1988) using the fundamental parameter (FP) approach of TOPAS (Cheary et al., 2007), allowing for the determination of microstructural properties such as domain size and microstrain. For the modelling of the background, fourth-order Chebychev polynomials were employed. The crystal structure was solved by the global optimization method of simulated annealing (SA) in real space as implemented by DASH (David, 2006). The relative positions of the molecules were not known *a priori*, thus two independent molecular models were used using standard bond lengths and angles. Slack bond length, bond angle and planarity restraints were introduced to stabilise the subsequent Rietveld refinement (Rietveld, 1969). For the final Rietveld refinement, all profile and lattice parameters were released and all atomic positions were subjected to refinement using soft bond and angle constraints. Final agreement factors (R-values) are listed in Table 3.6. The full lists of atomic coordinates, together with intramolecular distances and

angles, can be found in Appendix 2, Table A.2.3–Table A.2.7). The program Mercury 2.3 (Mercury CSD 2.0, 2008) was used for illustrating the molecular structures.

3.2.2.17 Single crystal X-ray diffraction (SC-XRD)

The analysis was performed by Kirsten Christensen (Department of Chemistry, University of Oxford, Oxford, United Kingdom) in collaboration with Helge Müller-Bunz (School of Chemistry & Chemical Biology, University College Dublin, Ireland). Crystal data were collected at Diamond Light Source, Beamline I19 the Small Molecule Single Crystal diffraction Beamline. A full sphere of data was collected at 100 K on a Rigaku Saturn 724+ CCD diffractometer with $\lambda = 0.6889$ Å. Data integration and numerical absorption correction were carried out by the CrysAlisPro software package from Agilent. The data was solved and refined using the program JANA 2006 (Petricek et al., 2006).

3.2.2.18 Statistical analysis

as described in Chapter 2

3.3 Results and Discussion

3.3.1 Solid state characterisation

PXRD analysis revealed that products obtained by dry milling displayed diffraction patterns with peaks at the same positions regardless of the ratio in the mixture and all diffraction peaks could be superimposed with those of the single compounds. Furthermore, the intensity of the diffraction peaks decreased with increasing milling time which was assumed to be attributed to amorphisation induced by milling time (Figure 3.1).
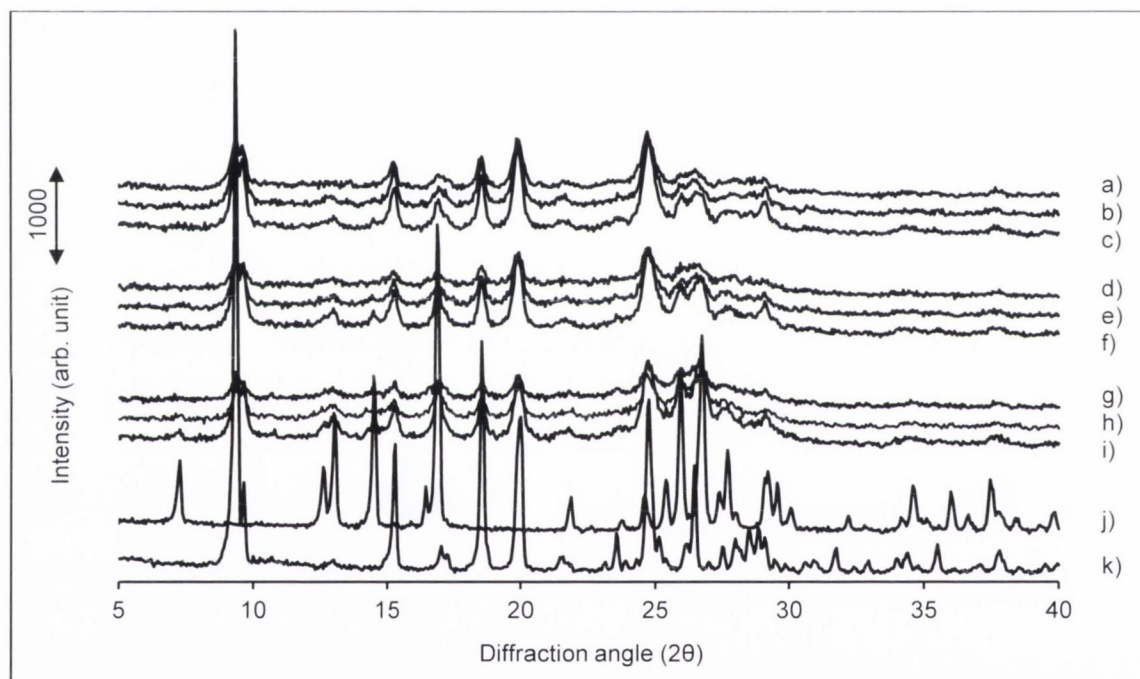

Figure 3.1: PXRD patterns of SD and 4-ASA, dry milled in different molar ratios: a) SD:4-ASA 2:1 milled 45 min, b) SD:4-ASA 2:1 milled 30 min, c) SD:4-ASA 2:1 milled 15 min, d) SD:4-ASA 1:1 milled 45 min, e) SD:4-ASA 1:1 milled 30 min, f) SD:4-ASA 1:1 milled 15 min, g) SD:4-ASA 1:2 milled 45 min, h) SD:4-ASA 1:2 milled 30 min, i) SD:4-ASA 1:2 milled 15 min, j) 4-ASA, raw material and k) SD, raw material.

In contrast, the liquid-assisted milled products showed patterns with characteristic diffraction peaks, which differed from those of the single components. However, the mixture ratios of 1:2 (Figure 3.2 g–i) and 2:1 (Figure 3.2 a–c) showed additional diffraction peaks which superimposed with that of 4-ASA raw material and/or SD raw material, respectively. The milling time was not found to have an influence on the PXRD patterns (Figure 3.2).
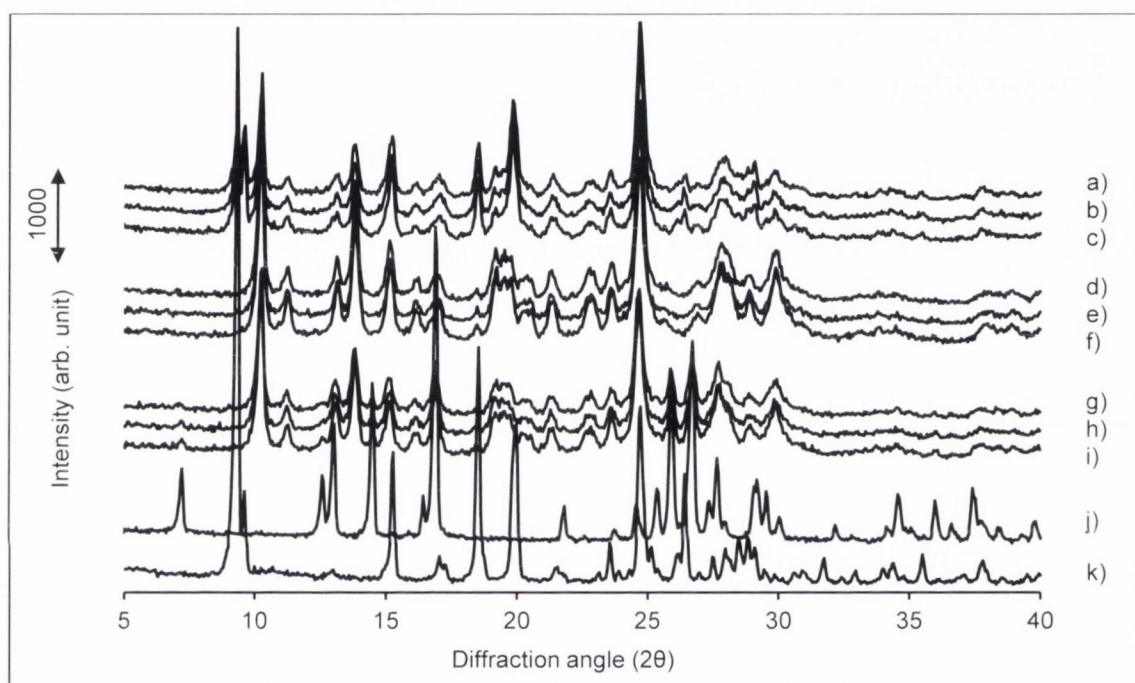

Figure 3.2: PXRD patterns of SD and 4-ASA, liquid-assisted milled using EtOH in different molar ratios: a) SD:4-ASA 2:1 milled 45 min, b) SD:4-ASA 2:1 milled 30 min, c) SD:4-ASA 2:1 milled 15 min, d) SD:4-ASA 1:1 milled 45 min, e) SD:4-ASA 1:1 milled 30 min, f) SD:4-ASA 1:1 milled 15 min, g) SD:4-ASA 1:2 milled 45 min, h) SD:4-ASA 1:2 milled 30 min, i) SD:4-ASA 1:2 milled 15 min, j) 4-ASA, raw material and k) SD, raw material.

PXRD patterns of the spray-dried products are shown in Figure 3.3. All three spray-dried products differed from each other and from the single components as well as from the dry and liquid-assisted milled products. The products of the SD:4-ASA 1:1 (Figure 3.3 b) and 1:2 ratio (Figure 3.3 c) showed similar diffraction patterns, whereas the 1:2 product revealed some additional diffraction peaks at around 26 and 27 degree 2θ which can be attributed to 4-ASA. Spray drying from a 2:1 component mixture resulted in a

product that showed a broad halo, characteristic of the amorphous state, with some diffraction peaks with very low intensity (Figure 3.3 a).
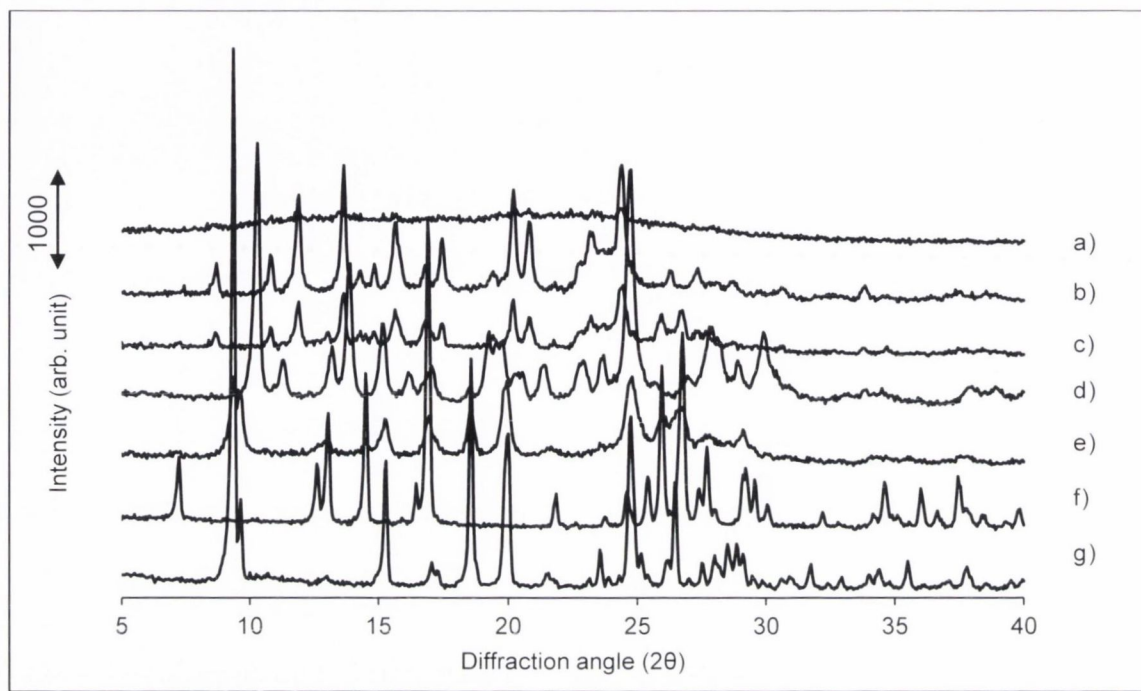

Figure 3.3: PXRD patterns of a) SD:4-ASA 2:1, spray-dried, b) SD:4-ASA 1:1, spray-dried, c) SD:4-ASA 1:2, spray-dried, d) SD:4-ASA 1:1 liquid-assisted milled, e) SD:4-ASA 1:1 dry milled, f) 4-ASA, raw material and g) SD, raw material.

Results of thermal analysis by DSC and TGA of the dry milled SD:4-ASA products are shown in Figure 3.4, 3.5 and Table 3.1. As the content of SD increased in the mixture, the endothermic melting event shifted towards the melting temperature of SD (T_m = 197.16 ± 0.43 °C, ΔH_f = 130.45 ± 6.60 J/g) (Figure 3.4). Melting of all dry milled products was associated with a significant mass loss and thus with degradation (Figure 3.5). The 1:1 mixtures showed a single melting event (Figure 3.4 d–f), while the non-equimolar mixtures revealed, as in the case of the 1:2 ratio, a double peak endotherm shifted towards the melting temperature of 4-ASA (T_m = 139.07 ± 0.93 °C, ΔH_f = 392.80 ± 7.33 J/g) (Figure 3.4 g–i) and in the case of the 2:1 ratio a second, small melting event attributed to SD was observed (Figure 3.4 a–c). From these results it was concluded that in contrast to the 1:1 product, the non-equimolar mixtures contained excess amount of either SD or 4-ASA raw material (Figure 3.4). For all dry milled

products, regardless of the mixture ratio, an exotherm in the temperature range between 65 and 95 °C which increased with increasing milling time was observed (Figure 3.4) and was not associated with a significant mass loss by TGA (Figure 3.5). This was assumed to be attributed to crystallisation of an amorphous content induced by milling, which is known to result for milled materials (Willart and Descamps, 2008; Willart et al., 2007). DSC analysis of the single components when milled separately under the same conditions showed, in the case of SD, a similar exothermic event prior to melting as for the co-milled systems. This was not observed for milled 4-ASA for which no thermal event until melting, associated with decomposition, typical for 4-ASA (Rotich et al., 2001), was found. Details can be found in Appendix 2, Figure A.2.1. These results suggest that the exothermic event was attributable to crystallisation of amorphous SD induced by milling, whereas 4-ASA remained crystalline at the given milling conditions.
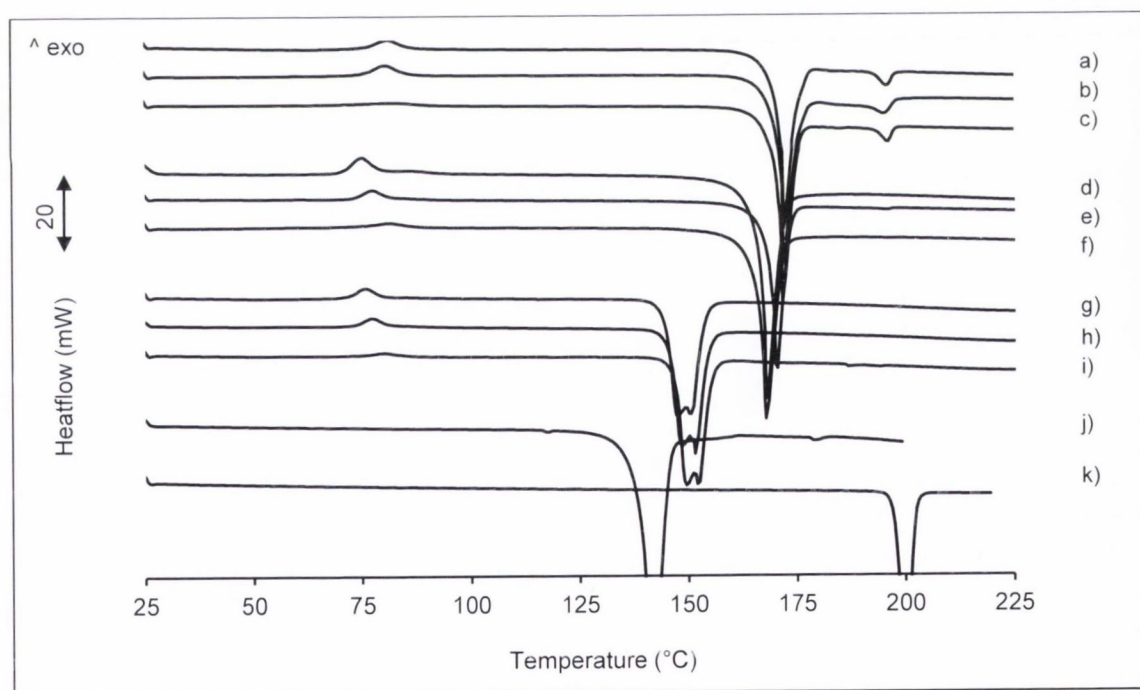

Figure 3.4: DSC thermograms of SD and 4-ASA, dry milled in different molar ratios: a) SD:4-ASA 2:1 milled 45 min, b) SD:4-ASA 2:1 milled 30 min, c) SD:4-ASA 2:1 milled 15 min, d) SD:4-ASA 1:1 milled 45 min, e) SD:4-ASA 1:1 milled 30 min, f) SD:4-ASA 1:1 milled 15 min, g) SD:4-ASA 1:2 milled 45 min, h) SD:4-ASA 1:2 milled 30 min, i) SD:4-ASA 1:2 milled 15 min, j) 4-ASA, raw material and k) SD, raw material.
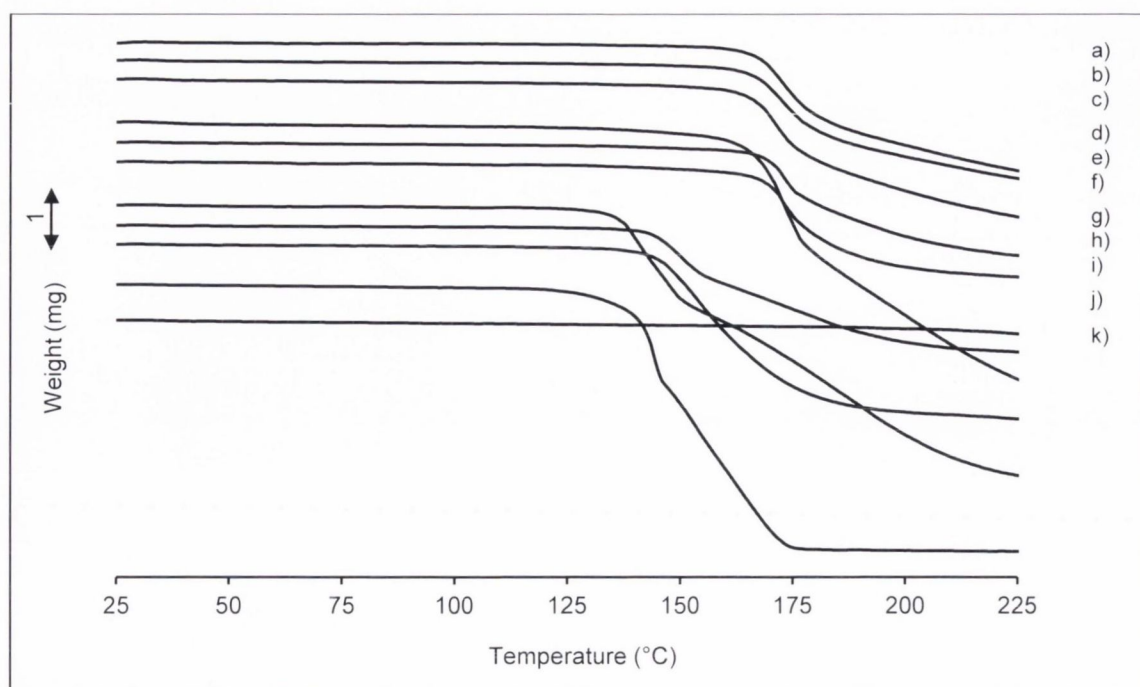
Figure 3.5: TGA thermograms of SD and 4-ASA, dry milled in different molar ratios: a) SD:4-ASA 2:1 milled 45 min, b) SD:4-ASA 2:1 milled 30 min, c) SD:4-ASA 2:1 milled 15 min, d) SD:4-ASA 1:1 milled 45 min, e) SD:4-ASA 1:1 milled 30 min, f) SD:4-ASA 1:1 milled 15 min, g) SD:4-ASA 1:2 milled 45 min, h) SD:4-ASA 1:2 milled 30 min and i) SD:4-ASA 1:2 milled 15 min, j) 4-ASA, raw material and k) SD, raw material.

Table 3.1: Melting onset temperatures (T_m) and corresponding enthalpies of fusion (ΔH_f) of SD:4-ASA dry milled, liquid-assisted milled and spray-dried products.

Method	Milling time (min)	SD:4-ASA ratio	T_m,°C (ΔH_f, J/g)*
Dry milling	15	2:1	170.48 ± 0.11 (157.91 ± 4.09)
		1:1	165.95 ± 0.40 (208.35 ±1.21)
		1:2	144.52 ± 1.08 (242.17 ± 4.08)
	30	2:1	170.81 ± 0.02 (145.31 ± 1.61)
		1:1	167.28 ± 0.94 (203.04 ± 2.08)
		1:2	144.31 ± 2.30 (239.34 ± 6.26)
	45	2:1	171.39 ± 0.27 (157.52 ± 0.27)
		1:1	166.46 ± 0.11 (205.19 ± 10.57)
		1:2	144.03 ± 1.07 (239.72 ± 4.18)
Liquid-assisted milling	15	2:1	171.65 ± 0.08 (166.46 ± 7.83)
		1:1	168.82 ± 0.21 (228.35 ± 22.34)
		1:2	149.08 ± 0.36 (251.94 ± 1.49)
	30	2:1	171.72 ± 0.21 (166.89 ± 2.42)
		1:1	170.38 ± 0.89 (240.81 ± 16.62)
		1:2	148.98 ± 0.36 (257.39 ± 5.75)
	45	2:1	171.39 ± 0.12 (170.08 ± 0.65)
		1:1	169.12 ± 0.35 (233.73 ± 16.22)
		1:2	149.42 ± 0.39 (255.48 ± 6.65)
Spray drying	–	2:1	176.01 ± 0.21 (170.45 ± 2.75)
		1:1	170.61 ± 0.94 (209.78 ± 9.20)
		1:2	140.85 ± 0.81 (244.44 ± 1.63)

refers to onset temperature of main melting event (n=3)

For the liquid-assisted milled products, it was found that, similar to the dry milled products, an increasing amount of SD in the mixture resulted in a shift of the endothermic melting event towards the melting temperature of SD (Figure 3.6). The melting endotherms occurred at similar temperatures and showed similar enthalpies of fusion (ΔH_f) to those of the dry milled materials (Figure 3.6, 3.4 and Table 3.1). However, the thermograms did not show any evidence of amorphisation since no exothermic events prior to melting were observed (Figure 3.6). All products melted with decomposition (Figure 3.7).
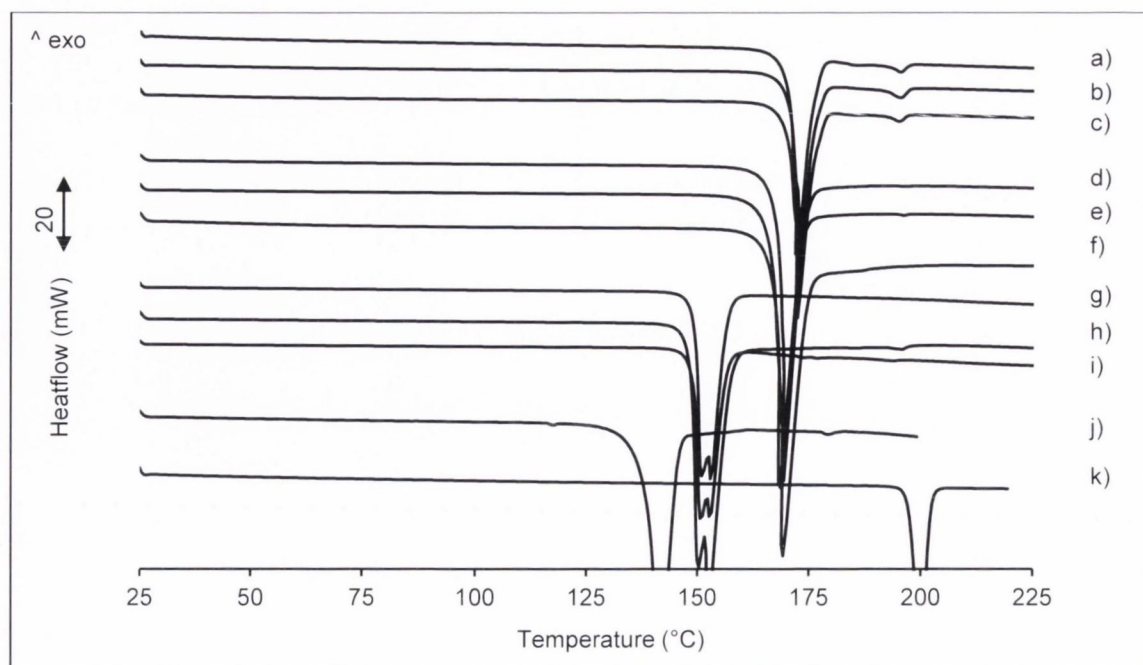
Figure 3.6: DSC thermograms of SD and 4-ASA, liquid-assisted milled using EtOH in different molar ratios of a) SD:4-ASA 2:1 milled 45 min, b) SD:4-ASA 2:1 milled 30 min, c) SD:4-ASA 2:1 milled 15 min, d) SD:4-ASA 1:1 milled 45 min, e) SD:4-ASA 1:1 milled 30 min, f) SD:4-ASA 1:1 milled 15 min, g) SD:4-ASA 1:2 milled 45 min, h) SD:4-ASA 1:2 milled 30 min, i) SD:4-ASA 1:2 milled 15 min, j) 4-ASA, raw material and k) SD, raw material.
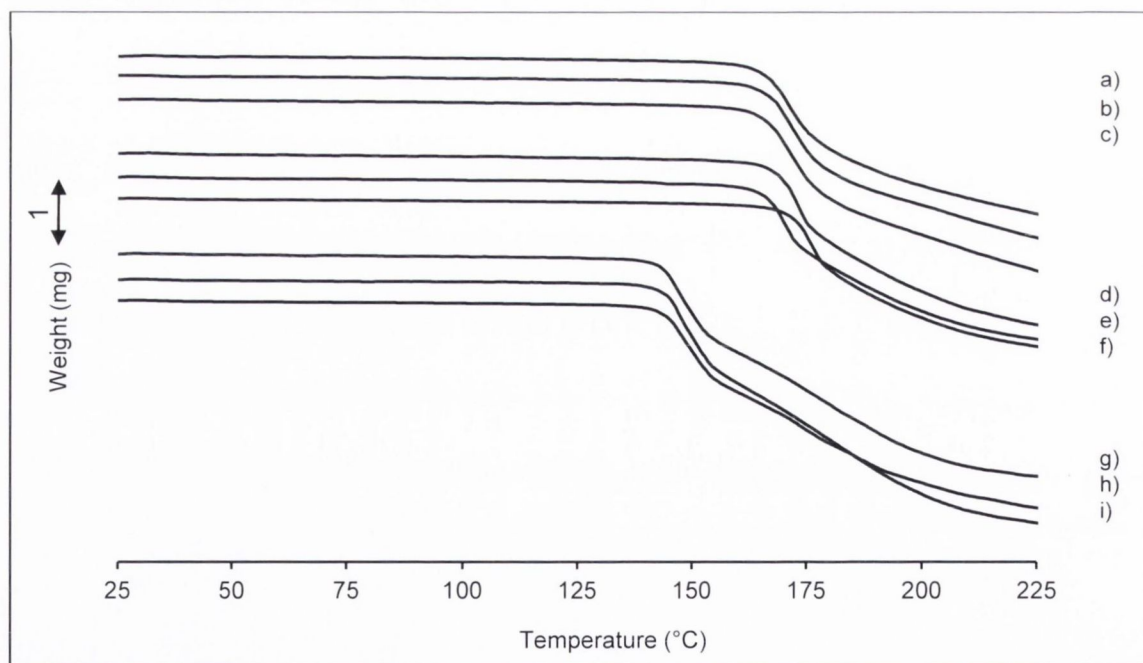

Figure 3.7: TGA thermograms of SD and 4-ASA, liquid-assisted milled using EtOH in different molar ratios of a) SD:4-ASA 2:1 milled 45 min, b) SD:4-ASA 2:1 milled 30 min, c) SD:4-ASA 2:1 milled 15 min, d) SD:4-ASA 1:1 milled 45 min, e) SD:4-ASA 1:1 milled 30 min, f) SD:4-ASA 1:1 milled 15 min, g) SD:4-ASA 1:2 milled 45 min, h) SD:4-ASA 1:2 milled 30 min and i) SD:4-ASA 1:2 milled 15 min.

In the case of the co-spray-dried materials, the product of the 1:2 SD:4-ASA ratio (Figure 3.8 c) showed a broad asymmetric melting event shifted towards the melting temperature of 4-ASA (T_m = 139.07 ± 0.93 °C), similar to the 1:2 SD:4-ASA dry milled (Figure 3.4 g–i) and liquid-assisted milled (Figure 3.6 g–i) products, indicative of excess amount of 4-ASA. For the SD:4-ASA 2:1 spray-dried product (Figure 3.8 a) a glass transition (T_g) at 68.46 ± 0.20 °C, characteristic of the amorphous state and thus consistent with the PXRD data (Figure 3.3 a), followed by two exothermic crystallisation events corresponding to crystallisation of the amorphous phase and melting were observed. The amorphous phase may be attributed to amorphous SD induced by spray drying as it has been found, that when spray drying the components separately under the same conditions, SD showed an exothermic event in the same temperature range as observed for the SD:4-ASA 2:1 spray-dried product prior to melting, while 4-ASA revealed a melting event only (Appendix 2, Figure A.2.2). Based on further evidence by PXRD analysis of spray-dried SD and 4-ASA (Appendix 2, Figure A.2.3), these results indicated that SD transforms to a partially amorphous phase by spray drying, whereas 4-ASA remains crystalline. In contrast, co-spray drying from a 1:1 ratio revealed a product with a single melting peak (Figure 3.8 b) occurring at the same temperature as the melting peak of the 1:1 liquid-assisted milled material (Table 3.1). Melting of each product was found to be associated with decomposition, as evidenced by TGA analysis (Figure 3.9).
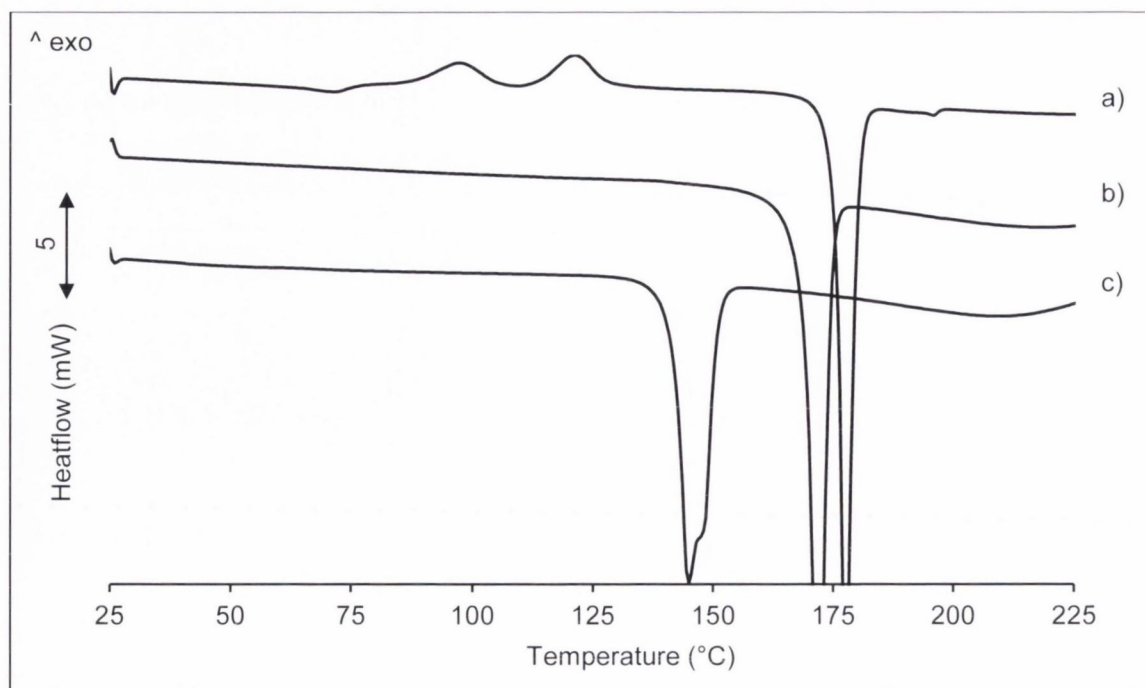
Figure 3.8: DSC thermograms of spray-dried composite systems of a) SD:4-ASA 2:1, b) SD:4-ASA 1:1 and c) SD:4-ASA 1:2.
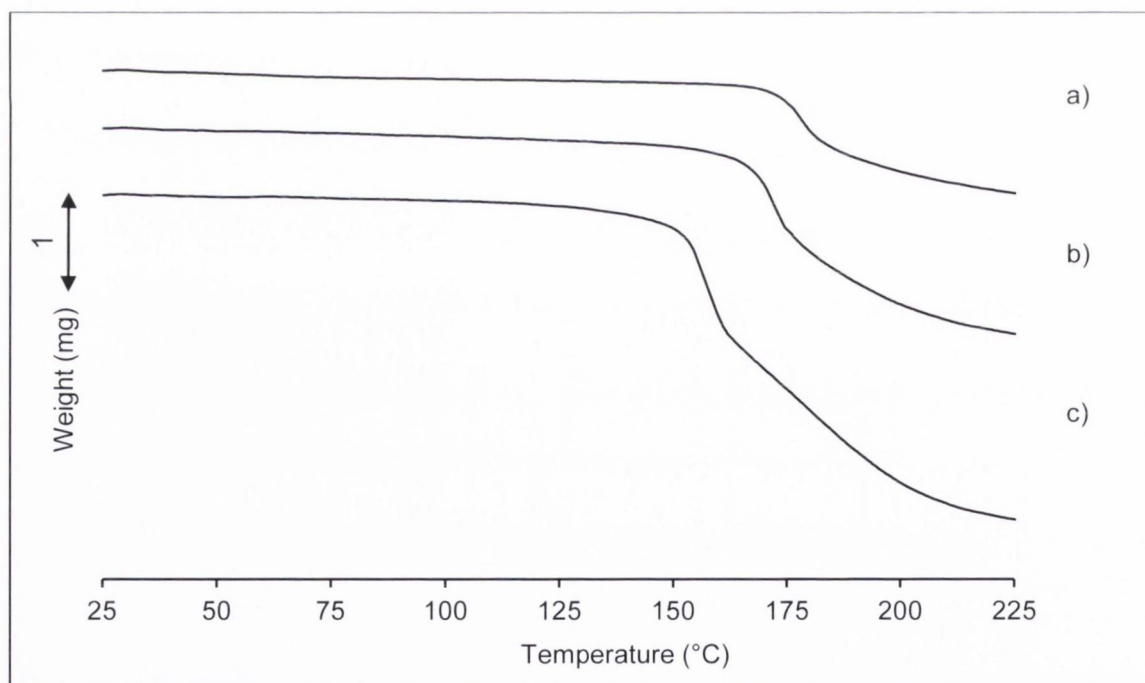

Figure 3.9: TGA thermograms of spray-dried composite systems of a) SD:4-ASA 2:1, b) SD:4-ASA 1:1 and c) SD:4-ASA 1:2.

In summary, from the results obtained by PXRD and thermal analysis, it was concluded, that dry co-milling and co-spray drying of SD and 4-ASA induced amorphisation to different extents, while this was not evident for liquid-assisted milling. Influence of the milling time was only observed during dry milling, which resulted in products with increased amorphous content and reduced crystallinity with increasing milling time. All products melted with decomposition. Non-equimolar ratios of SD:4-ASA resulted in either binary crystalline mixtures or binary crystalline mixtures with some amorphous content. Single phase products (based on PXRD and DSC analysis) with unique diffraction peaks different from the pure components, indicative of cocrystal formation, were only observed for liquid-assisted milling and spray drying when the mixture contained equimolar amounts of SD and 4-ASA.

Referring to the objective of this work in studying cocrystal systems, all further investigations were therefore focused on the SD:4-ASA 1:1 liquid-assisted milled and spray-dried products.

3.3.2 SD:4-ASA 1:1 liquid-assisted milled and spray-dried product – further solid state characterisation

In order to ascertain if one of the processing methods has resulted in formation of the same SD:4-ASA 1:1 cocrystal as obtained by crystallisation from ethanol and reported previously by Caira (1992), the single crystal X-ray data were transformed into a theoretical powder diffractogram and compared with the experimental patterns obtained for the two solid products. As shown in Figure 3.10, it was found that the PXRD pattern of the 1:1 liquid-assisted milled product was consistent with the calculated pattern. However, the spray-dried product in the equivalent ratio showed different diffraction peaks which also differed from the pure components and it was assumed that a polymorphic cocrystal might have formed (Figure 3.10). The lower intensity of the diffraction peaks of the milled and spray-dried product compared to the product crystallised from ethanol can be explained by crystal imperfections induced by ball milling and spray drying.
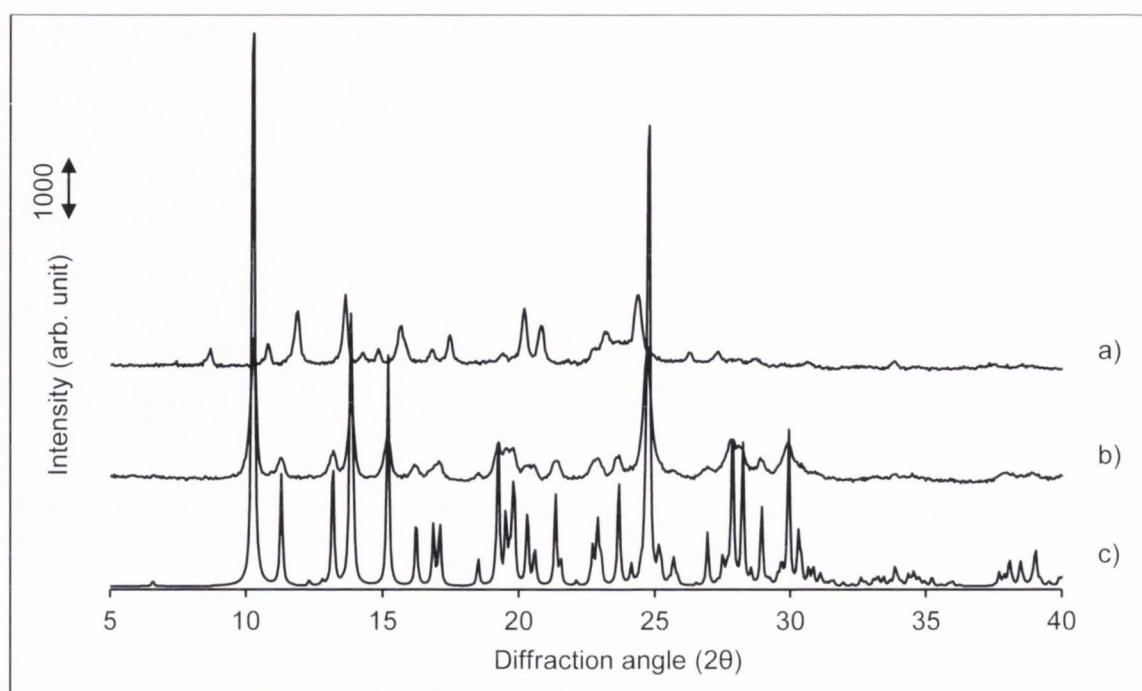
Figure 3.10: Theoretical PXRD patterns of SD:4-ASA 1:1 products obtained by a) spray drying, b) liquid-assisted milling compared to SD:4-ASA 1:1 cocrystal, crystallised from ethanol, calculated on the basis of single crystal data (Caira, 1992).

Characterisation by elemental analysis of the carbon, hydrogen and nitrogen composition of the liquid-assisted milled and spray-dried product is shown in Table 3.2. For both products the same elemental composition was detected and showed consistency with the known cocrystal molecular formula, $C_{12}H_{14}N_4O_2S$.

Table 3.2: Elemental analysis of SD:4-ASA 1:1 composite systems, produced by liquid-assisted milling and spray drying.

Sample	Element	Theory (%)	Found (%)
SD:4-ASA 1:1, liquid-assisted milled	C	52.90	52.66 ± 0.03
	H	4.87	4.85 ± 0.04
	N	16.24	16.04 ± 0.04
SD:4-ASA 1:1, spray-dried	C	52.90	52.51 ± 0.02
	H	4.87	4.87 ± 0.01
	N	16.24	16.20 ± 0.03

Analysis by IR spectroscopy is illustrated in Figure 3.11. Distinctive bands in the higher frequency range were observed for the single components such as in the case of SD (Figure 3.11 d) which showed three characteristic IR bands: two bands at around 3441 cm^{-1} and 3338 cm^{-1} attributed to the asymmetric and symmetric NH_2 stretching bands of the amine group respectively and one stretching band at approximately 3235 cm^{-1} attributed to the sulfonamide or amidine NH group, while 4-ASA (Figure 3.11 c) displayed two characteristic bands at around 3493 cm^{-1} and 3386 cm^{-1} referring to the asymmetric and symmetric NH_2 stretching bands of the amine group respectively. The SD:4-ASA 1:1 liquid-assisted milled product (Figure 3.11 b) showed bands at 3468, 3415, 3369 and 3339 cm^{-1} corresponding to the NH_2 stretching vibrations of the amine groups and thus shifts to different wavenumbers with respect to the pure components (Figure 3.11 c-d). The sulfonamide/amidine NH stretching was not prominent, but a small attributable band at 3233 cm^{-1} was visible. Moreover, a shift of the band corresponding to the OH bending of the carboxylic acid group in 4-ASA merging with the band attributed to the sulfone (SO_2) group in SD (at 1300 cm^{-1}) was found at 1274 cm^{-1} (Figure 3.11 b). The observed shifts are indicative of molecular interactions such as hydrogen bonding. As was previously shown for the SD:4-ASA 1:1 cocrystal reported by Caira (1992), the molecular association between SD and the acid occurs through hydrogen bonding formation (Figure 3.12). These findings were consistent with the PXRD results and confirmed formation of the SD:4-ASA 1:1 cocrystal (Caira, 1992) via liquid-assisted milling.
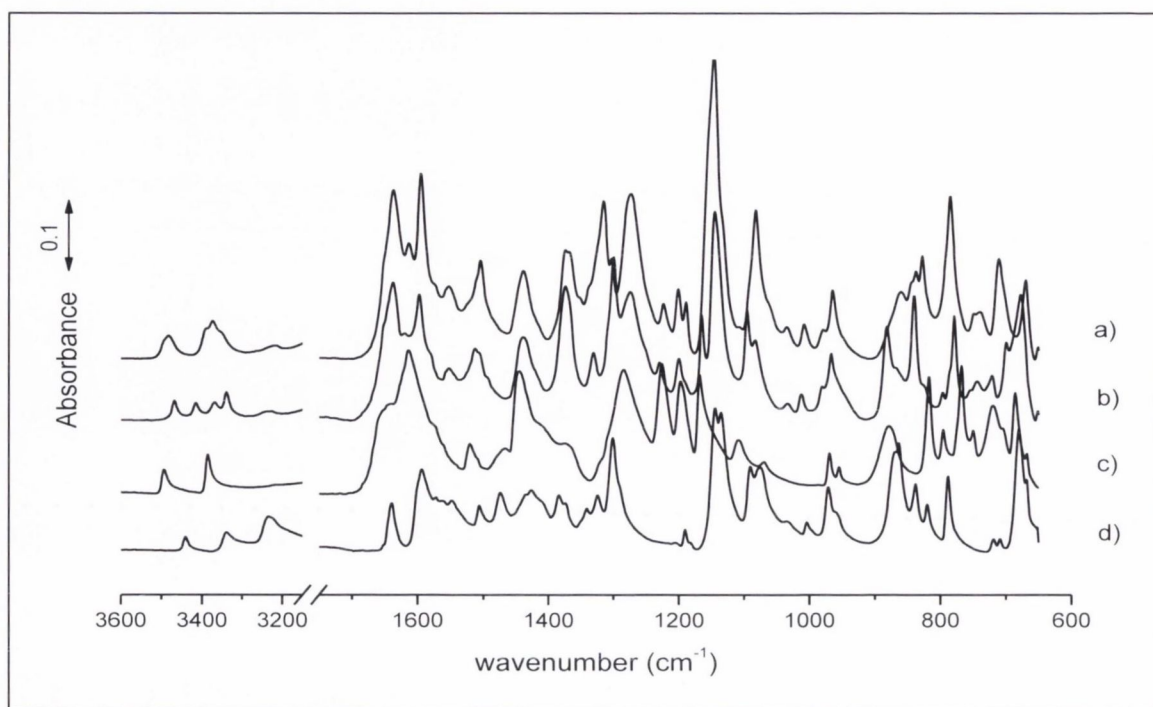
Figure 3.11: FTIR spectra of a) SD:4-ASA 1:1 spray-dried product, b) SD:4-ASA 1:1 liquid-assisted milled product, c) 4-ASA, raw material and d) SD, raw material.
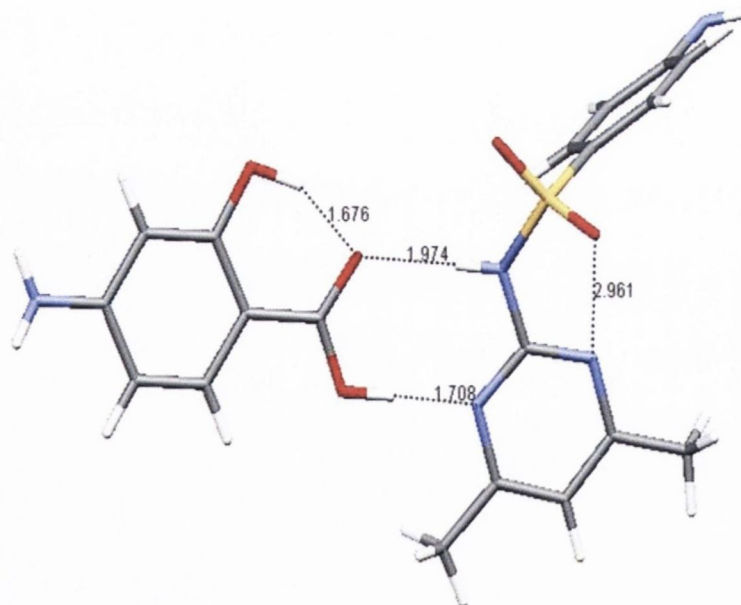

Figure 3.12: Molecular structure of the SD:4-ASA 1:1 cocrystal (dotted black lines indicate hydrogen bonds) (Caira, 1992).

The spray-dried material showed a different result compared to the liquid-assisted milled product. As shown in Figure 3.11 a, two broad bands, one at 3482 cm^{-1} and one at 3372 cm^{-1} with some shoulders attributable to the NH$_2$ stretching bands of the amine groups and a small weak band at 3230 cm^{-1} referring to the sulfonamide/amidine NH stretching were observed. Compared to the single components, the bands at 3482 and 3372 cm^{-1} displayed shifts towards other wavenumbers and are therefore attributable to intermolecular interactions which differed to those of the liquid-assisted milled product. Further differences between the two products were observed in the fingerprint region by shifts of bands corresponding to the sulfone (SO$_2$) stretching vibrations in SD and to the carboxyl group (OH bending) in 4-ASA at 1315 and 1275 cm^{-1}, respectively (Figure 3.11 a).

To elucidate the structural differences between the SD:4-ASA 1:1 liquid-assisted milled and spray-dried product, solid state NMR analysis was performed. The obtained ^{13}C CPMAS spectra are shown in Figure 3.13. As a reference and for assignment of the chemical signals, the single components were analysed. Their spectra are illustrated in Figure 3.13 c and d. A list of all peak assignments is presented in Table 3.3. Both SD and 4-ASA revealed sharp and narrow signals indicative of highly ordered (crystalline) structures. The relaxation time constants (T_1) were found to be 48 seconds and 220 seconds for SD and 4-ASA, respectively. Generally, highly ordered, crystalline samples tend to have long relaxation times and thus high T_1 due to the long distances between individual nuclei in crystals. On the other hand, short relaxation times corresponding to low T_1 values are usually observed for amorphous materials due to the proximity of each nucleus to surrounding nuclei (Apperley et al., 2012).

For the liquid-assisted milled product the T_1 constant was 16 seconds and therefore significantly lower than the corresponding values for the single components, indicating that the product is less ordered than SD and 4-ASA raw materials. The NMR spectrum of the liquid-assisted milled product is shown in Figure 3.13 b. Similar to SD and 4-ASA the peaks were found to be sharp and narrow, attributable to an ordered structure. However, most signals have shifted towards higher or lower ppm numbers with respect to the single components (Figure 3.13 b, Table 3.3). Characteristic changes were, for example, observed for peaks corresponding to the carbons 8 and 12 and 7 of SD which have shifted and possibly exchanged their position appearing as overlapping signal at 127.8 and 129.6 ppm, respectively. The peak at 23.4–21.6 ppm attributed to the two methyl groups (carbons 1 and 5) of SD has shifted towards higher ppm numbers and

appeared to have further separated indicating an increased distance between the two methyl groups. Furthermore, peaks at 173.9, 169.1, 132.9 and 105.0 ppm corresponding to the carbons 1, 7, 3 and 2 of 4-ASA displayed characteristic shifts compared to single 4-ASA. The peak attributed to the carbons 4 and 6 of 4-ASA has separated into two discrete signals appearing at 100.5 and 98.1 ppm indicating that these carbons are no longer equivalent when compared to 4-ASA raw material. Overall, these findings show that liquid-assisted milling has changed the crystal structure of SD and 4-ASA and highlights the closer chemical contact and therefore the presence of molecular interactions between the components.
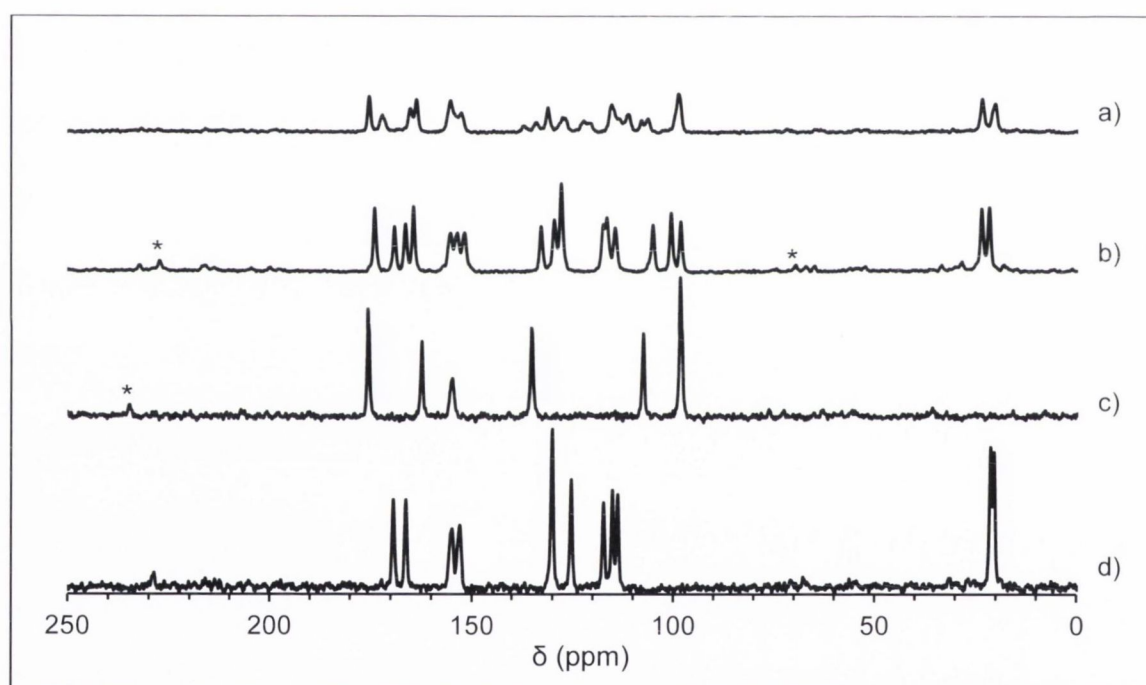

Figure 3.13: ^{13}C CPMAS spectra of a) SD:4-ASA 1:1 spray-dried product, b) SD:4-ASA 1:1 liquid-assisted milled product, c) 4-ASA, raw material and d) SD, raw material. The signals labelled by the asterisks indicate spinning side bands.

Table 3.3: ^{13}C chemical shifts (ppm) with assignment to the appropriate C-atom observed for SD, 4-ASA, the SD:4-ASA 1:1 liquid-assisted milled (LAM) and spray-dried (SPD) product.

^{13}C assignment*	SD	4-ASA	SD:4-ASA, LAM	SD:4-ASA, SPD
N-**C**=C (SD-C4)	169.3	–	166.4	172.0
N=**C**-C (SD-C2)	166.3	–	164.4	165.2
N-**C**=N (SD-C6)	154.8	–	155.2[a)]	155.2[c)]
C-NH$_2$ (SD-C10)	152.9	–	151.8[a)]	
C-**C**=C (SD-C8, C12)	130.1	–	127.8[b)]	133.9, 131.2
-**C**-SO$_2$ (SD-C7)	125.4	–	129.6[b)]	127.5
C-**C**=C (SD-C3)	117.3	–	117.3	122.3, 120.5
C-**C**=C (SD-C9, C11)	115.1, 113.7	–	116.5, 114.4	115.3, 111.1
CH$_3$ (SD-C1, C5)	21.3, 20.4	–	23.4, 21.6	23.3, 20.1
COOH (4ASA-C1)	–	175.5	173.9	175.3
C=**C**-OH (4ASA-C7)	–	162.4	169.1	163.7
C-NH$_2$ (4ASA-C5)	–	154.8	153.5[a)]	152.6[c)]
C=**C**-C (4ASA-C3)	–	135.2	132.9	137.1
C=**C**-COOH (4ASA-C2)	–	107.4	105.0	107.9, 106.2
C=**C**-C (4ASA-C4, C6)	–	98.2	100.5, 98.1	98.7

refers to molecular structures of SD and 4-ASA as shown below
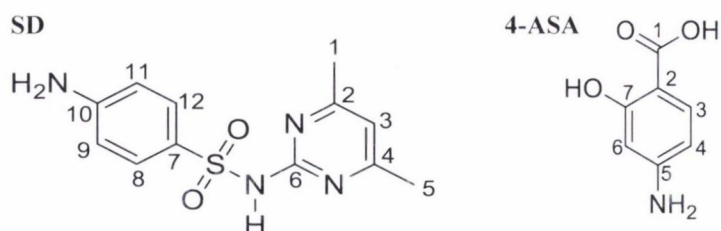
a) overlapping signals
b) overlapping signals
c) overlapping signals

For the SD:4-ASA 1:1 spray-dried product a T_1 of 7.5 seconds was found. This value was lower than the values for the liquid-assisted milled sample and the single components and indicates that the spray-dried product is less ordered in nature. The ^{13}C NMR spectrum is shown in Figure 3.13 a. It was found that all peaks appeared broader and signals were superimposing with one another when compared to the liquid-assisted milled material and the single components. This is often observed for less ordered (amorphous) materials and thus consistent with the result of T_1 determination. The spectrum of the spray-dried product showed distinct differences to those of the other materials. For example, the signals attributed to the carbons 4 and 2 of SD have drifted further apart from each other appearing at 172.0 and 165.2 ppm and thus in close proximity to the signals attributed to carbons 1 and 7 of 4-ASA at 175.3 and 163.7 ppm, respectively. The peaks corresponding to carbons 6 and 10 of SD merge with the peak attributed to carbon 5 of 4-ASA at 155.2–152.6 ppm. Moreover, the peak appearing at 137.1 ppm attributable to carbon 3 of 4-ASA showed a shift towards higher ppm numbers. The single peak referring to the carbons 8 and 12 of SD seemed to have separated into two signals, appearing at 133.9 and 131.1 ppm. Characteristic shifts towards higher ppm numbers were observed for peaks at 127.5 ppm and 122.3–120.5 ppm, corresponding to carbon 7 and 3 of SD. The signals attributed to carbons 9 and 11 of SD have drifted further apart from each other by around 2.8 ppm appearing at 115.3–111.1 ppm, whereas the peak present at 107.8–106.2 ppm attributable to carbon 2 of 4-ASA, showed separation. In contrast to the liquid-assisted milled sample, the peak referring to the carbons 4 and 6 of 4-ASA appeared as a single peak at 98.7 ppm, as in pure 4-ASA. Moreover, the signals at 23.3–20.1 ppm corresponding to the two methyl groups (carbons 1 and 5) of SD were found to have drifted further apart than was observed for the liquid-assisted milled product and single SD. These results showed that spray drying has altered the structure of the components, possibly rendering it amorphous to some extent. The characteristic shifts observed in the spectrum, different to those of the liquid-assisted milled sample were indicative of molecular interactions between the components.

Further conclusions were drawn by analysing a physical mixture of SD and 4-ASA in 1:1 molar ratio and SD and 4-ASA after being spray-dried separately. The ^{13}C spectra can be found in Appendix 2, Figure A.2.4. For the physical mixture the T_1 value was 65 seconds and therefore between the corresponding values of the single components. In contrast to the liquid-assisted milled and spray-dried product, all peaks in the spectrum

were found to superimpose with those of SD and 4-ASA (Appendix 2, Figure A.2.4 a), proving that simply mixing of the two components did not alter the chemical structure. Spray-dried SD and 4-ASA showed T_1 values of 12.5 and 19.5 seconds, respectively. These values were significantly lower when compared to unprocessed SD (by 35.6 seconds) and 4-ASA (by 200.5 seconds) indicating that the components became more disordered by spray drying. These findings were consistent with the corresponding ^{13}C spectra of spray-dried SD and 4-ASA which displayed broader peaks than the unprocessed materials (Appendix 2, Figure A.2.4 b-e). Moreover, the observed peak broadening of the single components was not found to be attributable to the peak broadening of the SD:4-ASA co-spray-dried material. Therefore, it was concluded that the broader peaks obtained from co-spray-drying associated with shifts are not only a result of a more disordered state, but confirm that the carbon atoms are chemically different to those of the liquid-assisted milled product, a physical mixture and the single components.

In summary, further solid state characterisation of the SD:4-ASA 1:1 liquid-assisted milled and spray-dried product has shown that liquid-assisted milling of SD and 4-ASA in 1:1 ratio results in the formation of the same cocrystal as reported by Caira (1992). On spray drying, a product with the same molecular formula as the liquid-assisted milled sample is obtained. Based on findings from IR and ^{13}C ssNMR spectroscopy, the spray-dried product revealed noticeable differences which are attributed on the one hand to different molecular interactions between SD and 4-ASA and on the other hand to a different solid state nature. These differences gave further indication that a polymorphic form of the SD:4-ASA 1:1 cocrystal has been generated by spray drying.

In the following, the term "form I" cocrystal is used for the SD:4-ASA 1:1 liquid-assisted milled product and "form II" is used for the spray-dried product.

3.3.3 SD:4-ASA 1:1 form I and form II cocrystal – solubility studies

The equilibrium and apparent solubility of pure SD and pure 4-ASA were found to be $2.30 \times 10^{-3} \pm 0.02 \times 10^{-3}$ mmol/ml and $14.90 \times 10^{-3} \pm 0.00 \times 10^{-3}$ mmol/ml, respectively.

As demonstrated in work by Good and Rodríguez-Hornedo (2009), cocrystal solubility can be estimated through only a single measurement from the transition concentration (C_{tr}) at which the cocrystal and drug are in equilibrium with the solution. A good estimation of the cocrystal solubility based on C_{tr} measurements requires that solution complexation does not play a role (Good and Rodríguez-Hornedo, 2009). To determine whether solution complexation is present, phase-solubility studies were performed. As shown in Figure 3.14, increasing 4-ASA concentrations in solution did not have an impact on the concentration of SD in solution. The measured SD concentration for solutions which contained ≥ 0.0026 mmol/ml 4-ASA did not change significantly and was $2.45 \times 10^{-3} \pm 0.03 \times 10^{-3}$ mmol/ml. When compared to S_0 (= SD concentration in the absence of 4-ASA, $S_0 = 2.30 \times 10^{-3} \pm 0.02 \times 10^{-3}$ mmol/ml), the measured increase and thus solution complexation of SD in the presence of 4-ASA was considered to be negligible.
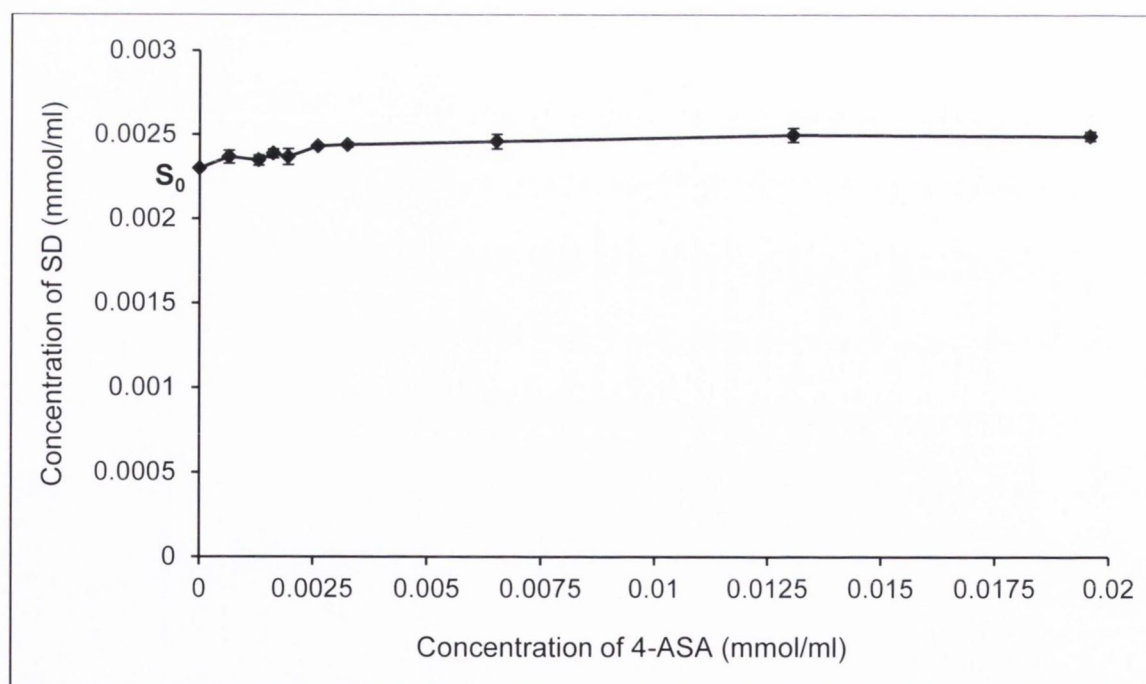

Figure 3.14: Phase-solubility profile of SD (mmol/ml) as a function of 4-ASA concentration. S_0 is the equilibrium solubility of SD in the absence of 4-ASA.

The determination of the cocrystal solubility or rather solubility product (K_{sp}) from the transition concentration is based on the following theoretical principle:

$$K_{sp} = [A]_{tr}^{\alpha} [B]_{tr}^{\beta} \qquad (3.1)$$

where [A] and [B] are the molar concentrations of cocrystal components, and the superscripts, α and β, refer to the stoichiometric amounts of A and B, respectively (Good and Rodríguez-Hornedo, 2009).

For the SD:4-ASA 1:1 form I cocrystal (produced by liquid-assisted milling) transition concentrations (C_{tr}) of $2.39 \times 10^{-3} \pm 0.13 \times 10^{-3}$ mmol/ml for SD and $3.37 \times 10^{-3} \pm 0.08 \times 10^{-3}$ mmol/ml for 4-ASA (pH=4.12) were measured resulting in a solubility product of $8.05 \times 10^{-6} \pm 0.53 \times 10^{-6}$ M^2 using equation 3.1. Analysis by PXRD of the solid remaining phase after equilibration verified that the transition point was reached by the presence of a mixed phase composed of cocrystal and SD (Appendix 2, Figure A.2.5).

However, equation 3.1 is only applicable to non-ionisable components (Good and Rodriguez-Hornedo, 2009; Nehm et al., 2006). As both components in the SD:4-ASA 1:1 cocrystal have an amphoteric character, ionisation and thus the pH in solution plays an important role.

The prediction of cocrystal solubility dependence on pH has been previously described for different components by Bethune et al. (2009). However, no model has been reported for a cocrystal containing two amphoteric components. Therefore, for the SD:4ASA 1:1 cocrystal a new theoretical model has been established from which the pH-dependent cocrystal solubility and solubility product was predicted by the following equation:

$$S_{cocrystal} = \sqrt{K_{sp}\left(1 + \frac{[H^+]}{K_{a1,SD}} + \frac{K_{a2,SD}}{[H^+]}\right)\left(1 + \frac{[H^+]}{K_{a1,4ASA}} + \frac{K_{a2,4ASA}}{[H^+]}\right)} \qquad (3.2)$$

where K_{sp} is the solubility product and K_{a1} and K_{a2} are the acid ionisation constants for the SD (drug) and 4-ASA (coformer), respectively.

The model was derived based on the equilibrium reactions for cocrystal dissociation and ionisation and is described in detail in the following paragraphs.

For the SD:4-ASA 1:1 cocrystal composed of an amphoteric drug and an amphoteric coformer the following equations can be established:

$$SD:4ASA_{solid} \rightleftharpoons SD_{soln} + 4ASA_{soln} \tag{3.3}$$

$$K_{sp} = [SD][4ASA] \tag{3.4}$$

For SD the equilibrium reactions and the thereof derived mass constants can be described by:

$$SDH^+ \rightleftharpoons SD + H^+ \tag{3.5}$$

$$K_{a1,SD} = \frac{[SD][H^+]}{[SDH^+]} \tag{3.6}$$

$$SD \rightleftharpoons SD^- + H^+ \tag{3.7}$$

$$K_{a2,SD} = \frac{[SD^-][H^+]}{[SD]} \tag{3.8}$$

For 4-ASA the equilibrium reactions and the thereof derived mass constants can be expressed by:

$$4ASAH^+ \rightleftharpoons 4ASA + H^+ \tag{3.9}$$

$$K_{a1,4ASA} = \frac{[4ASA][H^+]}{[4ASAH^+]} \tag{3.10}$$

$$4ASA \rightleftharpoons 4ASA^- + H^+ \tag{3.11}$$

$$K_{a2,4ASA} = \frac{[4ASA^-][H^+]}{[4ASA]} \tag{3.12}$$

The total SD and 4-ASA concentrations (SD_t and $4-ASA_t$) are then calculated by the sum of the ionised and nonionised species as described below:

$$[SD]_t = [SDH^+] + [SD] + [SD^-] \tag{3.13}$$

$$[4ASA]_t = [4ASAH^+] + [4ASA] + [4ASA^-] \tag{3.14}$$

The equilibrium constants (K_{sp} and K_a) can be used to substitute equations 3.13 and 3.14:

$$[SD]_t = \frac{K_{sp}}{[4ASA]} \left(1 + \frac{[H^+]}{K_{a1,SD}} + \frac{K_{a2,SD}}{[H^+]}\right) \tag{3.15}$$

$$[4ASA]_t = [4ASA] \left(1 + \frac{[H^+]}{K_{a1,4ASA}} + \frac{K_{a2,4ASA}}{[H^+]}\right) \tag{3.16}$$

$$[4ASA] = \frac{[4ASA]_t}{\left(1 + \frac{[H^+]}{K_{a1,4ASA}} + \frac{K_{a2,4ASA}}{[H^+]}\right)} \tag{3.17}$$

Substituting equation 3.17 into equation 3.15:

$$[SD]_t = \frac{K_{sp}}{[4ASA]_t} \left(1 + \frac{[H^+]}{K_{a1,SD}} + \frac{K_{a2,SD}}{[H^+]}\right) \left(1 + \frac{[H^+]}{K_{a1,4ASA}} + \frac{K_{a2,4ASA}}{[H^+]}\right) \tag{3.18}$$

For a 1:1 cocrystal considering stoichiometric conditions, $S_{cocrystal} = [SD]_t = [4ASA]_t$ and thus equation 3.18 can be rewritten resulting in equation 3.2.

At the transition (tr) point equation 3.18 can be rewritten as:

$$[SD]_{tr} = \frac{K_{sp}}{[4ASA]_{tr}} \left(1 + \frac{[H^+]}{K_{a1,SD}} + \frac{K_{a2,SD}}{[H^+]}\right) \left(1 + \frac{[H^+]}{K_{a1,4ASA}} + \frac{K_{a2,4ASA}}{[H^+]}\right) \tag{3.19}$$

Hence, the solubility product (K_{sp}) can be determined by:

$$K_{sp} = \frac{[SD]_{tr}\,[4ASA]_{tr}}{\left(1 + \frac{[H^+]}{K_{a1,SD}} + \frac{K_{a2,SD}}{[H^+]}\right)\left(1 + \frac{[H^+]}{K_{a1,4ASA}} + \frac{K_{a2,4ASA}}{[H^+]}\right)} \tag{3.20}$$

Based on the measured C_{tr}, the pH and the known acid constants for the SD:4-ASA 1:1 form I cocrystal a K_{sp} of $1.91 \times 10^{-6} \pm 0.16 \times 10^{-6}$ M^2 was calculated using equation 3.20. The obtained K_{sp} allowed further prediction of the cocrystal solubility for other pH values using equation 3.2.

Figure 3.15 shows the resulting cocrystal solubility profile, dependent on the pH. For the single components the pH-dependent solubility was derived from the Henderson-Hasselbalch relationship (Florence and Attwood, 2011).

Experimentally measured solubilities of the cocrystal at other pH values were determined according to the following equation for a 1:1 cocrystal referring to Nehm et al. (2006) (Figure 3.15).

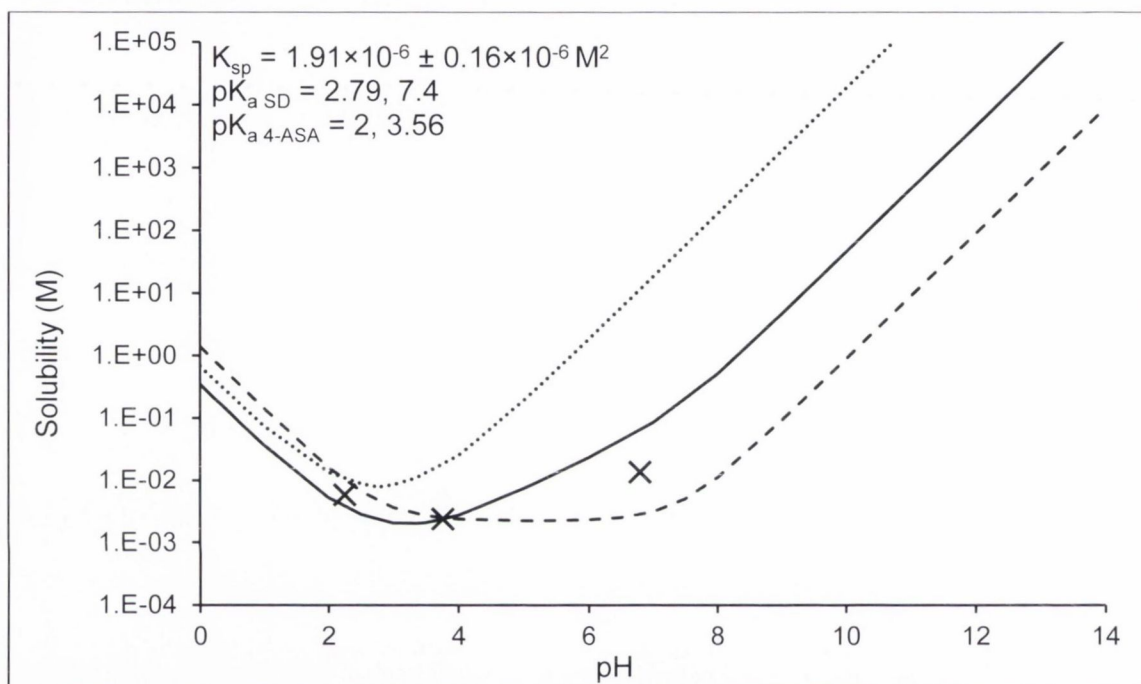$$S_{cocrystal} = \sqrt{[\mathbf{drug}][\mathbf{coformer}]} \quad\quad (3.21)$$

Figure 3.15: Theoretical pH solubility profile (37 °C) for the SD:4ASA 1:1 form I cocrystal containing two amphoteric components. The solid line represents the cocrystal solubility, the dashed and dotted lines show the theoretical SD and 4-ASA solubility dependent on the pH (derived from the Henderson-Hasselbalch relationship) and the cross symbols are experimentally obtained solubility data for the cocrystal.

From the established pH-solubility profile, it was concluded that the SD:4-ASA 1:1 form I cocrystal is less soluble than its single components in the acidic region at pH < 4 and becomes more soluble than SD at pH > 4. Experimentally determined solubilities at pH = 2.3 and pH = 3.76 were found to be in good agreement with the predictions.

PXRD analysis of the solid phases at equilibrium confirmed the presence of cocrystal as a single phase and thus its stability at the given pH (Figure 3.16 b and c). In contrast, at pH = 6.8 the measured concentration was found to be lower than the predicted

solubility (Figure 3.15). PXRD analysis of the solid phase detected a mixed phase of cocrystal and SD attributed to the presence of the diffraction peak at 9.35° 2θ (Figure 3.16 a). This result showed that at pH = 6.8 the cocrystal was unstable by transforming to SD and explained the deviation of the experimentally determined solubility from the predicted profile (Figure 3.15).
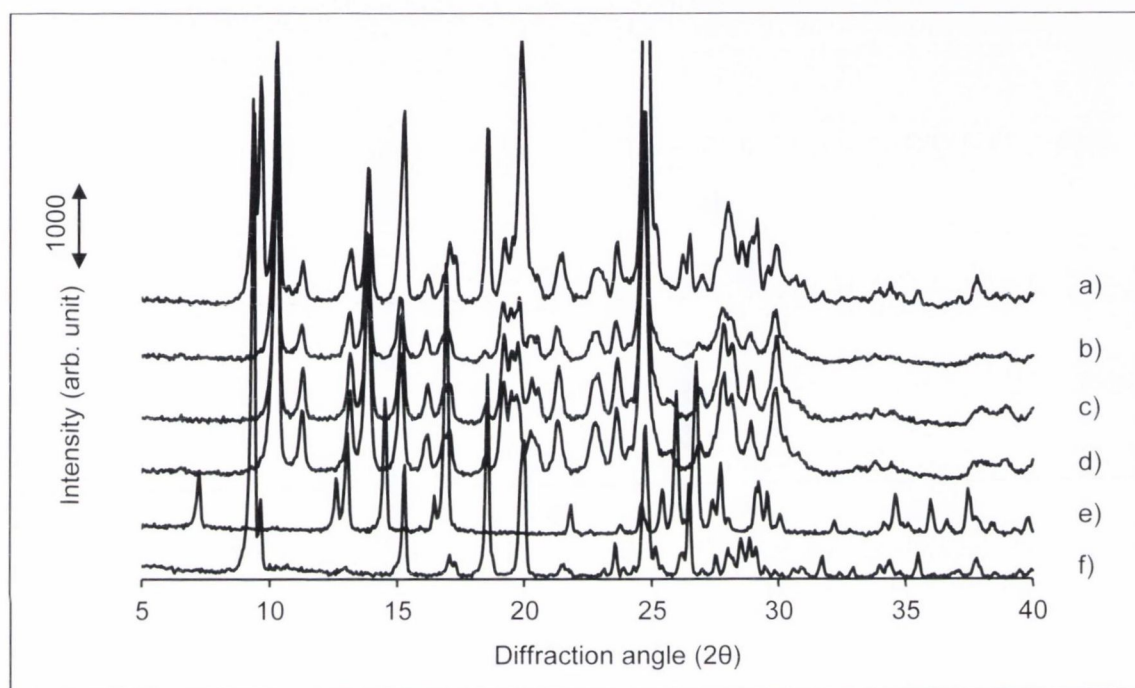

Figure 3.16: PXRD patterns of SD:4-ASA 1:1 form I cocrystal phases at different solution pH compared to the cocrystal before the study and the single components. a) cocrystal at pH = 6.8, b) cocrystal at pH = 3.76, c) cocrystal at pH = 2.30, d) form I cocrystal, e) 4-ASA, raw material and f) SD, raw material.

For determination of the solubility of the SD:4-ASA 1:1 form II cocrystal, initial solubility experiments using the shake-flask method were performed. However, it was found that, after 1 hour equilibration time, the solid phase had fully converted to the form I cocrystal and SD (verified by PXRD, data not shown). For more detailed information, dynamic solubility studies were performed for the form II cocrystal and the phase stability was analysed by PXRD. The results are presented in Figure 3.17 and Figure 3.18.
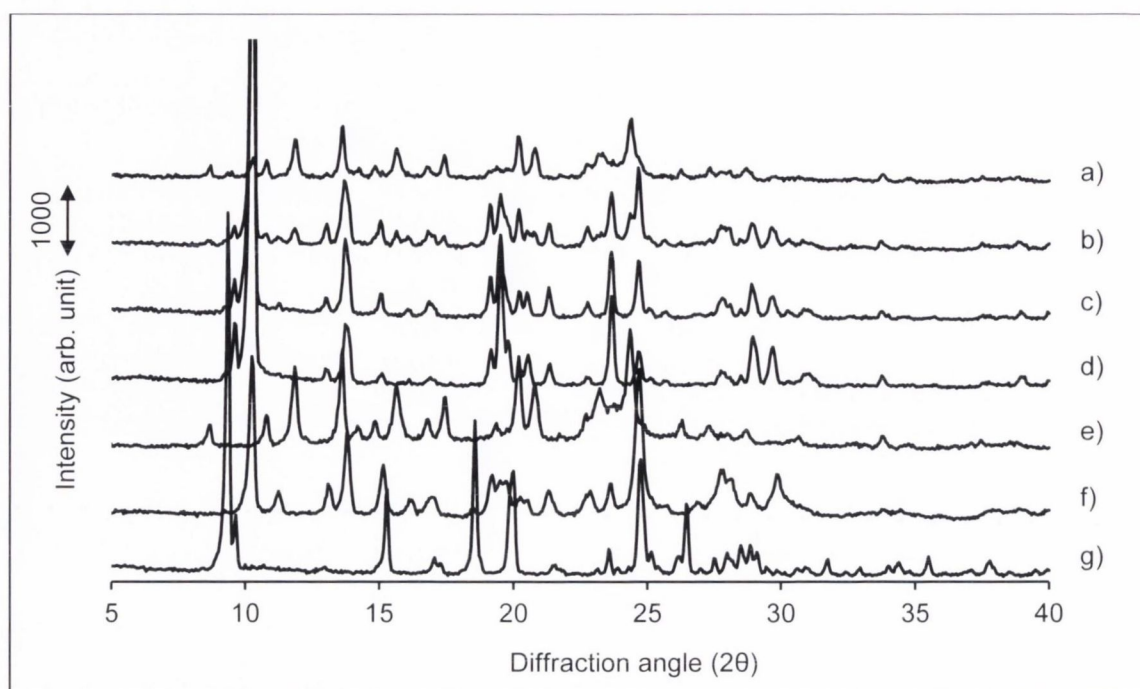
Figure 3.17: PXRD patterns of the solid phase during dynamic solubility studies performed in water (37 °C) of the SD:4-ASA 1:1 form II cocrystal: a) at 30 seconds, b) at 10 minutes, c) at 20 minutes, d) at 60 minutes compared to e) SD:4-ASA 1:1 form II before subjected to solubility test, f) SD:4-ASA 1:1 form I cocrystal before subjected to solubility test and g) SD, raw material.

It was found that, after only 30 seconds, the form II cocrystal converted, to some extent, to the form I cocrystal attributed to the presence of the diffraction peak at 10.25° 2θ (Figure 3.17 a). At 10 minutes, a third phase was detected in the solid residue, corresponding to SD as shown by the characteristic diffraction peak at 9.35° 2θ (Figure 3.17 b). At 20 minutes almost all diffraction peaks attributed to the form II cocrystal had disappeared (Figure 3.17 c) and at 60 minutes form II had fully converted to form I cocrystal and SD (Figure 3.17 d).

The concentration-time profile, as illustrated in Figure 3.18 revealed that the solution concentrations of SD and 4-ASA were non-equimolar, whereas for SD initially a significantly higher concentration was measured with a peak at 8 minutes followed by a decrease after 10 minutes with the trend to level out with the 4-ASA concentration with increasing time. The decrease was explained by the phase transformation as it has been shown by PXRD analysis.

As a reference, the study was also conducted for the SD:4-ASA form I cocrystal and pure SD (data can be found in Appendix 2, Figure A.2.6 and Figure A.2.7). In contrast to form II, the form I cocrystal showed equimolar solution concentrations of SD and 4-ASA and was stable over 60 minutes as confirmed by PXRD analysis of the solid residue at each time point. The initial SD concentration of form I was considerably lower than that obtained for form II, but was similar and at t=60 minutes the same as the SD concentration of pure SD (Appendix 2, Figure A.2.6). Considering the pH at t=60 minutes, which was approximately 3.80, the concentration of the form I cocrystal was expected to be similar to pure SD based on the pH-solubility predictions, as was demonstrated in Figure 6.2.
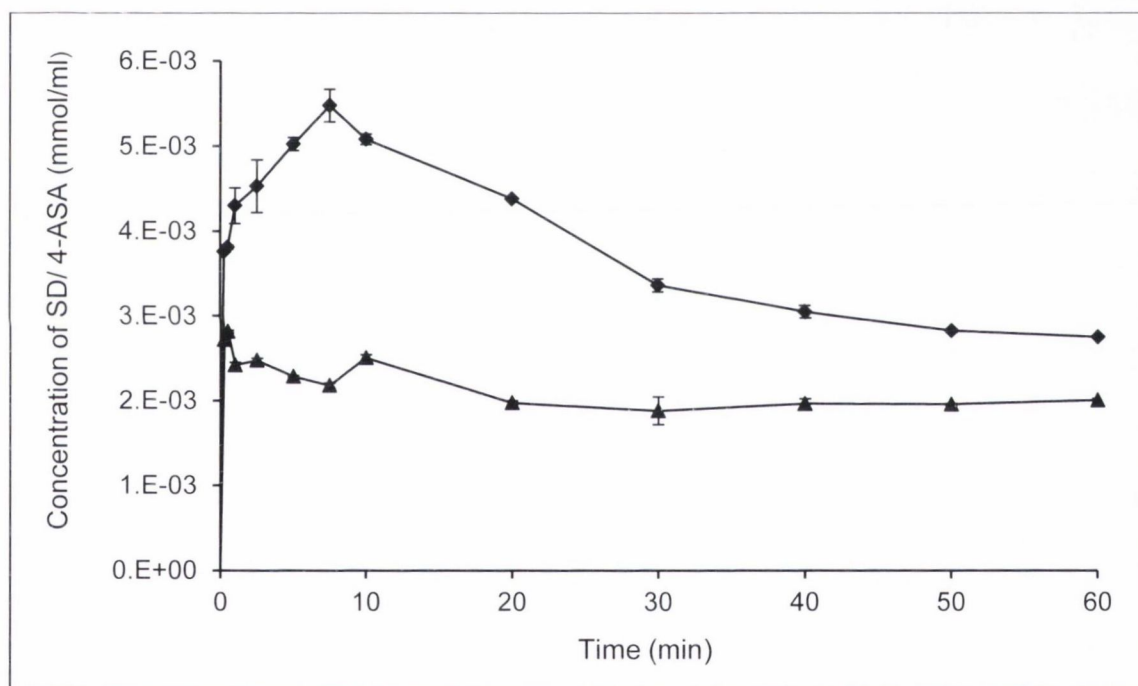

Figure 3.18: Concentration – time profiles of the SD:4-ASA 1:1 form II cocrystal in water at 37 °C. Diamonds symbolise SD, triangles represent 4-ASA.

Overall, these results indicated that the SD:4-ASA 1:1 form II cocrystal forms an unstable, supersaturated solution which undergoes a rapid solution-mediated transformation into the more stable form I associated with precipitation of SD. It was concluded, that the findings can be referred to the "spring" effect as is described for the "spring and parachute" approach by Guzmán et al. (2007). The "spring" is induced by a

higher energy form and reveals a higher apparent solubility ("apparent" because the material is not in the most stable form), which is a known phenomenon for amorphous materials, but has also been reported for crystalline materials (Guzmán et al., 2007; Vogt et al., 2008). In the case of the SD:4-ASA 1:1 form II cocrystal, the "spring" was observed at < 10 minutes and associated with conversion to the form I cocrystal. Therefore, it was not possible to determine the solubility of form II considering the given conditions. However, as has been demonstrated by Guzmán et al. (2007) such issues can be eliminated by maintaining or stabilising the unstable supersaturated state (parachute effect), where the use of polymers has been reported many times in the literature (Overhoff et al., 2008; ; Appel et al., 2006; Raghavan et al., 2001; Suzuki and Sunada, 1998; Usui et al., 1997). For example Warren et al. (2010) have reported on the effect of several polymers to inhibit precipitation from supersaturated solution using low polymer concentrations ranging from 0.001–0.1% (w/v). Among others, PVP (10, 40, 360) was found to be an effective inhibitor.

Therefore, for the SD:4-ASA 1:1 form II cocrystal dynamic solubility studies were performed in 0.1 % (w/v) aqueous PVP solution. As it is known that PVP can enhance the solubility of sulfa drugs such as sulfamethoxazole (Loftsson et al., 1996) and sulfathiazole (Simonelli et al., 1976), the study was initially performed for pure SD and also for the form I cocrystal. The results showed, that no considerable increase in the SD concentration in 0.1% (w/v) PVP solution compared to water was observed for both pure SD and the form I cocrystal (Appendix 2, Figure A.2.8). In the case of pure SD, for early time points the concentration was rather decreased in 0.1% (w/v) PVP in comparison to water (Appendix 2, Figure A.2.8). Besides, the 4-ASA concentration of the form I cocrystal remained unchanged in both solution media (data not shown).

Based on these findings, the form II cocrystal was investigated under the same conditions, which revealed that the cocrystal remained stable over the entire time of the study. No phase changes were observed, as shown by analysis of the solid remaining phase by PXRD (Figure 3.19). The resulting concentration-time profile was consistent with the PXRD data. As illustrated in Figure 3.20, the addition of PVP stabilised and maintained the concentrations of both cocrystal components and thus the supersaturated state. The concentrations of SD and 4-ASA at t=60 minutes were $4.96 \times 10^{-3} \pm 0.11 \times 10^{-3}$ mmol/ml and $2.81 \times 10^{-3} \pm 0.09 \times 10^{-3}$ mmol/ml, respectively. When compared to the equivalent concentrations measured for the form I cocrystal in 0.1% (w/v) PVP solution (Appendix 2, Figure A.2.8) the form II cocrystal showed a more than 2-fold and an

approximately 1.2-fold higher SD and 4-ASA concentration, respectively. Likewise, the SD concentration of the form II cocrystal was 2-fold higher compared to pure SD, under the same experimental conditions (Figure 3.20).
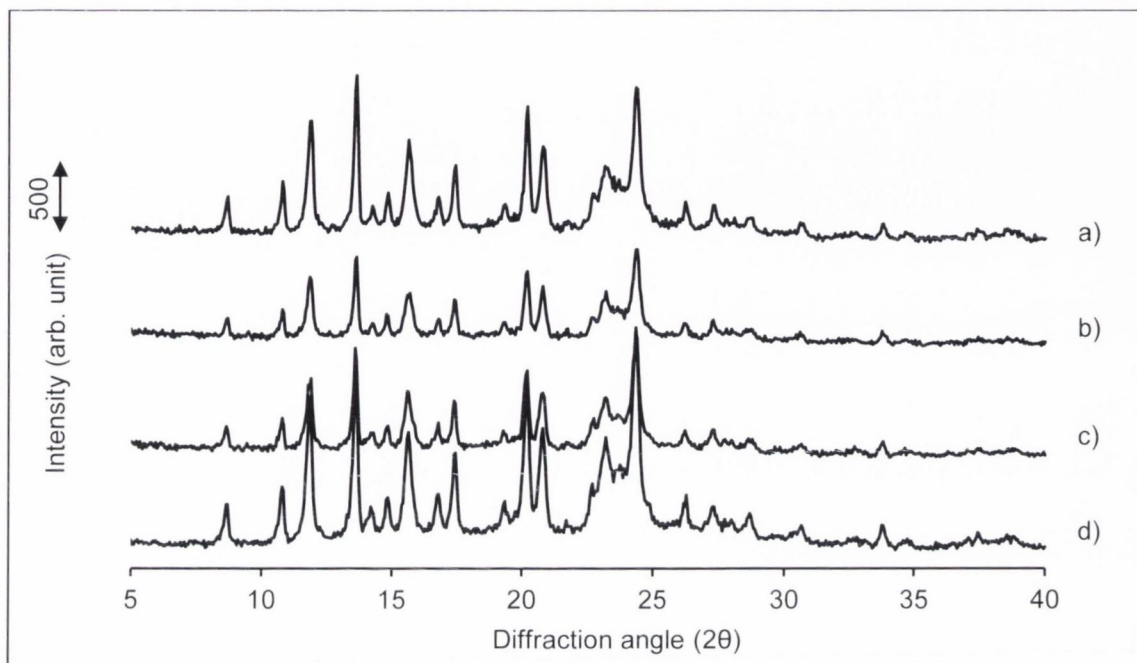

Figure 3.19: PXRD patterns of the solid phase of the SD:4-ASA 1:1 form II cocrystal during dynamic solubility studies in 0.1% (w/v) PVP solution. a) at 5 minutes, b) at 10 minutes, c) at 60 minutes compared to d) form II before subjected to solubility test.
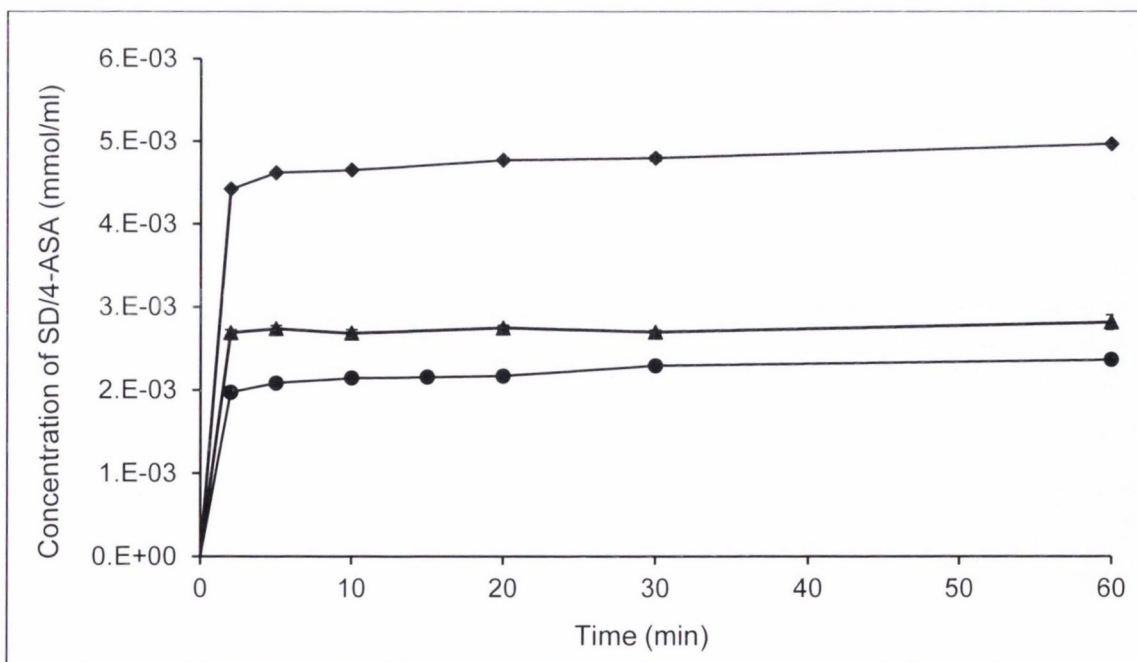

Figure 3.20: Concentration – time profile of the SD:4-ASA 1:1 form II cocrystal and pure SD in 0.1% (w/v) PVP solution (37 °C). Diamonds and triangles symbolise SD and 4-ASA concentrations of the form II cocrystal, respectively. Circles represent the concentrations of pure SD.

Overall, the solubility studies have shown that the SD:4-ASA 1:1 form I cocrystal is stable in water at 37 °C and its pH-dependent solubility can be predicted by a model established for a cocrystal composed of two amphoteric components. The SD:4-ASA 1:1 form II cocrystal was found to be unstable, transforming very rapidly to form I and SD by generating a supersaturated solution in water at 37 °C. The addition of 0.1% (w/v) PVP to the solution enabled the form II cocrystal to be stabilised and the supersaturated state to be maintained. The form II cocrystal revealed higher component concentrations compared to the form I cocrystal. For SD, which is the less water soluble component, the form II cocrystal showed a more than 2-fold higher concentration compared to form I and pure SD.

Based on the results obtained by ssNMR analysis which have emphasised the differences between the form I and form II cocrystal not only as a result of a difference in the molecular structure, but also due to a difference in the nature of the solid form, the higher component concentrations (supersaturated state) of the form II cocrystal were assumed to be attributed to its rather amorphous nature that has been observed. In experiments performed later (see section 3.3.5, pp. 96–102) it was found that in contrast to the liquid-assisted milled form I cocrystal, the spray-dried form II cocrystal revealed a non-equimolar stoichiometry with SD:4-ASA of 1:0.92 as a result of the spray drying conditions. The obviously higher SD molar amount was assumed to be free amorphous SD induced by spray drying and the reason for the observed higher SD solution concentrations. This assumption has been confirmed in a solubility experiment using a stoichiometrically equimolar form of the form II cocrystal with a higher degree of crystallinity, produced by solvent evaporation (see section 3.3.6, pp. 103–109). The equimolar form II cocrystal revealed a similar 4-ASA concentration to the non-equimolar (spray-dried) form II cocrystal and to the form I cocrystal. However, in the case of SD, the concentration difference with respect to form I was of a much lower order of magnitude (only around 1.2-fold higher) than it was observed for the non-equimolar form II (spray-dried) cocrystal. It was concluded that, despite the difference in stability, the actual solubilities of the form I and form II cocrystals are similar. Details of these results can be found in Appendix 2, Figure A.2.9 and Figure A.2.10.

3.3.4 The SD:4-ASA 1:1 form I and form II cocrystal – dissolution studies

Further investigations were performed by intrinsic dissolution rate studies. The intrinsic dissolution profiles of the pure components are shown in Figure 3.21. The dissolution of both components was linear over time ($R^2 > 0.97$), whereas 4-ASA dissolved around nine times faster than SD (Table 3.4). Analysis of the compact surface at the end of the study by IR and PXRD verified that no phase changes occurred (Appendix 2, Figure A.2.11 and Figure A.2.12).
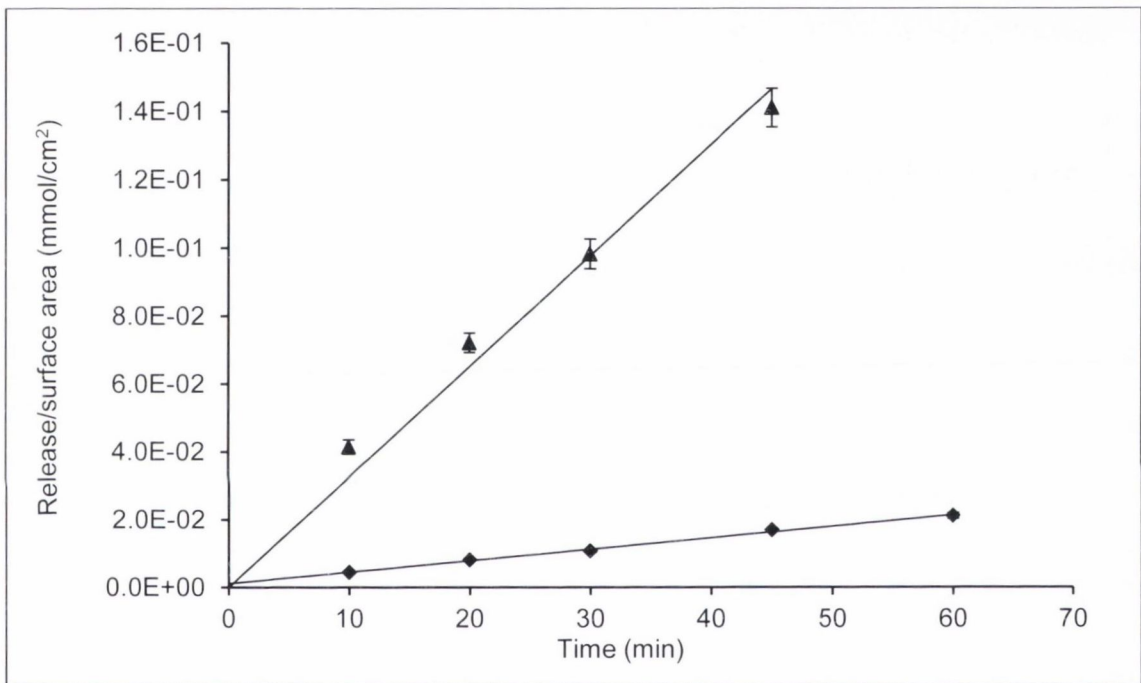

Figure 3.21: Dissolution profiles of SD (diamonds) and 4-ASA (triangles) in water at 37 °C.

Table 3.4: Intrinsic dissolution rates of the SD:4-ASA 1:1 form I and form II cocrystal (CC), a 1:1 physical mixture (PM) and the pure components. Where not otherwise stated, the data refer to water (37 °C).

Material	IDR (mmol/min/cm^2)	Difference (α=0.05)
SD	$3.64\times10^{-4} \pm 0.12\times10^{-4}$	–
4-ASA	$32.6\times10^{-4} \pm 1.26\times10^{-4}$	–
form I CC	SD: $5.09\times10^{-4} \pm 0.27\times10^{-4}$ 4-ASA: $6.52\times10^{-4} \pm 0.33\times10^{-4}$	SD: n.s. to form II CC (in PVP), s. to all others 4-ASA: s. to all
form II CC	SD: $6.08\times10^{-4} \pm 0.13\times10^{-4}$ 4-ASA: $5.25\times10^{-4} \pm 0.02\times10^{-4}$	SD: s. to all 4-ASA: s. to all
form II CC (in 0.1% PVP)	SD: $4.66\times10^{-4} \pm 0.06\times10^{-4}$ 4-ASA: $3.58\times10^{-4} \pm 0.00\times10^{-4}$	SD: n.s. to form I CC, s. to all others 4-ASA: n.s. to PM**, s. to all others
PM	SD: $3.89\times10^{-4} \pm 0.09\times10^{-4}$ 4-ASA: $9.78\times10^{-4} \pm 0.67\times10^{-4}$* 4-ASA: $4.05\times10^{-4} \pm 0.28\times10^{-4}$**	SD: n.s. to pure SD, form II CC (in PVP), s. to all others 4-ASA*: s. to all 4-ASA**: n.s. to form II CC (in PVP), s. to all others

*initial rate (estimated from t=0 until t of 1st measuring point)

** limiting rate

s. = significantly different (p<0.05)

n.s. = not significantly different (p>0.05)

The SD:4-ASA 1:1 form I cocrystal showed linear (R^2 > 0.99), non-equimolar release with a ratio of 1:1.3 of SD:4-ASA at each time point (Figure 3.22). However, no changes of the surface composition were detected as confirmed by IR and PXRD analysis (Appendix 2, Figure A.2.11 and Figure A.2.12). It was found that SD had a 1.4-fold higher and 4-ASA a 5-fold lower dissolution rate compared to the pure components (Table 3.4).
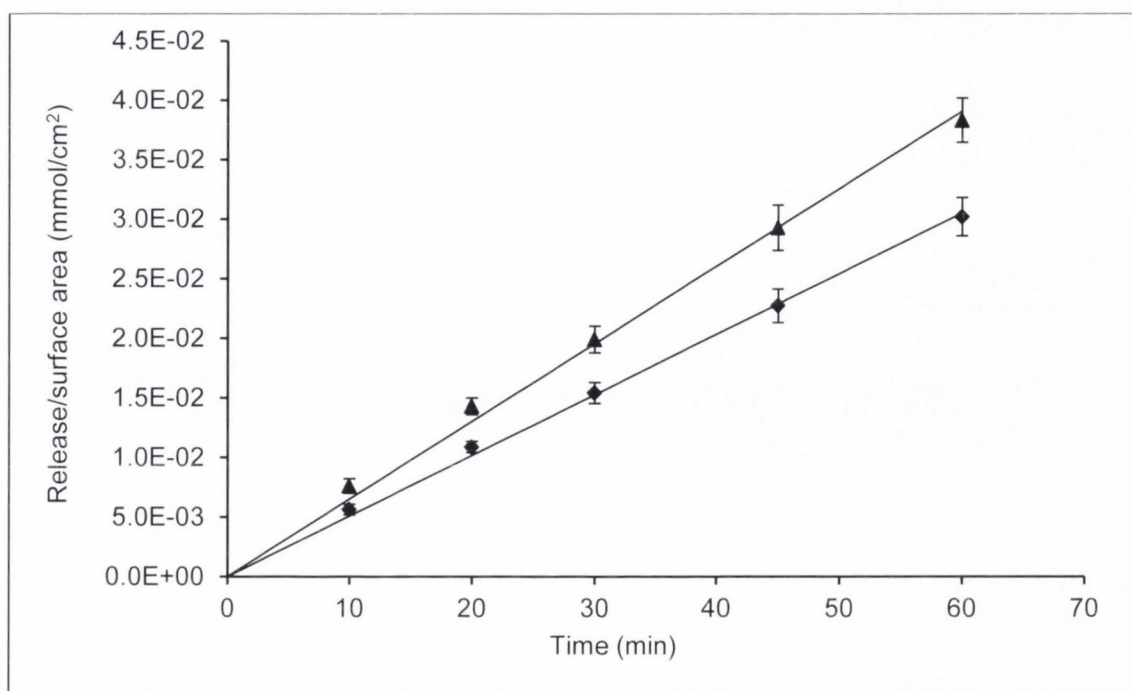
Figure 3.22: Dissolution profiles of the SD:4-ASA 1:1 form I cocrystal in water at 37 °C. Diamonds symbolise SD, triangles represent 4-ASA.

In the case of SD:4-ASA 1:1 form II cocrystal the dissolution was initially measured from 10–60 minutes. However, at the end of the study the surface composition revealed changes. Analysis by IR spectroscopy of the compact surface detected the appearance of two weak bands at 3442 and 1477 cm^{-1} corresponding to SD and for the bands at 3372 and 671 cm^{-1} shoulders, attributable to the form I cocrystal and/or SD were visible (Figure 3.23 a). Additional analysis by PXRD revealed the presence of diffraction peaks at 9.35 and 10.25° 2θ, characteristic of SD and the form I cocrystal, respectively (Figure 3.24 a). These results showed that the form II cocrystal transformed to form I and SD during dissolution, which was also observed in solubility studies, as has been demonstrated earlier.
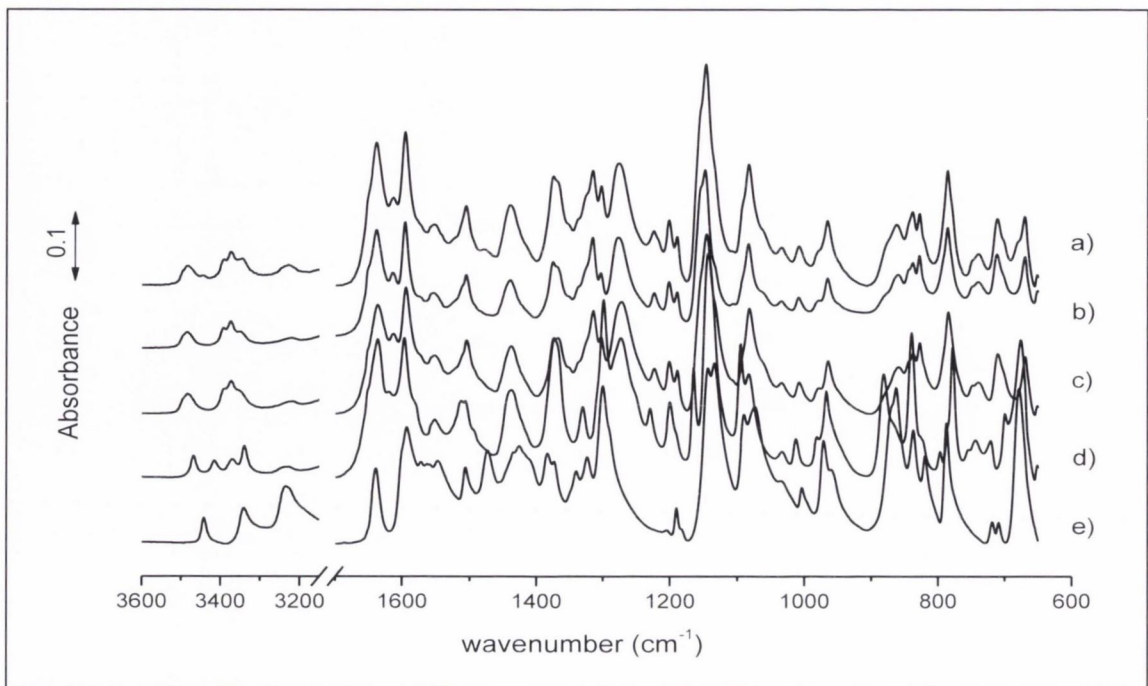
Figure 3.23: IR spectra of compact surface after intrinsic dissolution studies: a) SD:4-ASA 1:1 form II, at 60 minutes, b) SD:4-ASA 1:1 form II, at 10 minutes compared to compacts before dissolution: c) SD:4-ASA 1:1 form II, d) SD:4-ASA 1:1 form I and e) SD, raw material.
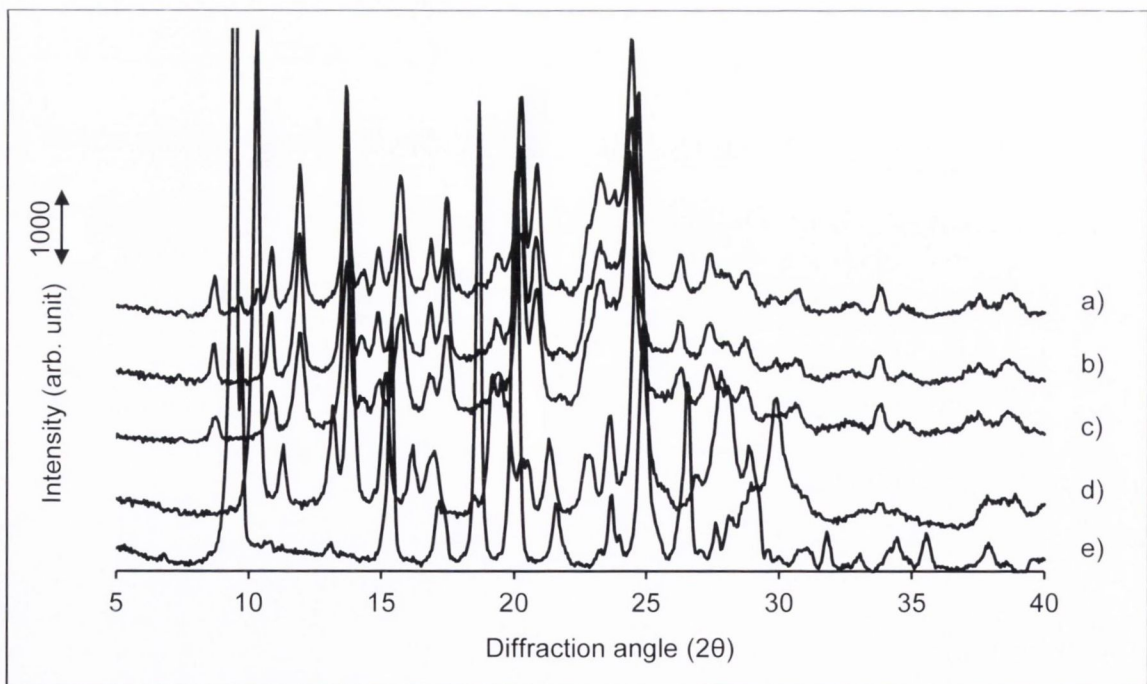

Figure 3.24: PXRD patterns of compact surface after intrinsic dissolution studies: a) SD:4-ASA 1:1 form II, at 60 minutes, b) SD:4-ASA 1:1 form II, at 10 minutes compared to compacts before dissolution: c) SD:4-ASA 1:1 form II, d) SD:4-ASA 1:1 form I and e) SD, raw material.

Further studies were therefore performed for lower time points (2–10 minutes) and no phase changes at the surface of the compact were detected at 10 minutes as confirmed by IR and PXRD analysis (Figure 3.23 b, Figure 3.24 b). The dissolution profiles are shown in Figure 3.25. The dissolution of both components was linear ($R^2 > 0.98$) and nearly equimolar (1:0.9 SD:4-ASA) over time. For SD, the dissolution rate was around 1.7-fold and 1.2-fold higher compared to pure SD and the form I cocrystal, respectively, while 4-ASA showed a more than 6-fold and approximately 1.2-fold lower dissolution than pure 4-ASA and the form I cocrystal, respectively (Table 3.4).

The same experiment was conducted in 0.1% (w/v) PVP solution, as it has been shown in solubility studies that PVP prevents phase transformation of the form II cocrystal. A linear ($R^2 > 0.99$) release of both components (Figure 3.25) was observed. However, the dissolution rates differed significantly from those obtained in water for the form II cocrystal. It was found that SD dissolved at a 1.3-fold lower rate and 4-ASA at a 1.5-fold lower rate than the corresponding pure components in water (Table 3.4).
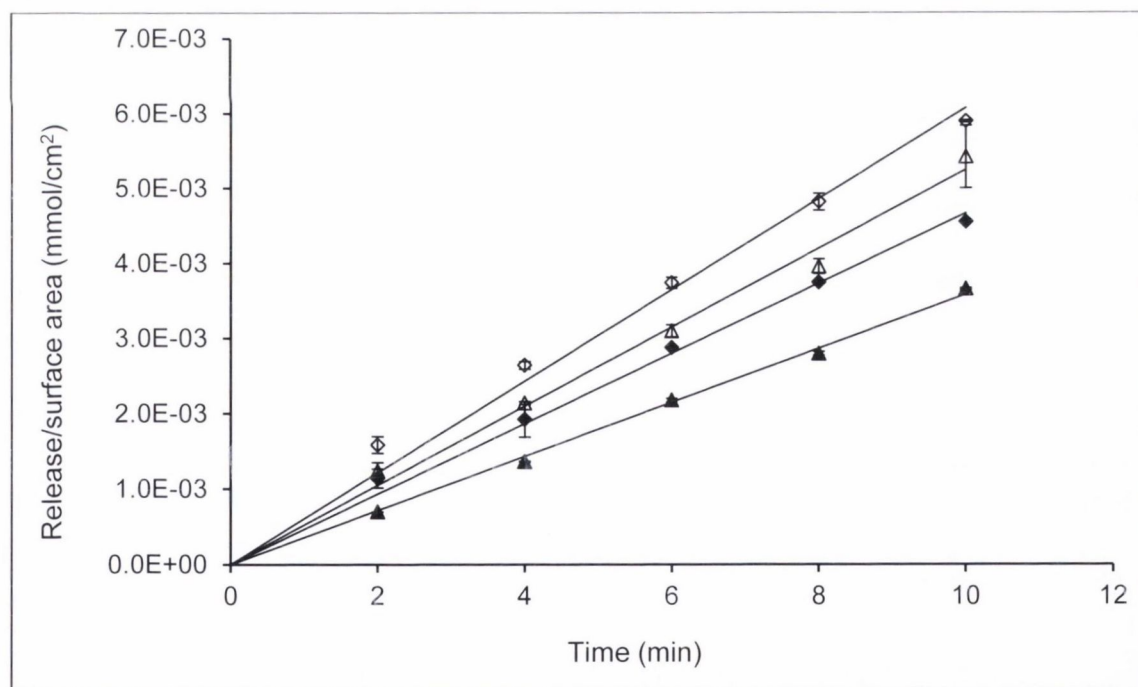

Figure 3.25: Dissolution profiles of the SD:4-ASA 1:1 form II cocrystal in water and in 0.1% (w/v) PVP solution at 37 °C. Open diamonds and triangles symbolise SD and 4-ASA in water, respectively. Closed diamonds and triangles represent SD and 4-ASA in PVP solution, respectively.

For comparison, the dissolution behaviour of a physical equimolar mixture of SD and 4-ASA was studied. The corresponding dissolution profiles are shown in Figure 3.26. Both components showed linear profiles ($R^2 > 0.99$), although 4-ASA dissolved initially faster, followed by a slower linear release. The dissolution rate of SD from the physical mixture did not differ significantly to pure SD, but was 1.3-fold and 1.5-fold lower than from the form I and form II (in water) cocrystal, respectively (Table 3.4). The dissolution rate of 4-ASA from the physical mixture was initially high, but more than 3-fold lower than pure 4-ASA, and revealed a slower dissolution from 10–60 minutes (limiting rate) of more than half of the initial rate (Table 3.4, Figure 3.26). When compared to the form I and form II cocrystal (in water), the 4-ASA dissolution rate was 1.6-fold and 1.3-fold lower from the physical mixture (with respect to its limiting rate) (Table 3.4).
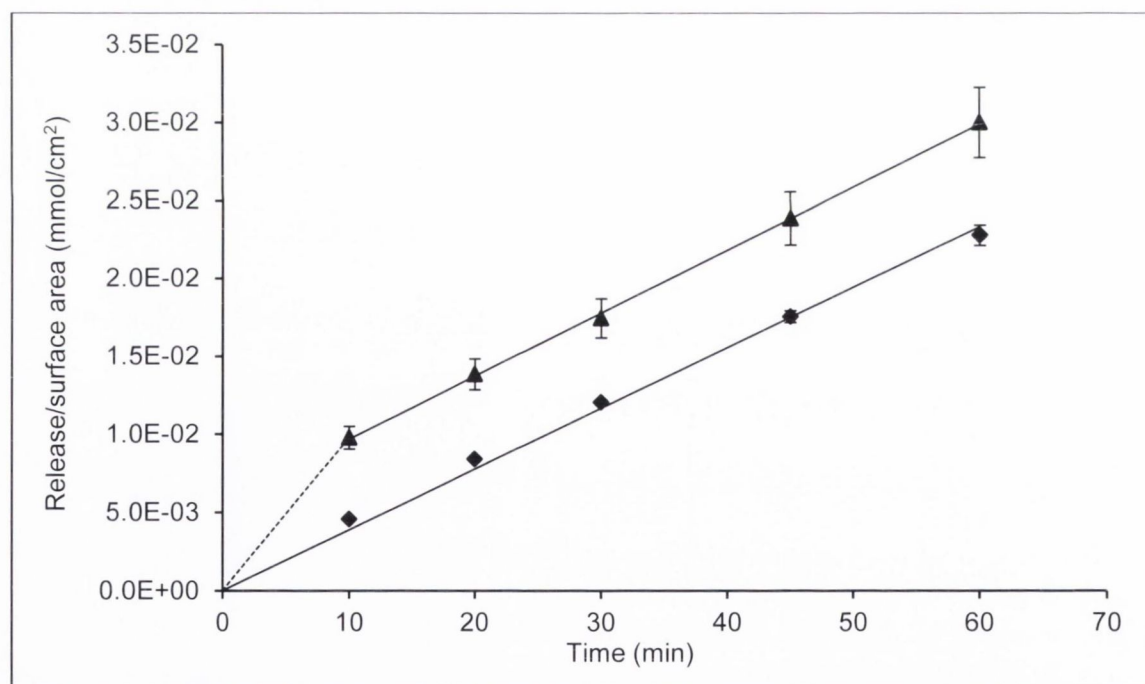

Figure 3.26: Dissolution profiles of SD:4-ASA 1:1 physical mixture in water at 37 °C. Diamonds symbolise SD, triangles represent 4-ASA. The dashed line refers to the initial rate of 4-ASA.

Analysis of the physical mix compact surface at the end of the study by IR and PXRD showed that the surface composition had changed. As illustrated in Figure 3.27 a, IR spectroscopy detected the absence of bands attributed to 4-ASA and the appearance of two weak bands, visible at around 778 and 700 cm^{-1} indicative of the form I cocrystal. Analysis by PXRD confirmed the presence of the form I cocrystal attributed to the characteristic diffraction peaks at around 10.25 and 13.75° 2θ (Figure 3.28 a). In contrast to the IR analysis, the PXRD pattern of the physical mixture after dissolution displayed still diffraction peaks corresponding to 4-ASA. This may be explained by a greater penetration depth of the X-rays into the compact compared to the IR beam using the ATR-FTIR technique.
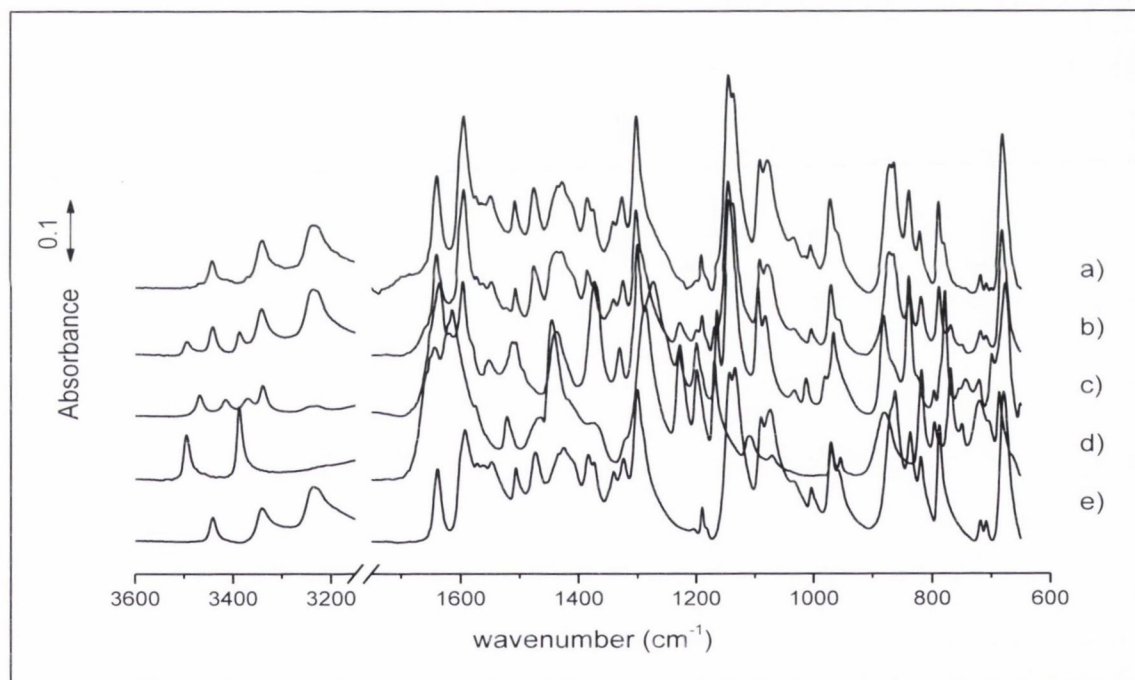

Figure 3.27: IR spectra of compact surfaces of a) SD:4-ASA 1:1 physical mixture, after dissolution compared to b) SD:4-ASA 1:1 physical mixture, before dissolution, c) SD:4-ASA 1:1 form I cocrystal, before dissolution, d) 4-ASA, before dissolution and e) SD, raw material, before dissolution.

Figure 3.28: PXRD patterns of compact surfaces of a) SD:4-ASA 1:1 physical mixture, after dissolution compared to b) SD:4-ASA 1:1 physical mixture, before dissolution, c) SD:4-ASA 1:1 form I cocrystal, before dissolution, d) 4-ASA, before dissolution and e) SD, raw material, before dissolution.
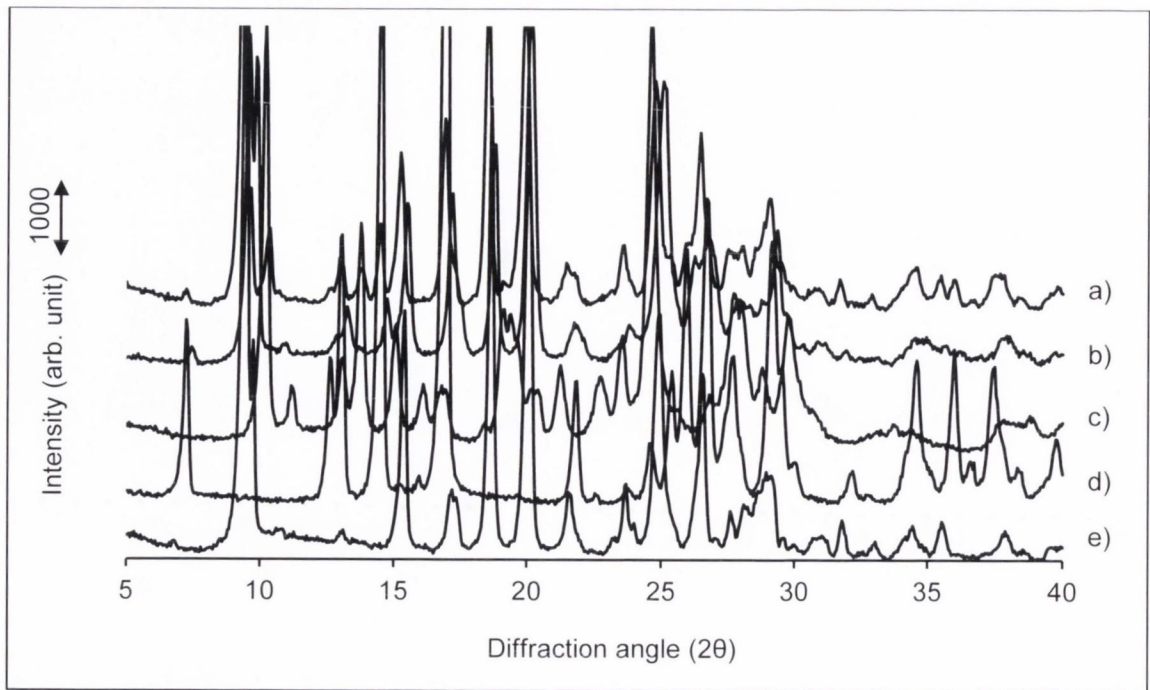
Characterisation of the surface morphology of the compacts before and after dissolution was performed by SEM analysis. The pictures are illustrated in Figure 3.29 and Figure 3.30.
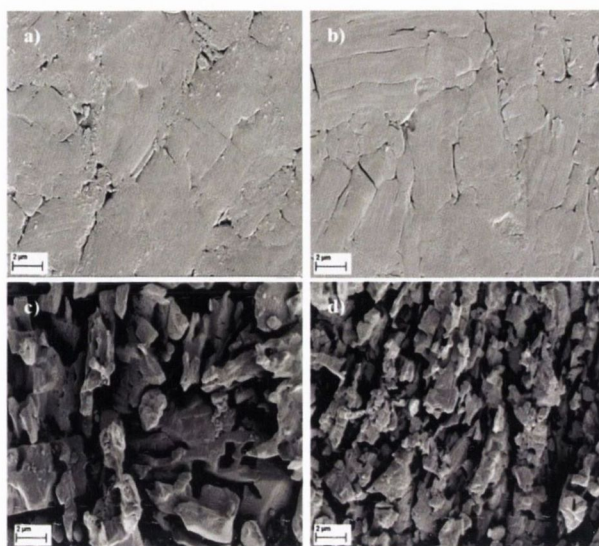

Figure 3.29: SEM images of disk surfaces before dissolution of a) SD, b) 4-ASA compared to disk surfaces after dissolution of c) SD and d) 4-ASA.
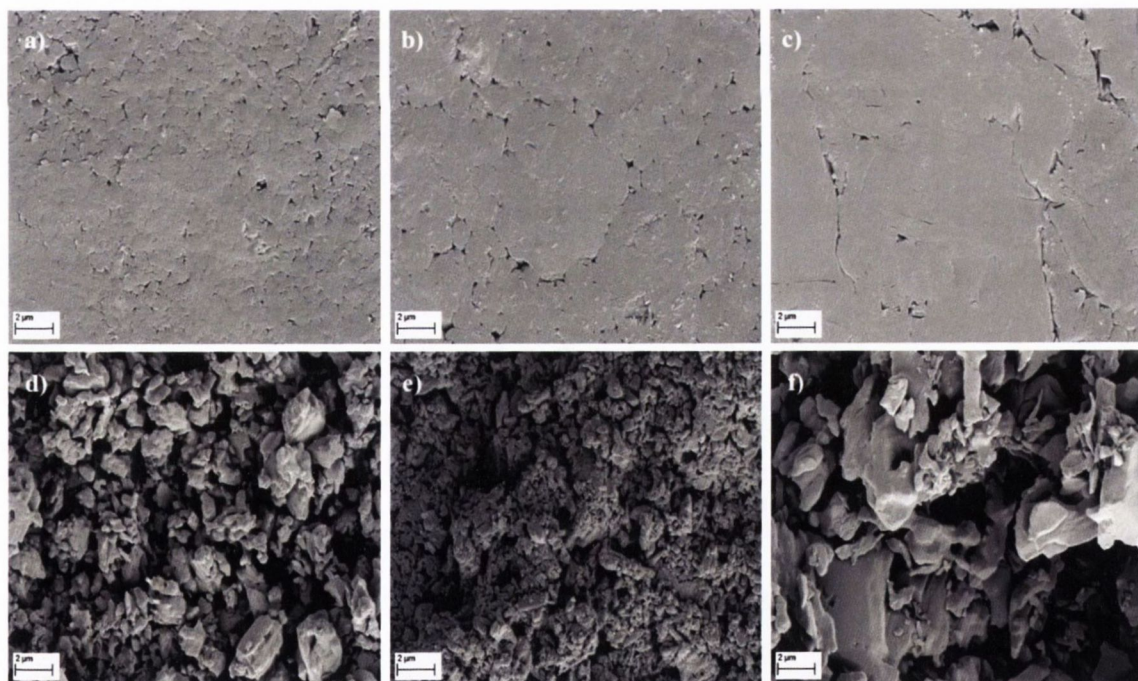

Figure 3.30: SEM images of disk surfaces before dissolution of a) SD:4-ASA 1:1 form I cocrystal, b) SD:4-ASA 1:1 form II cocrystal, c) a physical mixture compared to disk surfaces after dissolution of d) SD:4-ASA 1:1 form I cocrystal, e) SD:4-ASA 1:1 form II cocrystal and f) a physical mixture.

Each compact surface before dissolution appeared relatively smooth and homogenous (Figure 3.29 a–b, Figure 3.30 a–c), whereas after dissolution distinctly texturised surfaces with voids indicative of the release of component(s) were observed (Figure 3.29 c–d, Figure 3.30 d–f). When comparing the pure components, 4-ASA showed larger voids than SD, likely to be a result of its faster dissolution (Figure 3.29 c–d). The surface of the form I cocrystal after dissolution (Figure 3.30 d) revealed smaller cavities than the pure components, but larger and less uniform in morphology than the form II cocrystal (Figure 3.30 d–e). On the other hand, the physical mixture (Figure 3.30 f) showed a less uniform surface with larger gaps than the form I cocrystal, but the surface morphology was different compared to the single components. From all materials, the form II cocrystal revealed the smallest gaps after dissolution (Figure 3.30 e). Considering the dissolution behaviour of the composite systems, the larger gaps of the physical mixture compared to the form I cocrystal might be a result of the faster initial release of 4-ASA from the physical mixture, while the little gaps observed for the form II corystal might be attributed to the lower 4-ASA dissolution when compared to the form I cocrystal and the physical mixture (with respect to its initial rate).

In summary, the results from the dissolution studies have shown that both SD:4-ASA 1:1 cocrystals, form I and form II, revealed enhanced dissolution rates of the poorly water soluble SD in comparison to a physical equimolar mixture and pure SD. Besides, the component dissolution rates were in the same rank order as the corresponding solubilities. For example, for the form I cocrystal, the ratio of SD:4-ASA was 1:1.3 for the dissolution rates and 1:1.4 for the solubilities. Similarly, for the form II cocrystal, the SD:4-ASA ratios were found to be 1:0.8 in the case of the dissolution rates and 1:0.6 in the case of the solubilities (refers to data in PVP solution). When comparing the two cocrystal forms, form II revealed a higher dissolution rate of SD and a lower dissolution rate of 4-ASA than form I. These findings were in agreement with the results from solubility studies (referring to dynamic solubilities in the case of form II and referring to solubilities from transition concentrations - equilibrium solubility in the case of form I). Furthermore, the dissolution rates of the form II cocrystal measured in water and in 0.1% (w/v) PVP solution differed significantly, although the dissolution kinetics were linear (with zero origin) in both media. The dissolution rates of both, SD and 4-ASA were significantly lower in 0.1% (w/v) PVP solution than those determined in water.

These results might relate to the findings from the dynamic solubility studies, at least in the case of SD, where, for pure SD, the concentrations at the early sampling times were lower in 0.1% (w/v) PVP solution compared to water. A similar case has been reported by Gibaldi and Weintraub (1968) for the dissolution and solubility of salicylic acid/PVP compressed mixtures. The decreased dissolution rate of salicylic acid in the presence of PVP was explained as a result of the increased viscosity in the diffusion layer and the consequently smaller diffusion coefficient (Gibaldi and Weintraub, 1968). The same assertion can be made for the obtained dissolution rates of SD and 4-ASA since the measured viscosity of a 0.1% (w/v) PVP solution was 0.79 mPa·s in comparison to water, which revealed a lower value of 0.72 mPa·s.

For a physical equimolar mixture of SD and 4-ASA it was shown that 4-ASA dissolved fast initially, leaving a layer of SD and form I cocrystal behind. The presence of the form I cocrystal at the surface of the compact indicated that the cocrystal can be formed from water, possibly induced by the initially faster release of 4-ASA compared to SD, generating a saturated solution (with respect to 4-ASA) in the surrounding layer, from which the cocrystal precipitates after SD has been released into solution. These findings can be expected from the established pH-solubility profile (Figure 6.2) as presented under section 3.3.3, p. 77. Besides, the physical mixture revealed a faster initial release of 4-ASA than the form I and form II cocrystal which is assumed to be a result of the absence of intermolecular forces such as hydrogen-bonds. Similar findings have been demonstrated for the physical mixture and the cocrystal of benzamide and dibenzyl sulfoxide described in Chapter 2.

Characterisation of the compact surfaces after dissolution by SEM analysis revealed for all materials distinctively texturised surface morphologies with voids of different sizes attributable to the component(s) release rates.

3.3.5 SD:4-ASA 1:1 form I and form II cocrystal – stability studies

Dynamic vapour sorption (DVS)

The dynamic vapour sorption and desorption isotherms of the form I and form II cocrystal are illustrated in Figure 3.31. In comparison to the form II cocrystal, the form I cocrystal sorbed less water over the entire humidity range. The maximum water sorption of the form I cocrystal was below 0.3%, where most water was sorbed between 70 and 90%. The desorption behaviour was similar with a slight hysteresis effect in the humidity range of 90 to 40% RH, followed by merging with the sorption profile below 40% RH. In contrast, the form II cocrystal showed a maximum water sorption below 1% and showed a relatively strong increase in water sorption between 70 and 90% RH. The desorption behaviour was similar and associated with a small hysteresis effect over the entire humidity range.

PXRD analysis of the materials recovered at the end of the experiment (0% RH) and at 90% RH revealed no changes compared to the starting materials (Figure 3.32), which confirmed that both cocrystal forms remained unchanged under DVS experimental conditions.
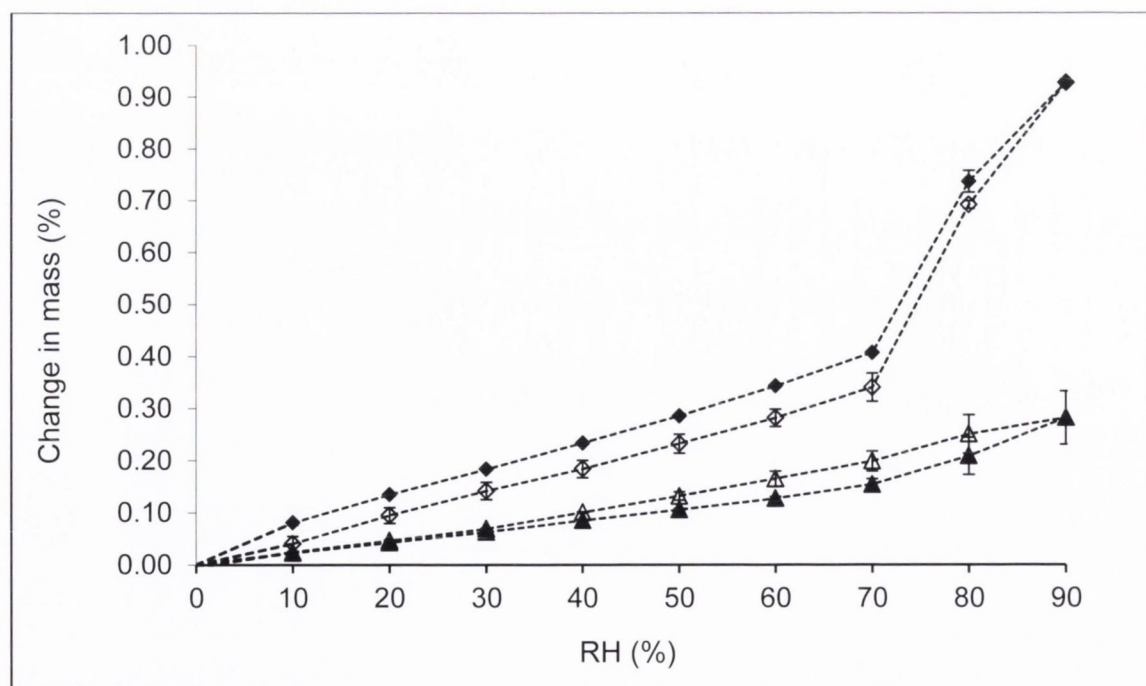

Figure 3.31: Moisture sorption and desorption profiles of SD:4-ASA 1:1 form I (closed and open triangles) and form II (closed and open diamonds) cocrystal at 25 °C.
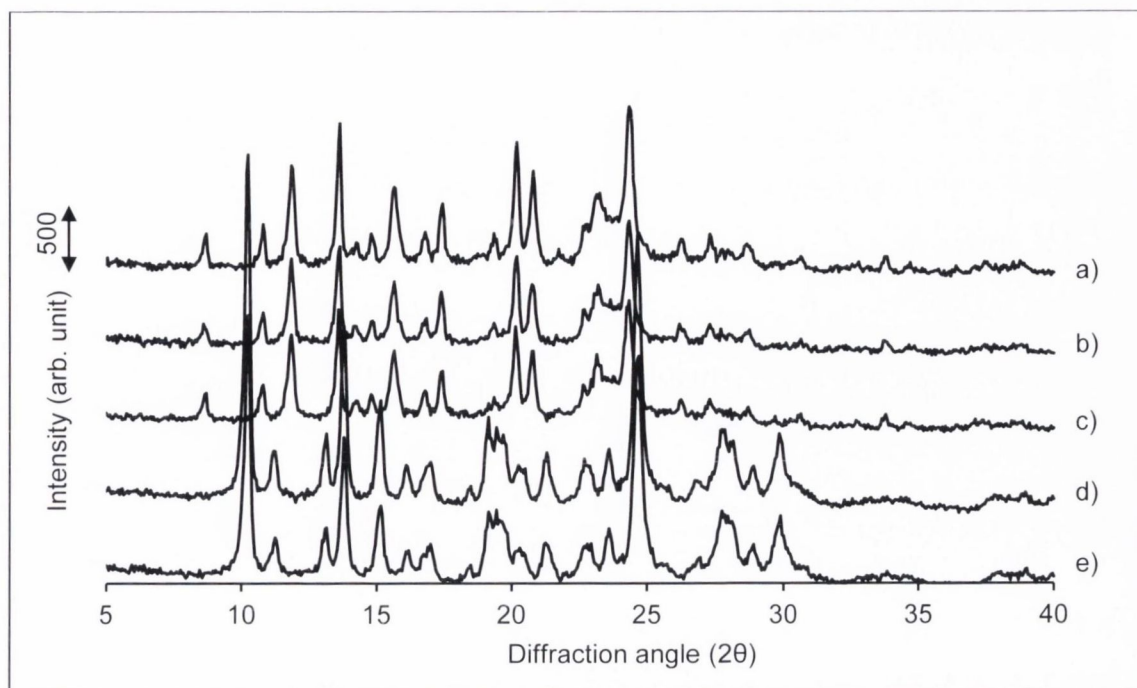
Figure 3.32: PXRD patterns before and after DVS experiments. a) SD:4-ASA 1:1 form II cocrystal, recovered after DVS at 90% RH, b) SD:4-ASA 1:1 form II cocrystal, recovered after DVS at 0% RH, c) SD:4-ASA 1:1 form II cocrystal, before DVS study, d) SD:4-ASA 1:1 form I cocrystal, recovered after DVS at 0% RH and e) SD:4-ASA 1:1 form I cocrystal, before DVS study.

From the DVS studies, it can be summarised that the form I and form II cocrystals were stable when exposed to different humidities between 0 and 90% RH. Referring to the hygroscopicity classification system established by Murikipudi et al. (2013) on the basis of sorption analysis, the form I and form II cocrystals can be classified as "slightly hygroscopic" due to their water uptake ranging between 0.2–2% (w/w). The generally higher water sorption of the form II cocrystal compared to the form I cocrystal is possibly attributed to differences in the specific surface area of the materials (not controlled) resulting from the different methods which have been used for cocrystal production. As it was shown from characterisation by solid state NMR, the form I cocrystal was more ordered (crystalline), whereas the form II cocrystal showed amorphous-like behaviour. Amorphous materials tend to sorb more water vapour than crystalline materials, which would explain the DVS results of the form II cocrystal relative to form I.

Long-term stability studies

The investigation of the form I and form II cocrystals vary in their stability with time revealed that both forms did not undergo changes over 12 months storage under conditions of 60% RH at 25 °C. This was confirmed by PXRD analysis as displayed in Figure 3.33 and Figure 3.34, which showed that the diffraction patterns remained unchanged over the entire time for both, the form I (Figure 3.33) and the form II cocrystal (Figure 3.34).
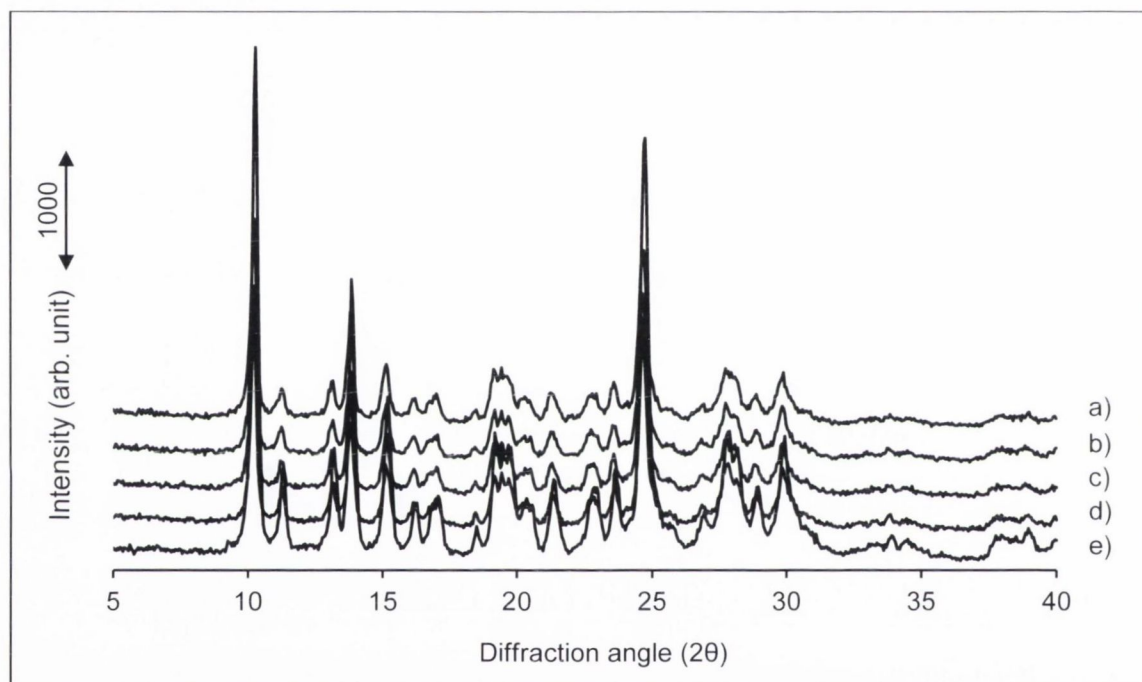

Figure 3.33: PXRD patterns of the SD:4-ASA 1:1 form I cocrystal. a) Before the study and analysed at different time points during long-term stability test: b) 1 month c) 2 months d) 6 months e) 12 months.

Figure 3.34: PXRD patterns of the SD:4-ASA 1:1 form II corystal. a) Before the study and analysed at different time points during long-term stability test: b) 1 month c) 2 months d) 6 months e) 12 months.

Further characterisation by DSC (Figure 3.35, Figure 3.36) and IR spectroscopy (Appendix 2, Figure A.2.13 and Figure A.2.14) was consistent with the results from PXRD. No substantial changes in the thermal behaviour and the IR spectra of the form I (Figure 3.35, Appendix 2 - Figure A.2.13) and form II (Figure 3.36, Appendix 2 - Figure A.2.14) cocrystal occurred over 12 months at the given storage conditions.

Figure 3.35: DSC thermograms of the SD:4-ASA 1:1 form I cocrystal. a) Before the study and analysed at different time points during long-term stability test: b) 1 month c) 2 months d) 6 months e) 12 months.
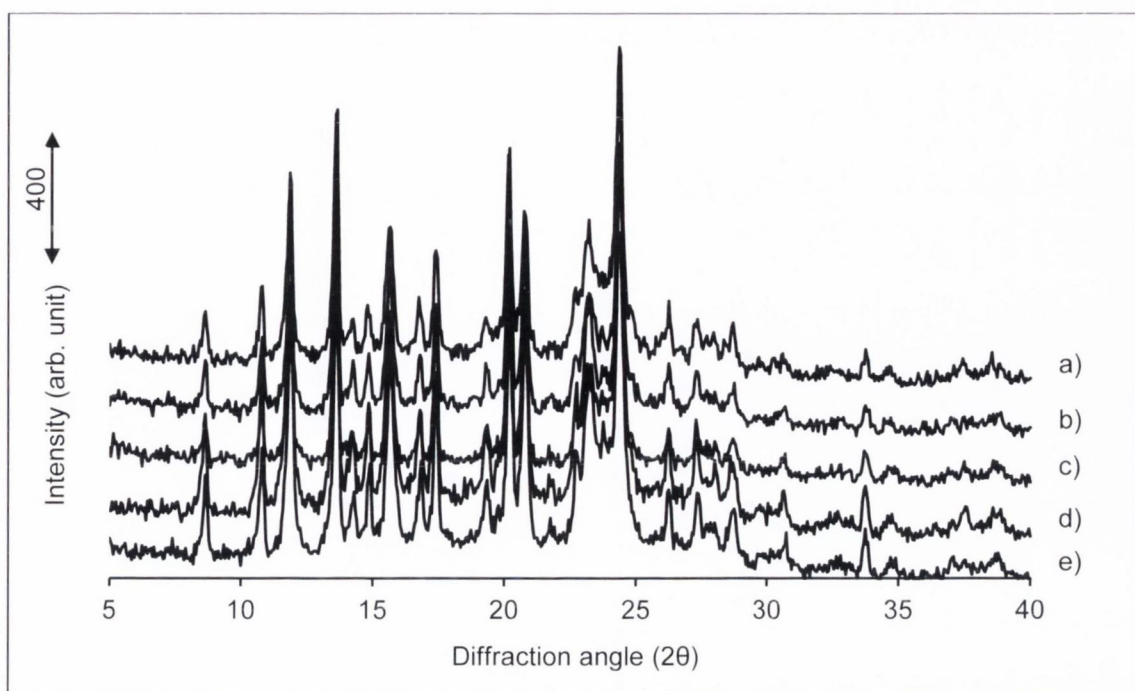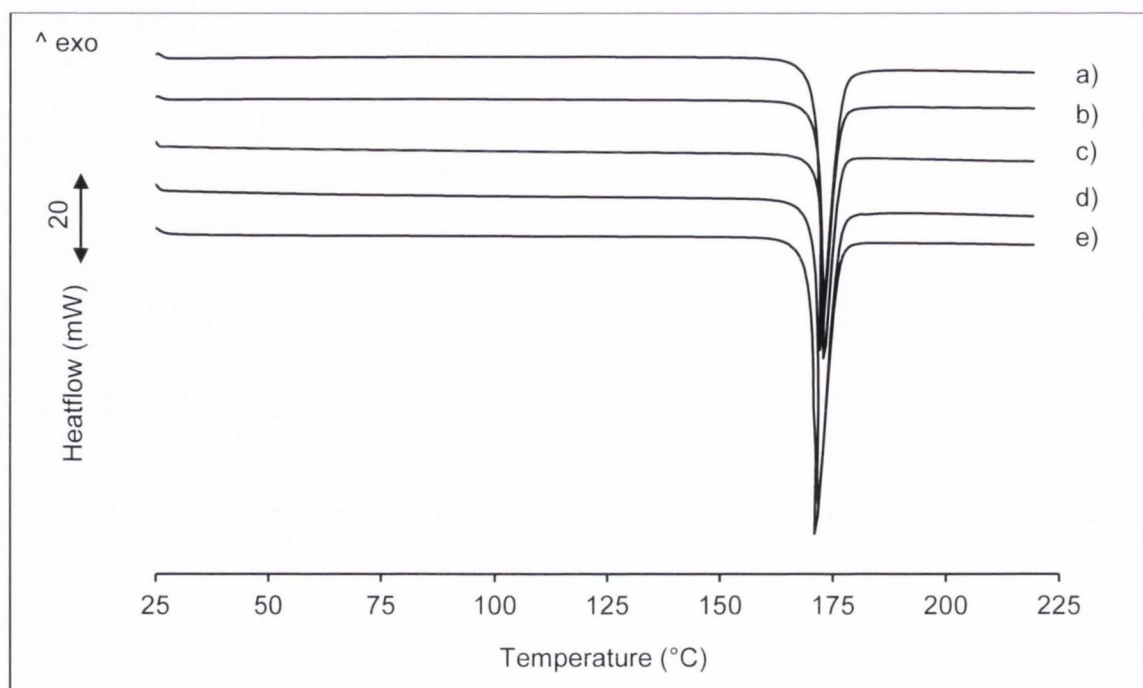

Figure 3.36: DSC thermograms of the SD:4-ASA 1:1 form II corystal. a) Before the study and analysed at different time points during long-term stability test: b) 1 month c) 2 months d) 6 months e) 12 months.
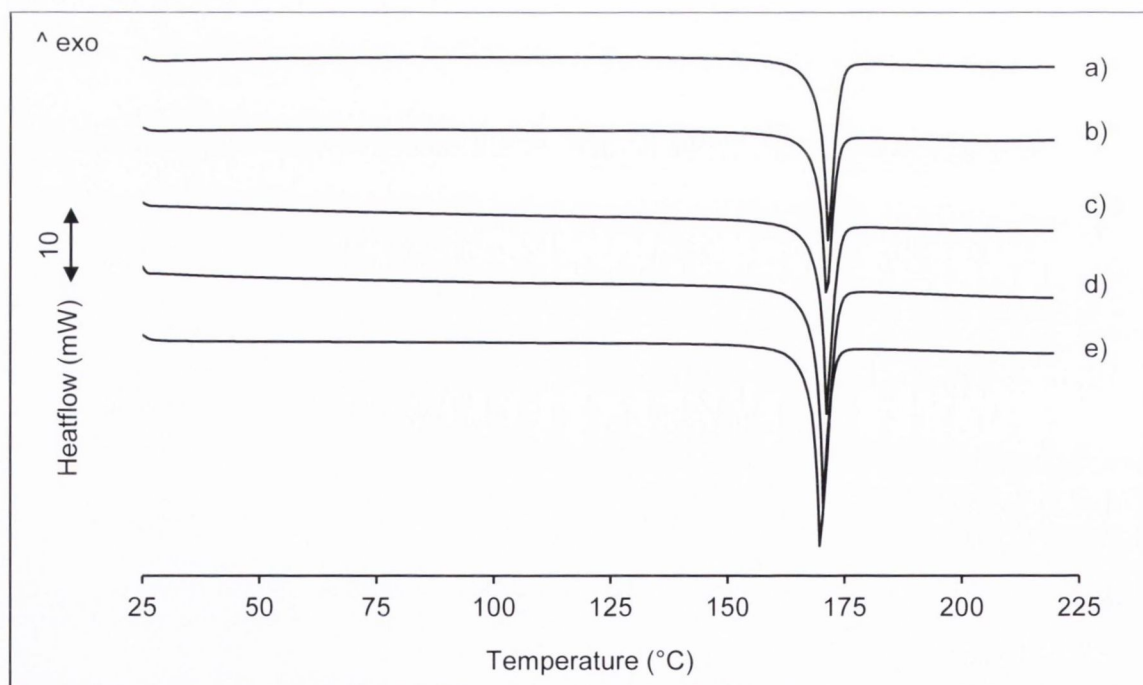
Analysis by HPLC showed that both materials did not undergo chemical changes during the stability study. As shown in Figure 3.37 and Table 3.5, the concentrations of the form I and form II cocrystal have not changed significantly (ICH guidelines October, 1993) and the SD:4-ASA molar ratio remained stable over time. However, the SD:4-ASA molar ratio differed between form I and form II. The form II cocrystal revealed an approximately 6% lower molar 4-ASA amount than form I (Table 3.5). Analysis by liquid NMR has further confirmed this difference in stoichiometry of the two forms. Details can be found in Appendix 2, Figure A.2.15 and Table A.2.2.
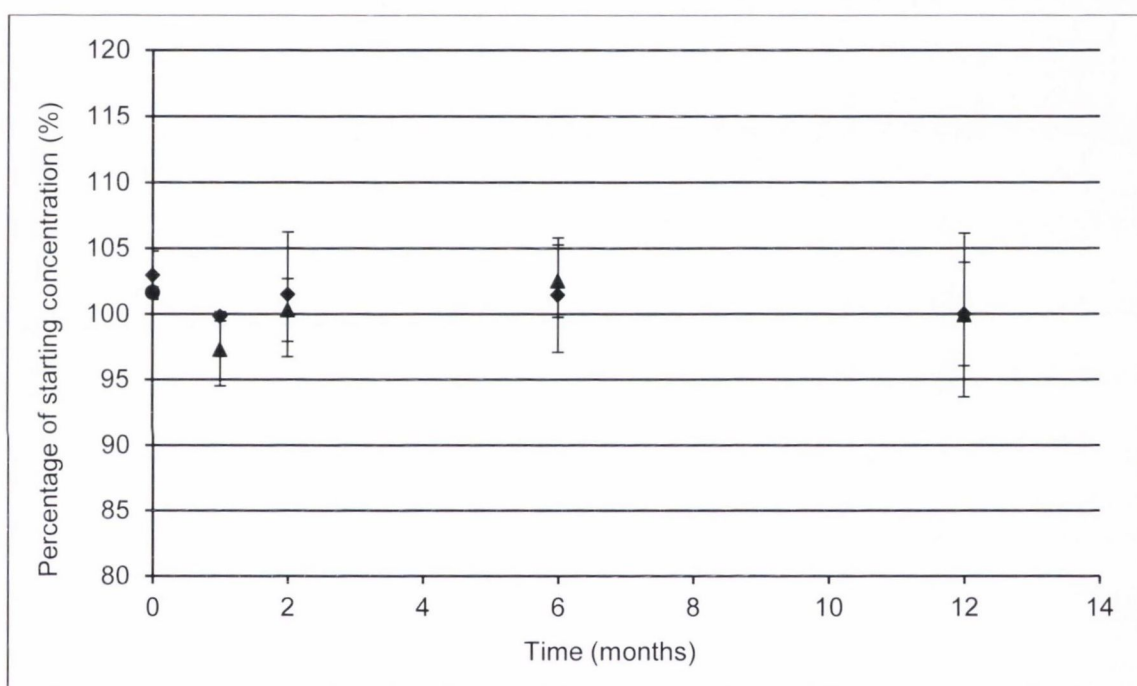

Figure 3.37: Chemical stability of the SD:4-ASA 1:1 form I (triangles) and form II (diamonds) cocrystal over 12 months storage at 60% RH and 25 °C, analysed by HPLC. The SD:4-ASA molar ratio corresponding to each data point is presented in Table 3.5.

Table 3.5: Molar concentration ratios of the SD:4-ASA 1:1 form I and form II cocrystal determined by HPLC during long-term stability test.

Test time (months)	form I cocrystal	form II cocrystal
0	1:0.97	1:0.92
1	1:0.98	1:0.90
2	1:0.97	1:0.92
6	1:0.98	1:0.93
12	1:0.97	1:0.91

In summary, the results of the long-term stability study have shown that the form I and form II cocrystal were stable over 12 months at storage conditions of 60% RH and 25 °C, which was confirmed by the consistency of PXRD, DSC, FTIR and HPLC data. Moreover, it was found that the form II cocrystal (produced by spray drying) differed from the form I cocrystal (produced by liquid-assisted milling) in its stoichiometry, where the molar 4-ASA amount was found to be approximately 6% lower compared to form I.

When comparing the different methods used to produce the cocrystals, spray drying is a technique which requires heat and works under fast evaporation from a liquid into a solid material, conditions which are different to liquid-assisted milling. It is suggested that the lower 4-ASA amount of the form II cocrystal, obtained by spray drying might be a result of sublimation or evaporation occurring during processing.

3.3.6 SD:4-ASA 1:1 form II cocrystal - structure determination

For determination of the crystal structure using single crystal X-ray diffraction (SC-XRD), several attempts were made to grow single crystals of sufficient size of the form II cocrystal, where it was found that single crystals in the form of needles can grow from ethanol and acetone by solvent evaporation at elevated temperature using a 1:1.1 SD:4-ASA ratio (for details, see method description 3.2.2.15). Characterisation of the obtained crystals by PXRD and DSC confirmed consistency with the spray-dried product (Appendix 2, Figure A.2.16 and Figure A.2.17). The stoichiometry was determined by HPLC and a molar ratio of SD:4-ASA of 1:0.99 was found (data not shown).

However, due to observed non-crystallographic systematic absences, the structure could not be solved in a first step. Further investigations were undertaken and will be explained later.

Alternatively, the PXRD technique was used to determine the crystal structure, which has been reported to be a successful tool when single crystal data cannot be obtained (Harris and Cheung, 2004; Lapidus et al., 2010). The use of high resolution laboratory X-ray powder diffraction data enabled the crystal structure of the form II cocrystal to be solved and refined and confirmed the presence of a polymorphic form of the SD:4-ASA 1:1 cocrystal. It was found that the form II cocrystal reveals an orthorhombic unit cell with $P2_12_12_1$ space group, whereas the form I cocrystal was reported to exist in a triclinic unit cell with space group P-1 (Caira, 1992). A summary of the crystallographic data is presented in Table 3.6 and full details can be found in Appendix 2, Tables A.2.3–A.2.7.

Table 3.6: Crystallographic data of the SD:4-ASA 1:1 form I cocrystal (Caira, 1992) compared to the form II cocrystal (based on PXRD calculations).

Lattice parameter	form I	form II
Space group	Triclinic, P-1	Orthorhombic, $P2_12_12_1$
Appearance	Prisms	Needles
Unit cell parameters		
a	8.205 (6) Å	23.8057 (16) Å
b	9.449 (3) Å	7.8125 (5) Å
c	14.161 (2) Å	11.2661 (9) Å
α	107.02 (2) °	90 °
β	92.29 (4) °	90 °
γ	105.85 (4) °	90 °
Volume	1001.27 (1) Å^3	2095.3 (3) Å^3
Temperature (K)	298	298
ρ (calc.) / g cm^{-3}	1.431	1.3342
Wavelength (Å)	–	1.5406
R-exp (%)[*]	–	1.682
R-p (%)[*]	–	5.142
R-wp (%)[*]	–	7.633
R_Bragg	–	5.84
χ^2	–	4.538
Starting angle (° 2θ)	–	5.0
Final angle (° 2θ)	–	95.0
Step width (° 2θ)	–	0.0086

The crystal structure of the form II cocrystal calculated from PXRD data is illustrated in Figure 3.38 and was compared to the structure of the form I cocrystal, based on single crystal data (Caira, 1992) (Figure 3.39). The unit cell volume of the form II was found to be almost doubled to that of the form I cocrystal, possibly due to a difference in molecular packing flexibility, thus posing torsional restrictions (Table 3.6). The SD molecules in the new cocrystal adopt a cage-like arrangement, with 4-ASA molecules aligned diagonally across the cavity (Figure 3.38). Unlike, in the form I cocrystal (Caira, 1992), the 4-ASA and the dimethylpyrimidine portion of SD are essentially coplanar, forming sheets with an interlayer distance of 3.409 Å and resulting in a slight increase in density (Figure 3.39).
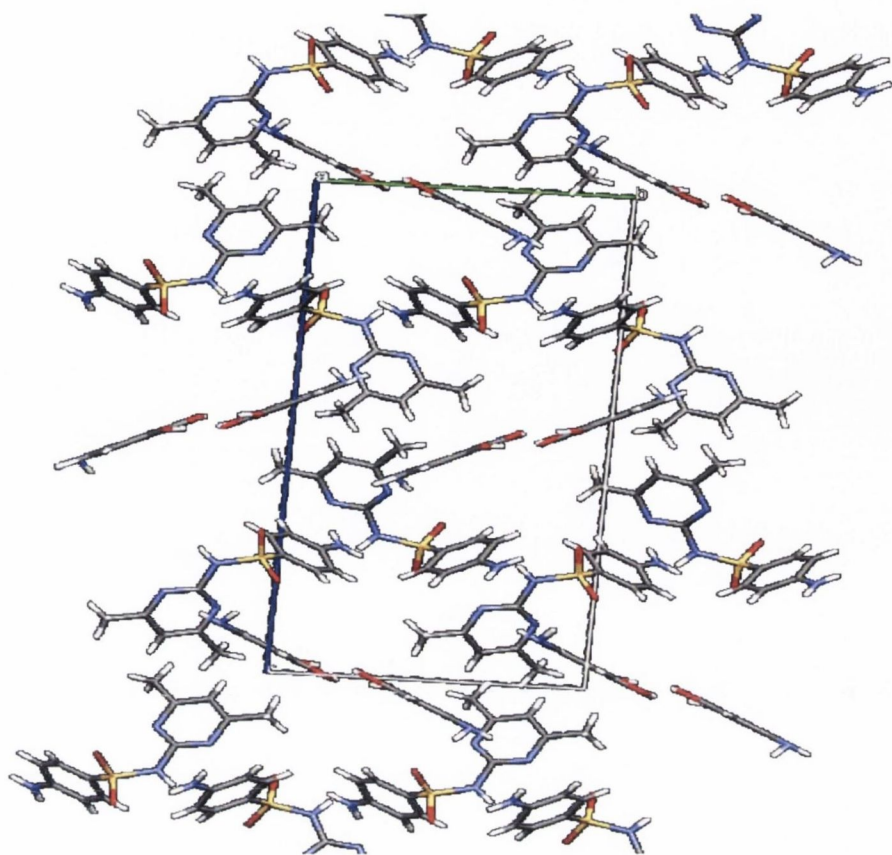
Figure 3.38: Crystal structure of the SD:4-ASA 1:1 form II cocrystal (calculated from PXRD data) viewed along the *a* axis.
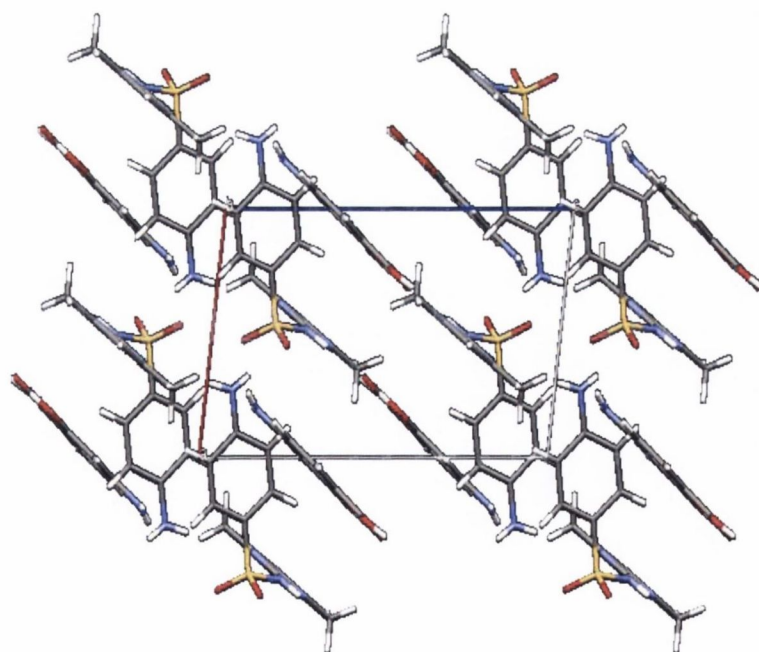

Figure 3.39: Crystal structure of the SD:4-ASA 1:1 form I cocrystal (determined from single crystal data by Caira, 1992) viewed along the *b* axis.

Intermolecular interactions in the form of hydrogen bonding of SD and 4-ASA in the form II cocrystal were found between C-H···N and C-H···O involving the amidine and sulfoxy group of SD and the aromatic hydrogens of 4-ASA (Figure 3.40). In contrast, the form I cocrystal (Caira, 1992) shows hydrogen-bond preferences of O-H···N and N-H···O between the amidine moiety of SD and the acid group of 4-ASA (illustrated earlier in Figure 3.12).
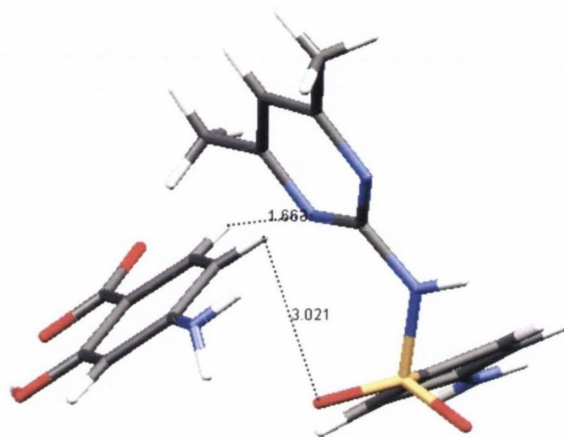

Figure 3.40: Molecular interactions in the SD:4-ASA 1:1 form II cocrystal calculated from PXRD data (dotted black lines indicate hydrogen bonds and the numbers represent the corresponding bond length).

These findings clearly elucidated the structural difference of the form II cocrystal to the form I cocrystal and therefore confirmed that a polymorph has been generated.

On closer inspection of the initially obtained data from single crystal X-ray diffraction it was hypothesised that the SD:4-ASA 1:1 form II cocrystal could be a modulated phase: Instead of a typical 3-dimensional periodic crystal, an aperiodic crystal is present.

Further data were collected at Diamond Light Source, the British national synchrotron facility. The use of synchrotron radiation (a higher intensity source) was chosen in order to ensure measurement of all possible reflections, including weaker satellite reflections.

From the resulting data an orthorhombic unit cell of a=22.349(4) Å, b=7.6597(5) Å, c=47.138(3) Å could be indexed. However, by carefully examining the reconstructed precession images, it became apparent that this molecular structure reveals an unusual form of twinning (twinning is described as the intergrowth of two individual crystals of the same species (Buerger, 1945)), where not all reflections could be indexed by a twin model. From this observation it was concluded that the actual crystal is composed of two phases: One orthorhombic unit cell and one monoclinic twinned unit cell that result in three individuals as illustrated in Figure 3.41. The identified orthorhombic unit cell (above) index all collected reflections which embeds the two phases. These phases could be indexed with a twinned monoclinic unit cell (marked in blue and red) and an orthorhombic unit cell (marked in green), whereas the monoclinic (twinned) unit cell revealed parameters of a=22.3967(18) Å, b=7.6645(2) Å, c=26.0793(13) Å and β = 115.306(8) ° and the parameters of the orthorhombic unit cell were a=22.347(4) Å, b=7.6617(6) Å, c=23.5748(16) Å (Figure 3.41).
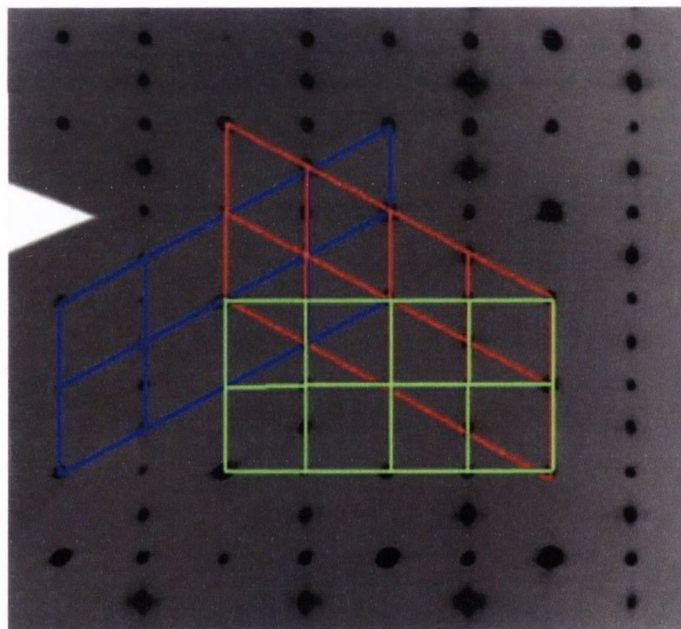

Figure 3.41: The reconstructed *h1l* layer of the SD:4-ASA 1:1 form II cocrystal with an overlay of the three possible unit cells. The green unit cell is the orthorhombic unit cell and the blue and red unit cells are the two twinned monoclinic cells.

Such a crystal pattern arises when the molecules have a free choice of either packing in a monoclinic or an orthorhombic fashion and can be described by a scheme as illustrated in Figure 3.42. A similar structure has been reported for one metal oxo-halide (Hugonin et al., 2009).
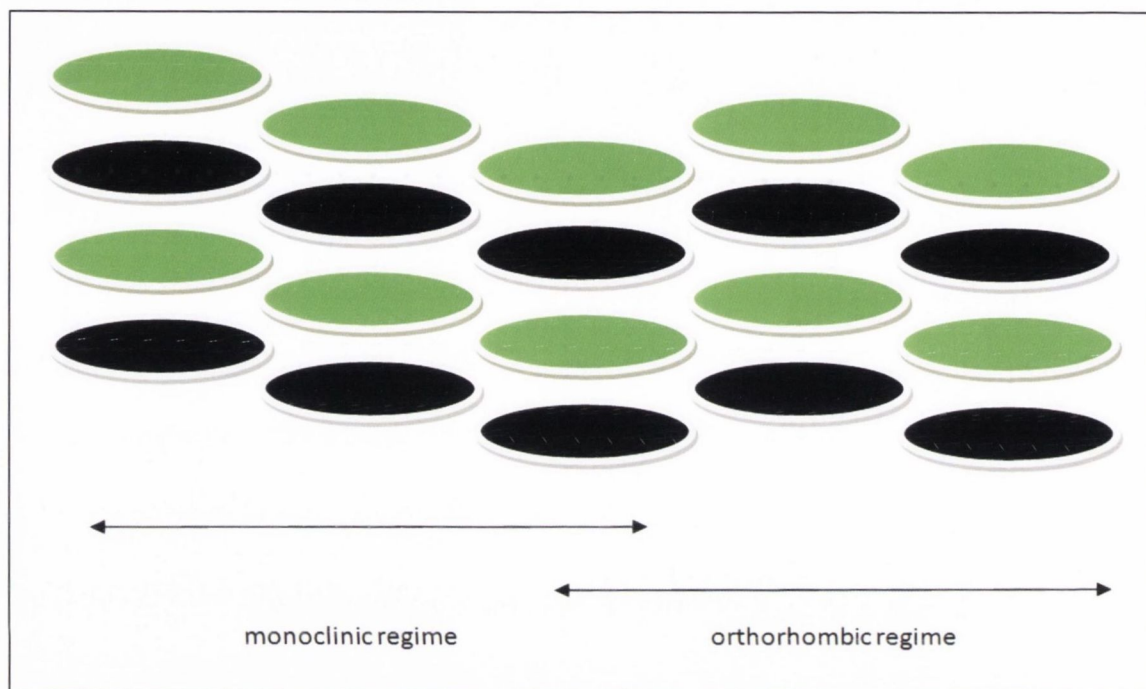

Figure 3.42: Schematic illustration of two crystals phases (monoclinic and orthorhombic) in one crystal. The black and green circles symbolise one molecule each.

The difficulty is that the two phases need to be solved and refined together from the overall (total) orthorhombic unit cell. The parameters of the two phases determined so far are of non-standard space group settings and the symmetry of them has to be established before a final crystal structure can be produced. Nevertheless, it is already observed that the hydrogen bonding preferences of SD and 4-ASA in the structures occur between the amidine moiety of SD and the acid group of 4-ASA as is reported for the form I cocrystal (Caira, 1992) and in contrast to the result obtained from the PXRD derived crystal structure data. Moreover, once the correct symmetry of the cocrystal structures has been resolved, the scheme shown in Figure 3.42 can be described more precisely for the case of this cocrystal.

It can be summarised that the SD:4-ASA 1:1 form II cocrystal can also be formed by solvent evaporation from ethanol or acetone by forming needle-like crystals. Elevated temperatures and non-equimolar starting amounts with 4-ASA in excess were required in order to obtain an equimolar product. These findings indicated that the form II cocrystal requires energy in the form of heat to be generated which, however, leads to a mass loss of 4-ASA and has to be balanced.

The use of PXRD data enabled a crystal structure to be determined, showing that the cocrystal exists in an orthorhombic unit cell, in which the SD molecules interact with 4-ASA by forming hydrogen bonds in the form of C-H···N and C-H···O involving the amidine and sulfoxy group of SD and the aromatic hydrogens of 4-ASA.

However, investigations from single crystal X-ray diffraction (SC-XRD) analysis showed that the cocrystal structure is more complex. It is suggested that the form II cocrystal exists in two intergrown polymorphs. The use of synchrotron radiation enabled confirmation of the presence of two cocrystal cells, which are embedded in a large orthorhombic unit cell. The hydrogen bonding motifs of SD and 4-ASA in the structures are expected to be similar to the form I cocrystal (Caira, 1992) and thus different to the results from PXRD data. However, due to the complexity, crystallographic details of the two cocrystal structures are not yet available and are currently under investigation.

Although not complete, the obtained single crystal X-ray diffraction data are of high quality due to the high standard of the technique using synchrotron radiation. In the case of more complex structures such as the SD:4-ASA form II cocrystal, crystal structure results based on PXRD data will be inferior compared to SC-XRD. Further advancement in the methodology of crystal structure indexing using the PXRD technique would be required.

3.4 Conclusions

In this study, dry and liquid-assisted milling and spray drying were examined for the formation of sulfadimidine:4-aminosalicylic acid (SD:4-ASA) cocrystals using different molar ratios (1:2, 1:1, 2:1). Solid state, solubility and dissolution properties were investigated. It was shown that cocrystals can be generated by liquid-assisted milling and spray drying, while this was not possible using dry milling. SD and 4-ASA formed only 1:1 cocrystals. Cocrystals of other stoichiometry (1:2 and 2:1) have not been observed. Dry co-milling and co-spray drying of SD and 4-ASA induced amorphisation to different extents, which was not evident for liquid-assisted milling. By liquid-assisted milling the SD:4-ASA 1:1 form I cocrystal was formed. By spray drying a polymorphic form (form II) of the SD:4-ASA 1:1 cocrystal was discovered which could also be obtained by solvent evaporation from ethanol and acetone. Liquid-assisted milling from a 1:1 component ratio generated a cocrystal of equivalent molar ratio. In contrast, spray drying had shown to induce a mass loss of 4-ASA which resulted in the formation of a non-equimolar cocrystal after being spray-dried from an equimolar SD:4-ASA solution. The solubility of the SD:4-ASA 1:1 cocrystal was dependent on the pH and could be predicted by a model established for a two amphoteric component cocrystal. The form I cocrystal was found to be thermodynamically more stable in aqueous solution than form II, which showed transformation to form I. The addition of PVP to the solution enabled the form II cocrystal to be stabilised. Despite the stability difference, the solubilities of the form I and form II cocrystal were found to be similar. The presence of amorphous uncomplexed SD in the form II cocrystal induced a supersaturated solution with respect to SD. Intrinsic dissolution studies revealed that the dissolution rate of the poorly water soluble SD from both cocrystal forms was enhanced when compared to a physical equimolar mixture and SD alone. The dissolution rates were consistent with the corresponding solubilities. Both cocrystal forms were slightly hygroscopic and stable on a long-term storage.

Structure determination of the discovered SD:4-ASA 1:1 form II cocrystal revealed an unusual and complex crystal structure. The presence of two polymorphic forms in one cocrystal is suggested and will be further investigated.

Chapter 4:

Investigating the potential for cocrystallisation on spray drying sulfadimidine with aromatic carboxylic acids

4.1 Introduction

A recent approach to the formation of cocrystals is the use of spray drying, as demonstrated by Alhalaweh and Velaga (2010) and further by the study described in Chapter 3 of this thesis. The work presented in Chapter 3 has shown that liquid-assisted milling of sulfadimidine (SD) and 4-aminosalicylic (4-ASA) in an equimolar ratio using ethanol results in the formation of the same SD:4-ASA 1:1 cocrystal (form I) as that reported previously by Caira (1992), while spray drying from ethanol (and solvent evaporation at elevated temperature) leads to a new, polymorphic form (form II) of the cocrystal. These results suggested that spray drying offers the potential to screen for new cocrystal forms or polymorphic forms of cocrystals which cannot be obtained by the liquid-assisted milling route. Hence, one of the objectives of the following study was to investigate if other cocrystals, composed of sulfadimidine and an aromatic carboxylic acid are able to form polymorphic forms of known cocrystals when prepared by spray drying. Therefore, two known cocrystals were selected: the sulfadimidine:benzoic acid (SD:BA) 1:1 cocrystal (Caira et al., 1995; Arman et al., 2010) and the sulfadimidine:salicylic acid (SD:SA) 1:1 cocrystal (Patel et al., 1988; Caira et al., 1995). For each of the cocrystals only one crystalline form has been reported, which can be obtained by crystallisation from solution or by solid state grinding (dry grinding) (Caira et al., 1995). In addition, the formation of the SD:4-ASA 1:1 cocrystal using crystallisation methods other than those reported in Chapter 3 was studied in this work. Another objective was to screen if sulfadimidine can form cocrystals with other aromatic carboxylic acids such as nicotinic acid (NA) and pyrazine-2-carboxylic acid (PCA).

The final goal was the overall evaluation of cocrystallisation of sulfadimidine with aromatic carboxylic acids by means of spray drying and to compare the products formed with those obtained by other crystallisation methods such as liquid-assisted milling, solvent evaporation and cooling crystallisation.

4.2 Materials and Methods

4.2.1 Materials

Sulfadimidine (SD), benzoic acid (BA), salicylic acid (SA), 4-aminosalicylic acid (4-ASA), nicotinic acid (NA), pyrazine-2-carboxylic acid (PCA) and pyridine-2-carboxylic acid (PA) were purchased from Sigma-Aldrich (Ireland). Ethanol (EtOH)

and acetone (Me_2CO) were supplied from Corcoran Chemicals (Ireland). Methanol (MeOH) and acetonitrile (MeCN) were purchased from Fisher Scientific (Ireland).

4.2.2 Methods

4.2.2.1 Milling (liquid-assisted, LAM)

Liquid-assisted milling was performed for 30 minutes using a 1:1 molar ratio of sulfadimidine and the relevant aromatic carboxylic acid. Further details of the process are described in Chapter 3.

4.2.2.2 Spray drying (SPD)

Spray drying was performed using a Büchi B-290 Mini Spray Dryer operating in the closed-mode using nitrogen as drying gas. The drying gas was recirculated using the B-295 inert loop. Solution concentrations of 0.5–2% (w/v) of sulfadimidine and acid in a 1:1 molar ratio were prepared using different solvents such as ethanol, methanol, acetonitrile and acetone. The solutions were delivered to a 2-fluid atomization nozzle using a peristaltic pump at a pump speed of 30 % (9–10 ml/min) and the aspirator was operated at 100%. The flowmeter for the standard 2-fluid nozzle was set at 4 cm which is equivalent to 473 Normlitres per hour (Nl/h) of gas flow in normal conditions (p=1013.25 mbar and T=273.15 K) (Büchi Labortechnik, 93001). The inlet temperature varied between 70–82 °C, depending on the solvent used. Details of spray drying conditions can be found in Appendix 3, Table A.3.1.

4.2.2.3 Solvent evaporation (SEV)

Equimolar mixtures of SD and the acid of 20–100 mg were dissolved in an excess of solvent at ambient temperature. The solutions were covered with a pierced parafilm and left under ambient conditions until the solvent was completely evaporated.

4.2.2.4 Cooling crystallisation (CCR)

Cooling crystallisation experiments were performed in a heated water bath. Physical mixtures of equimolar ratio of SD and acid were used and saturated solutions were prepared by dissolving a sufficient amount of the mix in 2 ml of the relevant solvent at the boiling point of the solvent. The tubes were sealed with a lid and the water bath was turned off to allow slow cooling until ambient temperature was reached.

4.2.2.5 X-ray Diffraction

4.2.2.5.1 Powder X-ray diffraction (PXRD)

as described in Chapter 2

4.2.2.5.2 Single crystal X-ray diffraction (SC-XRD)

The analysis was performed by Thomas McCabe (School of Chemistry, Trinity College Dublin, Ireland). Crystal data were collected on a Rigaku Saturn 724 CCD Diffractometer. A suitable crystal was selected and mounted on a glass fiber tip and placed on the goniometer head in a 123K N_2 gas stream. The data was collected using Crystalclear-SM 1.4.0 software. Data integration, reduction and correction for absorption and polarization effects were all performed using Crystalclear-SM 1.4.0 software. Space group determination, structure solution and refinement were obtained using Bruker Shelxtl Ver. 6.14 software. The structure was solved with Direct Methods using the SHELXTL program and refined by full matrix least-squares on F^2 for all data using SHELXL-97. Non-hydrogen atoms were refined with anisotropic thermal parameters. Hydrogen atoms were placed into geometrically calculated positions and refined using a riding model. The programs Ortep-3 (Faruggia, 1997) and Mercury 2.3 (Mercury CSD 2.0, 2008) were used for illustrating the molecular structures. For calculation of X-ray powder patterns on the basis of the single crystal data, the program Mercury 2.3 (Mercury CSD 2.0, 2008) was used. Crystallographic cif files and supplementary data are available at http://www.ccdc.cam.ac.uk/data_request/cif (Cambridge Crystallograhpic Data Centre, CCDC 903503).

4.2.2.6 Thermal analysis

as described in Chapter 2, whereas the temperature range varied between 25 and 270 °C

4.2.2.7 Attenuated Total Reflection - Fourier Transform Infra-red (ATR-FTIR) Spectroscopy
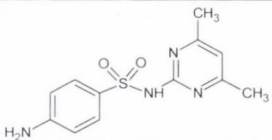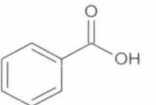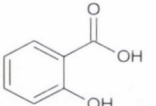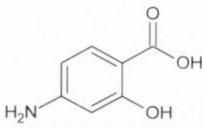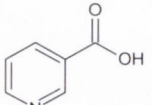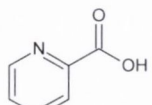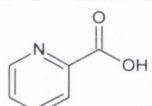
as described in Chapter 2

4.2.2.8 Dynamic vapour sorption (DVS)

as described in Chapter 3

4.3 Results and Discussion

An overview of the cocrystal components and their physical properties is given in Table 4.1.

Table 4.1: Physical and chemical properties of sulfadimidine (SD) and aromatic carboxylic acids selected as cocrystal formers. The melting temperatures (T_m) and corresponding enthalpies of fusion (ΔH_f) refer to experimental data shown in Chapter 3 (for SD and 4-ASA) and in Appendix 3 (for all other components).

Cocrystal compound	Structure	Molecular weight (g/mol)	pK$_a$ values	T_m, °C (ΔH_f, J/g)
SD		278.33	pK$_{a1}$ = 2.79[a] pK$_{a2}$ = 7.4[a]	197.16 ± 0.43 (130.45 ± 6.60)
BA		122.12	pK$_a$ = 4.21[b]	121.14 ± 0.69 (139.43 ± 0.32)*
SA		138.12	pK$_{a1}$ = 3.00[c] pK$_{a2}$ = 13.4[c]	158.07 ± 0.68 (170.06 ± 5.99)*
4-ASA		153.14	pK$_{a1}$ = 2.0[d] pK$_{a2}$ = 3.56[d]	139.07 ± 0.93 (392.80 ± 7.33)**
NA		123.11	pK$_{a1}$ = 2.14[e] pK$_{a2}$ = 4.82[e]	235.65 ± 0.59 (205.67 ± 7.43)*
PCA		124.10	pK$_a$ = 2.90[f]	224.74 ± 0.37 (798.72 ± 32.11)*
PA		123.11	pK$_{a1}$ = 1.01[g] pK$_{a2}$ = 5.39[g]	136.60 ± 1.03 (177.35 ± 5.02)***

a) Sukul and Spiteller, 2006
b) Harris, 2010
c) Kolthoff and Stenger, 1942
d) Newton and Kluza, 1978
e) Nagy and Takács-Novák, 1997
f) Zhang et al., 2003
g) Abdullah and Tofiq, 2010

*sublimes before melting showing a one stage mass loss (Appendix 3, Figures A.3.1 and A.3.2)
** associated with decomposition showing a two stage mass loss (see Chapter 3 for details)
***associated with decomposition showing a one stage mass loss (Appendix 3, Figures A.3.1 and A.3.2)

Sulfadimidine and benzoic acid

Co-processing of SD with BA was initially performed using EtOH and MeOH as solvents. In earlier work published by Caira et al. (1995), it was reported that the SD:BA 1:1 cocrystal can be formed from EtOH, MeCN and Me$_2$CO. Therefore, additionally MeCN and Me$_2$CO were selected for cocrystal screening by the different techniques such as spray drying, liquid-assisted milling, solvent evaporation and cooling crystallisation. For each solvent, Table 4.2 presents a summary of the resulting products obtained by co-processing of SD with BA, based on analysis by PXRD and DSC. Full details of the results are shown in Appendix 3.

Table 4.2: Products resulting from co-processing of SD with BA using spray drying (SPD), liquid-assisted milling (LAM), solvent evaporation (SEV) and cooling crystallisation (CCR). The results are based on PXRD and DSC analysis. All diffractograms and thermograms and a table with the values of the melting temperatures (T_m) and corresponding enthalpies of fusion (ΔH_f) can be found in Appendix 3, Figures A.3.3 – A.3.10 and Table A.3.2.

Solvent	Method and resulting solid phase(s)			
	SPD	**LAM**	**SEV**	**CCR**
EtOH[1]	CC[a]*	CC[a]	CC[a] + SD + BA	CC[a] + SD
MeOH[2]	CC[a]*	CC[a]	CC[a]*	CC[a] + SD
MeCN[3]	CC[a]*	CC[a]	CC[a] + SD + BA	CC[a] + SD
Me$_2$CO[4]	CC[a]**	CC[a]	CC[a]* + SD	CC[a]*

1) analysis is shown in Appendix 3, Figure A.3.3 and Figure A.3.4

2) analysis is shown in Appendix 3, Figure A.3.5 and Figure A.3.6

3) analysis is shown in Appendix 3, Figure A.3.7 and Figure A.3.8

4) analysis is shown in Appendix 3, Figure A.3.9 and Figure A.3.10

a) consistent with cocrystal (CC) reported by Arman et al., 2010

*contains traces of SD and/or BA which are only detectable by DSC but not by PXRD

**pure phase (by DSC analysis) when 30% excess molar amount of BA is added

The results showed that irrespective of the formation technique and the solvent, the same cocrystal was generated and identified as the SD:BA 1:1 cocrystal, reported previously (Arman et al., 2010; Caira et al., 1995). The PXRD patterns were consistent with the PXRD pattern calculated based on single crystal X-ray data (Arman et al., 2010). In general, the PXRD patterns of the spray dried and liquid-assisted milled products showed broader peaks with lower diffraction intensities when compared with those of products obtained by solvent evaporation and cooling crystallisation. This was assumed to be attributed to crystal imperfections and/or the preferred orientation effect, as was observed for other spray-dried and milled samples (Grant and York, 1986; Corrigan, 1995; Paul et al., 2007; Khatirkar and Murty, 2010). Not all cocrystals formed were a single phase product, as indicated by the presence of additional diffraction peaks of the starting materials in the PXRD patterns and/or deviations from the reported melting behaviour of the cocrystal (Caira et al., 1995; Arman et al., 2010) in the DSC scans.

All spray-dried products showed PXRD patterns which superimposed with the theoretical PXRD pattern of the reported single crystal data with no other diffraction peaks visible (Figures A.3.3, A.3.5, A.3.7, A.3.9). However, the corresponding thermograms of the products spray-dried from a solution containing SD and BA in an equimolar ratio resulted in usually two broad melting endotherms, merging and appearing at lower temperatures (184–189 °C) than the melting range reported (T_m=208–220 °C) for the SD:BA 1:1 cocrystal (Arman et al., 2010) (Figures A.3.4, A.3.8, A.3.10). In the case of the sample spray dried from MeOH, the two endotherms were clearly separated, the first one was small and appeared at 185.90 ± 1.30 °C with an enthalpy of fusion of 7.50 ± 1.59 J/g and the second one was larger, appearing at 208.59 ± 4.82 °C with an enthalpy of fusion of 174.47 ± 17.35 J/g and attributed to melting of the cocrystal (Figure A.3.6). As previously observed for the SD:4-ASA cocrystal discussed in Chapter 3, spray drying induced a mass loss of the 4-ASA component, presumably as a result of sublimation or evaporation occurring during processing. Thus, it was suggested that similarly to 4-ASA, spray drying led to a mass loss of BA and hence a non-equimolar product composed of the cocrystal with some excess SD leading to a melting point depression. This assumption was further investigated using Me_2CO as a solvent for spray drying SD with excess BA of different molar amounts in order to balance the mass loss. It was found that the addition of 30 % excess molar amount (1.3) of BA to the spray drying solution resulted in a single phase product, as confirmed by

PXRD and DSC. The PXRD pattern of this sample superimposed in each diffraction peak with the calculated pattern based on single crystal X-ray data (Figure A.3.9 a), while the DSC thermogram showed a single melting endotherm, shifted towards the melting temperature of the cocrystal (T_m=218.39 ± 2.23 °C) (Figure A.3.10 a) when compared with the products spray-dried from a 1:1 ratio, indicative of an equimolar product. It was therefore concluded that spray drying induced a mass loss of BA which needs to be balanced in order to generate a cocrystal with an equimolar ratio of components.

In contrast, liquid-assisted milling of SD and BA in a 1:1 molar ratio revealed single phase products, as evidenced by the results of both PXRD and DSC analysis (see Figure references in Table 4.2). Irrespective of the solvent used, the products showed PXRD patterns which superimposed in each peak with the PXRD pattern of the reported cocrystal. DSC showed thermograms with a single melting event in the temperature range of 208–217 °C and corresponding enthalpies of fusion of 205–284 J/g, indicative of the SD:BA 1:1 cocrystal.

Solvent evaporation from a 1:1 SD:BA solution resulted in the formation of a mix of the cocrystal and the single components (Table 4.2). The presence of SD was shown by the appearance of a characteristic diffraction peak at 9.35° 2θ, as for example when EtOH and MeCN were used as solvents (Figures A.3.3 c and A.3.7 c). In the case of BA, characteristic diffraction peaks at 8.15° and 23.8° 2θ appeared, however the first one was not always visible. The DSC thermograms revealed two melting events, one at around 119–121 °C attributable to BA and a second endotherm, often broad, at 212–213 °C indicative of the cocrystal and melting of SD (see Figure references in Table 4.2).

For the products crystallised by evaporation from MeOH and Me₂CO, the presence of the single components in the product was mainly detectable by DSC analysis and not by PXRD, presumably as a result of a higher limit of detection for PXRD. The overall product quality, in terms of cocrystal purity based on DSC results, was found to be best when MeOH was used as solvent (Figure A.3.6 c).

Binary crystalline products composed of the cocrystal and SD were observed to form when cooling crystallisation from EtOH, MeOH and MeCN was employed, indicating that the coformer was more soluble than the cocrystal and SD in these solvents. This was confirmed by PXRD analysis, where the presence of SD was attributed to the characteristic diffraction peak at 9.35° 2θ (Figures A.3.3 d, A.3.5 d, A.3.7 d).

DSC analysis of the products revealed thermograms with two melting endotherms

(Figures A.3.4 d, A.3.6 d, A.3.8 d), one, small endotherm at around 190–192 °C and in the case of EtOH and MeOH (Figures A.3.4 d, A.3.6 d) merging with the second endotherm, which appeared between 207–219 °C, attributed to the cocrystal.

Cooling crystallisation from Me$_2$CO (Figures A.3.9 e, A.3.10 e) revealed a product composed of the cocrystal with a small amount of SD, detected by DSC only and attributable to the melting endotherms at 190.08 ± 1.52 °C and 219.48 ± 1.55 °C with corresponding enthalpies of fusion of 0.40 ± 0.03 J/g and 170.60 ± 12.30 J/g, respectively. With respect to the cocrystal purity based on DSC results, the use of Me$_2$CO as solvent resulted in the best product quality by cooling crystallisation.

Overall, these results showed that from each technique and solvent the same cocrystal, the SD:BA 1:1 cocrystal (Caira et al., 1995; Arman et al., 2010) was generated. Thus, spray drying did not result in the formation of a polymorphic form as previously observed for SD:4-ASA. When comparing the techniques, it was observed that spray drying induced a mass loss of BA, which needed to be balanced by the addition of 30% excess molar amount of BA prior to processing in order to generate a cocrystal of equimolar stoichiometry. Liquid-assisted milling produced cocrystals with no evidence of traces attributable to the single components. In contrast, solvent evaporation and cooling crystallisation resulted in the cocrystal formation with concomitant crystallisation of either BA and/or SD. The best product quality was obtained from MeOH and Me$_2$CO in the case of solvent evaporation and cooling crystallisation, respectively.

Sulfadimidine and salicylic acid

As for BA, co-processing of SD with SA by the techniques described above was initially performed using EtOH and MeOH and further using MeCN and Me$_2$CO, based on literature data which showed that the SD:SA 1:1 cocrystal crystallises from EtOH, MeCN and Me$_2$CO (Patel et al., 1988; Caira, 1995). A summary of the results is presented in Table 4.3.

Table 4.3: Products resulting from co-processing of SD with SA using spray drying (SPD), liquid-assisted milling (LAM), solvent evaporation (SEV) and cooling crystallisation (CCR). The results are based on PXRD and DSC analysis. All diffractograms and thermograms and a table with the values of the melting temperatures (T$_m$) and corresponding enthalpies of fusion (ΔH$_f$) can be found in Appendix 3, Figures A.3.11 – A.3.18 and Table A.3.2.

Solvent	Method and resulting solid phase(s)			
	SPD	**LAM**	**SEV**	**CCR**
EtOH[1]	CC[b]*	CC[b]	CC[b]*	CC[b] + SD
MeOH[2]	CC[b]*	CC[b]	CC[b] + SD + SA	CC[b] + SD
MeCN[3]	CC[b]**	CC[b]	CC[b]*	CC[b]*
Me$_2$CO[4]	CC[b]*	CC[b]	CC[b]* + SD	CC[b]*

1) analysis is shown in Appendix 3, Figure A.3.11 and Figure A.3.12

2) analysis is shown in Appendix 3, Figure A.3.13 and Figure A.3.14

3) analysis is shown in Appendix 3, Figure A.3.15 and Figure A.3.16

4) analysis is shown in Appendix 3, Figure A.3.17 and Figure A.3.18

b) consistent with cocrystal reported by Patel et al., 1988

*contains traces of SD and/or SA which are only detectable by DSC but not by PXRD

**pure phase (by DSC analysis) when 20% excess molar amount of SA is added

Similar to the use of BA as a coformer, it was found that regardless of which formation technique and solvent was used, the same cocrystal was generated. The cocrystal was identified as the SD:SA 1:1 cocrystal, previously reported (Patel et al., 1988; Caira, 1995) by comparing the calculated PXRD pattern based on single crystal X-ray data (Patel et al., 1988) and the literature melting point of the SD:SA 1:1 cocrystal (T$_m$=196

°C, Caira, 1995) with the experimental data for the resulting products. As discussed in the previous example for SD and BA, PXRD analysis revealed reduced diffraction peak intensities and less sharp peaks for the spray-dried and liquid-assisted milled products when compared to those of samples produced by solvent evaporation and cooling crystallisation, attributable to crystal imperfections and/or the preferred orientation effect.

As shown in the case of BA as coformer, it was also observed that spray drying induced a mass loss of SA. As a consequence, the resulting products were of a non-equimolar ratio, verified by DSC analysis which showed for each product two merging melting endotherms occurring at lower temperatures, between 180–197 °C, than the melting point of the cocrystal (see Figure references in Table 4.3). In order to balance the mass loss and to obtain a product with an equimolar ratio of components (based on DSC analysis), the addition of 20% excess SA molar amount (1.2) prior to spray drying was required. This was demonstrated using MeCN as a solvent and verified by DSC analysis which revealed a product with a single sharp melting event at 197.01 ± 1.87 °C (Figure A.3.16 a) indicative of the SD:SA 1:1 cocrystal (Caira, 1995). PXRD analysis confirmed the formation of the cocrystal. Each diffraction peak of the 1:1.2 spray-dried product (Figure A.3.15 a) superimposed with the equivalent pattern of the cocrystal based on single crystal data (Patel et al., 1988).

In the case of liquid-assisted milling using a 1:1 component ratio, a pure cocrystal, determined by PXRD and DSC analysis (see Figure references in Table 4.3) was generated from each solvent. All products showed PXRD patterns which superimposed in each diffraction peak with the PXRD pattern of the SD:SA 1:1 cocrystal (Patel et al., 1988) and revealed thermograms with a single melting endotherm between 196–197 °C and corresponding enthalpies of 138–145 J/g.

Cocrystallisation of a 1:1 SD:SA ratio by solvent evaporation resulted in formation of the cocrystal and was accompanied by crystallisation of the single components. Based on PXRD analysis, the presence of SD and SA in the product was verified by the characteristic peak at 9.35° and 28.05° 2θ, respectively. In most cases however, analysis by PXRD was not sufficiently sensitive and identity of the resulting products was determined by DSC analysis. The thermograms showed for each product a melting endotherm at 142–153 °C (ΔH_f = 7–58 J/g) indicative of SA, followed by a melting endotherm occurring at lower temperatures than the literature melting point of the SD:SA 1:1 cocrystal (Caira, 1995) at 186–195 °C, and thus attributable to melting of

cocrystal and SD (see Figure references in Table 4.3). When comparing the solvents used, the best product quality, in terms of cocrystal purity as evaluated by DSC, was obtained from EtOH and MeCN.

Cooling crystallisation from EtOH and MeOH resulted in the cocrystal formation associated with crystallisation of SD indicating that the coformer was more soluble than the cocrystal and SD in these solvents. Analysis of products formed by PXRD confirmed the presence of SD by the characteristic diffraction peak at 9.35° 2θ (Figures A.3.11 d, A.3.13 d). DSC analysis revealed two merging melting endotherms, one occurring at 184–185 °C, followed by a second at around 191–194 °C (Figures A.3.12 d, A.3.14 d). Cooling crystallisation from MeCN and Me$_2$CO showed the best product quality (based on cocrystal purity analysed by DSC) in comparison to EtOH and MeOH, by the formation of the cocrystal with only a small amount of unreacted SD, verified by DSC only (Figures A.3.16 e, A.3.18 d) and attributable to the presence of two endotherms, a small one at 184–185 °C (ΔH_f = 0.9–1.3 J/g) and a larger one at around 198 °C (ΔH_f = 143–146 J/g).

In summary, these findings showed that spray drying did not result in the formation of a polymorphic form of the SD:SA 1:1 cocrystal, the same finding as was observed using SD and BA. Each technique and solvent generated the same form. Spray drying induced a mass loss of SA, and it was found that, in order to obtain a cocrystal of equimolar ratio (based on DSC results), the addition of 20% excess molar amount to the spray drying solution was required. Liquid-assisted milling produced cocrystals with no evidence of the single components. In general, solvent evaporation and cooling crystallisation resulted in cocrystal formation associated with crystallisation of both BA and/or SD. When comparing the two methods and the solvents used, both methods revealed the best product quality (in terms of purity based on DSC analysis) when SD and SA were crystallised from MeCN. Solvent evaporation revealed a better product quality than cooling crystallisation for crystallisation from EtOH, while the opposite was observed when Me$_2$CO was used as the solvent.

Sulfadimidine and 4-aminosalicylic acid

As described in the previous Chapter, it was found that co-spray drying of SD with 4-ASA using EtOH and solvent evaporation at elevated temperatures using EtOH and Me_2CO resulted in the formation of a new form, a polymorph (form II) of the SD:4-ASA 1:1 cocrystal, while liquid-assisted milling using EtOH led to the production of the previously reported SD:4-ASA 1:1 form I cocrystal (Caira, 1992). Further studies on the formation of the SD:4-ASA 1:1 cocrystal by spray drying and liquid-assisted milling using Me_2CO and by using other crystallisation methods such as solvent evaporation at room temperature and cooling crystallisation have been investigated. The results are summarised in Table 4.4.

Table 4.4: Products resulting from co-processing of SD with 4-ASA using spray drying (SPD), liquid-assisted milling (LAM), solvent evaporation (SEV) and cooling crystallisation (CCR). The results are based on PXRD and DSC analysis. All diffractograms and thermograms and a table with the values of the melting temperatures (T_m) and corresponding enthalpies of fusion (ΔH_f) can be found in Appendix 3, Figures A.3.19 – A.3.22 and Table A.3.2.

Solvent	Method and resulting solid phase(s)			
	SPD	**LAM**	**SEV**	**CCR**
$EtOH^{1)}$	$CC^{d)}$	$CC^{c)}$	$CC^{c)} + SD + 4\text{-}ASA$	$CC^{c)} + SD$
$Me_2CO^{2)}$	$CC^{d)}$	$CC^{c)}$	$CC^{c)}*$	$CC^{c)}*$

1) analysis is shown in Figure A.3.19 and Figure A.3.20

2) analysis is shown in Figure A.3.21 and Figure A.3.22

c) consistent with SD:4-ASA 1:1 form I cocrystal reported by Caira, 1992

d) consistent with SD:4-ASA 1:1 form II cocrystal reported in Chapter 3

*contains traces of SD and/or 4-ASA which are only detectable by DSC but not by PXRD

It was found that the use of Me_2CO as solvent led to the formation of the same product as when EtOH was employed. In the case of spray drying the SD:4-ASA 1:1 form II cocrystal was generated, while in the case of liquid-assisted milling the SD:4-ASA form I cocrystal was obtained. The identity of the forms was confirmed by PXRD analysis (Figures A.3.19, A.3.21). DSC analysis (Figures A.3.20 and A.3.22) showed, in the case of spray drying from both EtOH and Me_2CO, thermograms with a single melting

endotherm at 167–170 °C ($\Delta H_f = 200$–201 J/g). For liquid-assisted milling using EtOH and Me$_2$CO as solvents, both products showed thermograms with a single melting event occurring at 167–170 °C ($\Delta H_f = 207$–225 J/g) and indicated that the thermal behaviour of both form I and form II cocrystals is similar.

Methods such as solvent evaporation and cooling crystallisation from EtOH and Me$_2$CO resulted in the formation of the form I cocrystal (Table 4.4). This was shown by PXRD analysis which revealed diffraction patterns which superimposed with the PXRD pattern of the previously reported form I cocrystal (Caira, 1992). However, in the case of EtOH the cocrystal purity was poorer when compared to that obtained with Me$_2$CO. This impurity using EtOH was demonstrated by PXRD and DSC analysis (Figures A.3.19, A.3.20). For example, for the product obtained by solvent evaporation PXRD analysis detected the presence of SD and 4-ASA attributable to the characteristic diffraction peak at 9.35° and 26.5° 2θ, respectively (Figure A.3.19 c). The corresponding thermogram (Figure A.3.20 c) showed a broad melting endotherm, shifted towards lower temperatures compared to the melting point of the pure cocrystal (167–170 °C) by 24 °C, indicative of an impure phase and thus consistent with the PXRD data. In the case of cooling crystallisation from EtOH, PXRD analysis showed the presence of SD in the product (attributable to the characteristic diffraction peak at 9.35° 2θ, Figure A.3.19 d) as a result of a lower solubility of SD in EtOH compared to 4-ASA. The DSC thermogram confirmed the results of PXRD analysis by showing a broad melting event at 171.29 ± 1.88 °C with an enthalpy of fusion of 170.30 ± 8.97 J/g (Figure A.3.20 d).

Overall, the findings showed that the SD:4-ASA 1:1 form II cocrystal can be generated by spray drying from both EtOH and Me$_2$CO, while all other methods resulted in the formation of the form I cocrystal from both solvents. These results led to the conclusion, as was suggested in the previous Chapter, that the generation of the form II cocrystal requires energy in the form of heat (constantly supplied) in order to be generated.

Moreover, solvent evaporation and cooling crystallisation from Me$_2$CO resulted in general in a better cocrystal quality (purity) than EtOH, based on PXRD and DSC analysis.

Sulfadimidine and nicotinic acid

The use of NA as a coformer in co-processing with SD resulted in the formation of a novel SD:aromatic carboxylic acid cocrystal, the SD:NA 1:1 cocrystal, confirmed by structure determination using single crystal X-ray analysis, as described below. The cocrystal was formed by each method using EtOH and MeOH. A summary of the products, determined by PXRD and DSC analysis is presented in Table 4.5.

Table 4.5: Products resulting from co-processing of SD with NA using spray drying (SPD), liquid-assisted milling (LAM), solvent evaporation (SEV) and cooling crystallisation (CCR). The results are based on PXRD and DSC analysis. All diffractograms and thermograms and a table with the values of the melting temperatures (T_m) and corresponding enthalpies of fusion (ΔH_f) can be found in Appendix 3, Figures A.3.23 – A.3.26 and Table A.3.2.

Solvent	Method and resulting solid phase(s)			
	SPD	**LAM**	**SEV**	**CCR**
EtOH[1]	CC[e]	CC[e]	CC[e] + SD	CC[e] + SD
MeOH[2]	CC[e]	CC[e]	CC[e]	CC[e]*

1) analysis is shown in Figure A.3.23 and Figure A.3.24

2) analysis is shown in Figure A.3.25 and Figure A.3.26

e) new cocrystal discovered, crystallographic data are shown in Figures 4.2-4.4 and Table 4.6

*contains traces of SD which is only detectable by DSC but not by PXRD

The results revealed that spray drying and liquid-assisted milling generated a single phase product composed of the SD:NA 1:1 cocrystal. This was confirmed by PXRD analysis by comparing the PXRD patterns of the products with the theoretical PXRD pattern based on single crystal data. Each product showed a diffraction pattern which was similar to the theoretical pattern. DSC analysis confirmed the purity of the product showing for each product a single sharp melting event at 204–205 °C with a corresponding enthalpy of fusion of 150–167 J/g (see Figure references in Table 4.5).

Solvent evaporation from a 1:1 molar ratio mix of SD:NA showed in the case of EtOH the formation of the cocrystal mixed with SD, verified by PXRD analysis by the presence of the characteristic diffraction peak for SD at 9.35° 2θ (Figure A.3.23 c). Distinctive diffraction peaks of NA which clearly differed from the cocrystal and SD

were not found. PXRD analysis of the product crystallised from MeOH did not show evidence of the presence of SD and/or NA (Figure A.3.25 c). DSC analysis revealed for both products thermograms with a single melting endotherm at 205–207 °C and enthalpies of fusion of 162–167 J/g, indicative of the SD:NA 1:1 cocrystal (Figures A.3.24 c, A.3.26 c).

In the case of cooling crystallisation, both solvents resulted in cocrystal formation with crystallisation of SD indicating that NA was more soluble than SD in EtOH and MeOH. This was confirmed by PXRD and DSC analysis. The presence of a characteristic diffraction peak at 9.35° 2θ attributable to SD was, for example, shown in the case of the product crystallised form EtOH (Figure A.3.23 d). DSC analysis of both the crystallised products from EtOH and MeOH, revealed two melting endotherms: a first one at 189–190 °C followed by a second at 205–206 °C indicative of a mixture of SD and the SD:NA 1:1 cocrystal (Figures A.3.24 d, A.3.26 d).

Overall, these findings showed that the SD:NA 1:1 cocrystal was generated using each technique. Spray drying and liquid-assisted milling using both solvents and solvent evaporation from MeOH resulted in a single phase product. In contrast, for solvent evaporation from EtOH and cooling crystallisation from both solvents concomitant crystallisation of the cocrystal and single components was observed.

In order to determine the crystal structure of the discovered SD:NA 1:1 cocrystal by single crystal X-ray analysis, the crystals obtained by solvent evaporation from MeOH were used. As shown in Figure 4.1, transparent, dipyramidal crystals were grown.
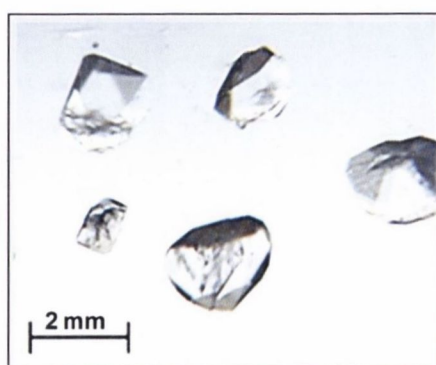

Figure 4.1: Morphology of the SD:NA 1:1 cocrystals obtained by solvent evaporation from MeOH.

It was found that SD and NA crystallised in the monoclinic space group P 2_1/c with one molecule of each component in the asymmetric unit (Figures 4.2–4.4 and Table 4.6). Based on the location and bond distances of atoms involved in molecular interactions between SD and NA, hydrogen bond formation was found between the sulfonyl moiety in SD and the carbonyl group in NA (N-H···O) and between the pyrimidine nitrogen (N3) in SD and the hydroxyl group in NA (N···H-O) (Figure 4.3). The molecules are packed by forming a ladder-like arrangement with alternating open sides along the b-axis (Figure 4.4). In each monomer the acid and the pyrimidine ring of SD are coplanar and are stabilised by the hydrogen bonds (Figure 4.4). There were other weaker hydrogen bonds observed involving the amino and the sulfoxy moiety of SD. Full crystallographic details are available at http://www.ccdc.cam.ac.uk/data_request/cif (Cambridge Crystallograhpic Data Centre, CCDC 903503). Furthermore, these results showed that the SD:NA 1:1 cocrystal revealed the same hydrogen bond motifs as has been reported for the SD:BA, SD:SA and SD:4-ASA form I cocrystal (Arman et al., 2011, Patel et al., 1988; Caira 1992) as well as for other cocrystals composed of SD and carboxylic acids (Ghosh et al., 2011). All revealed hydrogen-bond preferences between the amidine moiety and the acid group of the coformer.
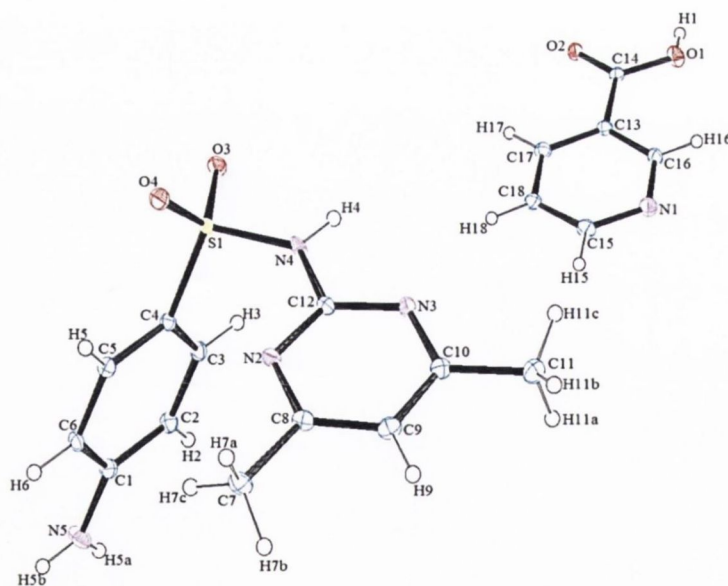

Figure 4.2: Ortep representation of the SD:NA 1:1 cocrystal structure with the thermal ellipsoids set at 50% probability.

Table 4.6: Crystallographic parameters of the SD:NA 1:1 cocrystal.

Parameter	SD:NA 1:1 cocrystal
Molecular formula	$C_{18}H_{19}N_5O_4S$
Molecular weight	401.44 g/mol
Space group	Monoclinic, $P\,2_1/c$
Unit cell parameters	
a	8.9450 (18) Å
b	14.944 (3) Å
c	14.193 (3) Å
α	90 °
β	105.48 (3) °
γ	90 °
Volume	1828.4 (6) Å^3
Temperature (K)	150
ρ (calc.) / g cm^{-3}	1.458
Reflections collected	13172
Unique reflections	3100
R_1	0.0460
wR_2	0.2178
Goodness-of-fit	1.188
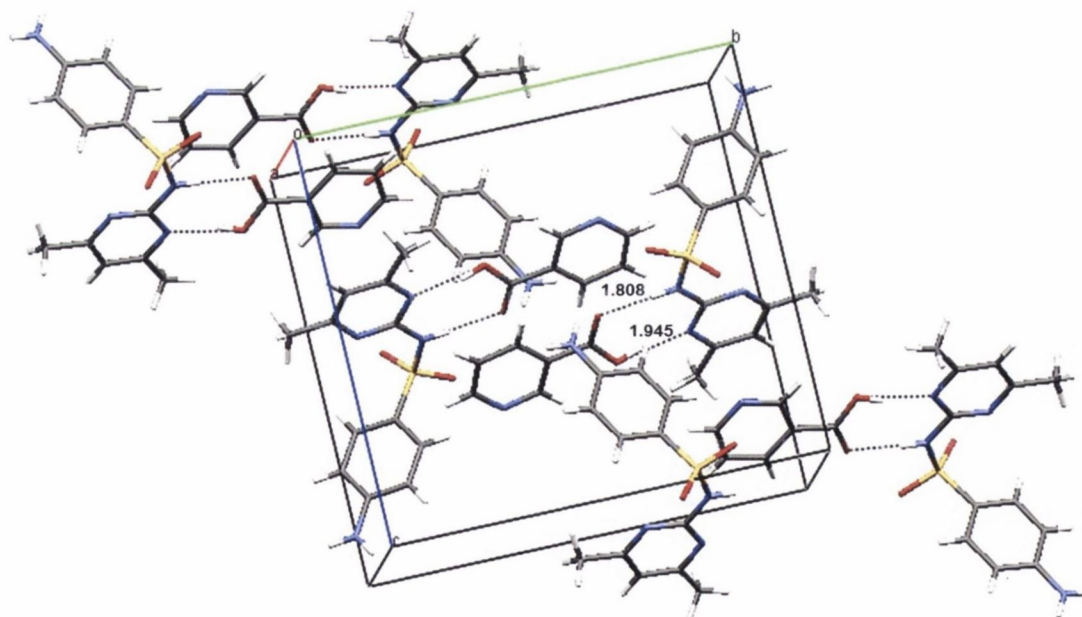
Figure 4.3: Molecular packing of the SD:NA 1:1 cocrystal (dotted black lines indicate hydrogen bonds and the values the appropriate lengths).
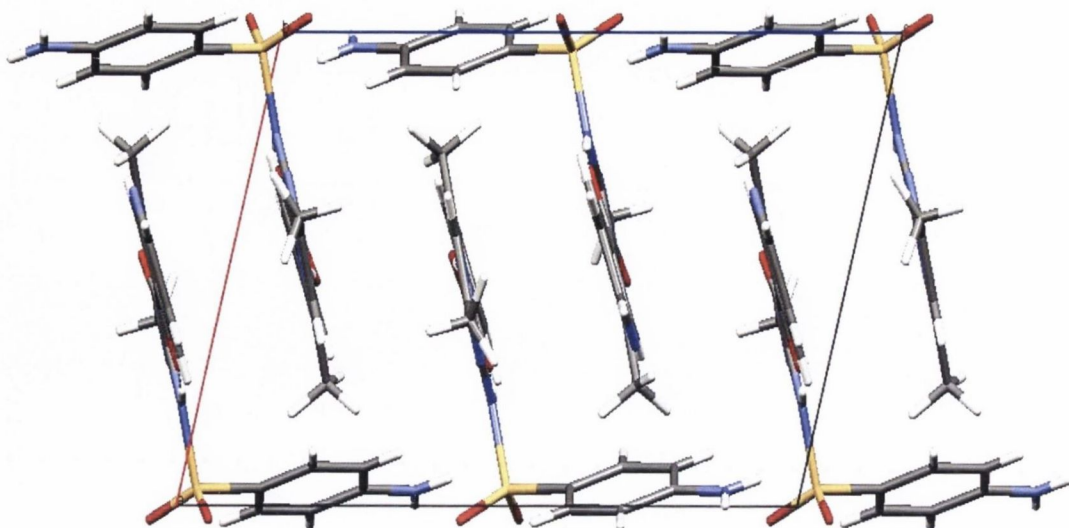
Figure 4.4: Crystal packing in the SD:NA 1:1 cocrystal, viewed along the b-axis.

Further characterisation of the SD:NA 1:1 cocrystal by IR spectroscopy confirmed the presence of molecular interactions between SD and NA in the form of hydrogen bonds. Figure 4.5 illustrates the IR spectrum of the SD:NA 1:1 cocrystal obtained from solvent evaporation using MeOH, in comparison to the IR spectra of the single components. The cocrystal revealed shifts of bands attributed to SD in the higher wavenumber region, where the asymmetric and symmetric NH_2 stretching bands of the amine group of SD (3441 cm^{-1} and 3342 cm^{-1}) were shifted towards higher wavenumbers by 32 cm^{-1} and 36 cm^{-1}, respectively. Moreover, the carbonyl stretching band of NA (1698 cm^{-1}) was shifted towards lower wavenumbers by 19 cm^{-1} and was less strongly pronounced than in the spectrum of NA alone. The sulfone (SO_2) stretching band of SD (1300 cm^{-1}) appeared broader and was shifted by 8 cm^{-1} towards higher wavenumbers in the cocrystal.
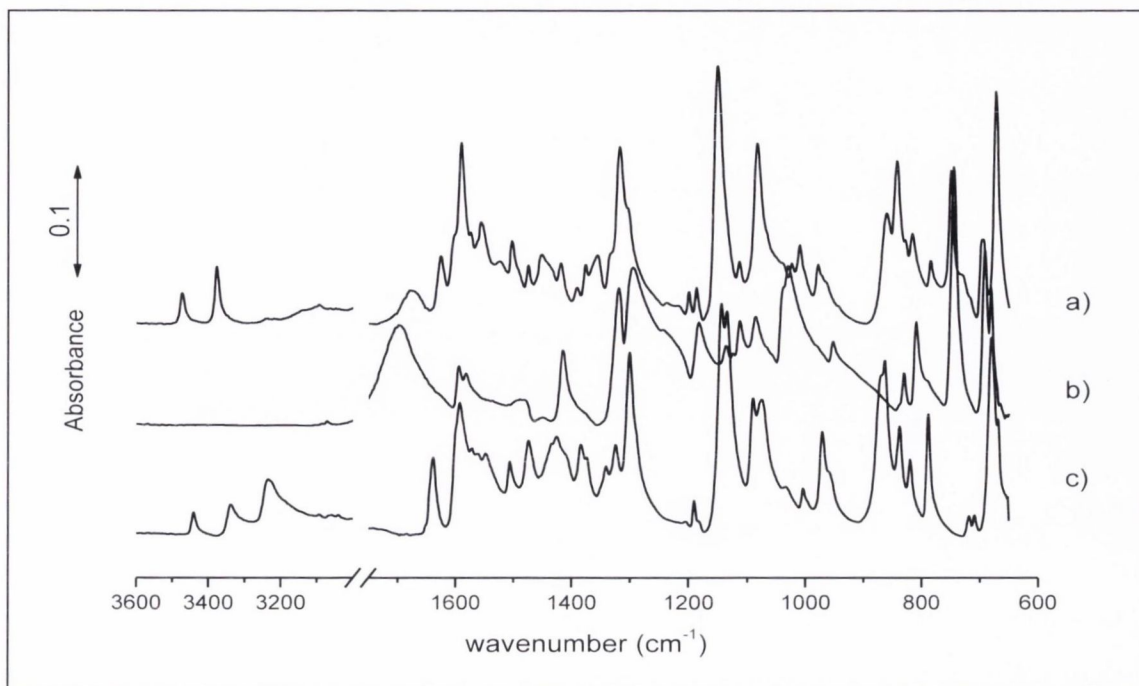
Figure 4.5: FTIR spectra of a) SD:NA 1:1 product obtained by SEV using MeOH, b) NA and c) SD.

Sulfadimidine and pyrazine-2-carboxylic acid

PCA, as another coformer from the aromatic carboxylic acid group, has also been investigated for its potential to form a cocrystal with SD using EtOH and MeOH as solvents. The results obtained from the different crystallisation techniques are shown in Table 4.7.

Table 4.7: Products resulting from co-processing of SD with PCA using spray drying (SPD), liquid-assisted milling (LAM), solvent evaporation (SEV) and cooling crystallisation (CCR). The results are based on PXRD and DSC analysis. All diffractograms and thermograms and a table with the values of the melting temperatures (T_m) and corresponding enthalpies of fusion (ΔH_f) can be found in Appendix 3, Figures A.3.27 – A.3.30 and Table A.3.2.

Solvent	Method and resulting solid phase(s)			
	SPD	**LAM**	**SEV**	**CCR**
EtOH[1]	SD + PCA*	SD + PCA	SD + PCA	SD + PCA
MeOH[2]	SD + PCA	SD + PCA	SD + PCA	SD + PCA

1) analysis is shown in Figure A.3.27 and Figure A.3.28

2) analysis is shown in Figure A.3.29 and Figure A.3.30

*contains amorphous phase

It was found that all products revealed mixtures of SD and PCA, regardless of the technique and solvent used. This was confirmed by PXRD analysis (Figures A.3.27, A.3.29) which showed diffraction patterns in which each peak was attributed to the single components. Each pattern was basically the sum of the diffraction patterns of SD and PCA and thus no evidence of cocrystal formation was shown. PXRD analysis of a physical mixture, prepared by simply mixing both components using a spatula, showed consistency with the results of the products and confirmed the presence of a mixture composed of SD and PCA. For the spray-dried product from EtOH (Figure A.3.27 a), the PXRD pattern revealed diffraction peaks with very low intensities in comparison to those of the spray-dried product from MeOH (Figure A.3.29 a) and to those resulting from the other techniques.

Thermal analysis by DSC showed for each product a melting endotherm, often broad, occurring at temperatures below the melting point of SD and PCA, between 173–176 °C (ΔH_f = 144–161 J/g), indicating the formation of a crystalline mixture composed of SD and PCA. In the case of the spray-dried product from EtOH, an exothermic event at 87.51 ± 2.63 °C prior to melting was observed, which was attributed to crystallisation of an amorphous content induced by spray drying and therefore in agreement with the results from PXRD analysis.

Overall, these results indicate that no cocrystal was formed with PCA as a coformer, in contrast to BA, SA, 4-ASA and NA. Further confirmation was obtained by IR spectroscopy as shown in Figure 4.6.

When compared to the SD:BA, SD:SA, SD:4-ASA form I and SD:NA 1:1 cocrystals, which revealed characteristic shifts of bands towards higher or lower wavenumbers, for example in the wavenumber regions between 3500–3300 cm^{-1} and 1400–1200 cm^{-1} (Figure 4.6 a, b, c, d), for the SD:PCA 1:1 product each IR band superimposed with bands of SD and PCA (Figure 4.6 e). No evidence of band shifts which indicate the presence of intermolecular interactions such as hydrogen bonds and thus cocrystal formation was found for the SD:PCA 1:1 product.
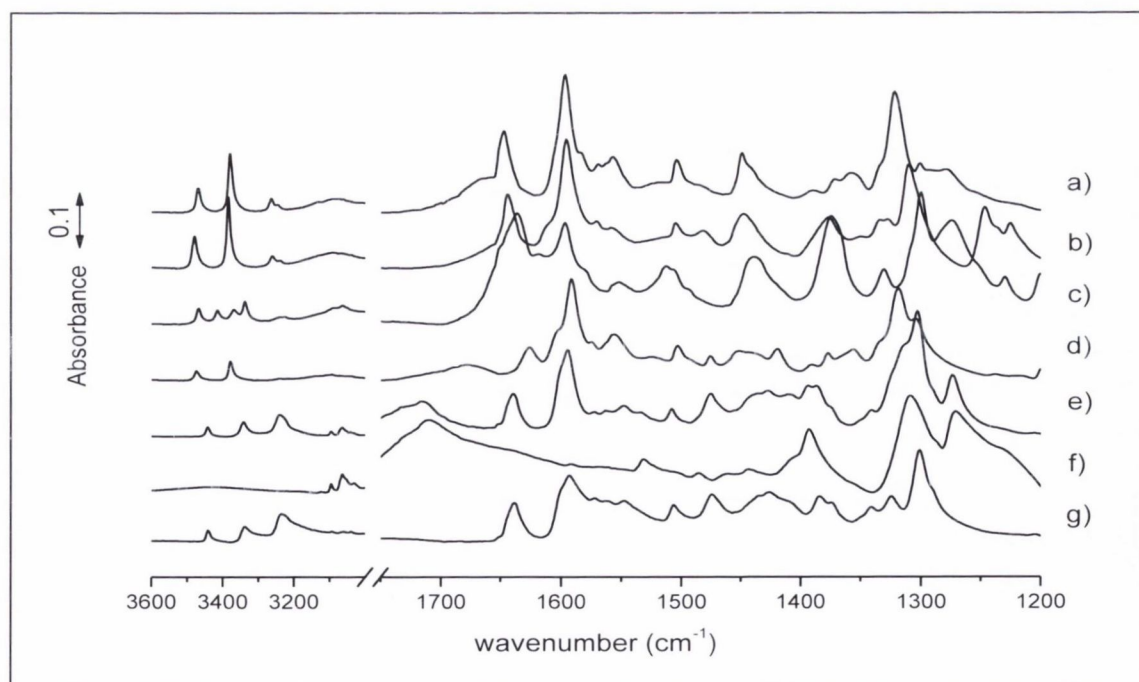

Figure 4.6: IR spectra of a) SD:BA 1:1 cocrystal, b) SD:SA 1:1 cocrystal, c) SD:4-ASA 1:1 form I cocrystal, d) SD:NA 1:1 cocrystal and e) SD:PCA 1:1 composite system (all produced by liquid-assisted milling) compared to f) PCA and g) SD raw materials.

When comparing the structural properties of all coformer acids described, it was obvious that PCA has a similar structure to NA (Figure 4.7) and similar pK_a values (Table 4.1), which can play a role in the formation of cocrystals (Lu et al., 2011). However, in contrast to NA, cocrystal formation with PCA was not observed. It was suggested that the additional nitrogen in the aromatic ring forming the pyrazine moiety and in direct vicinity to the carboxyl group in PCA might hinder cocrystal formation and thus hydrogen bond formation with SD. To verify this idea, pyridine-2-carboxylic acid (PA) was introduced as coformer. As shown in Figure 4.7, pyridine-2-carboxylic acid contains the same structural motif as PCA: an aromatic nitrogen in direct vicinity to the carboxyl group.
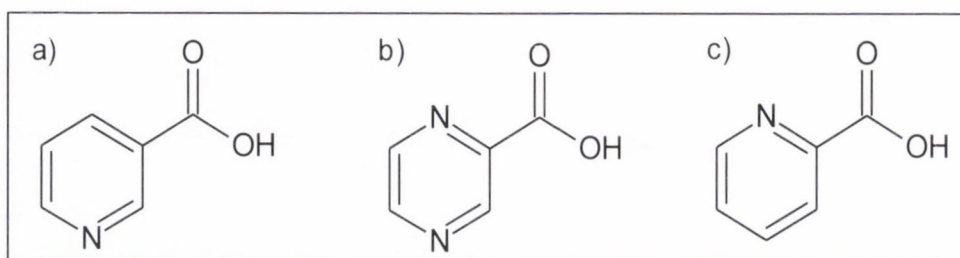
Figure 4.7: Molecular structure of a) NA, b) PCA and c) PA.

As liquid-assisted milling has been shown to be a very reliable technique in the formation of cocrystals, PA was co-milled with SD using the same solvents (EtOH and MeOH) as for PCA. Furthermore, MeCN and Me_2CO were used in order to examine whether the type of solvent influences the result. For comparison, a physical mixture of PA and SD was prepared by simply mixing both components using a spatula. The products were analysed by PXRD and DSC. As shown in Figure 4.8, PXRD revealed, for all liquid-assisted milled samples, identical diffraction patterns which superimposed in each diffraction peak with those of the physical mixture and the single components. DSC analysis showed, for all milled products and the physical mixture, thermograms with a single melting endotherm occurring at lower temperatures than the melting points of SD and PCA raw materials (Table 4.1) at 121–125 °C (Figure 4.9 and Table A.3.2 in Appendix 3), indicating the formation of a crystalline mixture.

These results were similar to those found for PCA, showing that co-processing with SD resulted in crystalline mixtures composed of the single components. Thus, the experiment using PA confirmed that the structural moiety in PCA consisting of an

aromatic nitrogen in direct vicinity to a carboxyl group (Figure 4.7) hinders cocrystal formation with SD, possibly as the result of an intramolecular hydrogen-bond formation, as the carboxyl group acts as donor and the aromatic nitrogen as acceptor.
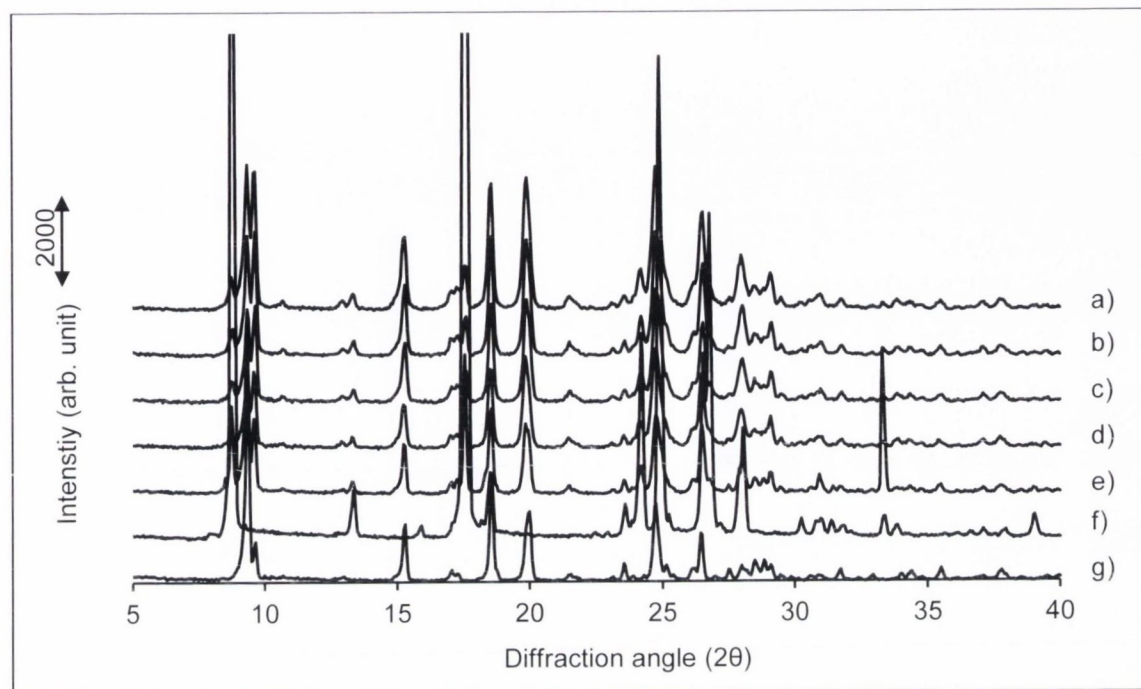

Figure 4.8: PXRD patterns of SD:PA 1:1 products obtained by liquid-assisted milling using a) EtOH, b) MeOH, c) MeCN, d) Me$_2$CO compared to e) SD:PA 1:1 PM, f) PA and g) SD.
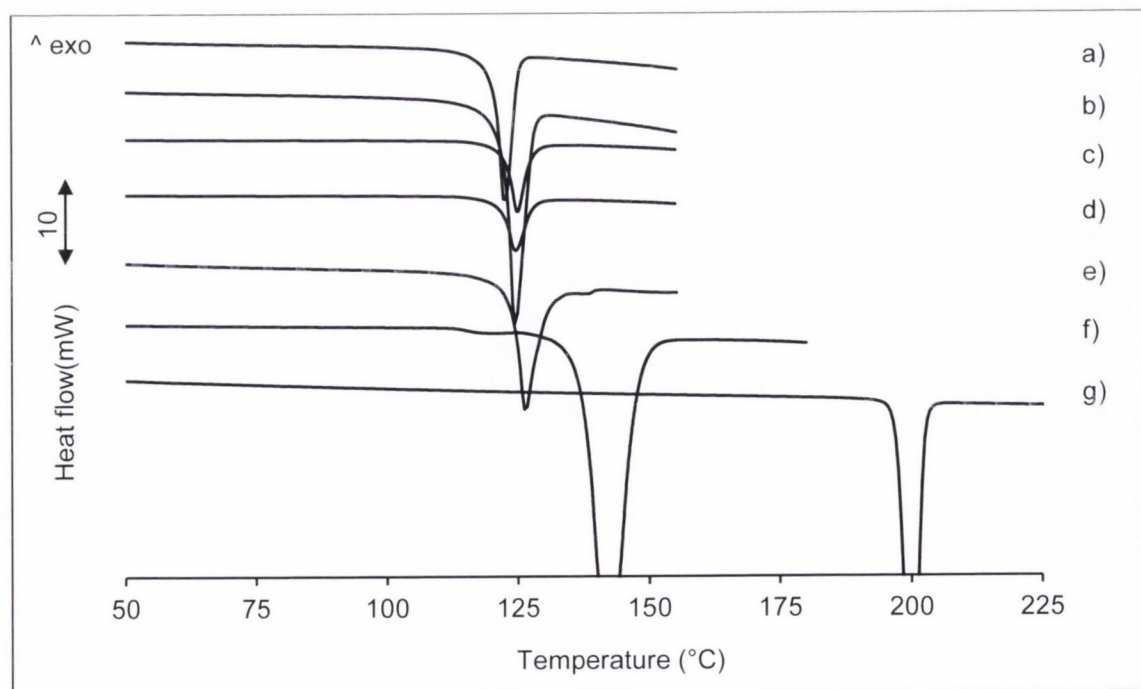

Figure 4.9: DSC thermograms of SD:PA 1:1 products obtained by liquid-assisted milling using a) EtOH, b) MeOH, c) MeCN, d) Me$_2$CO compared to e) SD:PA 1:1 PM, f) PA and g) SD.

In summary, when comparing the common crystallisation methods such as liquid-assisted milling, solvent evaporation and cooling crystallisation with spray drying in the formation of cocrystals, the study has shown that spray drying is a successful alternative. All SD:aromatic carboxylic acid cocrystals that were generated by liquid-assisted milling, solvent evaporation and cooling crystallisation, were also formed by spray drying. Only in one case, using 4-ASA as coformer, did spray drying result in the formation of a polymorphic cocrystal, the SD:4-ASA form II cocrystal, which could not be obtained by the other methods. This observation might be related to the presence of the aromatic amino group, which only exists in the 4-ASA molecule but not for the other acid coformers. In general, based on PXRD results, cocrystals produced by spray drying and liquid-assisted milling revealed a lower degree of crystallinity than those produced by solvent evaporation and cooling crystallisation.

Moreover, in contrast to solvent evaporation and cooling crystallisation, where cocrystal formation was usually associated with crystallisation of the single components and where the cocrystal quality (purity) varied, depending on the solvent used, for cocrystals produced by spray drying and liquid-assisted milling the solvent was not found to have an impact on the product result (based on PXRD and DSC analysis). However, a difference to liquid-assisted milling was observed for spray drying based on DSC analysis. In the case of the acid coformers BA and SA, spray drying from an equimolar component ratio induced a mass loss of the acid and the addition of excess BA and SA to the liquid feed was required in order to generate a cocrystal of equimolar ratio. In the case of 4-ASA and NA, DSC analysis did not show any evidence that a non-equimolar cocrystal was produced by spray drying. However, as described in Chapter 3, further analysis by HPLC for the 1:1 spray-dried SD:4-ASA cocrystal (form II) detected a non-stoichiometric component ratio, indicative of a mass loss of 4-ASA during processing. Hence, the product stoichiometry (by means of HPLC) was also analysed for the SD:NA cocrystal spray-dried from a 1:1 molar solution. The results showed that this cocrystal contained equimolar amounts of SD and NA.

Therefore, it was concluded that spray drying can result in the formation of pure (equimolar) cocrystals, but can also produce cocrystals with some unreacted amounts of the components. However, for detailed conclusions and an evaluation of the cocrystals purity, further analysis will be required.

Dynamic vapour sorption

The cocrystals of SD with BA, SA and NA and the mixture of SD with PCA produced by liquid-assisted milling were further examined by dynamic vapour sorption (DVS) experiments in order to study the effect of moisture sorption/desorption of the material (DVS studies of the SD:4-ASA 1:1 cocrystal have been reported in Chapter 3). Dynamic vapour sorption and desorption isotherms are shown in Figure 4.10. The SD:BA 1:1 cocrystal showed a maximum amount of water sorption of less than 0.09%, where most of the water was sorbed between 70 and 80% RH. The desorption profile showed a similar trend to the sorption profile. The SD:SA 1:1 cocrystal revealed a higher water uptake, with a maximum of 0.15% at 90% RH. Most water was sorbed between 70% and 90% RH. The desorption behaviour was similar with a slight hysteresis effect between 90 and 40% RH, while below 40% RH the curve merged with the sorption profile. The SD:NA 1:1 cocrystal sorbed, over the entire humidity range, more water than the SD:BA cocrystal. Compared to the SD:SA cocrystal, the water uptake was initially higher but decreased and was less between 70 and 90% RH. In general, the maximum amount of water sorbed by the SD:NA 1:1 cocrystal was 0.1% with similar sorption and desorption profiles. In comparison to the cocrystals, the SD:PCA 1:1 crystalline mixture showed the highest water uptake with a maximum of 0.23% at 90% RH. The sorption increased continually over the entire humidity range. The desorption profile revealed a similar trend with, in general, less water released than sorbed.
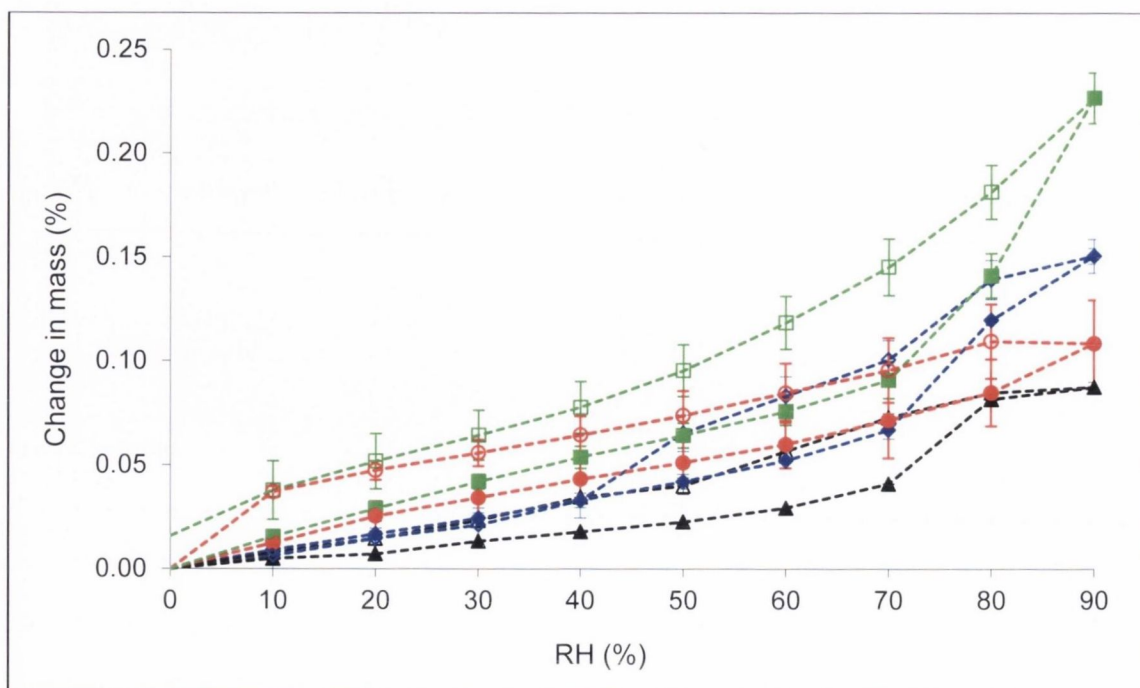
Figure 4.10: Moisture sorption and desorption profiles of SD:BA 1:1 cocrystal (closed and open black triangles), SD:SA 1:1 cocrystal (closed and open blue diamonds), SD:NA 1:1 cocrystal (closed and open red circles) and SD:PCA 1:1 mixed system (closed and open green squares) at 25 °C. The data refer to materials obtained by liquid-assisted milling.

PXRD analysis of the materials recovered at the end of the DVS experiments (0% RH) confirmed that no solid state transformation occurred (Figure 4.11).

In summary, these results showed that the SD:BA, SD:SA and SD:NA 1:1 cocrystals and the SD:PCA 1:1 mixture are physically stable, with only little water uptake (< 0.25 %) when exposed to humidities ranging from 0 to 90% RH. Referring to the hygroscopicity classification system established by Murikipudi et al. (2013) on the basis of sorption analysis, all cocrystals can be classified as "non-hygroscopic" (water uptake < 0.2%), while the SD:PCA 1:1 mixture is regarded as "slightly hygroscopic" (water uptake 0.2–2%).
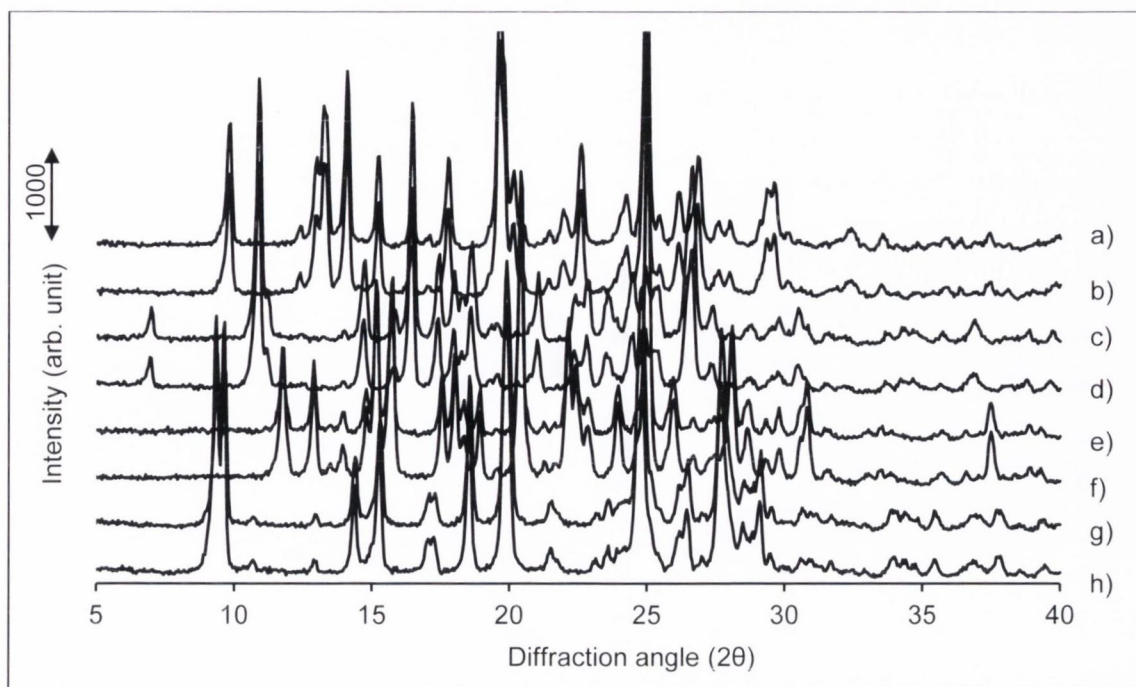
Figure 4.11: PXRD patterns before and after DVS experiments. a) SD:BA 1:1 cocrystal recovered after DVS at 0% RH, b) SD:BA 1:1 cocrystal before DVS study, c) SD:SA 1:1 cocrystal recovered after DVS at 0% RH, d) SD:SA 1:1 cocrystal before DVS study, e) SD:NA 1:1 cocrystal recovered after DVS at 0% RH, f) SD:NA 1:1 cocrystal before DVS study, g) SD:PCA 1:1 mixture recovered after DVS at 0% RH and h) SD:PCA 1:1 mixture before DVS study. The data refer to materials obtained by liquid-assisted milling.

4.4 Conclusions

This study has investigated the effect of spray drying compared to common crystallisation methods such as liquid-assisted milling, solvent evaporation and cooling crystallisation in the formation of SD:aromatic carboxylic acid cocrystals and the discovery of new and/or polymorphic forms.

It was demonstrated that 4-ASA was the only coformer which resulted in the formation of a polymorphic cocrystal by means of spray drying. This polymorph could not be generated from the other methods, which only formed the SD:4-ASA 1:1 form I cocrystal. Following the earlier studies (Chapter 3) which were based on EtOH as solvent, it was shown that the SD:4-ASA 1:1 form II cocrystal could also be generated by spray drying and liquid-assisted milling using Me_2CO.

The introduction of NA as coformer resulted in the formation of a new, previously unreported cocrystal, the SD:NA 1:1 cocrystal. The structure of the SD:NA cocrystal was determined by single crystal X-ray diffraction analysis. The discovered cocrystal revealed the same hydrogen-bond motifs as reported for the SD:BA, SD:SA and SD:4-ASA form I cocrystals.

The use of PCA as coformer from the aromatic carboxylic acid type did not result in cocrystal formation. Instead, a crystalline mixture of SD and PCA was formed from each technique and solvent used. It was shown that PCA inhibited cocrystal formation with SD due to structural features of PCA, attributable to intramolecular hydrogen-bond formation.

Overall, the study has demonstrated that spray drying is a successful alternative to common crystallisation methods such as liquid-assisted milling, solvent evaporation and cooling crystallisation in the formation of SD:aromatic carboxylic acid cocrystals.

In each case where liquid-assisted milling, solvent evaporation and cooling crystallisation formed a cocrystal, the same result was observed using spray drying (disregarding polymorph formation). In contrast to solvent evaporation and cooling crystallisation, for cocrystals produced by spray drying and liquid-assisted milling the solvent was not found to have an impact on the product result. Besides, it was shown that spray drying can induce a mass loss of one of the components, affecting the resulting cocrystal purity. For a precise evaluation of the techniques with respect to cocrystal formation, the product purity needs to be analysed in detail.

Moreover, based on DVS studies, it was shown that the generated sulfadimidine cocrystals were non-hygroscopic, while the sulfadimidine physical mixture (SD:PCA) was slightly hygroscopic when exposed to humidities ranging from 0–90% RH.

Chapter 5:

Solubility and dissolution behaviour of sulfadimidine:aromatic carboxylic acid cocrystals

5.1 Introduction

Besides formation and solid state characterisation, solubility and dissolution are important properties in studying cocrystals, in particular in order to predict stability in aqueous solution and to address biopharmaceutical parameters. In earlier studies by Rodríguez-Hornedo and co-workers, it was shown, based on carbamazepine cocrystals that cocrystal solubility is dependent on the solubility of the coformer (Good and Rodríguez-Hornedo, 2009; Nehm et al., 2006). For cocrystals with ionisable components mathematical models were established to predict cocrystal solubility at various pH (Bethune et al., 2009). However, there are only a few studies which confirm these predictions (Cooke et al., 2008; Reddy et al., 2009; Rodríguez-Hornedo et al., 2006). Dissolution on the other hand depends on solubility and is important to investigate changes which might, for example, occur in the case of solution-mediated solid state transformations.

In Chapter 3, the solubility and dissolution behaviour was demonstrated for the SD:4-ASA 1:1 cocrystal. Solubility was shown to be pH-dependent and predictable by a theoretical model established on the basis of the dual amphoteric character of the cocrystal. Dissolution studies revealed an improved dissolution rate of the poorly water-soluble SD from the cocrystal.

In the following work, the focus was to investigate the solubility and dissolution behaviour of other SD:aromatic carboxylic acid cocrystals such as SD:BA, SD:SA and SD:NA which have been characterised in Chapter 4. The primary objectives were (1) to predict the solubility pH-dependence by applying adequate models and (2) to compare the results with the earlier studied SD:4-ASA cocrystal in order to evaluate the role of the coformer on solubility and dissolution.

5.2 Materials and Methods

5.2.1 Materials

Sulfadimidine (SD), benzoic acid (BA), salicylic acid (SA) and nicotinic acid (NA) were purchased from Sigma-Aldrich (Ireland). Methanol, HPLC grade, was purchased from Fisher Scientific (Ireland), sodium hydrogen phosphate and citric acid were obtained from Sigma-Aldrich (Ireland). Water, analytical and HPLC grade, was prepared from an Elix 3 connected to a Synergy UV system (Millipore, UK). All other chemicals purchased from commercial suppliers were of analytical grade. The sulfadimidine:benzoic acid (SD:BA) 1:1, sulfadimidine:salicylic acid (SD:SA) 1:1 and

the sulfadimidine:nicotinic acid (SD:NA) 1:1 cocrystals were prepared by liquid-assisted milling using MeOH, MeCN and MeOH, respectively, as described in Chapter 4.

5.2.2 Methods

5.2.2.1 Solubility studies

5.2.2.1.1 Equilibrium solubility

The solubility was determined by the shake flask method at 12, 24, 48 and 72 hours. Excess cocrystal was added to 10 ml of water in glass ampoules, which were then heat sealed and placed horizontally in a thermostated waterbath at 37 °C and shaken at 100 cpm. The supernatant was filtered using 0.45 µm membrane filters (PVDF - Cronus®) and analysed for sample concentration by HPLC. The remaining solid phase was characterised by PXRD. Solubility studies were performed in triplicate for each sample.

5.2.2.1.2 Transition concentration (C_{tr}) measurement

The study was performed as described in Chapter 3, except that the equilibration time was 24 hours instead. In the case of the SD:NA 1:1 cocrystal, C_{tr} measurements were also performed at different pH by the addition of small volumes of 1M HCl and 1M NaOH.

5.2.2.1.3 pH-dependent solubility

The study was performed as described in Chapter 3, except that the equilibration time was 24 hours instead.

5.2.2.2 Powder X-ray Diffraction (PXRD)

as described in Chapter 2

5.2.2.3 Intrinsic dissolution studies

The studies were performed based on the method as described in Chapter 2. The compacts were compressed at a pressure of 6 or 8 tonnes for 30 seconds up to 2 minutes depending on the type of sample and to ensure no capping (details are attached in Appendix 4, Table A.4.3). The compact surface was analysed by ATR-FTIR and SEM.

5.2.2.4 High Performance Liquid Chromatography (HPLC)

HPLC was performed using a modification of the method described in Chapter 3. Therefore, SD, BA, SA and NA solution concentrations were determined using a Shimadzu HPLC Class VP series with a LC-10AT VP pump, SIL-10AD VP autosampler and SCL-10VP system controller. The mobile phase was vacuum filtered through a 0.45 μm membrane filter (Gelman Supor-450). Separation was performed on a Phenomenex Inertsil ODS (3) C18 column (150 mm length, diameter 4.6 mm, particle size 5 μm) at a UV detection wavelength of 235 nm (SD:BA and SD:SA cocrystal) or 260 nm (for SD:NA cocrystal). The injection volume was 10 μL. The mobile phase consisted of methanol/buffer pH 6.5 30/70 (v/v). The buffer was prepared from a 200 mM solution of sodium hydrogen phosphate solution adjusted to pH 6.5 with a 100 mM solution of citric acid. The elution was carried out isocratically at ambient temperature with a flow rate of 1 ml/min. For peak evaluation, Class-VP 6.10 software was used. For SD, BA and SA (detected at 235 nm) the calibration curves were prepared between 0.5–200 μg/ml. For SD and NA (detected at 260 nm) the calibration ranged from 2–400 μg/ml and from 2–200 μg/ml, respectively. All calibration curves displayed good linearity with $R^2 > 0.999$. Based on the ICH guidelines (ICH, 1996), for SD the calculated LOD was 0.1 μg/ml (235 nm) and 0.2 μg/ml (260 nm) and the LOQ was 0.3 μg/ml (235 nm) and 0.5 μg/ml (260 nm). In the case of BA, the the LOD was 0.2 μg/ml and the LOQ was 0.6 μg/ml. For SA the LOD and LOQ were calculated as 0.1 μg/ml and 0.4 μg/ml, respectively. For NA the LOD was 0.2 μg/ml and the LOQ was 0.6 μg/ml.

All other methods used such as ATR-FTIR, SEM and statistical analyses are described in Chapter 2.

5.3 Results and Discussion

5.3.1 Solubility

Equilibrium solubility

Initially, the SD:BA, SD:SA, SD:NA cocrystal and the coformer components were studied for equilibrium solubility in water. Figure 5.1 shows the solubility of the cocrystals measured after 12, 24, 48 and 72 hours. It was found that for all cocrystals the concentrations did not change significantly between 12 and 72 hours ($p > 0.05$).

Similarly, for all coformer components no changes occurred between 12 and 72 hours. The appropriate concentration-time profiles can be found in Appendix 4 (Figure A.4.1 and Table A.4.2).

Based on those results all further solubility studies were performed with an equilibration time of 24 hours and thus, in the following text solubility values refer to 24 hours data.

As illustrated in Figure 5.1, the SD:NA cocrystal showed the highest solubility ($1.52 \times 10^{-2} \pm 0.07 \times 10^{-2}$ mmol/ml), followed by the SD:SA cocrystal ($2.47 \times 10^{-3} \pm 0.02 \times 10^{-3}$ mmol/ml), whereas the SD:BA cocrystal revealed the lowest solubility ($1.16 \times 10^{-3} \pm 0.00 \times 10^{-3}$ mmol/ml). For the coformer components the solubility increased in the order of SA<BA<NA, where solubility values of $2.55 \times 10^{-2} \pm 0.04 \times 10^{-2}$ mmol/ml, $4.04 \times 10^{-2} \pm 0.01 \times 10^{-2}$ mmol/ml and $19.3 \times 10^{-2} \pm 0.15 \times 10^{-2}$ mmol/ml were found, respectively (Appendix 4, Figure A.4.1 and Table A.4.2).
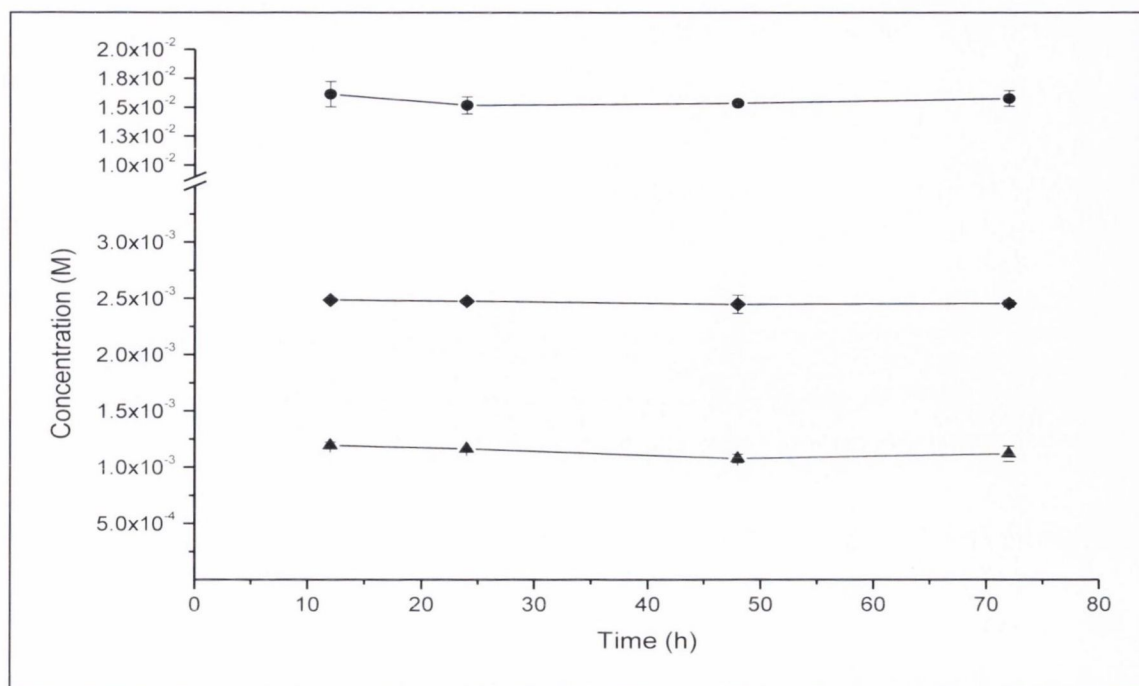
Figure 5.1: Concentration-time profiles of SD:BA (triangles), SD:SA (diamonds) and SD:NA (circles) 1:1 cocrystals over 72 hours in water at 37 °C.

Stability of the cocrystals was analysed by PXRD after each equilibration time. It was found that the SD:BA and SD:SA cocrystals were stable over 72 hours since no changes in the diffraction patterns were detected when compared with the initially added cocrystal (t=0) (Figure 5.2, Figure 5.3). These results indicated that both cocrystals were congruently saturating in water. In contrast, for the SD:NA 1:1 cocrystal the presence of a SD characteristic diffraction peak at 9.35° 2θ was observed at each equilibration time (Figure 5.4). It was concluded that the SD:NA cocrystal was not stable and incongruently saturating in water, probably as a result of a high solubility difference between the components, as NA is approximately 84 times more soluble than SD (see Chapter 3 for SD solubility).
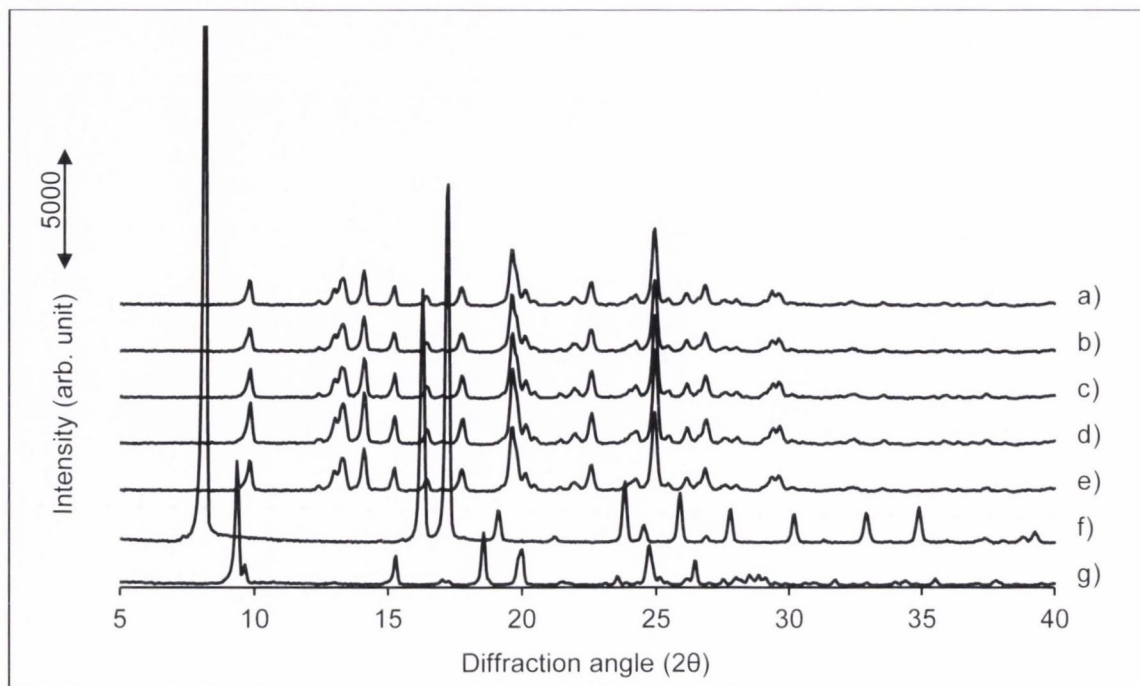
Figure 5.2: PXRD analysis of SD:BA 1:1 cocrystal during equilibrium solubility study after a) 72 hours, b) 48 hours, c) 24 hours, d) 12 hours, e) 0 hours compared to f) BA and g) SD.
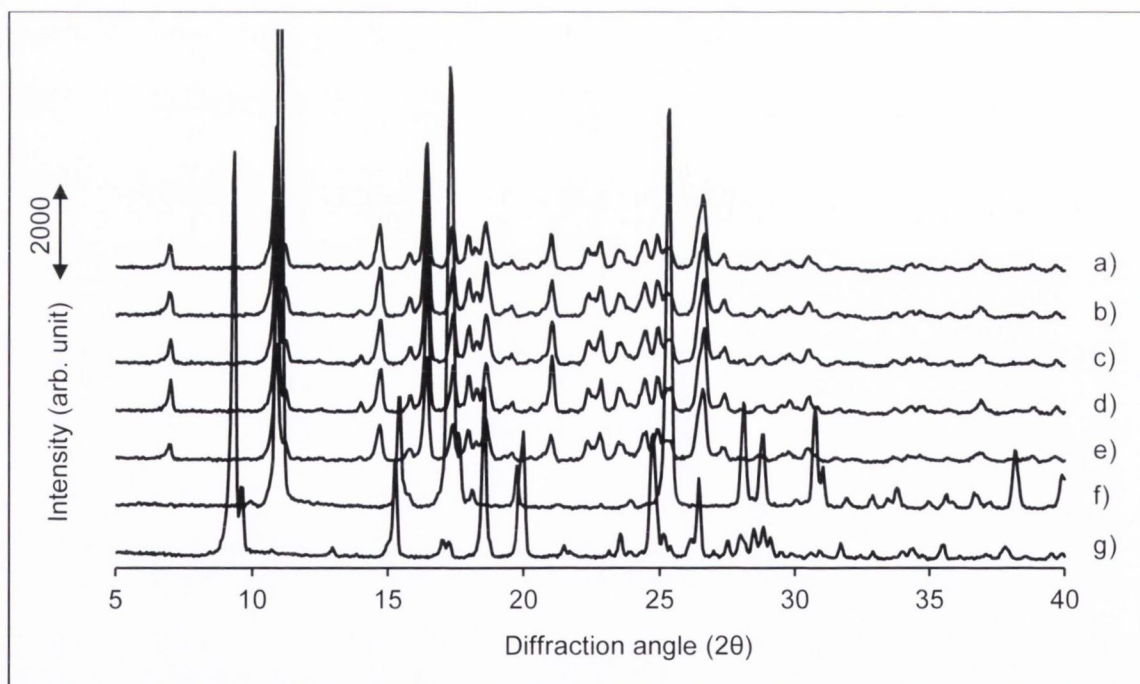
Figure 5.3: PXRD analysis of SD:SA 1:1 cocrystal during equilibrium solubility study after a) 72 hours, b) 48 hours, c) 24 hours, d) 12 hours, e) 0 hours compared to f) SA and g) SD.
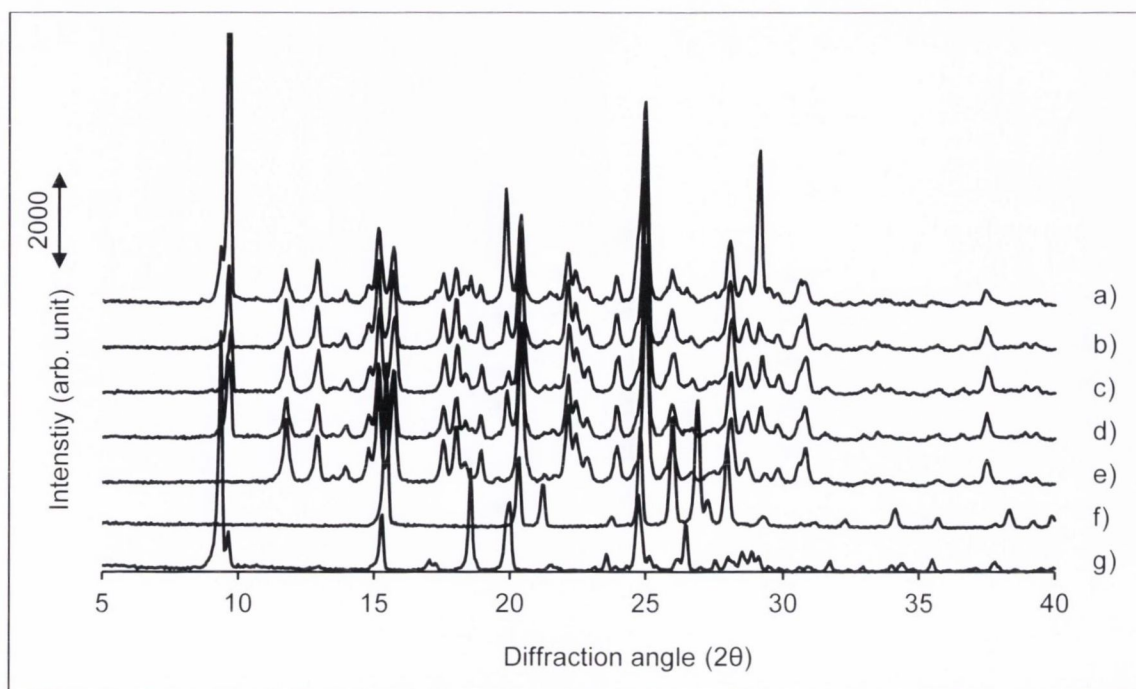
Figure 5.4: PXRD analysis of SD:NA 1:1 cocrystal during equilibrium solubility study after a) 72 hours, b) 48 hours, c) 24 hours, d) 12 hours, e) 0 hours compared to f) NA and g) SD.

Transition concentration measurement/pH-dependent solubility

The stability of cocrystals in water is an important property to investigate because many drugs exhibit low solubility in water. In previously reported work by Good and Rodríguez-Hornedo (2009) and as demonstrated in Chapter 2 and 3, the transition concentration (C_{tr}), at which cocrystal and drug coexist in equilibrium with the solution was found to be the key parameter in indicating the thermodynamic stability and solubility of cocrystals (Good and Rodríguez-Hornedo, 2009). To control crystallisation processes, knowledge of the C_{tr} is an essential requirement. Furthermore, for unstable cocrystals the C_{tr} was shown to be the nearest measurable equilibrium from which the cocrystal solubility can be estimated. The C_{tr} is defined at a given pH, which allows, in the case of ionisable cocrystals such as the SD:BA, SD:SA and SD:NA cocrystals, determination of the pH dependent solubility product. Therefore, the actual solubility was determined based on C_{tr} measurements.

By analysing the solid phase after equilibration using PXRD it was verified that transition concentrations were reached. Figure 5.5 confirms for the SD:BA, SD:SA and SD:NA cocrystal the detection of a mixed phase composed of cocrystal and SD at C_{tr}. The presence of SD was identified by the characteristic diffraction peak at 9.35° 2θ.
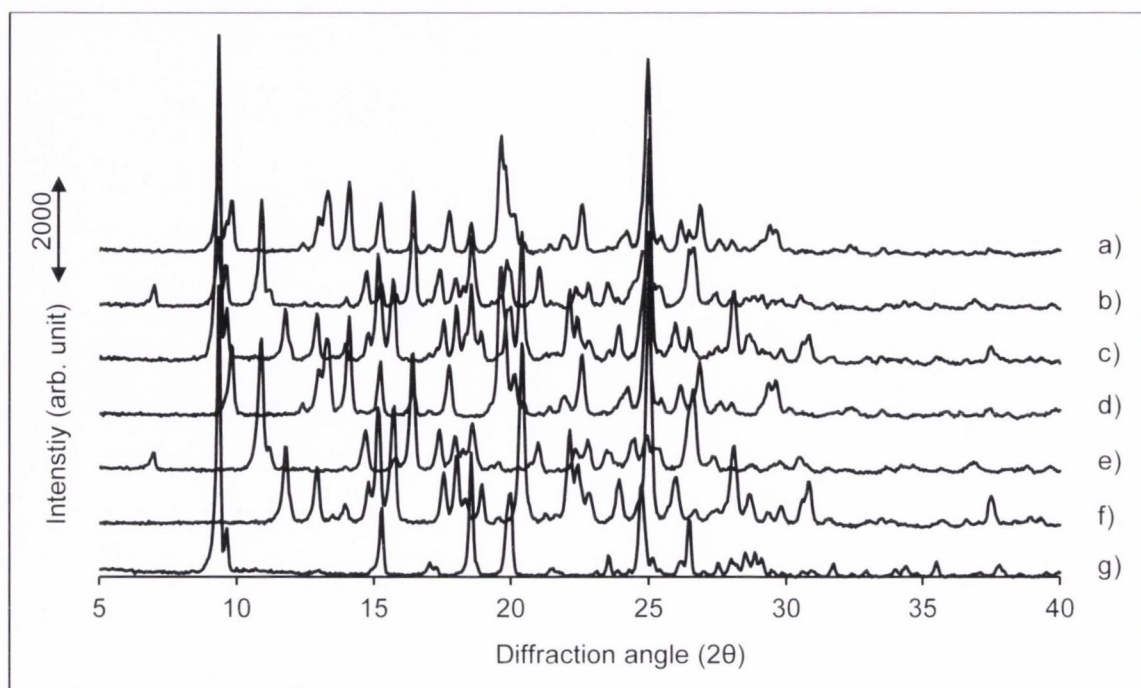
Figure 5.5: PXRD analysis of solid at the transition concentration (C_{tr}) of a) SD:BA, b) SD:SA and c) SD:NA 1:1 cocrystal compared to d) pure SD:BA, e) pure SD:SA, f) pure SD:NA 1:1 cocrystal and g) SD.

The SD:BA cocrystal represents an example of a cocrystal composed of one amphoteric (SD) and one monoprotic acidic component (BA). The equation describing the solubility of such a cocrystal type was derived previously (Bethune et al., 2009) and can be presented for the SD:BA cocrystal as:

$$S_{cocrystal} = \sqrt{K_{sp}\left(1 + \frac{K_{a,BA}}{[H^+]}\right)\left(1 + \frac{[H^+]}{K_{a1,SD}} + \frac{K_{a2,SD}}{[H^+]}\right)} \qquad (5.1)$$

where K_{sp} is the solubility product and K_a and K_{a1}/K_{a2} are the acid ionization constants for BA and SD, respectively.

At the transition concentration equation 5.1 can be rewritten and K_{sp} can be expressed by the following equation

$$K_{sp} = \frac{[SD]_{tr}\,[BA]_{tr}}{\left(1 + \frac{K_{a,BA}}{[H^+]}\right)\left(1 + \frac{[H^+]}{K_{a1,SD}} + \frac{K_{a2,SD}}{[H^+]}\right)} \qquad (5.2)$$

where $[BA]_{tr}$ and $[SD]_{tr}$ are the transition concentrations of BA and SD, respectively.

In contrast, the SD:SA cocrystal contains one amphoteric and one diprotic acidic component, which solubility can be described by the following equations based on the mathematical derivations established by Reddy et al. (2009):

$$S_{cocrystal} = \sqrt{K_{sp}\left(1 + \frac{K_{a1,SA}}{[H^+]} + \frac{K_{a1,SA}K_{a2,SA}}{[H^+]^2}\right)\left(1 + \frac{[H^+]}{K_{a1,SD}} + \frac{K_{a2,SD}}{[H^+]}\right)} \quad (5.3)$$

where K_{sp} is the solubility product and K_{a1} and K_{a2} are the acid ionization constants of SA and SD, respectively.

Further derivations of equation 5.3 enable K_{sp} to be determined using the eutectic/transition (tr) concentrations by:

$$K_{sp} = \frac{[SD]_{tr}\,[SA]_{tr}}{\left(1 + \frac{K_{a1,SA}}{[H^+]} + \frac{K_{a1,SA}K_{a2,SA}}{[H^+]^2}\right)\left(1 + \frac{[H^+]}{K_{a1,SD}} + \frac{K_{a2,SD}}{[H^+]}\right)} \quad (5.4)$$

where $[SA]_{tr}$ and $[SD]_{tr}$ are the transition concentrations of SA and SD, respectively. A detailed description of the mathematical derivations of equations 5.1 to 5.4 can be found in Appendix 4.

The SD:NA cocrystal contains two amphoteric components with similar dissociation behaviour as the previously studied SD:4-ASA 1:1 cocrystal (see Chapter 3). Thus, the solubility can be expressed by the same equations:

$$S_{cocrystal} = \sqrt{K_{sp}\left(1 + \frac{[H^+]}{K_{a1,SD}} + \frac{K_{a2,SD}}{[H^+]}\right)\left(1 + \frac{[H^+]}{K_{a1,NA}} + \frac{K_{a2,NA}}{[H^+]}\right)} \quad (5.5)$$

where K_{sp} is the solubility product and K_{a1} and K_{a2} are the acid ionization constants of SD and NA, respectively. Rewritten, equation 5.5 allows determination of K_{sp} from the eutectic/transition (tr) concentrations using

$$K_{sp} = \frac{[SD]_{tr}\,[NA]_{tr}}{\left(1 + \frac{[H^+]}{K_{a1,SD}} + \frac{K_{a2,SD}}{[H^+]}\right)\left(1 + \frac{[H^+]}{K_{a1,NA}} + \frac{K_{a2,NA}}{[H^+]}\right)} \quad (5.6)$$

$[SD]_{tr}$ and $[NA]_{tr}$ are the transition concentrations of SD and NA, respectively. A detailed description of the derivations of equation 5.5 and 5.6 was presented in Chapter 3 for the SD:4-ASA 1:1 cocrystal as example.

Based on the experimentally measured transition concentrations and the pH as well as the known acid constants, the solubility products (K_{sp}) of the SD:BA, SD:SA and SD:NA cocrystals were determined using equation 5.2, equation 5.4 and equation 5.6, respectively. The equations 5.1, 5.3 and 5.5 were further used to calculate the solubility of the cocrystals at other pH values. In order to evaluate the predictions with experimental data, cocrystal solubilities were also determined at different pH value. In the case of the SD:BA and SD:SA cocrystal it was shown that both cocrystals were stable in water at 37 °C as it was shown by PXRD analysis in Figure 5.2 and Figure 5.3. Therefore, the solubility could be directly measured by equilibrating excess cocrystal in water according to the following equation for a 1:1 cocrystal:

$$S_{cocrystal} = \sqrt{[\mathbf{drug}][\mathbf{coformer}]} \tag{5.7}$$

For the SD:NA 1:1 cocrystal the solubility at different pH values was determined at the transition concentration. This was required because it was observed that the cocrystal was unstable in water at 37 °C showing conversion to the SD component (Figure 5.4). Using the transition concentration the solubility was calculated by:

$$S_{cocrystal} = \sqrt{[\mathbf{drug}]_{tr}\,[\mathbf{coformer}]_{tr}} \tag{5.8}$$

The determined solubility products and the resulting solubility profiles at different pH values are shown in Figure 5.6, Figure 5.8 and Figure 5.10. In order to predict the solubility and stability of all solid phases, the pH-dependent solubility of the single components was derived from the Henderson-Hasselbalch relationship, as described earlier in Chapter 3.

The SD:BA 1:1 cocrystal had a solubility product (K_{sp}) value of $7.71\times10^{-7} \pm 0.51\times10^{-7}$ M^2 and the predicted pH-dependent solubility is shown in Figure 5.6. From the profile it was concluded that the cocrystal is stable below pH 5 when compared with the theoretical solubility profiles of the single components. At pH $\leq$ 5 the cocrystal is less soluble or as soluble as SD and BA, whereas at pH > 5 the cocrystal becomes more soluble than SD. The experimentally determined solubility at pH 3.60 was in good agreement with the calculated profile and is consistent with the PXRD analysis of the solid phase which showed that the cocrystal was stable under the given conditions

(Figure 5.7). For solubilities measured at higher pH (pH 9.19 and 8.11) the values deviated from the predictions and were found to be lower and in close proximity to the solubility curve of SD (Figure 5.6). However, this was not surprising with respect to the theoretical solubility profiles which predicted that at pH > 5 the cocrystal is more soluble than SD and thus may transform to SD. PXRD analysis of the solid phase confirmed the presence of SD attributed to the characteristic diffraction peak at 9.35° 2θ (Figure 5.7). At these pH values more coformer would have been required to keep the cocrystal stable in solution.
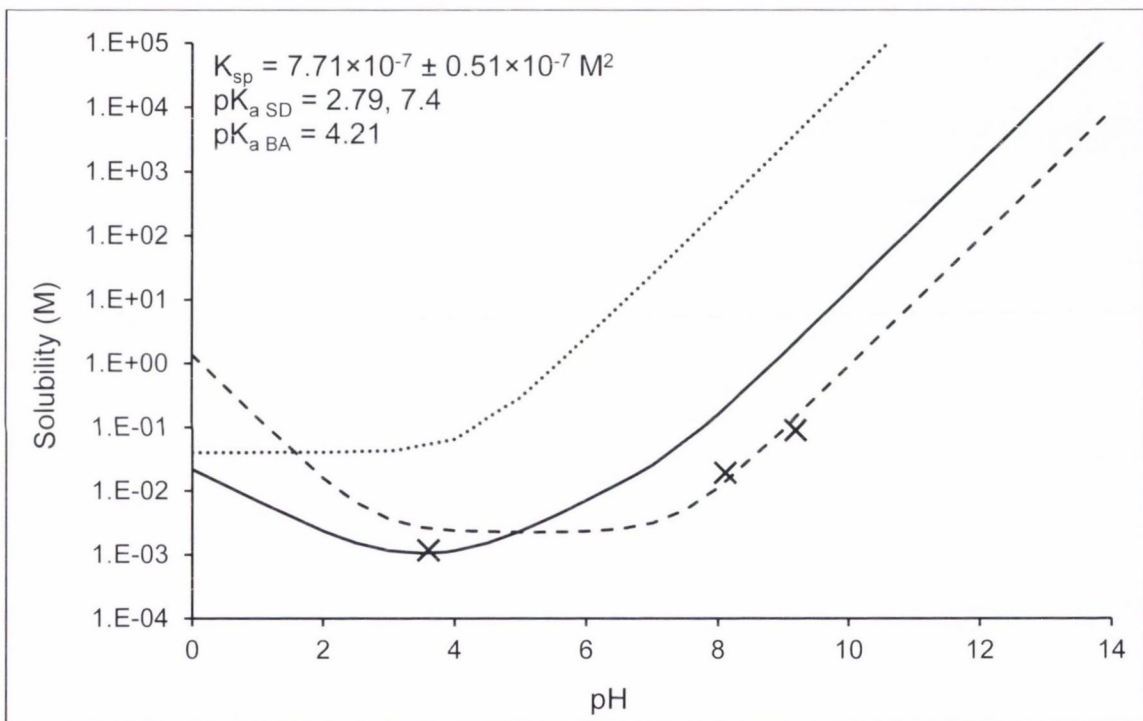
Figure 5.6: Theoretical – pH solubility profile for the SD:BA 1:1 cocrystal in water at 37 °C. The solid line represents the cocrystal solubility, the dashed and dotted lines show the theoretical SD and BA solubility dependent on the pH (derived from the Henderson-Hasselbalch relationship) and the cross symbols are experimentally obtained solubility data for the cocrystal.
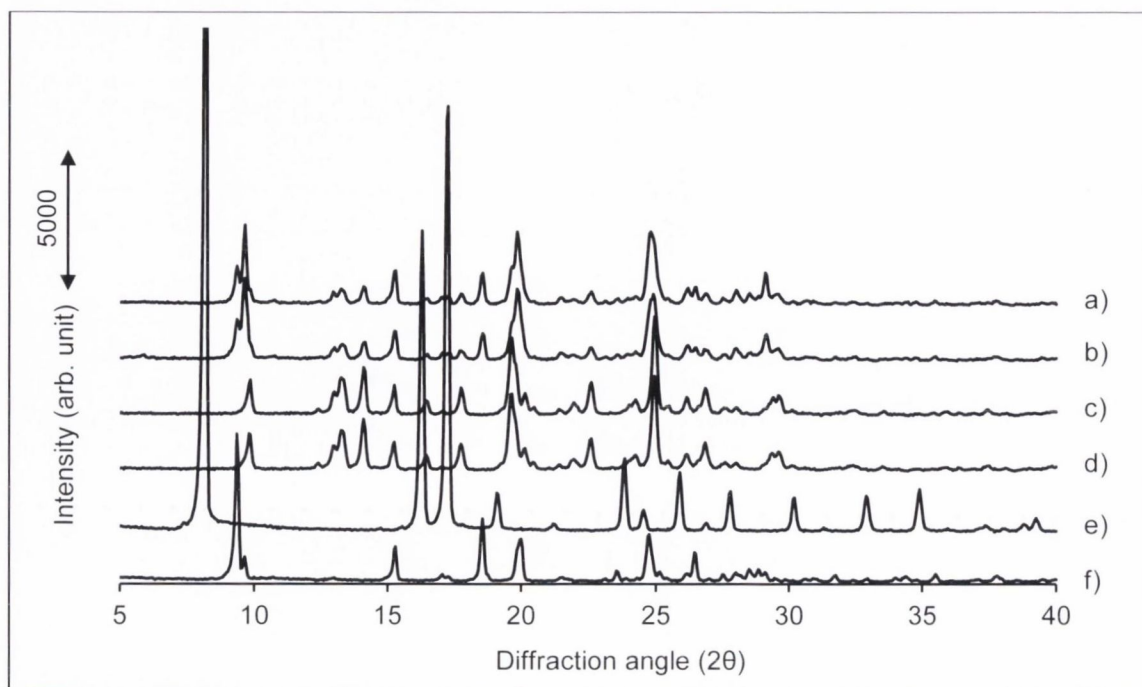
Figure 5.7: PXRD patterns of the SD:BA 1:1 cocrystal phases at different solution pH compared to the initially added cocrystal and the single components. a) cocrystal at pH = 9.19, b) cocrystal at pH = 8.11, c) cocrystal at pH = 3.60, d) initially added cocrystal, e) BA and f) SD.

For the SD:SA 1:1 cocrystal an approximately 1.8-fold higher solubility product (K_{sp}) than for the SD:BA cocrystal was determined with a value of $1.39 \times 10^{-6} \pm 0.08 \times 10^{-6}\, M^2$. The predicted solubility profile for different pH values is illustrated in Figure 5.8. A comparison with the calculated solubility curves of the single components showed that the cocrystal is stable below pH 3.5 at which it is more soluble than SA and SD. Experimentally obtained solubility data at pH 3.20 were consistent with the predicted solubility curve and PXRD analysis confirmed the presence of cocrystal as the only phase (Figure 5.9). Solubility values determined at pH 6.06 and 9.19 deviated from the calculated cocrystal solubility curve and were found to be a result of SD formation. PXRD analysis confirmed the presence of SD by the characteristic peak at 9.35° 2θ (Figure 5.9). However, at pH 6.06 SD was only weakly detectable indicating that SD formed to a smaller extent than at higher pH. These results confirmed the predictions that at pH > 3.5 formation of SD occurs. In order to stabilise the cocrystal at pH > 3.5 the addition of excess SA and thus non-stoichiometric conditions would be required, similarly as was observed for the SD:BA cocrystal.
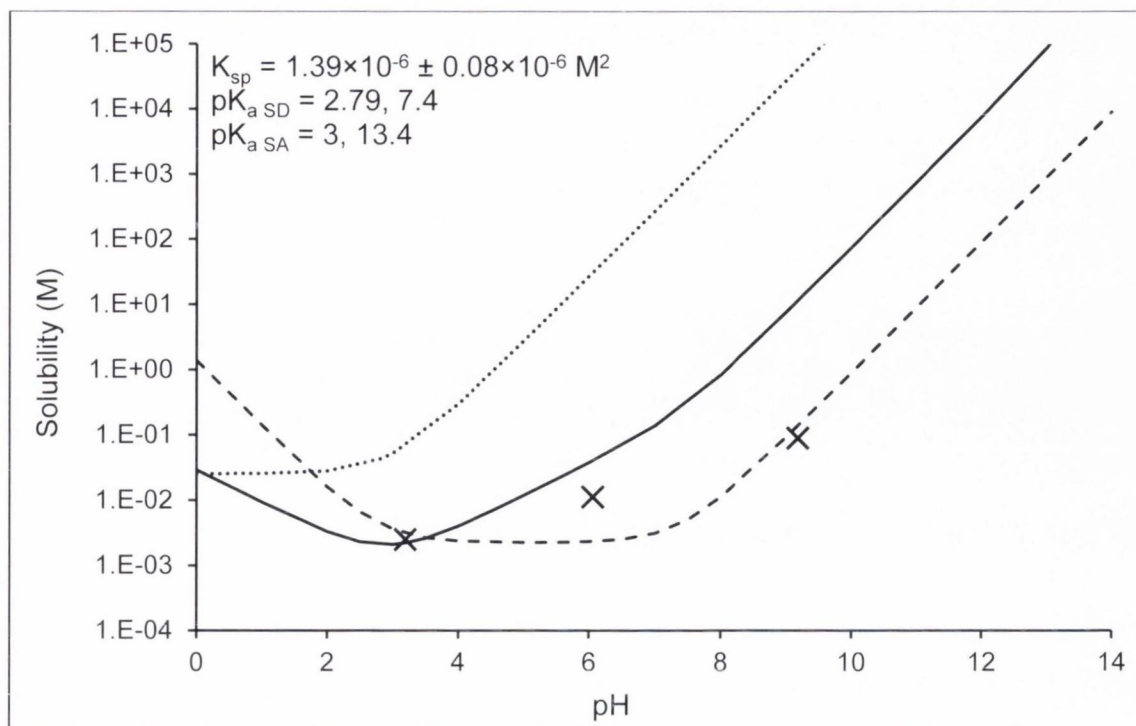
Figure 5.8: Theoretical – pH solubility profile for the SD:SA 1:1 cocrystal in water at 37 °C. The solid line represents the cocrystal solubility, the dashed and dotted lines show the theoretical SD and SA solubility dependent on the pH (derived from the Henderson-Hasselbalch relationship) and the cross symbols are experimentally obtained solubility data for the cocrystal.
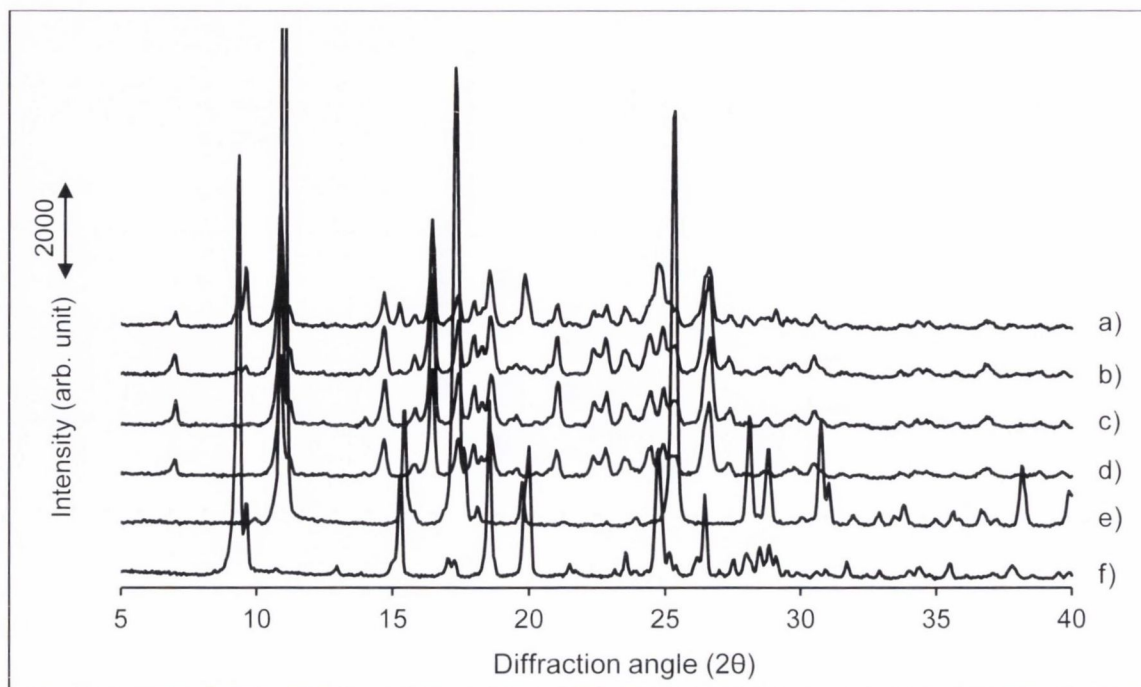
Figure 5.9: PXRD patterns of the SD:SA 1:1 cocrystal phases at different solution pH compared to the initially added cocrystal and the single components. a) cocrystal at pH = 9.19, b) cocrystal at pH = 6.06, c) cocrystal at pH = 3.20, d) initially added cocrystal, e) SA and f) SD.

The SD:NA 1:1 cocrystal revealed a solubility product (K_{sp}) value of $1.46 \times 10^{-4} \pm 0.01 \times 10^{-4}$ M^2 and was therefore the most soluble cocrystal. In Figure 5.10 the resulting pH-dependent solubility profile is illustrated which shows that the cocrystal is more soluble than SD over the entire pH range supporting the initial findings that this cocrystal is unstable in water (Figure 5.4). Experimentally determined solubilities at different pH based on the transition concentration (C_{tr}) at which cocrystal is in equilibrium with SD were in good agreement with the predicted solubility curve. These results confirmed the pH-dependence of the C_{tr} (Bethune et al., 2009) and showed on the other hand that the cocrystal was stable at the given conditions. PXRD analysis was consistent with the solubility data as displayed in Figure 5.11. At each pH the solid phase was a mixed phase of cocrystal and SD confirming that transition concentrations were reached.
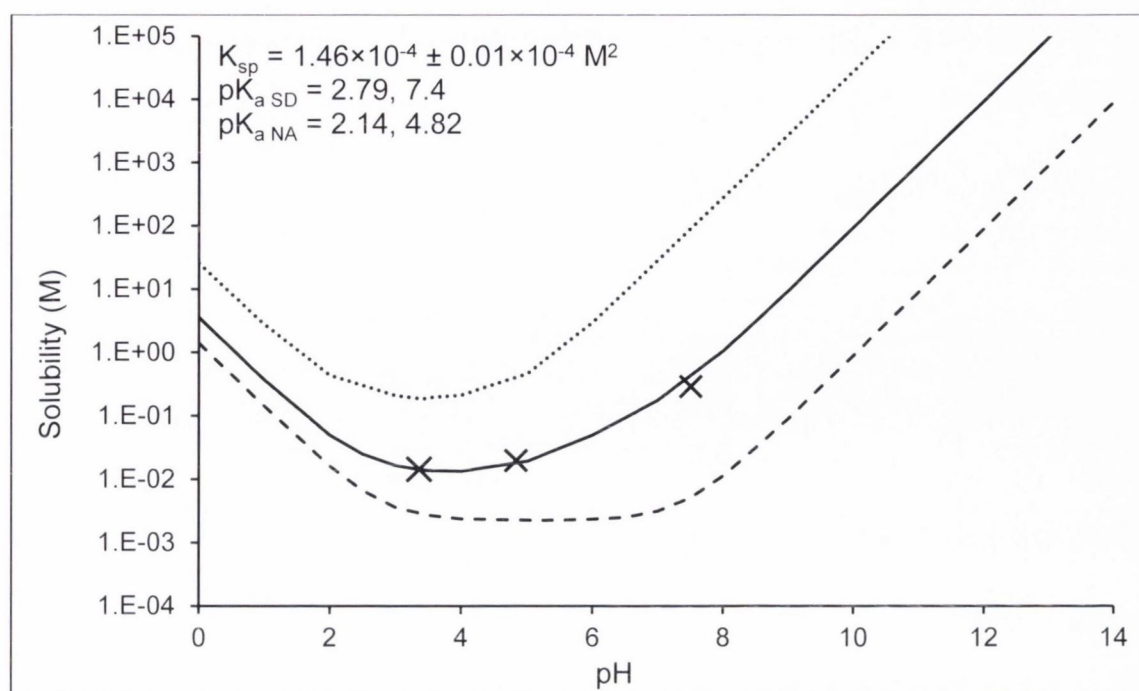
Figure 5.10: Theoretical – pH solubility profile for the SD:NA 1:1 cocrystal in water at 37 °C. The solid line represents the cocrystal solubility, the dashed and dotted lines show the theoretical SD and NA solubility dependent on the pH (derived from the Henderson-Hasselbalch relationship) and the cross symbols are experimentally obtained solubility data for the cocrystal.
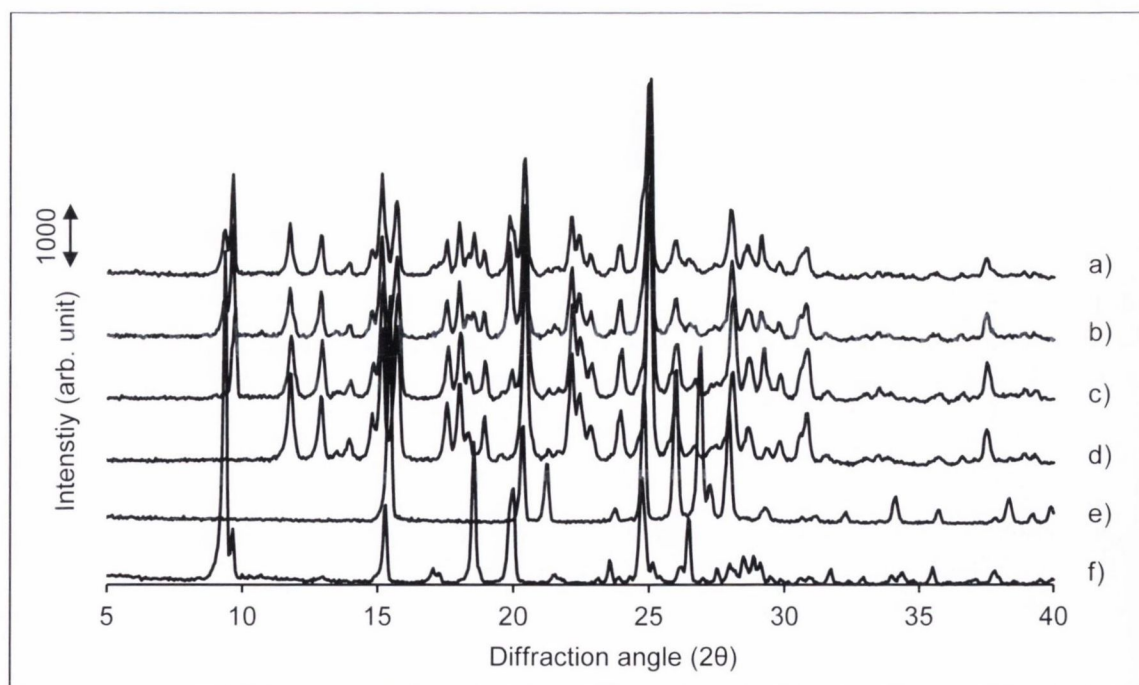

Figure 5.11: PXRD patterns of the SD:NA 1:1 cocrystal phases at the transition concentration (C_{tr}) at different solution pH compared to the initially added cocrystal and the single components. a) at pH = 7.51, b) at pH = 4.83, c) at pH = 3.36, d) initially added cocrystal, e) NA and f) SD.

Overall, it was shown that for each cocrystal the solubility was pH-dependent and could be predicted by mathematical models which have been reported previously for cocrystals composed of one amphoteric and one monoprotic, one amphoteric and one diprotic acidic component (Bethune et al., 2009; Reddy et al., 2009) and for cocrystals composed of two amphoteric components (see Chapter 3).

When comparing the solubilities obtained for the SD:BA, SD:SA and SD:NA cocrystal with those of the previously investigated SD:4-ASA form I cocrystal which has been described in detail in Chapter 3, the following trend was revealed: The cocrystal solubility product (K_{sp}) increased in the order of SD:BA<SD:SA<SD:4-ASA<SD:NA, whereas the coformer solubility increased in the order of 4-ASA<SA<BA<NA. A summary of the values is presented in Table 5.1.

These findings showed that the cocrystal solubility (represented by the solubility product, K_{sp}) did not correlate with the solubility of the coformer. In the cases where the cocrystal and thus the presence of SD revealed a higher solubility than the coformer, as shown for the SD:SA and SD:4-ASA cocrystals, it was suggested that solution complexation of SD by the coformer might be the reason. However, as it has been shown in Chapter 3 for the SD:4-ASA cocrystal, based on phase solubility studies solution complexation was found to be negligible. Besides, for both, the SD:4-ASA and the SD:SA cocrystal, the measured SD solubility at C_{tr}, $[SD]_{tr}$ was not significantly different from the solubility of SD, $[SD]_0$ indicating that SD was not solubilised by 4-ASA and SA, respectively.

In earlier work it was reported that a direct correlation between the cocrystal and coformer solubility is not always given and may be a result of different solid state interactions in the cocrystal lattice (Good and Rodríguez-Hornedo, 2009). Therefore, it was further investigated if a correlation between the cocrystal solubilities and lattice energies can be established, based on calculation of the ideal solubility (x_{ideal}) of the cocrystals using the following equation

$$\ln x_{ideal} = \frac{-\Delta H_m}{R} \left(\frac{T_m - T}{T_m * T} \right) \qquad (5.9)$$

where ΔH_m, T_m and R are the melting enthalpy (J/mol), the melting temperature (K) and the gas constant (J/mol K^{-1}), respectively. T represents the solution temperature which in this case is 37 °C.

However, as shown in Table 5.2, the calculated ideal solubilities increased in the order of SD:4-ASA<SD:BA<SD:NA<SD:SA and did therefore not correlate with the experimentally determined solubilities (Table 5.1). The ideal solubilities were in general $10^4 - 10^6$ times higher than the experimentally measured cocrystal solubilities, indicating non-ideal behaviour in water. These results let conclude that the cocrystal solubilities are controlled by the individual interactions between water, the solute and the solid state since no correlation can be established to either the lattice energies or the coformer solubilities. Similar findings have been reported by Good and Rodgriguez-Hornedo (2009).

Table 5.1: A summary of the results from solubility studies of four selected SD:aromatic carboxylic acid 1:1 cocrystals (CC) performed in water at 37°C.

Cocrystal	K_{sp} (M^2)	$[coformer]_0$[b]	CC solubility advantage $[CC]/[SD]_0$[d]
SD:BA	$7.71 \times 10^{-7} \pm 0.51 \times 10^{-7}$	$4.04 \times 10^{-2} \pm 0.01 \times 10^{-2}$	0.50
SD:SA	$1.39 \times 10^{-6} \pm 0.08 \times 10^{-6}$	$2.55 \times 10^{-2} \pm 0.04 \times 10^{-2}$	0.98
SD:4-ASA[a]	$1.91 \times 10^{-6} \pm 0.16 \times 10^{-6}$	$1.49 \times 10^{-2} \pm 0.00 \times 10^{-2}$ [c]	1.23
SD:NA	$1.46 \times 10^{-4} \pm 0.01 \times 10^{-4}$	$19.3 \times 10^{-2} \pm 0.15 \times 10^{-2}$	6.21

a) refers to form I cocrystal, details can be found in Chapter 3

b) refers to coformer solubility in absence of SD

c) refers to the apparent (non-equilibrium) solubility

d) calculation refers to Good and Rodríguez-Hornedo, 2009

Table 5.2: A summary of the melting temperatures (T_m), melting enthalpies (ΔH_m) and the thereof calculated ideal solubilities (S_{ideal}) of the SD:BA, SD:SA, SD:4-ASA and SD:NA 1:1 cocrystals using equation 5.9.

Cocrystal	T_m (°C)	ΔH_m (kJ/mol)[c]	S_{ideal} (mol/kg)[d]
SD:BA[a]	216.95 ± 1.23	41.06 ± 0.96	0.16
SD:SA[a]	196.65 ± 1.97	29.59 ± 0.57	1.15
SD:4-ASA[b]	170.38 ± 0.89	51.95 ± 3.59	0.13
SD:NA[a]	205.18 ± 0.71	33.63 ± 1.23	0.57

a) determined values for T_m and ΔH_m refer to Chapter 4

b) refers to form I cocrystal, details can be found in Chapter 3

c) the melting enthalpy was normalised by the cocrystal stoichiometry

d) calculated by converting mole fractions to molality in water

The extent to which the coformer increased the solubility of SD was demonstrated by the ratio of cocrystal solubility measured at C_{tr} [CC] to SD solubility in the absence of the coformer [SD]$_0$ (CC solubility advantage). As displayed in Table 5.1, BA and SA showed no solubility advantage, whereas 4-ASA improved the solubility by a factor of 1.23. NA revealed the highest increase in solubility with a value of 6.21. This order was consistent with the order of the cocrystal solubility (represented by K_{sp}). It was concluded that only sulfadimidine cocrystals composed of 4-ASA and NA as coformers showed a solubility advantage with respect to the low-water soluble SD, the SD:NA 1:1 cocrystal being superior.

However, cocrystal solubility is usually inversely related to cocrystal stability (Reddy et al., 2009). The SD:NA 1:1 cocrystal was found to be unstable over the entire pH range but revealed the highest solubility referring to its K_{sp} value. The SD:BA, SD:SA and SD:4-ASA cocrystals were found to be less soluble but on the other hand stable, based on the PXRD analysis of the remaining solid, in the acidic environment at pH ≤ 5, at ≤ 3.5 and at pH ≤ 4, respectively. From these results it was further concluded that in these pH regions optimal conditions exist at which the cocrystals can be formed from water.

5.3.2 Intrinsic dissolution studies

Single components

The dissolution profiles of BA, SA and NA are illustrated in Figure 5.12. For all components dissolution was linear ($R^2 > 0.99$) and analysis of the surface of the compacts at the end of the study by IR spectroscopy verified that no phase changes occurred (Appendix 4, Figure A.4.2). The calculated intrinsic dissolution rates were compared with the coformer studied in Chapter 3, 4-ASA. The dissolution rates increased in the order of 4-ASA<SA<BA<NA (Table 5.3) and were therefore consistent with the solubility results.

The dissolution rate of SD was between 9–63 times lower than those of the coformer components (Table 5.3). Details of the dissolution behaviour of SD can be found in Chapter 3.
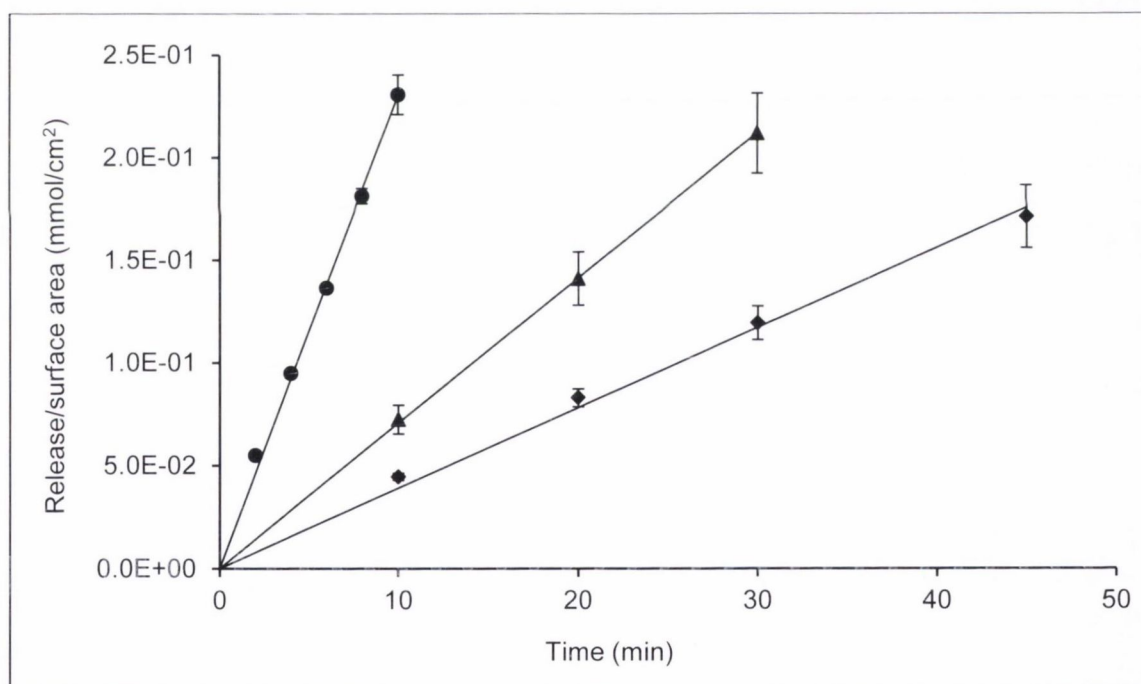
Figure 5.12: Dissolution-time profiles of coformer components: BA (triangles), SA (diamonds) and NA (circles).

Table 5.3: A summary of the intrinsic dissolution rates of the SD:BA, SD:SA, SD:4-ASA form I and SD:NA 1:1 cocrystal (CC) compared to equimolar physical mixtures (PM) and the pure components.

Type	Components	IDR (mmol/min/cm²)	Difference (α = 0.05)
Pure	SD	$3.64 \times 10^{-4} \pm 0.12 \times 10^{-4}$	–
	BA	$73.50 \times 10^{-4} \pm 5.68 \times 10^{-4}$	–
	SA	$39.10 \times 10^{-4} \pm 3.03 \times 10^{-4}$	–
	4-ASA	$32.60 \times 10^{-4} \pm 1.26 \times 10^{-4}$	–
	NA	$230.16 \times 10^{-4} \pm 5.93 \times 10^{-4}$	–
CC	SD:BA	SD: $1.54 \times 10^{-4} \pm 0.13 \times 10^{-4}$ BA: $1.66 \times 10^{-4} \pm 0.09 \times 10^{-4}$	SD: s. to pure SD and PM BA: s. to pure BA, n.s. to PM**
	SD:SA	SD: $3.97 \times 10^{-4} \pm 0.13 \times 10^{-4}$ SA: $4.01 \times 10^{-4} \pm 0.14 \times 10^{-4}$	SD: s. to pure SD and PM SA: s. to pure SA and PM
	SD:4-ASA	SD: $5.09 \times 10^{-4} \pm 0.27 \times 10^{-4}$ 4-ASA: $6.52 \times 10^{-4} \pm 0.33 \times 10^{-4}$	SD: s. to pure SD and PM 4-ASA: s. to pure 4-ASA and PM
	SD:NA	SD: $2.62 \times 10^{-4} \pm 0.02 \times 10^{-4}$ NA: $17.02 \times 10^{-4} \pm 1.18 \times 10^{-4}*$, $4.88 \times 10^{-4} \pm 0.35 \times 10^{-4}**$	SD: s. to pure SD and PM NA: s. to pure NA and PM**, n.s. to PM*
PM	SD:BA	SD: $2.39 \times 10^{-4} \pm 0.08 \times 10^{-4}$ BA: $3.51 \times 10^{-4} \pm 0.49 \times 10^{-4}*$, $1.75 \times 10^{-4} \pm 0.08 \times 10^{-5}**$	SD: s. to pure SD and CC BA: s. to pure BA, n.s. to CC**
	SD:SA	SD: $2.88 \times 10^{-4} \pm 0.17 \times 10^{-4}$ SA: $3.15 \times 10^{-4} \pm 0.17 \times 10^{-4}$	SD: s. to pure SD and CC SA: s. to pure SA and CC
	SD:4-ASA	SD: $3.89 \times 10^{-4} \pm 0.09 \times 10^{-4}$ 4-ASA: $9.78 \times 10^{-4} \pm 0.67 \times 10^{-4}*$, $4.05 \times 10^{-4} \pm 0.28 \times 10^{-4}**$	SD: n.s. to pure SD, s. to CC 4-ASA: s. to pure 4-ASA and CC
	SD:NA	SD: $2.24 \times 10^{-4} \pm 0.08 \times 10^{-4}$ NA: $17.97 \times 10^{-4} \pm 0.08 \times 10^{-4}*$, $3.94 \times 10^{-4} \pm 0.27 \times 10^{-4}**^{b)}$	SD: s. to pure SD and CC NA: s. to pure NA and CC**, n.s. to CC*

a) details can be found in Chapter 3

* initial rate (estimated from t=0 until t of 1ˢᵗ measuring point)

**limiting rate

b) based on 60–90 minutes data points

s. = significantly different (p < 0.05)

n.s. = not significantly different (p > 0.05)

SD:BA 1:1 cocrystal and physical mixture

As shown in Figure 5.13, the dissolution of SD and BA from the SD:BA 1:1 cocrystal was linear ($R^2 > 0.99$) and congruent over the entire time. The surface composition did not change, as confirmed by IR analysis (Figure 5.14). When compared to the pure components, the dissolution rates differed significantly. In comparison to dissolution rates of the single components, the dissolution rate of SD was more than 2-fold lower, whereas that of BA was more than 47 times lower (Table 5.3).
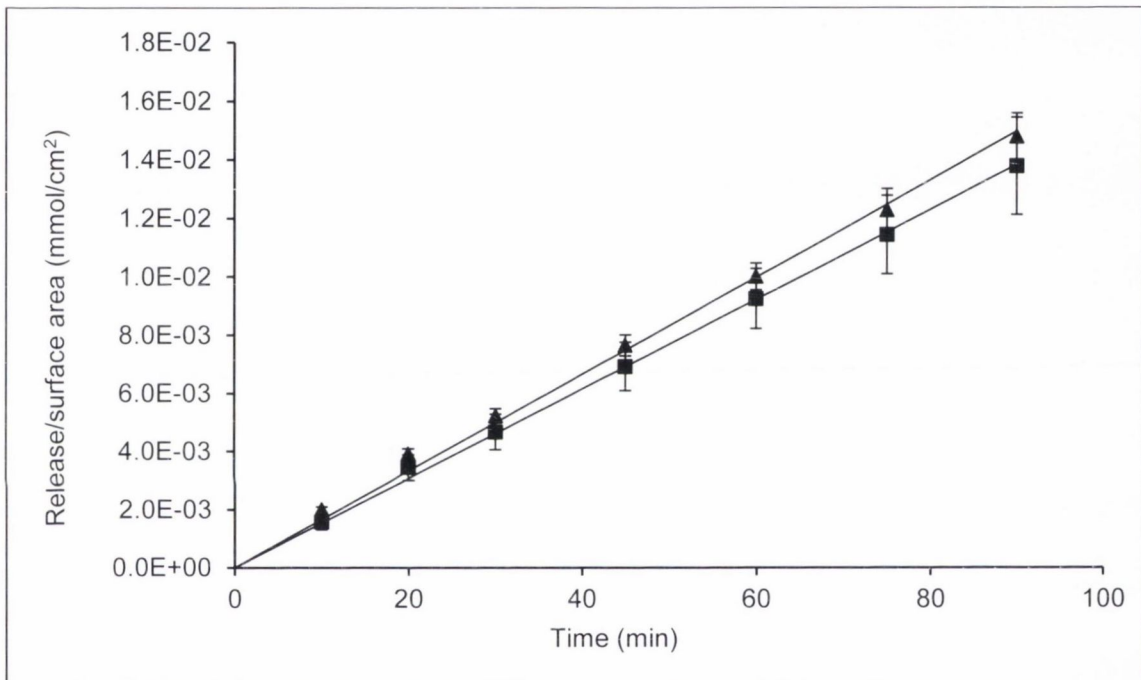
Figure 5.13: Dissolution profile of SD:BA 1:1 cocrystal in water at 37 °C. Squares symbolise SD, triangles represent BA.
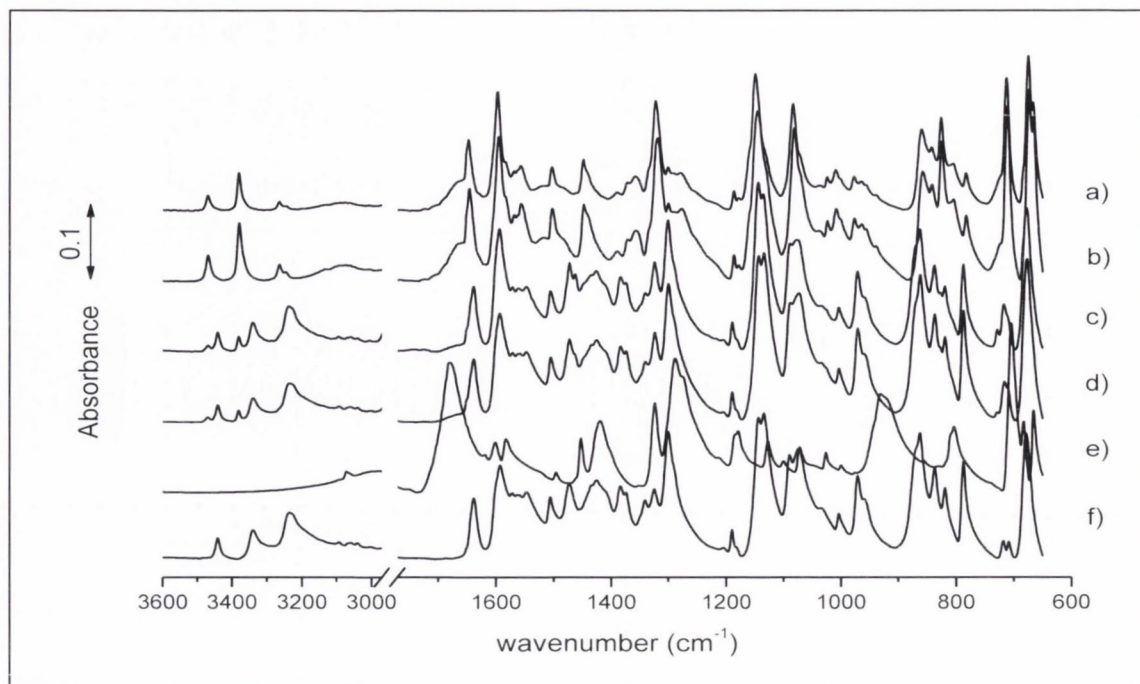
Figure 5.14: IR spectra of a) SD:BA CC after ID, b) SD:BA CC before ID, c) SD:BA PM after ID, d) SD:BA PM before ID compared to e) BA and f) SD.

For a stoichiometric equivalent physical mixture the dissolution profiles were also linear ($R^2 > 0.99$), however BA showed initially a faster release (Figure 5.15). Both components dissolved incongruently with SD dissolving faster than BA above 30 minutes of the dissolution study. However, no change in the surface composition was found by IR analysis (Figure 5.14). The dissolution rate was, in the case of SD, significantly lower (1.5-fold) than pure SD, but significantly higher (1.6-fold) than SD from the cocrystal (Table 5.3). In the case of BA, the initial dissolution was more than 20 times slower than pure BA and more than 2 times faster than from the cocrystal, however the limiting rate was not different to that of the cocrystal ($p > 0.05$) (Table 5.3).
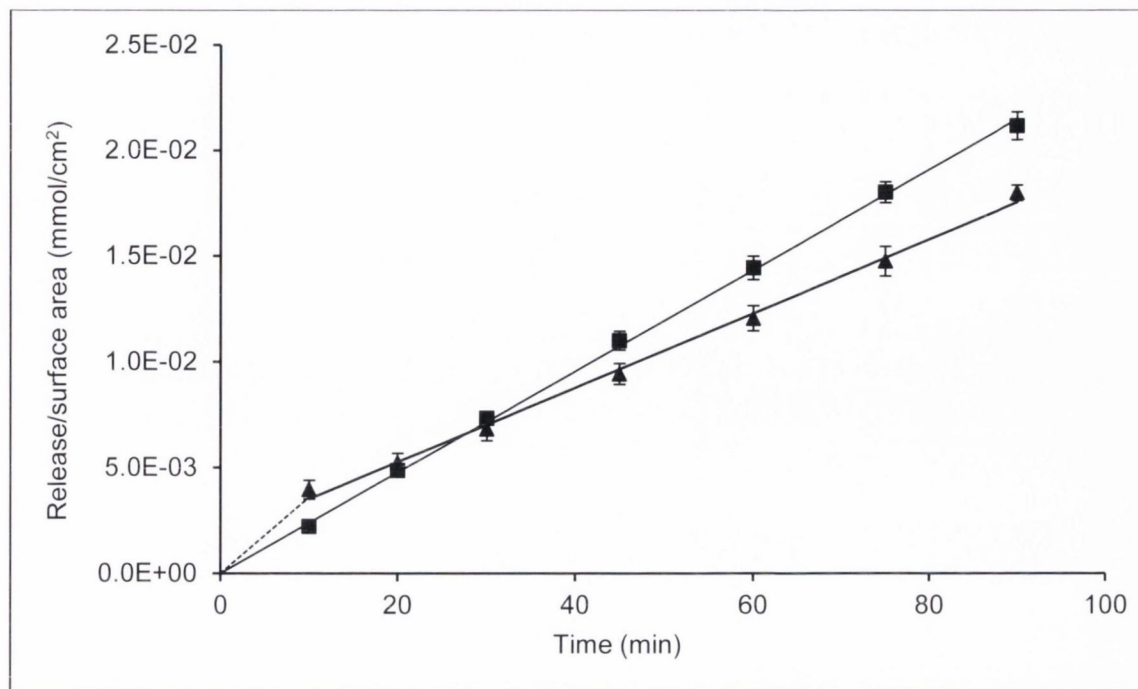
Figure 5.15: Dissolution profile of SD:BA 1:1 physical mixture in water at 37 °C. Squares symbolise SD, triangles represent BA. The dashed line refers to the initial rate of BA.

Analysis of the compact surface of the SD, BA, the SD:BA 1:1 cocrystal and the physical mixture by SEM is shown in Figure 5.16. For each material the surface morphology was found to be different. For example the surface of the single components and the SD:BA 1:1 physical mixture revealed a quite coarse texture compared to the cocrystal after dissolution. Furthermore, in contrast to the cocrystal, the physical mixture showed a non-uniform surface texture with relatively large voids at some regions, attributed to its faster release of BA. The cocrystal revealed the most consistent surface morphology with a finer structure which might be a result of the congruent dissolution of SD and BA from the surface of the compact.
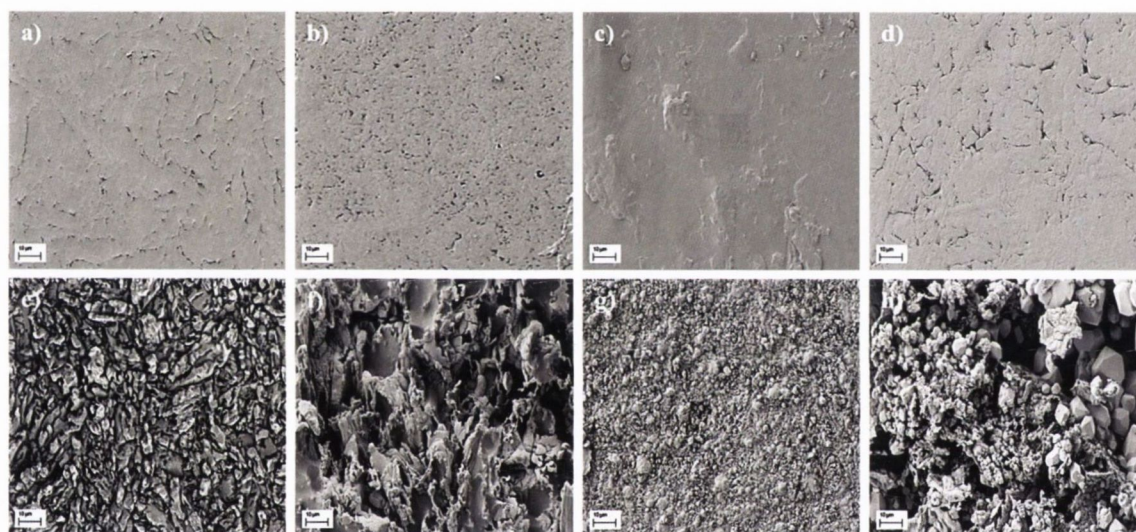

Figure 5.16: SEM images of disk surfaces before dissolution of a) SD, b) BA, c) SD:BA 1:1 cocrystal and d) SD:BA 1:1 physical mixture compared to disk surfaces after dissolution of e) SD, f) BA, g) SD:BA 1:1 cocrystal and h) SD:BA 1:1 physical mixture.

SD:SA 1:1 cocrystal and physical mixture

Figure 5.17 illustrates the dissolution behaviour of the SD:SA 1:1 cocrystal. Both components dissolved linearly ($R^2 > 0.99$) and congruently with dissolution rates of $3.97 \times 10^{-4} \pm 0.13 \times 10^{-4}$ for SD and $4.01 \times 10^{-4} \pm 0.14 \times 10^{-4}$ for BA (Table 5.3). IR analysis confirmed that the surface did not change after dissolution (Figure 5.18). When compared to the single components, SD revealed a slightly faster dissolution rate, whereas the dissolution rate of SA was almost 10 times lower than from the cocrystal (Table 5.3).
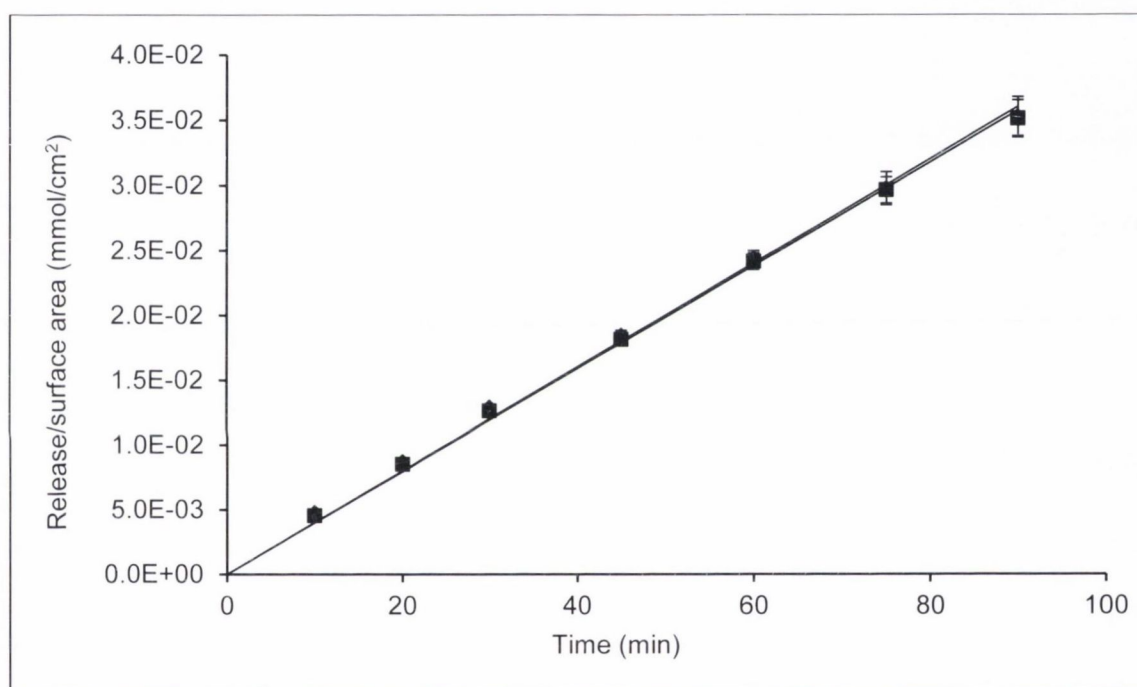
Figure 5.17: Dissolution profile of SD:SA 1:1 cocrystal in water at 37 °C. Squares symbolise SD, diamonds represent SA.
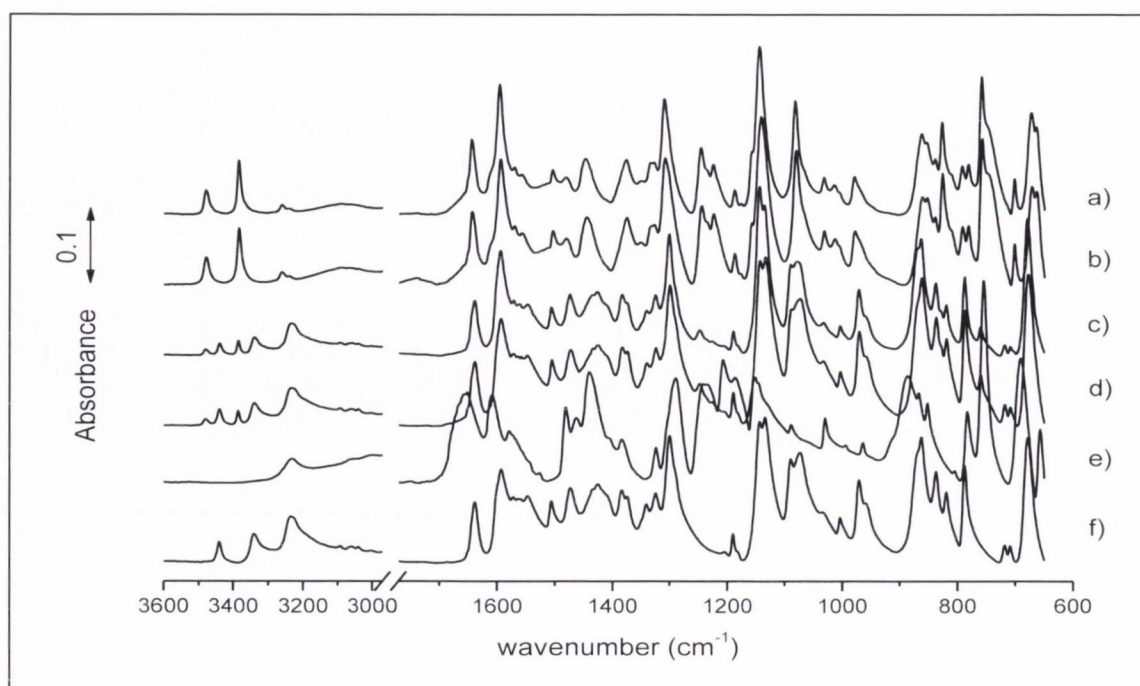
Figure 5.18: IR spectra of a) SD:SA CC after ID, b) SD:SA CC before ID, c) SD:SA PM after ID, d) SD:SA PM before ID compared to e) SA and f) SD.

An equimolar physical mixture of SD and SA showed a similar dissolution behaviour to the cocrystal. As shown in Figure 5.19 both components dissolved linearly ($R^2 > 0.99$) and up to 30 minutes congruently. IR analysis of the surface of the compact after dissolution revealed no changes (Figure 5.18). The dissolution rates of SD and SA from the physical mixture were significantly lower (for SD: 1.4 times and for SA: 1.3 times) to those of the cocrystal (Table 5.3). In comparison to the pure components, SD was found to dissolve 1.3 times slower and SA more than 12 times slower from the physical mixture (Table 5.3).
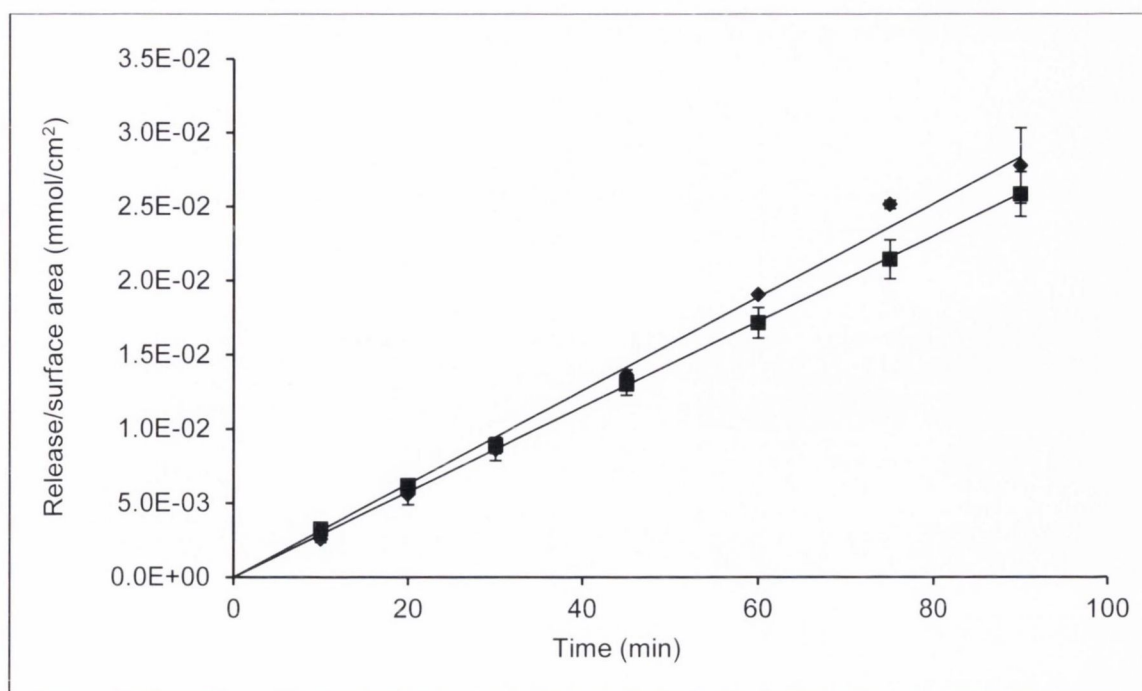
Figure 5.19: Dissolution profile of SD:SA 1:1 physical mixture in water at 37 °C. Squares symbolise SD, diamonds represent SA.

SEM analysis of the surface of the compacts before and after dissolution is shown in Figure 5.20. Similar to BA, SA revealed a quite rough morphology after dissolution, whereas the cocrystal and the physical mixture showed a finer structure. In general, relatively uniform textures were obtained for both, the cocrystal and the physical mixture after dissolution which was presumed to be a result of their similar dissolution behaviour showing congruent release from the compact surface.
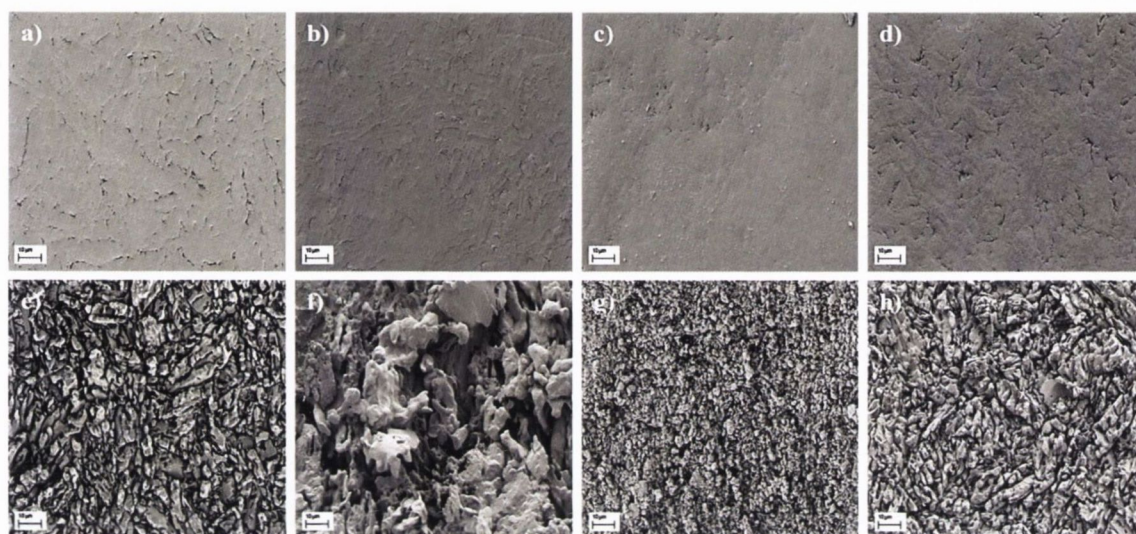

Figure 5.20: SEM images of disk surfaces before dissolution of a) SD, b) SA, c) SD:SA 1:1 cocrystal and d) SD:SA 1:1 physical mixture compared to disk surfaces after dissolution of e) SD, f) SA, g) SD:SA 1:1 cocrystal and h) SD:SA 1:1 physical mixture.

SD:NA 1:1 cocrystal and physical mixture

For the SD:NA 1:1 cocrystal linear dissolution over the entire time was observed in the case of SD ($R^2 > 0.97$), whereas NA dissolved initially very fast, followed by a slower but linear rate until the end of the study (Figure 5.21). Both components dissolved incongruently with NA being initially more than 6 times faster than SD (Table 5.3). Analysis of the compact surface by IR spectroscopy showed that the surface composition has changed. As shown in Figure 5.22, after dissolution only bands attributed to SD were detected indicating that NA dissolved very fast leaving SD as the remaining phase at the surface. The calculated dissolution rates were in the case of SD approximately 1.4 times lower, possibly as a result of the surface changes and in the case of NA more than 13 times (initial rate considered) lower than the pure components (Table 5.3).
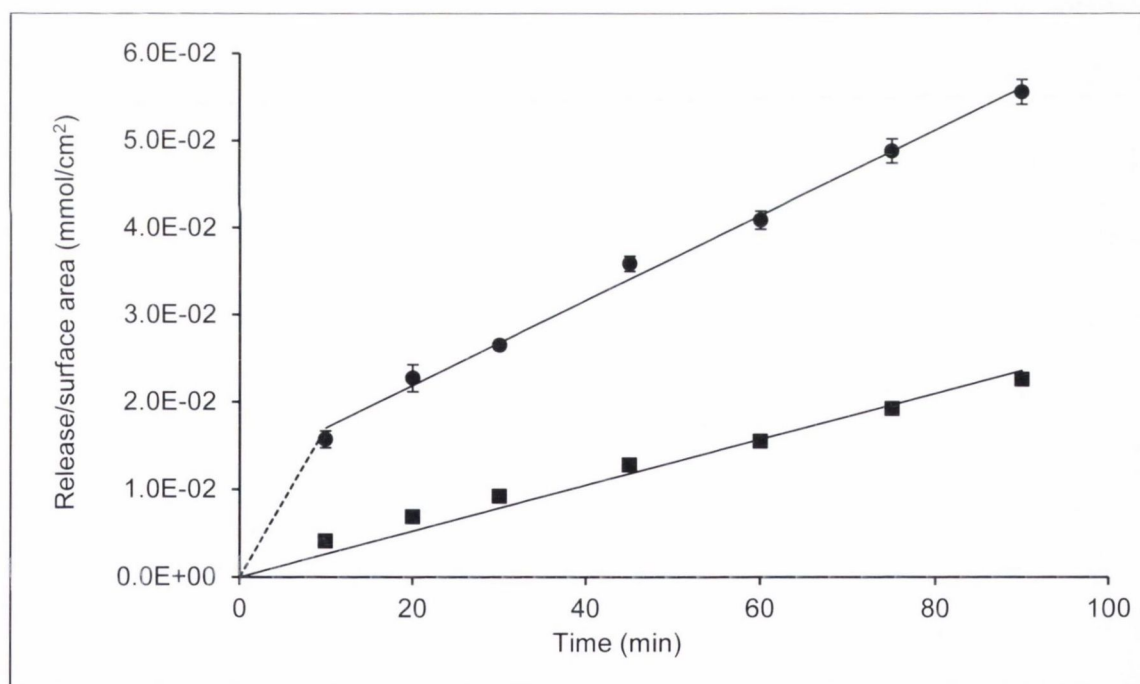

Figure 5.21: Dissolution profile of SD:NA 1:1 cocrystal in water at 37 °C. Squares symbolise SD, circles represent NA. The dashed line refers to the initial rate of NA.
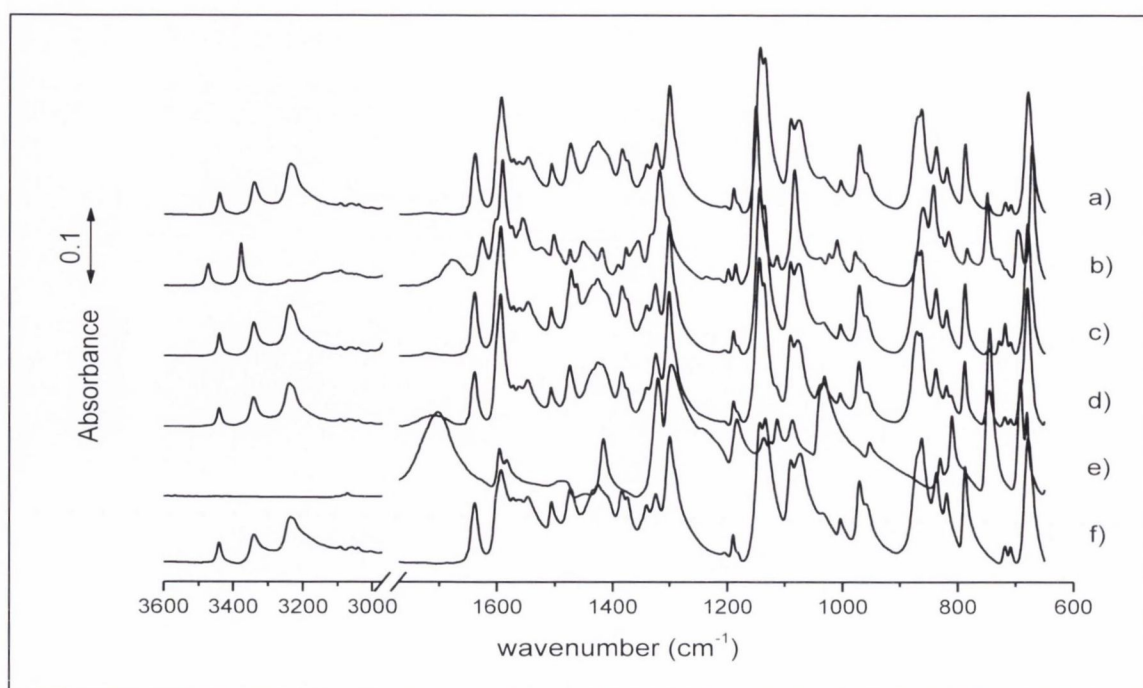
Figure 5.22: IR spectra of a) SD:NA CC after ID, b) SD:NA CC before ID, c) SD:NA PM after ID, d) SD:NA PM before ID compared to e) NA and f) SD.

A physical mixture of SD and NA showed similar dissolution profiles to the cocrystal (Figure 5.23). SD dissolved linearly over the entire time ($R^2 > 0.99$), while NA dissolved initially fast, however followed by a nonlinear release with declining rate over time. Like for the cocrystal IR analysis of the compact surface after the study detected SD as the sole remaining phase, indicative of the fast NA release (Figure 5.22). The calculated dissolution rate of SD was found to be approximately 1.2 times and 1.6 times lower than the cocrystal and pure SD, respectively (Table 5.3). For NA, the initial dissolution rate was nearly 13-fold lower than pure NA, but was not different to the initial rate of the cocrystal ($p > 0.05$). The limiting rate was calculated based on the time points between 60 and 90 minutes and was found to be more than 1.2-fold lower compared to the cocrystal. Moreover, the nonlinear dissolution behaviour of NA was found to be directly proportional to the square root of time ($R^2 > 0.99$) and thus approximated matrix diffusion controlled release (Higuchi, 1963) (Figure 5.23).

A similar dissolution behaviour was observed for a physical mixture composed of benzamide and dibenzyl sulfoxide as reported in Chapter 2. Benzamide, the more soluble component dissolved by diffusion controlled square-root of time kinetics, whereas dibenzyl sulfoxide, the less soluble component was remained at the surface of

the compact. These findings were attributed to the dissolution from an inert matrix system as described by Higuchi (1967), where the more soluble component dissolves through a matrix of the less soluble component as a result of a greatly higher solubility (> 75-fold) and a lower weight fraction of benzamide than dibenzyl sulfoxide in the mixture.

The solubility ratio of NA:SD was 83-fold, the same order of magnitude as compared to benzamide and dibenzyl sulfoxide. Therefore, it was concluded that the release of NA in the presence of SD in an equimolar ratio can be described in the same way as for benzamide and dibenzyl sulfoxide, where NA dissolves through a matrix of SD.
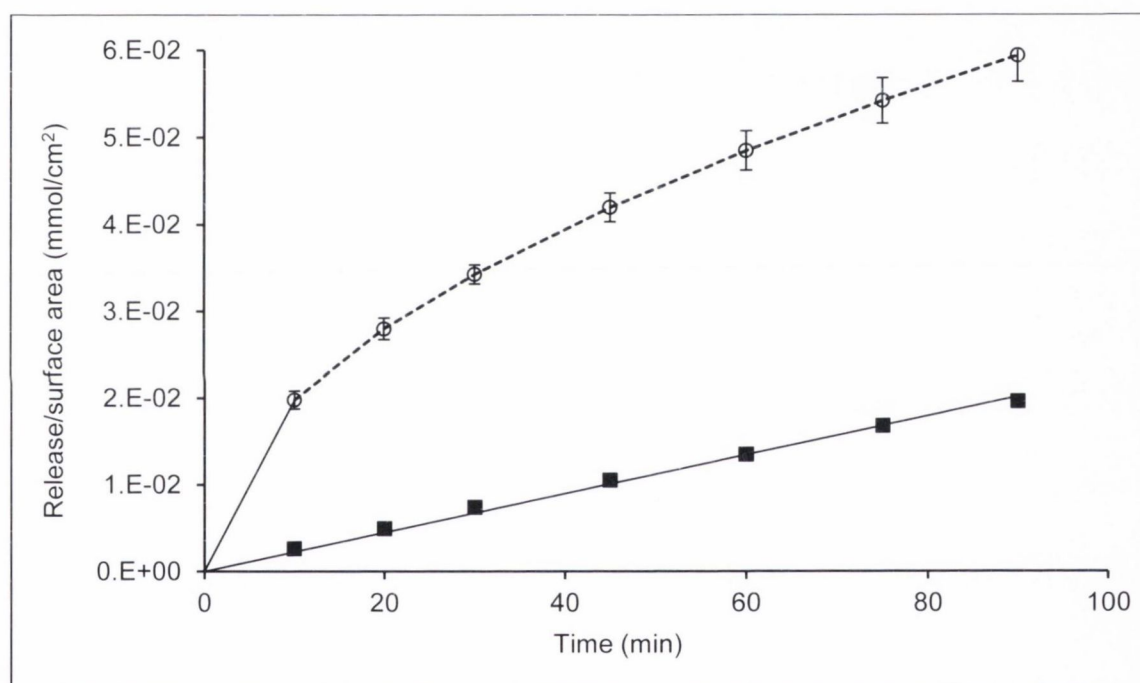

Figure 5.23: Dissolution profile of SD:NA 1:1 physical mixture in water at 37 °C. Squares symbolise SD, circles represent NA. The dashed line refers to the square-root of time fit.

From SEM analysis of the compact surface as shown in Figure 5.24, it was found that after dissolution SD and NA showed a relatively fine surface and more uniform in texture than the cocrystal and the physical mixture. The physical mixture revealed an inhomogeneous morphology with relatively large voids which was assumed to be attributed to the release of NA. The cocrystal also displayed voids on the surface after dissolution which was attributed to the NA release, similar to the physical mixture.

However, the surface of the cocrystal appeared rather ordered compared to the physical mixture which might be a result of the interactions such as hydrogen bonds between SD and NA in the cocrystal in the solid state. A similar surface morphology has been observed for the benzamide:dibenzyl sulfoxide cocrystal (see Chapter 2) and was thus presumed to be associated with the matrix controlled release of one of the components.
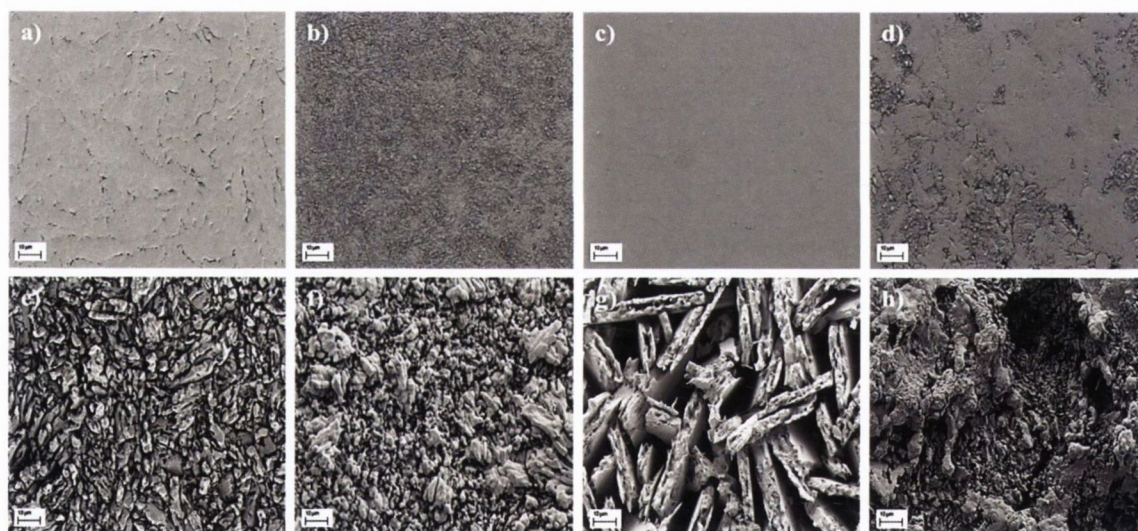

Figure 5.24: SEM images of disk surfaces before dissolution of a) SD, b) NA, c) SD:NA 1:1 cocrystal and d) SD:NA 1:1 physical mixture compared to disk surfaces after dissolution of e) SD, f) NA, g) SD:NA 1:1 cocrystal and h) SD:NA 1:1 physical mixture.

An overall summary of the results and a comparison to the previously discussed SD:4-ASA cocrystal (see Chapter 3) is presented in Table 5.4 and shows to what extent the cocrystal revealed an advantage in dissolution of the poorly water soluble SD. Based on the IDR ratio of SD from the cocrystal to SD of the pure component, it was found that the SD:BA and SD:NA cocrystal revealed a slower dissolution of SD with a ratio of 0.42 and 0.72, respectively and thus no improvement in dissolution of SD. Furthermore, the SD:BA cocrystal showed no advantage over a physical mixture, while the dissolution rate of SD from the SD:NA cocrystal was higher than from the physical mix (Table 5.3). These findings were attributed to the possibly greater difference in solid state interactions between the SD:NA cocrystal and the equivalent physical mixture than between the SD:BA cocrystal and the equivalent physical mixture. In contrast, the SD:SA cocrystal revealed a small advantage in dissolution compared to pure SD with an SD IDR ratio of 1.09 (Table 5.4), however the dissolution rate of SD from the cocrystal was considerably higher than that of the physical mixture (Table 5.3). The SD:4-ASA cocrystal also showed a dissolution advantage in comparison to the physical mixture (Table 5.3) and to the pure SD, where the SD IDR ratio was 1.40 (Table 5.4).

In general, physical mixtures of SD:BA, SD:SA and SD:NA revealed a lower dissolution rate for SD compared to pure SD (Table 5.3). These findings deviate from the theoretical model describing dissolution of polyphase mixtures of two non-interacting components, where SD should dissolve at a rate proportional to the solubility and the diffusion coefficient (Higuchi et al., 1965). In the case of the SD:BA and SD:NA cocrystals, the SD dissolution rate was lower than that of SD alone (Table 5.3); this suggests that interactions between the components may account for the lower than anticipated dissolution rate of SD from the physical mixtures.

Table 5.4: A summary of the results from intrinsic dissolution studies and solubility studies of four selected SD:aromatic carboxylic acid 1:1 cocrystals (CC) performed in water at 37 °C.

Cocrystal	IDR ratio IDR_{CC}/IDR_{SD}[b]	Component release	Solubility ratio $[CC]/[SD]_0$[c]	Stability[d]	Solubility ratio cof/SD[e]
SD:BA	0.42	congruent	0.50	congurently saturating	17.46
SD:SA	1.09	congruent	0.98	congruently saturating	10.99
SD:4-ASA [a]	1.40	incongruent	1.23	congruently saturating	6.42
SD:NA	0.72	incongruent	6.21	incongruently saturating	83.32

a) refers to form I cocrystal, details can be found in Chapter 3

b) refers to the ratio of SD dissolution rate from the cocrystal to SD dissolution rate of pure SD

c) Table 5.1

d) based on PXRD analysis

e) refers to the ratio of coformer/SD based on solubilities of single components

When comparing the IDR ratio (of SD from the cocrystal to SD alone) with the solubility ratios of the cocrystals to SD or coformer to SD (Table 5.4), a trend was found in the case of congruently saturating cocrystals composed of BA, SA and 4-ASA as conformers, which indicates that cocrystal dissolution, cocrystal solubility and the component solubility difference interrelate. As shown in Table 5.4 for these three systems, the rank order of the IDR ratio increased, as was the case for the solubility ratio, while the coformer/SD solubility ratio decreased. Thus, for congruently saturating cocrystals, it can be concluded that a high drug dissolution rate will result when the solubility of the cocrystal is high and the coformer/drug solubility difference is low. The SD:NA cocrystal, which is incongruently saturating, behaved differently to the other three systems. The IDR ratio was low, while the cocrystal/SD solubility ratio was high, as was coformer/SD solubility ratio. It was apparent that the NA/SD solubility difference was large (> 83-fold). As previously discussed, this can result in matrix-controlled dissolution and explains the discrepancy between dissolution and solubility. It can be concluded that a solubility difference between the coformer and SD of less

than 83, for the systems studied, results in thermodynamically stable (congruently saturating) cocrystals. However, an increase in the SD dissolution rate, compared to SD alone, can only be expected if the solubility difference of the coformer/SD is low, as shown for the SD:SA and SD:4-ASA cocrystal, where the components can dissolve congruently or incongruently (Table 5.4).

5.4 Conclusions

In summary, the study demonstrated that the pH-dependent solubility and stability of different SD:aromatic carboxylic acid cocrystals could be predicted by mathematical models which confirmed their use as a valuable tool in the development of pharmaceutical cocrystals. The predictions showed for all SD:aromatic carboxylic acid cocrystals a solubility advantage over the low water-soluble SD at neutral and basic pH, however precipitation of SD was observed. No correlation between the cocrystal solubility, the coformer solubility and the cocrystal lattice energies could be established, indicating that the cocrystal solubility is controlled by individual interactions between the solvent, solute and the solid state.

Intrinsic dissolution studies showed that, depending on the selected aromatic carboxylic acid chosen as coformer, cocrystals can enhance the dissolution rate of SD, but can also show no improvement or even a slower dissolution rate compared to SD alone and a physical mixture.

A relationship was shown for congruently saturating sulfadimidine cocrystals, where the intrinsic dissolution rate increased with increasing cocrystal solubility and decreasing coformer/SD solubility difference.

For incongruently saturating cocrystals, which exhibit a high coformer/SD solubility ratio (in the order of ≥ 83) no advantage in the dissolution rate of SD was observed. As a result of matrix-controlled release, SD can control the dissolution of the coformer.

Chapter 6: General discussion

6.1 Introduction

In the past years, pharmaceutical cocrystals have emerged as an interesting class of solid form with the potential for improving drug physicochemical and hence biopharmaceutical properties compared to traditional solid state forms such as salts, solvates/hydrates and polymorphs. However, in order for cocrystals to be of benefit and to become fully implemented in the pharmaceutical industry, studies on cocrystals which cover all stages of drug development are essential.

The formation of cocrystals has been reported in increasing numbers by a wide variety of researchers and various methods of production have been presented, whereas still relatively few studies have addressed solubility and dissolution, important parameters for the evaluation of new drugs.

This thesis has contributed to the fundamental understanding of cocrystals with a focus on solubility and dissolution studies and the investigation of production techniques with an emphasis on spray drying.

6.2 Solubility and dissolution studies

One of the objectives of this work was to study the solubility and dissolution of the benzamide:dibenzyl sulfoxide (BAM:DBSO) 1:1 cocrystal (Eccles et al., 2010), composed of the poorly water soluble dibenzyl sulfoxide (DBSO) and benzamide (BAM) as a coformer with a higher aqueous solubility. A graphical summary of the findings, which have been described in detail in Chapter 2, is presented in Figure 6.1.

Overall, the results from the solubility studies of the BAM:DBSO 1:1 cocrystal confirmed the theoretical models for binary cocrystals introduced by Rodríguez-Hornedo and co-workers (Nehm et al., 2006; Good and Rodríguez-Hornedo, 2009). It was demonstrated that the solubility of the BAM:DBSO 1:1 cocrystal is a function of the coformer, BAM, concentration in water and that it decreases with increasing coformer concentration (Figure 6.1), as was previously shown for different carbamazepine cocrystals (Nehm et al., 2006) and for two indomethacin cocrystals (Alhalaweh et al., 2011) in organic solvents. In general, the value of the solubility product and thus the cocrystal solubility was found to be relatively low in contrast to values reported in prior work on carbamazepine and indothemacin cocrystals (Nehm et al., 2006; Alhalaweh et al., 2011). Referring to the theoretical principles, low cocrystal solubility (represented by K_{sp}) and therefore low solubility of the components is inversely related to complexation in solution (represented by K_{11} assuming a 1:1

stoichiometry). As a consequence, a relatively high complexation constant, K_{11} was determined for the BAM:DBSO 1:1 cocrystal in water, indicating strong solute-solute interactions between the sulfoxide and amine functionality. This complexation resulted in an increase in the solubility of the poorly water-soluble DBSO and consequently the cocrystal was more soluble than DBSO alone.
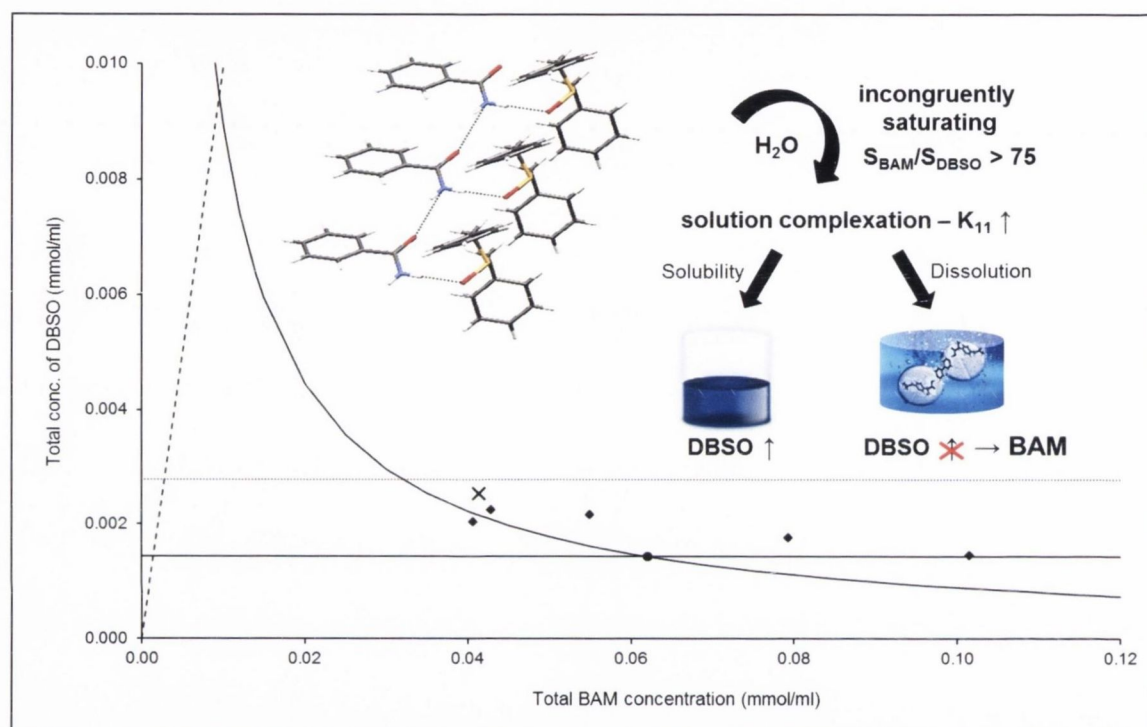

Figure 6.1: Phase solubility diagram of 1:1 BAM:DBSO cocrystal (CC). The horizontal line marks the solubility of pure DBSO; the curved line represents the cocrystal solubility curve; the dotted line represents the solubility limit of complex determined from phase-solubility studies of DBSO as a function of BAM; the filled diamonds mark the experimental cocrystal solubility values (BAM dependent); the dashed line represents stoichiometric concentrations of cocrystal components that dissolution could follow in the ideal case; the filled circle symbolises the transition concentration (DBSO/CC) and the cross illustrates the experimentally obtained transition concentration (DBSO/CC). K_{11} and S_{BAM}/S_{DBSO} represent the complexation constant of the cocrystal and the solubility ratio of BAM to DBSO, respectively.

However, the cocrystal was thermodynamically unstable in water which is expected when the components reveal a high solubility difference ($S_{BAM}/S_{DBSO} > 75$). According to reports by Good and Rodríguez-Hornedo (2009), if the coformer solubility is about 10-fold or more than that of the drug, this will result in the cocrystal being more soluble than the drug and being, as such, unstable in solution. These findings could be graphically presented by means of the phase solubility diagram (Figure 6.1) and the triangular phase diagram, discussed in Chapter 2 and have highlighted once again the use of such phase diagrams as valuable tools in the prediction of cocrystal solution stability.

Besides, it was demonstrated that determination of the BAM:DBSO 1:1 cocrystal solubility by means of the transition concentration (C_{tr}) is inaccurate and overestimates the result, as the cocrystal is incongruently saturating and the components show solution complexation. This was expected and has been reported elsewhere (Good and Rodríguez-Hornedo, 2009).

Despite the higher solubility of the cocrystal, the dissolution (based on intrinsic dissolution studies) of the poorly soluble DBSO was not enhanced in comparison to an equimolar physical mixture and DBSO alone. As the cocrystal solubility and thus complexation is a function of the coformer, dissolution studies performed in a dissolution medium containing the coformer might help to draw further conclusions. Similar studies have been reported by Lee et al., 2010 based on intrinsic dissolution studies of the acetaminophen:theophylline cocrystal using theophylline solution as the dissolution medium.

Instead, it was shown that the poorly soluble DBSO can control and retard dissolution of the more soluble coformer, BAM from the cocrystal. From a different perspective, these results indicate that a coformer with a low aqueous solubility can control the release of a drug with a high solubility. Therefore, cocrystals can also be used as systems for controlled drug release for example for drugs which have a narrow therapeutic window and for which controlled dosing is required to maintain therapeutic levels while avoiding toxic side effects. Maheshwari et al. (2012) have presented some work on this approach describing how to tailor the solubility of gabapentin lactam with several less soluble coformers.

Two further objectives in this thesis, with respect to solubility and dissolution, were to investigate different sulfadimidine:aromatic carboxylic acid cocrystals and to evaluate the impact of the acid coformers on the solubility and dissolution. Therefore, four sulfadimidine cocrystals were selected, three of them known and previously reported, i.e. the sulfadimidine:4-aminosalicylic acid (SD:4-ASA) 1:1 form I cocrystal (Caira et al., 1992) (presented in Chapter 3), the sulfadimidine:benzoic acid (SD:BA) 1:1 and the sulfadimidine:salicylic acid (SD:SA) 1:1 cocrystal (Caira et al., 1995; Arman et al, 2011; Patel et al., 1988) (presented in Chapter 5), and one previously unreported cocrystal, the sulfadimidine:nicotinic acid (SD:NA) 1:1 cocrystal (presented in Chapter 5) which was discovered in the study described in Chapter 4.

The overall findings are presented graphically in Figure 6.2 based on the SD:4-ASA 1:1 form I cocrystal as an example and in Table 6.1 which provides further details.

With the objective of understanding how ionisation properties influence cocrystal solubility, Bethune et al., (2009) and Reddy et al., (2009) introduced several models to predict the pH-dependent solubility and stability from studies using different carbamazepine cocrystals and a gabapentin cocrystal,.

These models were applied, with appropriate modifications to account for the different ionisation properties of components, to predict the pH-dependent solubility and stability of the sulfadimidine cocrystals (Table 6.1). In the case of the SD:4-ASA and SD:NA 1:1 cocrystals, a new, previously unreported model was established in order to enable the predictions for a cocrystal composed of two amphoteric components (Figure 6.2).
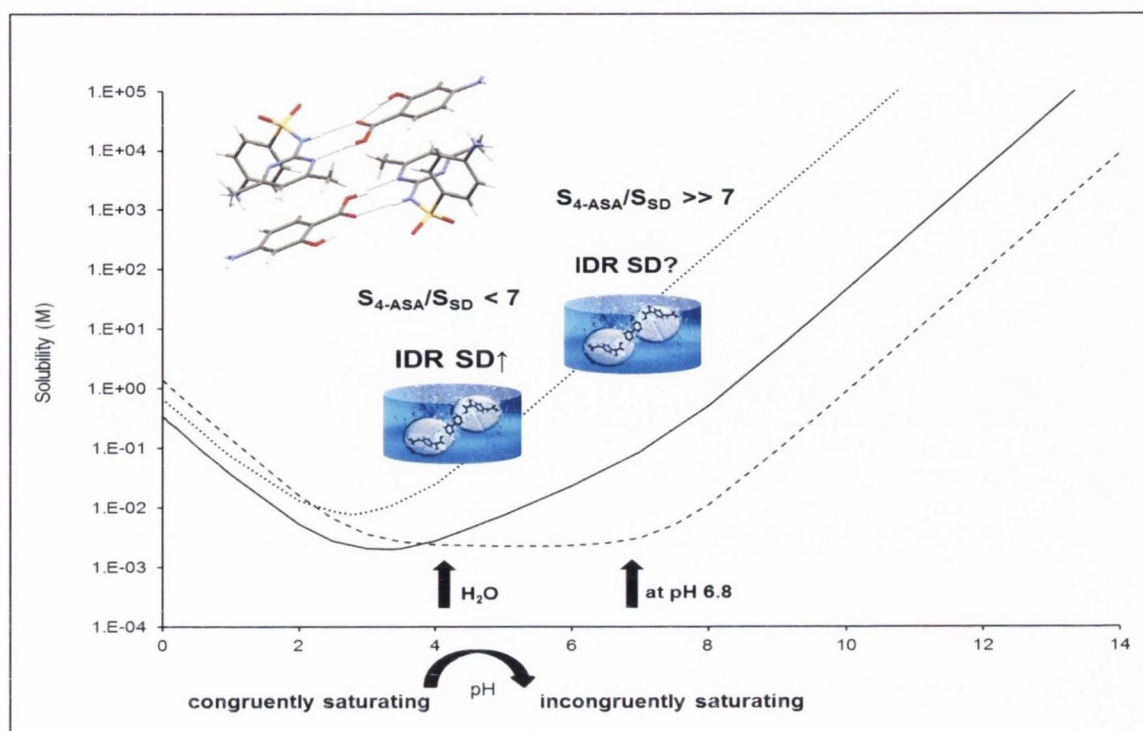
Figure 6.2: Theoretical pH solubility profile (37 °C) of the SD:4ASA 1:1 form I cocrystal containing two amphoteric components. The solid line represents the cocrystal solubility, the dashed and dotted lines show the theoretical SD and 4-ASA solubility dependent on the pH (derived from the Henderson-Hasselbalch relationship). S_{4-ASA}/S_{SD} and IDR SD represent the solubility ratio of 4-ASA to SD and the intrinsic dissolution rate of SD from the cocrystal, respectively.

The studies have confirmed the validity of each individual model and have highlighted, as was previously reported by other authors (Bethune et al, 2009; Reddy et al., 2009), that the pH-solubility predictions provide important insights of how pH, solubility and stability of cocrystals interrelate.

It was shown in Chapters 3 and 5 that the SD:aromatic carboxylic acid cocrystals resulted in U-shaped pH-solubility curves due to the amphoteric properties of SD and that they were more soluble compared to the poorly water-soluble SD at neutral and basic pH, where the solubility increased with increasing pH (see also Figure 6.2). At physiologically relevant pH of for example 6.8, a solubility advantage in the range of 8-56-fold for the cocrystals over SD can be expected, however precipitation of the drug was observed in the study.

In order to keep the cocrystal stable at the given pH, more coformer would be required to prevent drug precipitation. These findings can be deduced from the solubility product (K_{sp}) as it is a function of both drug and coformer concentration as described by Bethune et al, (2009).

Some studies have reported that cocrystal solubility is a function of the coformer solubility, where cocrystal solubility is high for coformers which exhibit high solubility (Good and Rodríguez-Hornedo 2009). Other studies have shown that this is not a general trend and depends on the crystal lattice energies and the interactions in the solid state of the individual cocrystal, in particularly in water (Good and Rodríguez-Hornedo 2009). Similar findings were observed for the SD:aromatic carboxylic acid cocrystals in water investigated in the current work. No correlation between the cocrystal solubility, the coformer solubility (Table 6.1) and the cocrystal lattice energies could be established, indicating that the cocrystal solubility is controlled by a multifactorial interplay between the solvent, solute and the solid state interactions of the cocrystal components.

From the results it can be concluded that for cocrystals composed of ionisable components, the coformer solubility and thus the coformer to drug solubility ratio cannot be considered as the only criterion for selecting a cocrystal with solubility advantage as pH of the medium may have a considerable influence on the solubility and stability (Table 6.1).

Conversely, considering the solubility product (K_{sp}), the same will apply for cocrystals composed of different drugs with the same coformer: the solubility can be improved for a cocrystal containing a less soluble drug compared to one with a more soluble drug. This was shown in studies by Alhalaweh et al., (2012) and was assumed to be a result of solvation effects.

Table 6.1: A summary of the results from solubility and intrinsic dissolution studies of four selected SD:aromatic carboxylic acid 1:1 cocrystals performed in water at 37 °C.

Cocrystal	Class	Solubility ratio cof/SD[b]	Solubility ratio $[CC]/[SD]_0$[c]	Stability[d]	IDR ratio IDR_{CC}/IDR_{SD}[e]	Component release
SD:BA	amphoteric:monoprotic acidic	17.46	0.50	congurently saturating	0.42	congruent
SD:SA	amphoteric:diprotic acidic	10.99	0.98	congruently saturating	1.09	congruent
SD:4-ASA[a]	amphoteric:amphoteric	6.42	1.23	congruently saturating	1.40	incongruent
SD:NA	amphoteric:amphoteric	83.32	6.21	incongruently saturating	0.72	incongruent

a) refers to form I cocrystal, details can be found in Chapter 3

b) refers to the ratio of coformer/SD based on solubilities of single components

c) calculation refers to Good and Rodríguez-Hornedo, 2009

d) based on PXRD analysis

e) refers to the ratio of SD dissolution rate from the cocrystal to SD dissolution rate of pure component

Intrinsic dissolution rate studies showed that, in the case of congruently saturating (thermodynamically stable) cocrystals the drug intrinsic dissolution rate increased with increasing cocrystal solubility and decreasing coformer to drug solubility ratio (Table 6.1). Thus, for an actual enhancement of the drug dissolution rate, a low coformer to drug solubility ratio seems to be preferred. However, this ratio can change with changing pH. As shown in Figure 6.2 the ratio will increase when the cocrystal becomes more soluble and consequently the congruently saturating cocrystal will transform to an incongruently saturating cocrystal.

Based on the findings for incongruently saturating cocrystals, such as the SD:NA 1:1 cocrystal (Table 6.1) and the BAM:DBSO 1:1 cocrystal (Figure 6.1) which exhibit a high coformer to drug solubility ratio, in the order of > 75 (molar solubility), dissolution can become matrix-controlled, where the less soluble component can control the dissolution of the more soluble component.

The findings of the solubility and dissolution studies described in this work showed that in general the solubility advantage through the cocrystal approach is associated with the lack of stability by transforming to the less soluble component, usually the drug. Whether this stability issue will result in an advantage in the dissolution rate may be influenced by the coformer to drug solubility ratio at a particular pH. However, this remains to be clarified in further studies under incongruent stability conditions at physiologically relevant pH. Few studies have investigated the intrinsic dissolution of cocrystals at different pH values (Lee et al., 2010; Cherukuvada et al., 2011). For example in the study by Cherukuvada et al. (2011) based on the nitrofurantoin-p-aminobenzoic acid cocrystal it was shown that the cocrystal showed improved intrinsic dissolution rates in water, in 0.1 N HCl and in pH 6.8 buffer compared to the reference drug (nitrofurantoin), however conversion to nitrofurantoin hydrate was observed.

6.3 Co-grinding and co-spray drying of sulfadimidine with 4-aminosalicylic acid

A further objective of this thesis was to compare co-grinding and co-spray drying as alternative techniques in the formation of sulfadimidine:4-aminosalicylic acid cocrystals. Experiments were carried out by milling in dry and liquid-assisted conditions at various times (15, 30, 45 minutes) and by spray drying using different molar ratios (1:2, 1:1, 2:1) of sulfadimidine (SD) and 4-aminosalicylic acid (4-ASA). The studies were presented in Chapter 3 and were extended for further details in Chapter 4. An overall summary of the findings is presented in Figure 6.3.
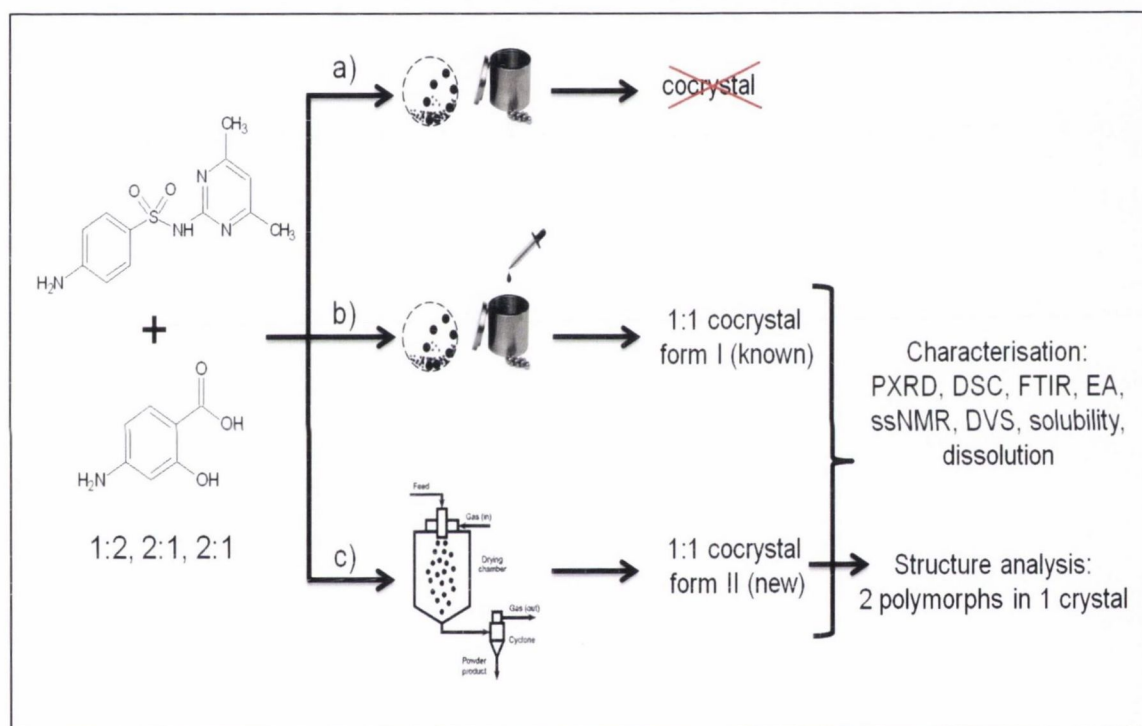
Figure 6.3: Co-processing of sulfadimidine and 4-aminosalicylic acid by a) dry milling, b) liquid-assisted milling and c) spray drying.

It was shown that SD and 4-ASA formed only 1:1 cocrystals. Cocrystals of other stoichiometry (1:2 and 2:1) have not been observed.

The use of dry milling of SD with 4-ASA as coformer did not result in cocrystal formation, while this method has been reported as successful in cocrystal formation for structurally related aromatic carboxylic acids such as benzoic and salicylic acid coformers (Caira et al., 1995). Although dry milling did not result in cocrystal formation, this may be a result of insufficient mechanical force that has been provided

under the given experimental conditions. Instead, binary crystalline mixtures with some amorphous phase which increased with increasing milling time (determined by the decreasing diffraction peak intensities by PXRD analysis and increasing enthalpies of the recrystallisation exotherm by DSC analysis) were obtained. Similar findings which showed that amorphisation is a function of milling time have been reported many times in the literature (Muñoz-Morris and Morris, 1991; Bhatt and Murty, 2008; Loureiro et al., 2009).

Liquid-assisted milling using ethanol and acetone as solvents resulted in the formation of the SD:4-ASA 1:1 form I cocrystal (discovered and previously reported by Caira in 1992); in a pure form when the starting materials were present in a 1:1 ratio. None of the liquid-assisted milled products showed evidence of amorphisation (based on PXRD and DSC analysis). In contrast to dry milling, these findings demonstrate the effectiveness of the liquid-assisted milling method in producing cocrystals, as was also reported previously by several authors (Shan et al., 2002; Childs et al., 2008; Karki et al., 2007; Friščić and Jones, 2009). Moreover, the formation of the SD:4-ASA 1:1 form I cocrystal via the liquid-assisted milling route has not been reported elsewhere and is therefore presented for the first time in this thesis.

By spray drying from ethanol and acetone as solvents a polymorphic form (form II) of the SD:4-ASA 1:1 cocrystal was discovered and could also be generated by solvent evaporation under elevated temperature conditions (for details see Chapter 3) from ethanol and acetone. However, in contrast to liquid-assisted milling, none of the three mixture ratios investigated (1:1, 1:2, 2:1) resulted in a pure crystalline cocrystal product; this was attributed to either the presence of excess crystalline 4-ASA (in the case of 1:2) or the presence of excess amorphous phase (in the case of 1:1 and 2:1), which was however not detectable by DSC for the 1:1 spray-dried product and thus not definitively assignable. According to the literature, it is known that crystalline SD can transform to the amorphous state by spray drying (Nolan, 2008). Based on evidence from stoichiometry analysis (by HPLC), where it was shown that the 1:1 spray-dried product contained 8% less molar amount of 4-ASA (as a result of a mass loss induced by spray drying), it was concluded that the observed amorphous phase is attributed to excess SD. Solubility studies of the spray-dried product compared to a reference product (with a higher degree of crystallinity and 1:1 stoichiometry) produced by solvent evaporation gave further evidence: in contrast to the reference product, the spray-dried product revealed a 2-fold higher apparent solubility of SD, which was

attributable to amorphous SD. Despite these findings, it should be considered that the amorphous phase induced by spray drying may also be a mixed phase composed of SD and SD:4-ASA complex. Attempts to produce an amorphous complex of SD and 4-ASA in order to draw further conclusions failed however (data not shown).

In general, the findings demonstrated the feasibility of cocrystal formation via spray drying using SD and 4-ASA as cocrystal formers. However, it was observed that the purity of the product can be affected due to the mass loss of one of the components induced by spray drying and as a consequence amorphisation of the excess component is likely. Furthermore, spray drying can result in the formation of polymorphic forms. These results prompted interest for further studies on cocrystal formation using spray drying as were presented in Chapter 4. A summary of the outcomes is described below in section 6.4.

In order to investigate the differences between the SD:4-ASA form I and the discovered form II cocrystal several characterisation techniques such as PXRD, DSC, elemental analysis (EA), FTIR, ssNMR and SC-XRD were used. Furthermore, solubility, dissolution, long-term (physical and chemical) stability and stability at different humidities by DVS were studied.

Considering all the findings, it can be summarised that, in comparison to form I the form II cocrystal is a higher energy form (due to the requirement of heat in order for it to be formed) with a similar melting behaviour, but is thermodynamically less stable. Solubility studies in water have demonstrated that the form II cocrystal transforms rapidly to form I, but can be stabilised by the addition of 0.1% PVP (w/v) to the solution to enable measurement of the solubility. The use of PVP to stabilise solid forms is known and has been reported many times in literature (Sekikawa et al., 1978; Raghavan et al., 2001; Lindfors et al., 2008; Alonzo et al., 2010; Warren et al., 2010).

The determined apparent solubility of the form II cocrystal was similar to the solubility of form I. As expected from the solubility results, and as for form I, the form II cocrystal revealed an improved dissolution rate of the poorly water-soluble SD in comparison to a physical mixture and pure SD.

However, it should be noted that, in contrast to the form I cocrystal (produced by liquid-assisted milling from a 1:1 ratio) for form II (produced by spray drying from a 1:1 ratio) the dissolution results refer to a product with a SD:4-ASA stoichiometry which is not exactly 1:1 (i.e. 8% less molar amount of 4-ASA). Nevertheless, considering that the 4-ASA loss is low, it is believed that a spray-dried product of

equimolar stoichiometry will have comparable dissolution rates to those of the form II cocrystal with a 1:0.92 SD:4-ASA stoichiometry as produced in the course of this work. This may be investigated in future work.

Characterisation by PXRD, FTIR and ^{13}C solid state NMR clearly indicated the structural difference of the form II cocrystal compared to form I, attributed to a different molecular arrangement and different molecular interactions. The use of advanced solid state NMR such as ^{1}H and ^{15}N NMR might have provided more detailed information.

Further clarification was obtained by crystal structure analysis of the SD:4-ASA 1:1 form II cocrystal. As described in Chapter 3, conventional single crystal X-ray analysis, although the most reliable technique, did not allow for solving of the structure due to the observation of non-crystallographic reflections. Alternatively, PXRD data were used from which a crystal structure could be calculated. However, based on a closer inspection of the single crystal X-ray data, followed by further data collection using synchrotron radiation it was demonstrated that the SD:4-ASA 1:1 form II cocrystal reveals an unusually complex structure. Although the investigations are not yet completed, there is evidence (Chapter 3) that the cocrystal is composed of two polymorphs, intergrown in one crystal. Such findings have so far only been reported once for a metal-oxo halide (Hugonin et al., 2009). Thus, these observations provide important insights, not only from a crystallographic point of view also from an industrial point of view, with respect to the production of materials.

In addition, the results demonstrate the superiority of the single crystal X-ray technique using synchrotron radiation as the X-ray source for structure determination in the case of more complex structures compared to the PXRD technique.

Stability tests based on long term storage and when exposed to different humidities by DVS analysis (using cocrystals produced by liquid-assisted milling and spray drying) have shown that both the SD:4-ASA 1:1 from I and form II cocrystals were physically and chemically stable over a storage time of 12 months at 60% RH and 25 °C and DVS analysis enabled these cocrystals to be classified as slightly hygroscopic according to the hygroscopicity classification system established by Murikipudi et al. (2013).

Other cocrystals from the SD:aromatic carboxylic acid type which have been investigated for stability by DVS (as described in Chapter 4) were classified as non-hygroscopic. Similar findings were reported by Andrew et al. (2006) and Basavoju et al. (2007) for theophylline and indomethacin cocrystals.

attributable to amorphous SD. Despite these findings, it should be considered that the amorphous phase induced by spray drying may also be a mixed phase composed of SD and SD:4-ASA complex. Attempts to produce an amorphous complex of SD and 4-ASA in order to draw further conclusions failed however (data not shown).

In general, the findings demonstrated the feasibility of cocrystal formation via spray drying using SD and 4-ASA as cocrystal formers. However, it was observed that the purity of the product can be affected due to the mass loss of one of the components induced by spray drying and as a consequence amorphisation of the excess component is likely. Furthermore, spray drying can result in the formation of polymorphic forms. These results prompted interest for further studies on cocrystal formation using spray drying as were presented in Chapter 4. A summary of the outcomes is described below in section 6.4.

In order to investigate the differences between the SD:4-ASA form I and the discovered form II cocrystal several characterisation techniques such as PXRD, DSC, elemental analysis (EA), FTIR, ssNMR and SC-XRD were used. Furthermore, solubility, dissolution, long-term (physical and chemical) stability and stability at different humidities by DVS were studied.

Considering all the findings, it can be summarised that, in comparison to form I the form II cocrystal is a higher energy form (due to the requirement of heat in order for it to be formed) with a similar melting behaviour, but is thermodynamically less stable. Solubility studies in water have demonstrated that the form II cocrystal transforms rapidly to form I, but can be stabilised by the addition of 0.1% PVP (w/v) to the solution to enable measurement of the solubility. The use of PVP to stabilise solid forms is known and has been reported many times in literature (Sekikawa et al., 1978; Raghavan et al., 2001; Lindfors et al., 2008; Alonzo et al., 2010; Warren et al., 2010).

The determined apparent solubility of the form II cocrystal was similar to the solubility of form I. As expected from the solubility results, and as for form I, the form II cocrystal revealed an improved dissolution rate of the poorly water-soluble SD in comparison to a physical mixture and pure SD.

However, it should be noted that, in contrast to the form I cocrystal (produced by liquid-assisted milling from a 1:1 ratio) for form II (produced by spray drying from a 1:1 ratio) the dissolution results refer to a product with a SD:4-ASA stoichiometry which is not exactly 1:1 (i.e. 8% less molar amount of 4-ASA). Nevertheless, considering that the 4-ASA loss is low, it is believed that a spray-dried product of

equimolar stoichiometry will have comparable dissolution rates to those of the form II cocrystal with a 1:0.92 SD:4-ASA stoichiometry as produced in the course of this work. This may be investigated in future work.

Characterisation by PXRD, FTIR and ^{13}C solid state NMR clearly indicated the structural difference of the form II cocrystal compared to form I, attributed to a different molecular arrangement and different molecular interactions. The use of advanced solid state NMR such as ^{1}H and ^{15}N NMR might have provided more detailed information.

Further clarification was obtained by crystal structure analysis of the SD:4-ASA 1:1 form II cocrystal. As described in Chapter 3, conventional single crystal X-ray analysis, although the most reliable technique, did not allow for solving of the structure due to the observation of non-crystallographic reflections. Alternatively, PXRD data were used from which a crystal structure could be calculated. However, based on a closer inspection of the single crystal X-ray data, followed by further data collection using synchrotron radiation it was demonstrated that the SD:4-ASA 1:1 form II cocrystal reveals an unusually complex structure. Although the investigations are not yet completed, there is evidence (Chapter 3) that the cocrystal is composed of two polymorphs, intergrown in one crystal. Such findings have so far only been reported once for a metal-oxo halide (Hugonin et al., 2009). Thus, these observations provide important insights, not only from a crystallographic point of view also from an industrial point of view, with respect to the production of materials.

In addition, the results demonstrate the superiority of the single crystal X-ray technique using synchrotron radiation as the X-ray source for structure determination in the case of more complex structures compared to the PXRD technique.

Stability tests based on long term storage and when exposed to different humidities by DVS analysis (using cocrystals produced by liquid-assisted milling and spray drying) have shown that both the SD:4-ASA 1:1 from I and form II cocrystals were physically and chemically stable over a storage time of 12 months at 60% RH and 25 °C and DVS analysis enabled these cocrystals to be classified as slightly hygroscopic according to the hygroscopicity classification system established by Murikipudi et al. (2013).

Other cocrystals from the SD:aromatic carboxylic acid type which have been investigated for stability by DVS (as described in Chapter 4) were classified as non-hygroscopic. Similar findings were reported by Andrew et al. (2006) and Basavoju et al. (2007) for theophylline and indomethacin cocrystals.

It can be concluded that the cocrystals investigated are stable solid state forms and provide thus a favoured property for drug formulation.

6.4 Evaluation of cocrystal formation by spray drying

With reference to the findings presented in Chapter 3, a further objective was to investigate the potential of spray drying for screening of new sulfadimidine cocrystals and for polymorphic forms of known sulfadimidine cocrystals and to provide an overall evaluation of cocrystal formation by spray drying compared to common crystallisation methods. The study was based on three known sulfadimidine (SD):aromatic carboxylic acid cocrystals composed of benzoic, salicylic and 4-aminosalicylic acid (BA, SA, 4-ASA) as coformers and two other aromatic carboxylic acids, nicotinic (NA) and pyrazine-2-carboxylic acid (PCA), as potential cocrystal formers with sulfadimidine. The production techniques used as comparators to spray drying were liquid-assisted milling, solvent evaporation and cooling crystallisation. A detailed discussion has been presented in Chapter 5. Figure 6.4 illustrates an overview of the study and the outcome.
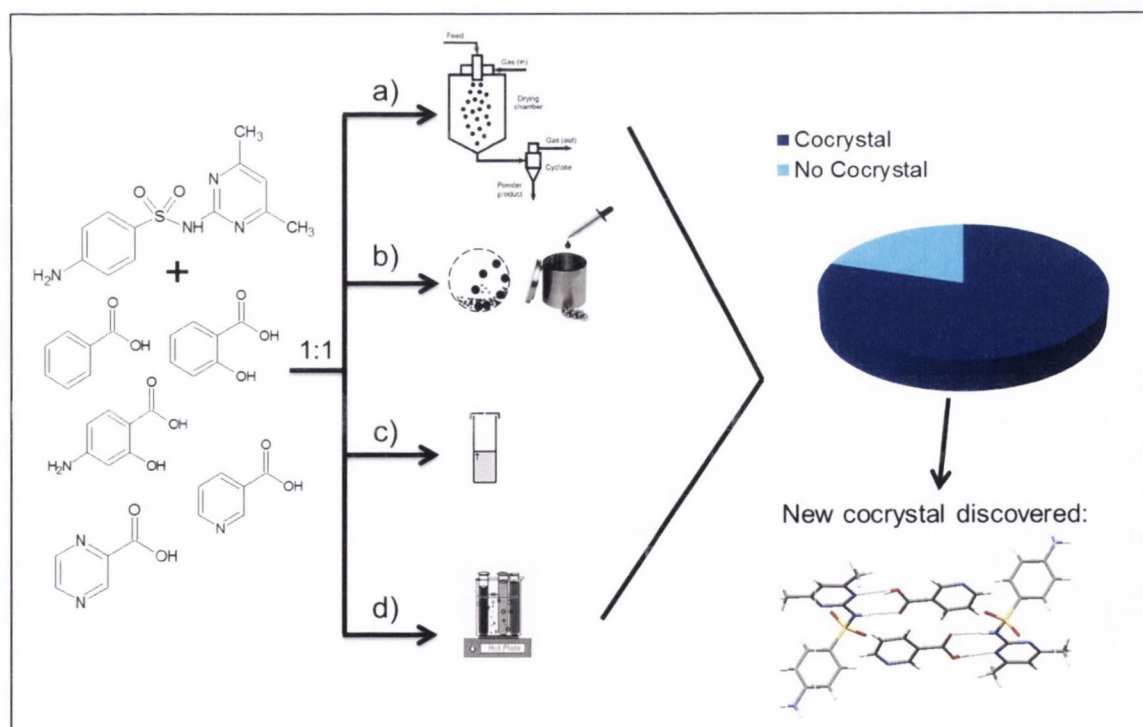
Figure 6.4: Co-processing of sulfadimidine with five aromatic carboxylic acids as coformers using a) spray drying, b) liquid-assisted milling, c) solvent evaporation and d) cooling crystallisation. Results are based on XRD and DSC analysis.

In summary the study has shown that spray drying is a successful alternative to common crystallisation methods such as liquid-assisted milling, solvent evaporation and cooling crystallisation in the formation of cocrystals.

From the five tested SD:aromatic carboxylic acid composite systems, four resulted in cocrystal formation, independently of the technique and solvent used.

By co-processing of SD and NA a new cocrystal has been discovered, the SD:NA 1:1 cocrystal and is thus presented for the first time in this thesis. Cocrystal formation was not successful in the case of the SD:PCA 1:1 systems using each crystallisation technique and solvent. It was shown that this is a result of the structural features of PCA, attributable to intramolecular hydrogen-bond formation which inhibits cocrystal formation.

Furthermore, 4-ASA was the only coformer where spray drying generated a cocrystal (a polymorphic form) which could not be obtained by the other techniques.

4-ASA is the only aromatic carboxylic acid with an amino group. It may therefore be interesting to screen for cocrystal polymorphs using SD and other amino aromatic carboxylic acids. Besides, it would be interesting to examine whether more cocrystals with such an unusual and complex crystal structure as observed for the SD:4-ASA 1:1 form II cocrystal (discussed in Chapter 3) will be discovered.

Although no broad conclusions can be drawn because the study was limited to a small selection of materials, it was observed in the current study that for spray drying and liquid-assisted milling the type of solvent had generally no impact on the product result, based on analysis by PXRD and DSC. Similar observations have been reported by Alhalaweh and Velaga (2010) for carbamazepine-glutaric acid and indomethacin-nicotinamide cocrystals produced by spray drying. However, according to the literature, in the case of liquid-assisted grinding the choice of solvent can have an impact on the result, where different cocrystals can be generated by the addition of different solvents (Friščić and Jones, 2009; Chierotti et al., 2010).

In contrast, for solvent evaporation and cooling crystallisation, depending on the solvent, the degree of purity of the product varied (based on DSC analysis). These findings are in agreement with the literature, where it is reported that cocrystal formation by solvent-based methods such as solvent evaporation and cooling crystallisation is influenced by the solubilities of the individual components in a given solvent (Wouters and Quéré, 2012).

In general, it has been observed that spray drying can induce a mass loss of one of the components, as in the case of BA, SA and 4-ASA as coformers; although the reason for this mass loss is unclear. Mass loss can, in fact, occur for both components. As a consequence, the resulting product can either contain some unreacted crystalline or amorphous phase or just reveal a lower yield. Since the mass loss can be very small, a careful product analysis is required.

It is obvious that for a detailed evaluation of cocrystal formation by spray drying, (with respect to the quality) further analysis of all generated products will be required. Besides, more studies using a broader solvent selection are necessary to elucidate what role the solvent plays in cocrystal formation by spray drying.

In spite of these limitations/issues and although liquid-assisted milling is the more environmentally-friendly of all methods, spray drying offers an interesting alternative with the possibility of faster cocrystal formation than solvent evaporation and cooling crystallisation as shown by Alhalaweh and Velaga (2010).

Main findings

- Based on the benzamide:dibenzyl sulfoxide cocrystal and four sulfdimidine:aromatic carboxylic acid cocrystals studied in this thesis it was demonstrated that the theoretical models describing the solubility and stability of cocrystals introduced by Rodríguez-Hornedo and co-workers are reliable and have highlighted their importance for the development of pharmaceutical cocrystals.

- Phase solubility and triangular phase diagrams have been confirmed to be valuable tools in the prediction of cocrystal stability.

- For the first time a model was presented which enables the pH-dependent solubility and stability of a cocrystal composed of two amphoteric components to be predicted.

- The aqueous solubility of cocrystals with ionisable character is a quite complex property; it seems to be controlled by the individual interactions between solvent, solute and solid state; more studies are required to elucidate the mechanisms and consequently to tailor the aqueous solubility.

- Cocrystals composed of components which reveal a large solubility difference, in the order of > 75 (molar solubility), were found to have no advantage in the dissolution rate of the poorly water-soluble drug over the drug alone.

- The studies have emphasised that the cocrystal approach provides advantages in the solubility compared to poorly water-soluble drugs, however this advantage is associated with the lack of stability by transforming to an incongruently saturating system, resulting in precipitation of the drug. What impact this transformation has on the dissolution rate is assumed to be dependent on the coformer to drug solubility ratio at the given pH conditions. However, further studies under incongruent stability conditions at physiologically relevant pH are necessary and will provide a better understanding, which is the essential requirement to render the cocrystal approach successful.

- For the first time formation of the sulfadimidine:4-aminosalicylic acid 1:1 form I cocrystal via a solid state route using liquid-assisted milling was presented.

- Two new cocrystals have been discovered: (1) A polymorphic form (form II) of the sulfadimidine:4-aminosalicylic acid 1:1 cocrystal. The polymorph reveals an unusually complex crystal structure indicating the presence of two polymorphs in one. (2) The sulfadimidine:nicotinic acid 1:1 cocrystal.

- 4-aminosalicylic acid was the only aromatic carboxylic acid coformer which formed a polymorphic cocrystal with sulfadimidine.

- None of the crystallisation techniques used enabled cocrystal formation of sulfadimidine with pyrazine-2-carboxylic acid as coformer.

- Spray drying was found to be a successful alternative in the formation of cocrystals compared to other common crystallisation methods such as liquid-assisted milling, solvent evaporation and cooling crystallisation. However, it was observed that the purity of the product can be affected due to a mass loss of one of the starting components during processing and as a consequence amorphisation of the unreacted component(s) is possible. Thus, a careful product analysis is required. These findings should be considered for process optimisation.

- All sulfadimidine:aromatic carboxylic acid cocrystals investigated were physically stable, as was supported by DVS studies and are classified as non-hygroscopic or slightly hygroscopic.

Future work

- Intrinsic dissolution studies of the sulfadimidine:aromatic carboxylic acid cocrystals under incongruent stability conditions (at neutral or basic pH) in order to evaluate the impact of an enhanced solubility, but deteriorated stability on the dissolution rate.

- Optimisation of the spray drying process for achieving the formation of a pure (stoichiometrically equimolar) sulfadimidine:4-aminosalicylic acid form II cocrystal followed by intrinsic dissolution studies of the resulting product.

- Completion of the crystal structure determination of the sulfadimidine:4-aminosalicylic acid 1:1 form II cocrystal.

- Analysis of the sulfadimidine:4-aminosalicylic acid 1:1 form II cocrystal by advanced solid state NMR, such as proton and nitrogen NMR such as ^1D ^1H MAS and CRAMPS, 2D ^1H DQ MAS, ^1H ^{13}C CPMAS and HETCOR and ^{15}N CPMAS.

- Purity analysis by HPLC of the sulfadimidine:aromatic carboxylic acid cocrystals produced by spray drying, liquid-assisted milling, solvent evaporation and cooling crystallisation in order to draw further conclusions for evaluating the overall product quality.

- Solubility, dissolution and stability studies of the sulfadimidine:aromatic carboxylic acid cocrystals presented in Chapter 4 that were produced by spray drying.

- Studies on the formation of polymorphic cocrystals using sulfadimidine and different amino aromatic carboxylic acids by spray drying and characterisation of their crystal structure.

References

Aakeröy, C.B., Beatty, A.M., Helfrich, B.A., Nieuwenhuyzen M., 2003. Do polymorphic compounds make good cocrystallising agents? A structural case study that demonstrates the importance of synthon flexibility. Cryst Growth Des. 3, 159–65.

Aakeröy, C.B., Salmon, D.J., 2005. Building co-crystals with molecular sense and supramolecular sensibility. Cryst. Eng. Comm. 7, 439–448.

Abdullah, M.A., Tofiq, D.I., 2010. Synthesis, characterization and kinetic studies of the formation of a new chromium(III) complex of mixed ligands L-cysteine and picolinic acid. Iraqi National Journal of Chemistry, 38, 265–278.

Ainouz, A., Authelin, J.-R., Billot, P., Lieberman, H., 2009. Modeling and prediction of cocrystal phase diagrams. Int. J. Pharm. 374, 82–89.

Alhalaweh, A., Kaialy,W., Buckton,G., Gill, H. Nokhodchi, A., Velaga, S.P., 2013. Theophylline Cocrystals Prepared by Spray Drying: Physicochemical Properties and Aerosolization Performance. Pharm Sci Tech 14, 265–276.

Alhalaweh, A., Sokolowski, A., Rodríguez-Hornedo, N., Velaga, S.P., 2011. Solubility Behavior and Solution Chemistry of Indomethacin Cocrystals in Organic Solvents. Cryst. Growth Des. 11, 3923–3929.

Alhalaweh, A., Velaga, S.P., 2010. Formation of cocrystals from stoichiometric solutions of incongruently saturating systems by spray drying. Cryst. Growth Des. 10, 3302–3305.

Alhalaweh, A., Roy, L., Rodríguez-Hornedo, N., Velaga, S.P., 2012. pH-dependent solubility of indomethacin-saccharin and carbamazepine-saccharin cocrystals in aqueous media. Mol. Pharmaceutics 9, 2605–2612.

Alonzo, D.E., Zhang, G.G., Zhou, D., Gao, Y., Taylor, L.S., 2010. Understanding the behavior of amorphous pharmaceutical systems during dissolution. Pharm Res 27, 608–618.

Amidon, G.L., Lennernas, H., Shah, V.P., Crison, J.R., 1995. A theroretical basis for a biopharmaeutic drug classification: the correleation of in vitro drug product dissolution and in vivo bioavailability. Pharm. Res. 12, 413–420.

Andrew, V.T., Motherwell, W.D.S., Jones, W., 2006. Physical stability enhancement of theophylline via co-crystallization. Int J Pharm. 320, 114–123.

Appel, L., Babcock, W., Friesen, D.T., Ray, R.J., Shamblin, S., Shanker, R., Smithey, D., 2006. Pharmaceutical dosage forms comprising a low-solubility drug and a polymer. Patent WO 2006/024944 A2.

Apperley, D.C., Harris, R.K., Hodgkinson, P., 2012. Solid State NMR: Basic Principles & Practice. Momentum Press, New York, USA.

Arman, H.D., Kaulguda, T., Tiekink, E.R.T., 2010. 4-Amino-N-(4,6-dimethylpyrimidin-2-yl)-benzenesulfonamide–benzoic acid (1/1). Acta Cryst. E66, 2430.

Ashkenazi, D., Eliaz, N., 2008. Minerals, Lattices And Gemstones – Crystallography and the Structure of Solids. PhysicsPlus, 11. (online magazine of the Israel Physics Society).

Avdeef, A., Tsinman, O., 2008. Miniaturized rotating disk intrinsic dissolution rate measurement: Effects of buffer capacity in comparisons to traditional wood's apparatus. Pharm. Res. 25, 2613–2627.

Bailey, M.A., Ingram, M.J., Naughton, D.P., Rutt, K.J., Dodd, H.T., 2008. Aminosalicylic acid conjugates of EDTA as potential anti-inflammatory pro-drugs: synthesis, copper chelation and superoxide dismutase-like activities. Transition Met. Chem. 33, 195–202.

Bailey Walsh, R.D., Bradner, M.W., Fleischman, S., Morales, L.A., Moulton, B., Rodríguez-Hornedo, N., Zaworotko, M.J., 2003. Crystal engineering of the composition of pharmaceutical phases. Chem. Commun. 9, 186–187.

Basavoju, S., Bostroem, D., Velaga, S.P., 2008. Indomethacin-saccharin cocrystal: Design, synthesis and preliminary pharmaceutical characterization. Pharm. Res. 25, 530–541.

Baxter, D.V., Chisholm, M.H., Lynn, M.A., Putilina, E.F., 1998. Studies of Thermotropic Properties and the Mesophase of Mixtures of *n*-Alkanoates and Perfluoro-*n*-alkanoates of Dimolybdenum (M-M). Chem. Mater. 10, 1758–1763.

Berge, S.M., Bighley, L.D., Monkhouse, D.C., 1977. Pharmaceutical salts. J.Pharm. Sci. 66, 1–19.

Bethune, S.J., Huang, N., Jayasankar, A., Rodríguez-Hornedo, N., 2009. Understanding and Predicting the Effect of Cocrystal Components and pH on Cocrystal Solubility. Cryst. Growth Des. 9, 3976–3988.

Bettinetti, G., Caira, M. R., Callegari, A., Merli, M., Sorrenti, M., Tadini, C., 2000. Structure and Solid-State Chemistry of Anhydrous and Hydrated Forms of the Trimethoprim-Sulfamethoxypyridazine 1:1 Molecular Complex. J. Pharm. Sci. 2000, 89, 478–489.

Bettinetti, G., Sardone, N., 1997. Methanol Solvate of the 1:1 Molecular Complex of Trimethoprim and Sulfadimidine. Acta Crystallogr. C53, 594–597.

Bhatt, J., Murty, B.S., 2008. On the conditions for the synthesis of bulk metallic glasses by mechanical alloying. J. Alloys Compd 459, 135–141.

Bighley, L.D., Berge, S.M., Monkhouse, D.C., 1996. Salt forms of drugs and absorption. In: Swarbrick, J., Boylan, J.C. (Eds.), Encycolpedia of Pharmaceutical Technology 13, 453–499. Marcel Dekker, New York.

Blagden, N., de Matas, M., Gavan, P.T., York, P., 2007. Crystal engineering of active pharmaceutical ingredients to improve solubility and dissolution rates. Adv. Drug Delivery Rev. 59, 617–630.

Braga, D., Giaffreda, S.L., Grepioni, F., Pettersen, A., Maini, L., Curzi, M., Polito, M., 2006. Mechanochemical preparation of molecular and supramolecular organometallic materials and coordination networks. Dalton Trans. 10, 1249–1263.

British Pharmacopoeia (BP), Appendix XII B (5), 2009.The Stationary Office, London.

Bruker. 2007. TOPAS. Version 4.2. BRUKER AXS Madison, Wisconsin, USA.

Brunner, E., 1904. Reaktionsgeschwindigkeit in heterogenen systemen.. Z. Phys. Chem., 47, 56–102.

Büchi Labortechnik: Operation Manual Mini Spray Dryer B-290, Version E, order number 93001.

Buerger, M.J., 1945. The Genesis of Twin Crystals. Am. Mineral. 30, 469–482.

Caira, M.R, 1991. Molecular complexes of sulfonamides. Part1. 1:1 complexes between sulfadimidine [4-amino-N-(4,6-dimethyl-2-pyrimidinyl)benzenesulfonamide] and 2- and 4-aminobenzoic acids. J. Crystallogr. Spectrosc. Res. 21, 641–648.

Caira, M.R., 1992. Molecular complexes of sulphonamides 2. 1:1 complexes between drug molecules: sulfadimidine-acetylsalicylic acid and sulfadimidine-4-aminosalicylic acid. J. Crystallogr. Spectrosc. Res. 22, 193–200.

Caira, M.R., 2007. Sulfa drugs as model cocrystal formers. Mol. Pharm. 4, 310–316.

Caira, M.R., Nassimbeni, L.R., Wildervanck, A.F. 1995. Selective formation of hydrogen bonded cocrystals between a sulfonamide and aromatic carboxylic acids in the solid state. J. Chem. Soc. Perkin Trans. 2, 2213–2216.

Carstensen, J.T., 2001. Advanced pharamaceutical solids. New York: Marcel Dekker.

Chadwick, K., Davey, R.J., Cross, W., 2007. How does grinding produce co-crystals? Insights from the case of benzophenone and diphenylamine. Cryst. Eng. Comm. 9, 732–734.

Cheary, R.W., Coelho, A.A., Cline, J.P., 2007. Fundamental parameters line profile fitting in laboratory diffractometers. J. Res. Nat. Inst. Stand. Technol. 109, 1–25.

ChemBase (ID: 75258) "(phenylmethanesulfinylmethyl)benzene", Chembasewebsite, www.chembase.cn/molecule-75258.html. (accessed 10. September 2013).

Cherukuvada, S., Babu, N.J., Nangia, A., 2011. Nitrofurantoin-p-aminobenzoic acid cocrystal: hydration stability and dissolution rate studies. J. Pharm. Sci. 100, 3233–3244.

Chetina, O., 2012. How to Grow Single Crystals for X-Ray Analysis by Solution Crystallisation. ENOD Press, United Kingdom.

Cheung, E.Y., Kitchin, S.J., Harris, K.D., Imai, Y., Tajima, N., Kuroda, R., 2003. Direct structure determination of a multicomponent molecular crystal prepared by a solid-state grinding procedure. J. Am. Chem. Soc.125, 14658–14659.

Chiarella, R.A., Davey, R.J., Peterson, M.L. 2007. Making co-crystals – the utility of ternary phase diagrams. Cryst. Growth Des.7, 1223–1226.

Chierotti, M.R., Ferrero, L., Garino, N., Gobetto, R., Pellegrino, L., Braga, D., Grepioni F., Maini, L., 2010. The richest collection of tautomeric polymorphs: The case of 2-thiobarbituric acid. Chem.–Eur. J. 16, 4347–4358.

Childs S.L., Zaworotko M.J., 2009. The Reemergence of Cocrystals: The Crystal Clear Writing Is on the Wall. Introduction to Virtual Special Issue on Pharmaceutical Cocrystals. Cryst. Growth Des. 9, 4208–4211.

Childs, S.L., Rodríguez-Hornedo, N., Reddy, L.S., Jayasankar, A., Maheshwari, C., McCausland, L., Shipplett, R., Stahly, B.C., 2008. Screening strategies based on solubility and solution composition generate pharmaceutically acceptable cocrystals of carbamazepine. Cryst. Eng. Comm. 10, 856–864.

Childs, S.L., 2009. Cocrystal design and packing analysis based on a family of crystal structures containing a common molecule. ACS Spring Meeting, Salt Lake City, USA.

Childs, S.L., Chyall, L.J., Dunlap, J.T., Smolenskaya, V.N., Stahly, B.C., Stahly, G.P., 2004. Crystal engineering approach to forming cocrystals of amine hydrochlorides with organic acids. Molecular complexes of fluoxetine hydrochloride with benzoic, succinic and fumaric acids. J. Am.Chem.Soc. 126, 13335–13342.

Childs, S.L., Hardcastel, K.I., 2007. Co-crystals of piroxicam with carboxylic acids. Cryst. Growth Des. 7, 1291–1304.

Chiou, D., Langrish, T., 2008. A comparison of crystallisation approaches in spray drying. J. Food Eng. 88, 177–185.

Clark, R.C., Reid, J.S., 1995. The analytical calculation of absorption in multifaceted crystals, Acta Cryst. A51, 887–897.

Coelho, A.A., 2003. Indexing of powder diffraction patterns by iterative use of singular value decomposition. J. Appl. Cryst. 36, 86–95.

Cooke, C.L., Davey, R.J., 2008. On the solubility of saccharinate salts and cocrystals. Cryst. Growth Des. 8, 3483–3485.

Corrigan, O.I., 1995. Thermal analysis of spray dried products. Thermochim. Acta 248, 245–258.

David, W.I.F., Shankland, K., van de Streek, J., Pidcock, E., Motherwell, W.D.S., Cole, J.C., 2006. DASH: A program for Crystal Structure Determination from Powder Diffraction Data. J. Appl. Cryst. 39, 910–915.

Desiraju, G.R., 1995. Supramolecular synthons in crystal engineering – A new organic synthesis. Angew Chem., Int. Ed. 34, 2311–2327.

Eccles, K.S., Elcoate, C.J., Stokes, S.P., Maguire, A.R., Lawrence, S.E., 2010. Sulfoxides: Potent co-crystal formers. Cryst.Growth Des. 10, 4243–4245.

Etter, M.C., 1990. Encoding and decoding hzdrogen bonds patterns of organic compounds. Acc. Chem. Res. 23, 120–126.

Etter, M.C., 1991. Hydrogen bonds as design elements in organic chemistry. J. Phys. Chem. 95, 4601–4610.

Etter, M.C., Reutzel, S.M., Choo, C.G., 1993. Self-Organization of Adenine and Thymine in the Solid State. J. Am. Chem. Soc. 115, 4411–4412.

European Pharmacopoeia (Ph.Eur.), Method 2.9.29., 2009. European Directorate for the Quality of Medicines, Council of Europe, France.

Farrugia, L.J., 1997. ORTEP-3 for Windows – a version of ORTEP-III with a Graphical User Interface (GUI). J. Appl. Cryst. 30, 565.

Florence, A.T., Attwood, D., ed., 2001. Physicochemical Principles of Pharmacy 5th edition. Royal Pharmaceutical Society of Great Britain, Pharmaceutical press, London, United Kingdom.

Forbes, R.T., York, P., Davidson, J.R., 1995. Dissolution kinetics and solubilities of p-aminosalicylic acid and its salts. Int. J. Pharm. 126, 199–208.

Friščić, T., Jones, W., 2009. Recent advances in understanding the mechanism of cocrystal formatin via grinding. Cryst. Growth Des. 9, 1621–1637.

Friščić, T., Trask, A.V., Jones, W., Motherwell, W.D.S., 2006. Screening for inclusion compounds and systematic construction of three-component solids by liquid-assisted grinding. Angew. Chem.,Int. Ed. 45, 7546–7550.

Ghosh, S., Bag, P.P., Reddy, C.M., 2011. Co-Crystals of Sulfamethazine with Some Carboxylic Acids and Amides: Co-Former Assisted Tautomerism in an Active Pharmaceutical Ingredient and Hydrogen Bond Competition Study. Cryst. Growth Des. 11, 3489–3503.

Gibaldi, M., Weintraub, H., 1968. Dissolution of salicylic acid and polyvinyl pyrrolidone from compressed mixtures. J. Pharm. Sci. 57, 832–835.

Good, D., Miranda, C., Rodríguez-Hornedo, N., 2011. Dependence of cocrystal formation and thermodynamic stability on moisture sorption by amorphous polymer. CrystEngComm, 13, 1181–1189.

Good, D.J., Rodríguez-Hornedo, N., 2009. Solubility advantage of pharmaceutical cocrystals. Cryst. Growth Des. 9, 2252–2264.

Good, D.J., Rodríguez-Hornedo, N., 2010. Cocrystal eutectic constants and prediction of solubility behavior. Cryst. Growth Des. 10, 1028–1032.

Grant, D.J.W., York, P., 1986. Entropy of processing: a new quantity for comparing the solid state disorder of pharmaceutical materials. Int. J. Pharmaceutics, 30, 161–180.

Guzmán, H., Tawa, M., Zhang, Z., Ratanabanangkoon P., Shaw, P., Gardner, C.R., Chen, H., Moreau, J., Almarsson, O., Remenar, J.F., 2007. Combined use of crystalline salt forms and precipitation inhibitors to improve oral absorption of celecoxib from solid oral formulations. J. Pharm. Sci. 96, 2686–2702.

Harris, D. 2010. Quantitative Chemical Analysis, 8th ed., New York: W. H. Freeman and Company.

Harris, K.D.M., Cheung, E.Y., 2004. How to determine structures when single crystals cannot be grown: opportunities for structure determination of molecular materials using powder diffraction data. Chem. Soc . Rev. 33, 526–538.

Healy, A.M., Corrigan, O.I., 1992. Predicting the dissolution rate of ibuprofen-acidic excipient compressed mixtures in reactive media. Int. J. Pharm. 84, 167–173.

Healy, A.M., Corrigan, O.I., 1996. The influence of excipient particle size, solubility and acid strength on the dissolution of an acidic drug from two-component compacts. Int. J. Pharm. 143, 211–221.

Healy, A.M., McCarthy, L.G., Gallagher, K.M., Corrigan, O.I., 2002. Sensitivity of dissolution rate to location in the paddle dissolution apparatus. J. Pharm. Pharmacol. 54, 441–444.

Hendriksen, B.A., Williams, J.D., 1991. Characterization of calcium fenoprofen 2. Dissolution from formulated tablets and compressed rotating discs. Int. J. Pharm. 69, 175–180.

Hickey, M.B., Peterson, M.L., Scoppettuolo, L.A., Morrisette, S.L., Vetter, A., Guzman, H., Remenar, J.F., Zhang, Z., Tawa, M.D., Haley, S., Zaworotko, M.J., Almarsson, O., 2007. Performance comparison of a co-crystal of carbamazepine with marketed product. Eur. J. Pharm. Biopharm. 67, 112–119.

Higuchi, T., 1963. Mechanism of sustained-action medication. Theorectical analysis of rate. J. Pharm. Sci. 52, 1145–1149.

Higuchi, T., Connors, K.A., 1965. Phase solubility techniques. Adv. Anal. Chem. Instrum. 4, 117–212.

Higuchi, W.I., 1967. Diffusional models useful in biopharmaceutics. Drug Release Rate Processes. Pharm. Sci. 56, 315–324.

Higuchi, W.I., Mir, N.A., Desai, S.J., 1965. Dissolution rates of polyphase mixtures. J. Pharm. Sci. 54, 1405–1410.

Hippel (von), A.R., 1962. Molecular designing of materials. Science 138, 91.

Hugonin, Z., Johnsson, M., Lidin, S., 2009. Two for the price of one – Resolvable polymorphism in a 'single cyrstal' of α- and β-Sb$_3$O$_4$I. Solid State Sci. 11, 24–28.

International Conference of Harmonisation (ICH) Harmonised Tripartite Guideline - Validation of Analytical Procedures: Methodology Q2. November, 1996.

International Conference of Harmonisation (ICH) Harmonised Tripartite Guideline - Stability Testing of new Drug Substances and Products: Methodology Q1. October, 1993.

Issa, N., Karamertzanis, P.G.; Welch, G.W.A.; Price, S.L., 2009. Computational attempts are ongoing to predict cocrystal formation. Cryst. Growth Des. 9, 442–453.

Jayasankar, A., Somwangthanaroj, A., Shao, Z.J., Rodríguez-Hornedo, N., 2006. Cocrystal formation during cogrinding and storage is mediated by amorphous phase. Pharm. Res. 23, 2381–2392.

Jivani, S.G., Stella, V.J., 1985. Mechanism of decarboxylation of p-aminosalicylic acid. J.Pharm. Sci.74, 1274–1282.

Jones, W., Motherwell, W.D., Trask, A.V., 2006. Pharmaceutical co-crystals: An emerging approach to physical property enhancement. MRS Bull. 341, 875–879.

Jung, M.S., Kim, J.S., Kim, M.S., Alhalaweh, A., Cho, W., Hwang, S.J., Velaga, S.P., 2010. Bioavailability of indomethacin-saccharin cocrystals. J Pharm. Pharmacol. 62, 1560–1568.

Karki, S., Friščić, T., Fábián, L., Laity, P.R., Day, G.M., Jones, W., 2009. Improving mechanical properties of crystalline solids by cocrystal formation: new compressible forms of paracetamol. Adv. Mater. 21, 3905–3909.

Karki, S., Friščić, T., Jones, W., Motherwell, W. D. S., 2007. Screening for pharmaceutical cocrystal hydrates via neat and liquid-assisted grinding. Mol. Pharm. 4, 347–354.

Khatirkar, R.K., Murty, B.S., 2009. Structural changes in iron powder during ball milling. Materials Chemistry and Physics 123, 247–253.

Kolthoff, I.M., Stenger, V.A., 1942. Volumetric Analysis, vol.1, ed. 2, Interscience Publishers, Inc. New York.

Kuliev, F.A., Aslanov, A.D., Denisov, E.T., 1984. Synthesis and spectra of dibenzyl sulfoxides and sulfones. Azerbaidzhanskii Khimicheskii Zhurnal 1, 72–75.

Kuroda, R., Imai, Y., Tajima, N., 2002. Generation of a co-crystal phase with novel coloristic properties via solid state grinding procedures. Chem. Comm. 23, 2848–2849.

Lapidus, S.H., Stephens, P.W., Arora, K.K., Shattock, T.R., Zaworotko, M.J., 2010. A Comparison of Cocrystal Structure Solutions from Powder and Single Crystal Techniques, Cryst. Growth Des. 10, 4630–4637.

Laudis, R.A., Holonyak, N. (Ed.), 1970. The Growth of Single Crystals. Solid State Physical Electronics Series. Prentice Hall, New York.

Le Bail, A., Duroy, H., Fourquet, J.L., 1988. Ab-initio structure determination of LiSbWO6 by X Ray powder diffraction. Mater. Res. Bull. 23, 447–452.

Lee, A.G., 1977. Lipid phase transitions and phase diagrams. II. Mixtures involving lipids. Biochim. Biophys. Acta. 472, 285–344.

Lee, H.-G., Zhang, G.G.Z., Flanagan, D.R., 2010. Cocrystal intrinsic dissolution behavior using a rotating disk. J. Pharm. Sci. 100, 1736–1744.

Levich, V.G., 1962. Physicochemical Hydrodynamics. Prentice-Hall, Englewood Cliffs, NY.

Lindfors, L., Forssén, S., Westergren, J., Olsson, U., 2008. Nucleation and crystal growth in supersaturated solutions of a model drug. J. Colloid Interface Sci. 325, 404–413.

Loftsson, T., Fririksdóttir, H., Gumundsdóttir, T.K., 1996. The effect of water-soluble polymers on aqueous solubility of drugs. Int. J. Pharm. 127, 293–296.

Loureiro, J.M., Costa, B.F.O., Le Caër, G., Delcroix, P., 2009. Partial amorphization of an α-FeCr alloy by ball-milling. Hyperfine Interactions 183, 109–115.

Lu, J., Li, Y.P., Wang, J., Li, Z., Rohani, S., Ching, C.B., 2011. Pharmaceutical cocrystals: a comparison of sulfamerazine with sulfamethazine. J. Cryst. Growth 335, 110–114.

Lu, J., Rohani, S., 2009. Preparation and characterization of theophylline-nicotinamide cocrystal. Org. Process Res. Dev. 13, 1269–1275.

Lynch, D.E., Smith, G., Byriel, K.A., Kennard, C.H.L., 1991. Molecular Cocrystals of Carboxylic Acids. I. The Crystal Structures of the Adducts of Indole-3-acetic-Acid With Pyridin-2(1H)-one, 3,5-Dinitrobenzoic Acid and 1,3,5-TrinitrobenzeneJ. Chem. 44, 809–819.

Maheshwari, C., André, V., Reddy, S., Roy, L, Duarte, T., Rodríguez-Hornedo, N., 2012. Tailoring aqueous solubility of a highly soluble compound *via* cocrystallization: effect of coformer ionization, pH_{max} and solute–solvent interactions. Cryst Eng Comm 14, 4801–4811.

Matsuda, Y., Kawaguchi, S., Kobayashi, H., Nishijo, J., 1984. Physicochemical characterization of spray-dried phenylbutazone polymorphs. J. Pharm. Sci. 73, 173–179.

Matthews, W.S., Bares, J.E., Bartmess, J.E., Bordwell, F.G., Cornforth, F.J., Drucker, G.E., Margolin, Z., McCallum, R.J., McCollum, G.J., Vanier, N.R., 1975. Equilibrium acidities of carbon acids. VI. Establishment of an absolute scale of acidities in dimethyl sulfoxide solution. J. Am. Chem. Soc. 97, 7006–7014.

Mauger, J., Ballard, J., Brockson, R., De, S., Gray, V., Robinson, D., 2003. Intrinsic Dissolution Performance Testing of the USP Dissolution Apparatus 2 (Rotating Paddle) Using Modified Salicylic Acid Calibrator Tablets: Proof of Principal. Dissolution Technol. 10, 6–15.

McNamara, D.P., Childs, S.L., Giordano, J., Iarriccio, A., Cassidy, J., Shet, M.S., Mannion, R., O'Donnell, E., Park, A., 2006. Use of a glutaric acid cocrystal to improve oral bioavailability of a low solubility API. Pharm. Res. 2, 1888–1897.

Mercury CSD 2.0, 2008. New Features for the Visualization and Investigation of Crystal Structures. Macrae, C.F., Bruno, I.J., Chisholm, J.A., Edgington, P.R., McCabe, P., Pidcock, E., Rodriguez-Monge, L., Taylor, R., van de Streek, J., Wood, P.A., J. Appl. Cryst., 41, 466–470.

Muñoz-Morris, M.A., Morris, D.G., 1991. Ball-milling of elemental powders-compound formation and/ or amorphization. Journal of Materials Science 26, 4687–4696.

Murikipudi, V., Gupta, P., Sihorkar, V., 2013. Efficient throughput method for hygroscopicity classification of active and inactive pharmaceutical ingredients by water vapor sorption analysis, Pharm. Dev. Technol. 18, 348–358.

Nagy, P.I., Takács-Novák, K., 1997. Theoretical and Experimental Studies of the Zwitterion - Neutral Form Equilibrium of Ampholytes in Pure Solvents and Mixtures J. Am. Chem. Soc. 119, 4999–5006.

Nakai, H., Takasuka, M., Shiro, M., 1984. X-Ray and Infrared Spectral Studies of the Ionic Structure of Trimethoprim-Sulfamethoxazole 1:1 Molecular Complex. J. Chem. Soc., Perkin Trans. 2, 1459–1464.

Nehm, S.J., Rodríguez-Spong, B., Rodríguez-Hornedo, N., 2006. Phase solubility diagrams of cocrystals are explained by solubility product and solution complexation. Cryst. Growth Des. 6, 592–600.

Nernst, W., 1904. Theorie der Reaktionsgeschwindigkeit in heterogenen Systemen. Z. Phys. Chem. 47, 52–55.

Newton, D.W., Kluza, R.B., 1978. pK$_a$ values. Drug Intell. Clin. Pharm. 12, 546–554.

Niazi, S.K. (ed.), 2006. Chapter 3: Handbook of Preformulation: Chemical, Biological, and Botanical Drugs. CRC Press, USA.

Nicklasson, M., Brodin, A., Nyqvist, H., 1981. Studies on the relationship between solubility and intrinsic rate of dissolution as a function of pH. Acta Pharm. Suec. 18, 119–128.

Nogami, H., Nagai, T., Suzuki, A., 1966. Studies on powdered preparations. XVII. Dissolution rate of sulfonamides by rotating disk method. Chem. Pharm. Bull. 14, 329–338.

Nolan, L.M., 2008. The production and characterisation of spray dried nanoporous microparticles (NPMPs) intended for dry powder inhalation drug delivery systems. PhD thesis, University of Dublin, Trinity College.

Noyes, A.A., Whitney, W.R., 1897. The rate of solution of solid substances in their own solutions. J. Amer. Chem. Soc. 19, 930–934.

O'Connor, K.M., Corrigan, O.I., 2001. Preparation and characterisation of a range of diclofenac salts. Int. J. Pharm. 226, 163–179.

O'Donnell, L.D., Arvind, A.S., Hoang, P. Cameron, D., Talbot, C., Jewell, D.P., Lennard-Jones, E., Farthing, M.J.G., 1992. Double blind, controlled trial of 4-aminosalicylic acid and prednisolone enemas in distal ulcerative colitis. Gut 33, 947–949.

O'Neil, M.J., Heckelman, P.E., Koch, C.B., Roman, K.J. (Eds.), 2006. The Merck Index: An Encyclopedia of Chemicals, Drugs, and Biologicals. 14th ed. Merck & Co. Inc., Whitehouse Station, N.J., USA.

Overhoff, K.A., McConville, J.T., Yang, W., Johnston, K.P., Peters, J.I., Williams, R. O. 3rd., 2008. Effect of stabilizer on the maximum degree and extent of supersaturation and oral absorption of tacrolimus made by ultra-rapid freezing. Pharm Res 25, 167–175.

Padrela, L., Rodrigues, M.A., Velaga, S.P., Matos, H.A., Gomes de Azevedo, E., 2009. Formation of indomethacin-saccharin cocrystals using supercritical fluid technology. Eur. J. Pharm. Sci. 38, 9–17.

Patel, U., Haridas, M., Singh, T.P., 1988. Structure of the 1:1 Complex between 4-Amino-N-(4,6-dimethyl-2-pyrimidinyl)-benzenesulfonamide (Sulfadimidine) and 2-Hydroxybenzoic Acid (Salicylic Acid). Acta Cryst. C44, 1264–1267.

Paul, K.T., Satpathy, S.K., Manna, I., Chakraborty, K.K., Nando, G.B., 2007. Preparation and Characterization of Nano structured Materials from Fly Ash: A Waste from Thermal Power Stations, by High Energy Ball Milling. Nanoscale Res Lett 2, 397–404.

Perrin, D.D., 1965. Dissociation Constants of Organic Bases in Aqueous Solution. Supplement (1972), Butterworths, London, United Kingdom.

Petricek, V., Dusek, M., Palatinus, L., 2006. Jana2006. The crystallographic computing system. Institute of Physics, Praha, Czech Republic.

Prescott, J.F., Baggot, J.D., 1988. Antimicrobial therapy in veterinary medicine. Blackwell Scientific Publications, Boston, USA.

Rager, R., Hilfiker, R., 2009. Stability domains of multi-component crystals in ternary phase diagrams, Z. Phys. Chem. 223, 793–813.

Raghavan, S.L., Trividic, A., Davis, A.F., Hadgraft, J., 2001. Crystallization of hydrocortisone acetate: influence of polymers. Int J Pharm 212, 213–221.

Rahman, Z., Samy, R., Sayeed, V.A., Khan, M.A., 2012. Physicochemical and mechanical properties of carbamazepine cocrystals with saccharin. Pharm. Dev. Technol. 17, 457–465.

Reddy, L.S., Bethune, S.J., Kampf, J.W., Rodríguez-Hornedo, N., 2009. Cocrystals and salts of gabapentin: pH dependent cocrystal stability and solubility. Cryst. Growth Des. 9, 378–385.

Remenar, J.F., Morissette, S.L., Peterson, M.L., Moulton, B., MacPhee, J.M., Guzmán, H.R., Almarsson, O., 2003. Crystal engineering of novel cocrystals of a triazole drug with 1,4-dicarboxylic acids. J Am Chem Soc. 125, 8456–8457.

Remington, J.P., 2005. The Science and Practice of Pharmacy. 21st Edition. Lippincott Williams & Wilkins, Philadelphia, PA, 1314.

Rietveld, H.M., 1969. A Profile Refinement Method for Nuclear and Magnetic Structures. J. Appl. Cryst. 2, 65–71.

Rodríguez-Hornedo, N., Nehm, S.J., Jayasankar, A., 2006. Cocrystals: Design, Properties and Formation Mechanisms. In Encyclopedia of Pharmaceutical Technology. Warbrick, J., Ed., Taylor & Francis Group: London.

Rotich, M.K., Glass, B.D., Brown, M.E., 2001. Thermal studies on some substituted aminobenzoic acids. J. Therm. Anal. Cal., 64, 681–688.

Sander, J.R.G., Bucar, D.K., Henry, R.F., Baltrusaitis, J., Zhang, G.G., MacGillivray, L.R., 2010. A red zwitterionic co-crystal of acetaminophen and 2,4-pyridinedicarboxylic acid. J. Pharm. Sci. 99, 3676–3683.

Schreiber, S., Howaldt, S., Raedler, A., 1994. Oral 4-aminosalicylic acid versus 5-aminosalicylic acid slow release tablets. Double blind, controlled pilot study in the maintenance treatment of Crohn's ileocolitis. Gut. 35, 1081–1085.

Schröder, I., 1893. Über die Abhänghigkeit der Löslichkeit eines festen Körpers von seiner Schmelztemperatur. Z. Phys. Chem., 11, 449–465.

Schultheiss, N., Newman, A., 2009. Pharmaceutical cocrystals and their physicochemical properties. Cryst. Growth Des. 9, 2950–2967.

Sekhon, B.S., 2009. Pharmaceutical co-crystals – a review. Ars Pharm 50, 99–117.

Sekikawa, H., Nakano, M., Arita, T., 1978. Inhibitory effect of poly(vinylpyrrolidone) on the crystallization of drugs. Chem Pharm Bull 26, 118–126.

Shan, N., Toda, F., Jones, W. 2002. Mechnochemistry and co-crystal formation: effect of solvent on reaction kinetics. Chem. Commun. 20, 2372–2373.

Sharma, D., Soni, M., Kumar, S., Gupta, G.D., 2009. Solubility enhancement – eminent role in poorly soluble drugs. Research J. Pharm. and Tech. 2, 220–224.

Shattock, T.R., Arora, K.K., Vishweshwar, P., Zaworotko, M.J., 2008. Hierarchy of Supramolecular Synthons: Persistent Carboxylic Acid·Pyridine Hydrogen Bonds in Cocrystals That also Contain a Hydroxyl Moiety. Cryst. Growth Des. 8, 4533–4545.

Simonelli, A.P., Mehta, S.C., Higuchi, W.I., 1976. Dissolution rates of high energy sulfathiazole–povidone coprecipitates II: characterization of form of drug controlling its dissolution rate via solubility studies. J Pharm Sci, 65, 355–361.

Skinner, M., Kanfer, I., 1992. Intrinsic dissolution rate and solubility studies on josamycin, a macrolide antibiotic. Int. J. Pharm. 88, 151–158.

Stahl, P.H., Wermuth, C.G. (Eds.), 2002. Handbook of pharmaceutical salts: Properties, selection and use., Wiley-VCH/VHCA, Weinheim/Zürich.

Stahly, G.P., 2007. Diversity in single and multiple component crystals. The search for and prevalence of plymorphs and co-crytstals. Cryst. Growth Des. 7, 1007–1026.

Stahly, G.P., 2009. A survey of cocrystals reported prior to 2000. Cryst. Growth. Des. 9, 4212–4229.

Stanton, M.K., Bak, A., 2008. Physicochemical Properties of Pharmaceutical Co-Crystals: A Case Study of Ten AMG 517 Co-Crystals. Cryst. Growth Des. 8, 3856–3862.

Sugano, K., 2009. Introduction to computational oral absorption simulation. Expert Opin. Drug Metab. Toxicol. 5, 529–293.

Sukul, P., Spiteller, M., 2006. Sulfonamides in the environment as veterinary drugs. Reviews of Environmental Contamination and Toxicology, 187, 67–101.

Suzuki, H., Sunada, H., 1998. Influence of watersoluble polymers on the dissolution of nifedipine solid dispersions with combined carriers. Chem. Pharm. Bull. 46, 482–487.

Tajber, L., Corrigan, O.I., Healy, A.M., 2005. Physicochemical evaluation of PVP-thiazide diuretic interactions in co-spray-dried composites – analysis of glass transition composition relationships. Eur. J. Pharm. Sci. 24, 553–563.

Tajber, L., Corrigan, D.O., Corrigan, O.I., Healy, A.M., 2009. Spray drying of budesonide, formoterol fumarate and their composites-I. Physicochemical characterisation. Int. J. Pharm. 367, 79–85.

Takata, N., Shiraki, K., Takano, R., Hayashi, Y., Terada, K., 2008. Cocrystal screening of stanolone and mestanolone using slurry crystallization. Cryst. Growth Des. 8, 3032–3037.

Tenchov, B.G., 1985. Nonuniform lipid distribution in membranes. Prog. Surf. Sci. 20, 273–340.

Tiwari, R.K., Haridas, M., Singh, T.P., 1984. Structure of 4-Amino-N-(4,6-dimethyl-2-pyrimidinyl)benzenesulphonamide (Sulfadimidine), $C_{12}H_{14}N_4O_2S$. Acta Cryst. C40, 655–657.

Trask, A.V.; Jones, W., 2005a. Crystal engineering of organic cocrystals by the solid-state grinding approach. Organic Solid State Reactions, 254, 41–70.

Trask A.V., Jones, W., edited by Toda, F., 2005b. Topics in Current Chemistry. Vol. 254, Springer, New York.

Trask, A.V., 2007. An overview of pharmaceutical cocrystals as intellectual property. J. Am. Chem. Soc. 4, 301–309.

Trask, A.V., Motherwell, W.D.S., Jones, W., 2004. Solvent-Drop Grinding: Green Polymorph Control of Cocrystallisation.Chem. Comm. 7, 890–891.

Trask, A.V., Motherwell, W.D.S., Jones, W., 2005. Pharmaceutical cocrystallization: Engineering a remedy for caffeine hydration. Cryst. Growth Des. 5, 1013–1021.

United States Pharmacopoeia and National Formulary USP 32–NF 27; 2009. The United States Pharmacopeial Convention, Inc., Rockville, MD, USA.

Usui, F., Maeda, K., Kusai, A., Nishimura, K., Yamamoto, K., 1997. Inhibitory effects of water-soluble polymers on precipitation of RS-8359. Int J Pharm 154, 59–66.

Vishweshwar, P., McMahon, J.A., Bis, J.A., Zaworotko, M.J., 2006. Pharmaceutical Co-crystals. J. Pharm. Sci. 95, 499–516.

Vogt, M., Vertzoni, M., Kunath, K., Reppas, C., Dressman, J.B., 2008. Cogrinding enhances the oral bioavailability of EMD 57033, a poorly water soluble drug, in dogs. Eur. J. Pharm. Biopharm. 68, 338–345.

Warren, D.B., Benameur, H., Porter, C.J.H., Pouton, C.W., 2010. Using polymeric precipitation inhibitors to improve the absorption of poorly water-soluble drugs: A mechanistic basis for utility. J. Drug Target. 18, 704–731.

Wenger, M., Bernstein, J., 2008. An alternate crystal form of gabapentin: A cocrystal with oxalic acid. Cryst. Growth Des. 8, 1595–1598.

Wermuth, C.G., 2008. The Practice of Medicinal Chemistry, 3rd ed. Elsevier, Ltd., pp. 750.

Willart, J.F., Caron, V., 2007. Descamps M. Transformations of crystalline sugars upon milling. J. Therm. Anal. Calorim. 90, 125–130.

Willart, J.F., Descamps, M., 2008. Solid state amorphization of pharmaceuticals. Mol. Pharm. 5, 905–920.

Wood, J.H., Syarto, J.E., Letterman, H., 1965. Improved holder for intrinsic dissolution rate studies. J. Pharm. Sci. 54, 1068.

Wouters, J., Quéré, L., (ed.) 2012. Pharmaceutical Salts and Co-Crystals. Royal Society of Chemistry.

Yu, L.X., Carlin, A.S., Amidon, G.L., Hussain, A.S., 2004. Feasibility studies of utilizing disk intrinsic dissolution rate to calssify drugs. Int. J. Pharm. 270, 221–227.

Zaworotko, M., 2005. Polymorphism in co-crystals and pharmaceutical co-crystals. XX Congress of the International Union of Crystallography, Florence.

Zhang, G.G.Z., Henry, R.F., Borchardt, T.B., Lou, X.C., 2007. Efficient co-crystal screening using solution mediated phase transformation. J. Pharm. Sci. 96, 990–995.

Zhang, Y., Zhang, H., Sun, Z., 2003. Susceptibility of Mycobacterium tuberculosis to weak acids. Journal of Antimicrobial Chemotherapy 52, 56–60.

Zughul, M.B., Badwan, A.A., 1997. Rigorous Analysis of S2 L Type Phase Solubility Digrams to Obtain Complex Formation and Solubility Product Constants. Int. J. Pharm. 151, 109–119.

Appendices

Appendix 1
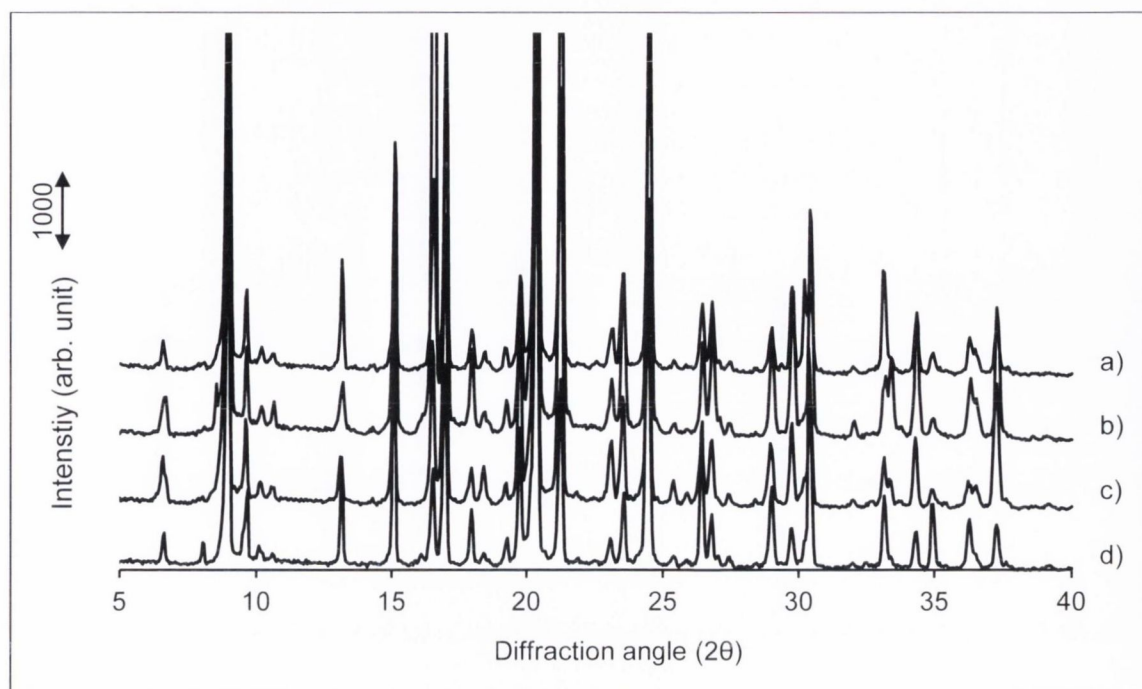
Figure A.1.1: PXRD pattern of remaining solid after 24 hours solubility study when cocrystal is the excess phase of a) 12mg/ml BAM added, b) 9mg/ml BAM added, c) 6mg/ml BAM added compared to d) 1:1 BAM:DBSO cocrystal.
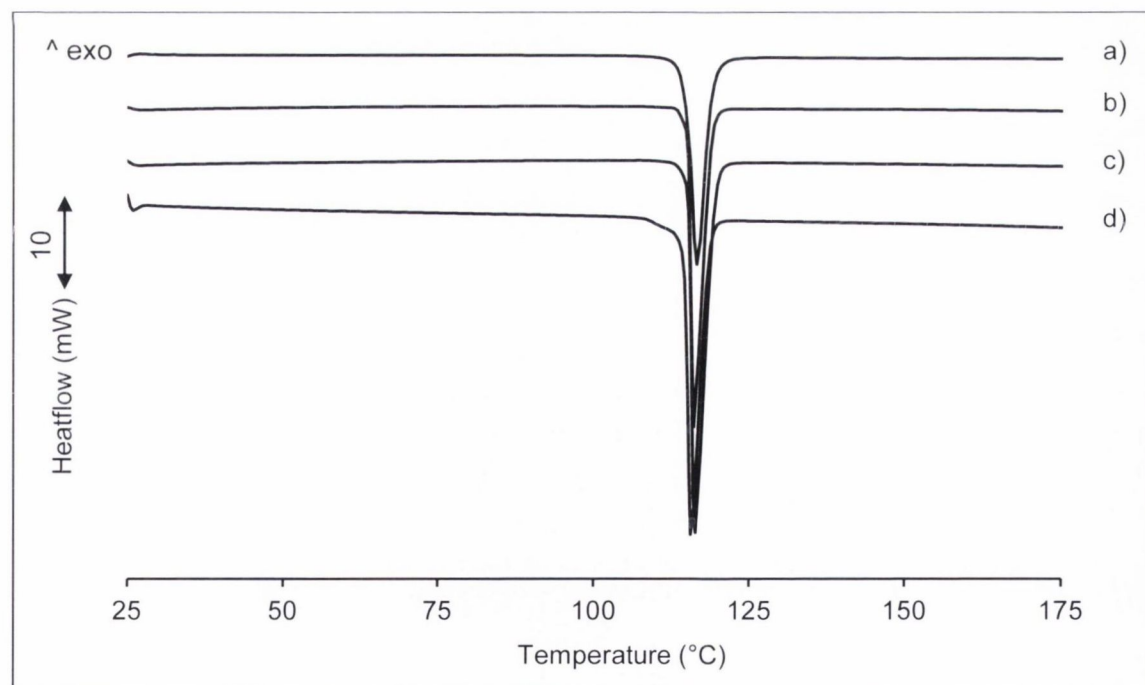
Figure A.1.2: DSC thermograms of remaining solid after 24 hours solubility study when cocrystal is the excess phase of a) 12mg/ml BAM added, b) 9mg/ml BAM added, c) 6mg/ml BAM added compared to d) 1:1 BAM:DBSO cocrystal.
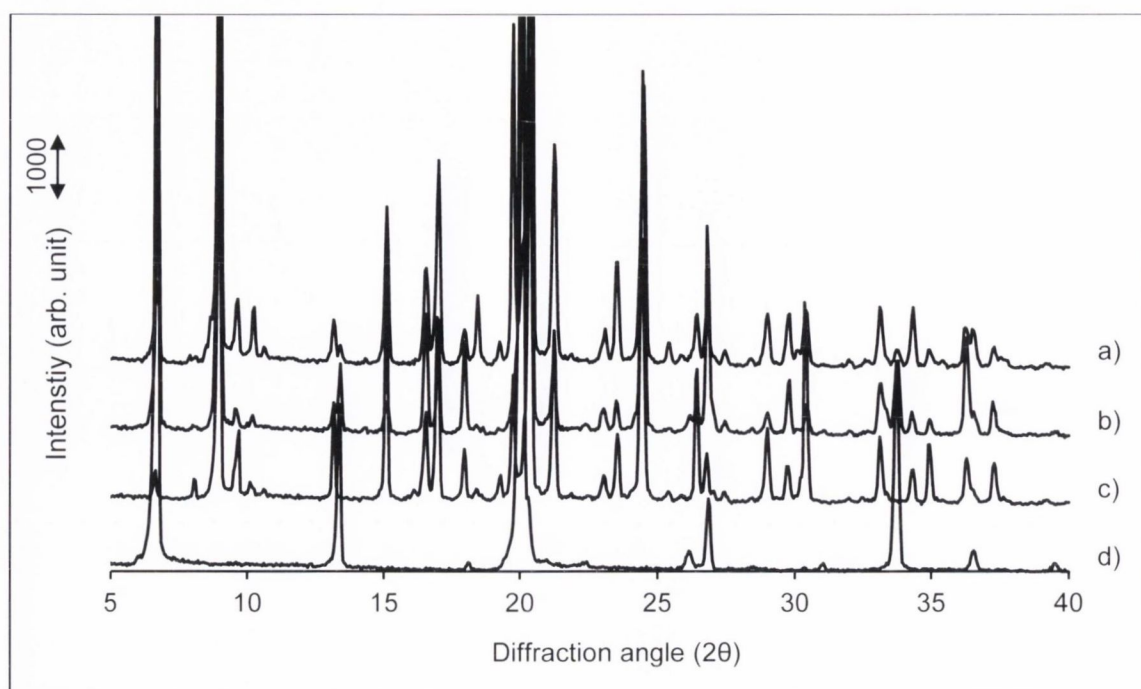
Figure A.1.3: PXRD pattern of remaining solid at the transition concentration after 24 hours equilibration of a) a slightly undersaturated BAM solution with excess DBSO and b) a presaturated DBSO solution with excess cocrystal compared to c) 1:1 BAM:DBSO cocrystal and d) DBSO.
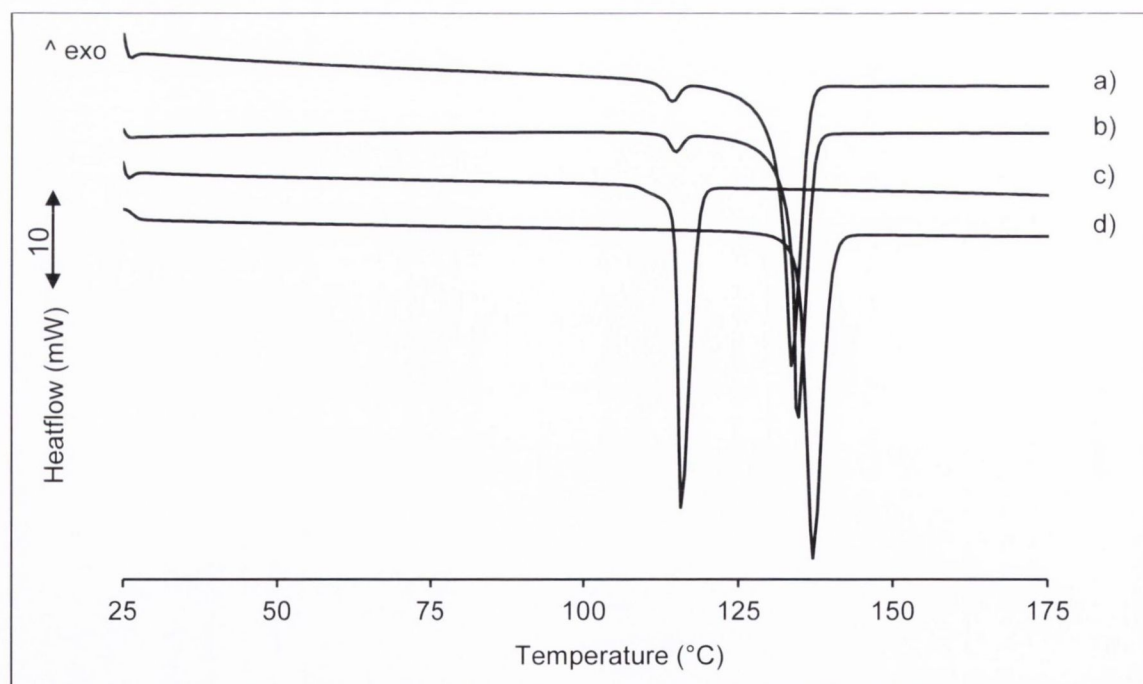
Figure A.1.4: DSC thermograms of remaining solid at the transition concentration after 24 hours equilibration of a) a slightly undersaturated BAM solution with excess DBSO and b) a presaturated DBSO solution with excess cocrystal compared to c) 1:1 BAM:DBSO cocrystal and d) DBSO.
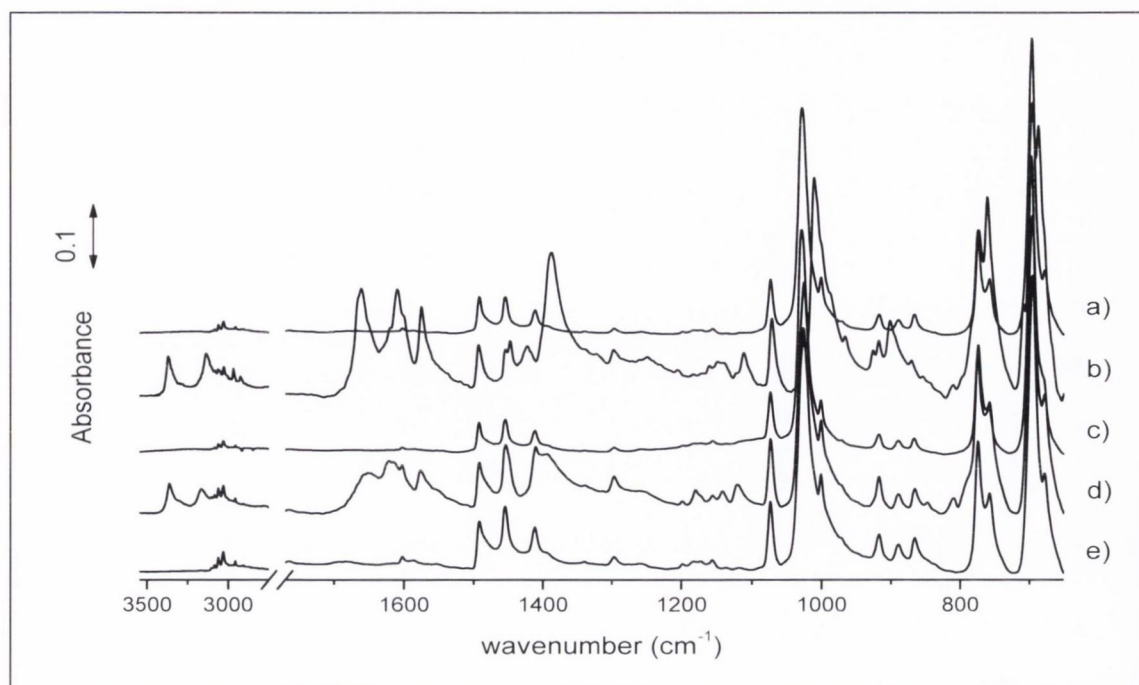
Figure A.1.5: IR spectra of compact surface before and after intrinsic dissolution (ID) studies of a) 1:1 BAM:DBSO cocrystal after dissolution, b) 1:1 BAM:DBSO cocrystal before dissolution, c) BAM:DBSO (1:1) physical mixture after dissolution, d) BAM:DBSO (1:1) physical mixture before dissolution compared to e) DBSO before dissolution.

Appendix 2
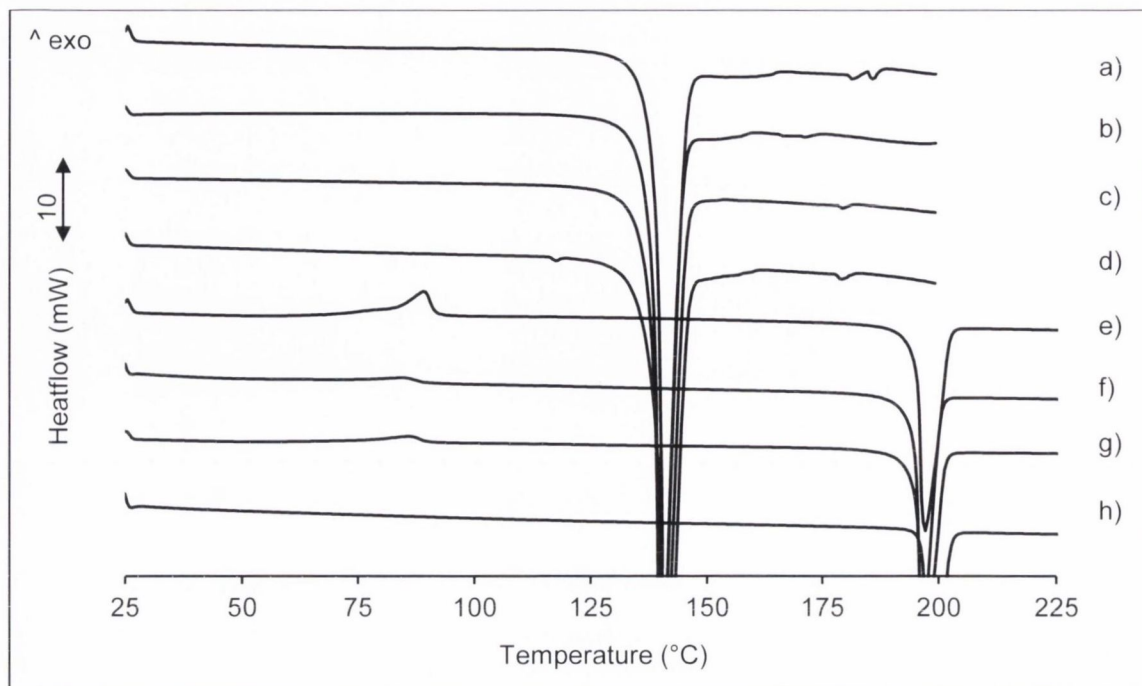
Figure A.2.1: DSC thermograms of a) 4-ASA, milled 45 min, b) 4-ASA, milled 30 min, c) 4-ASA, milled 15min, d) 4-ASA, raw material, e) SD, milled 45min, f) SD, milled 30min, g) SD, milled 15min and h) SD, raw material.
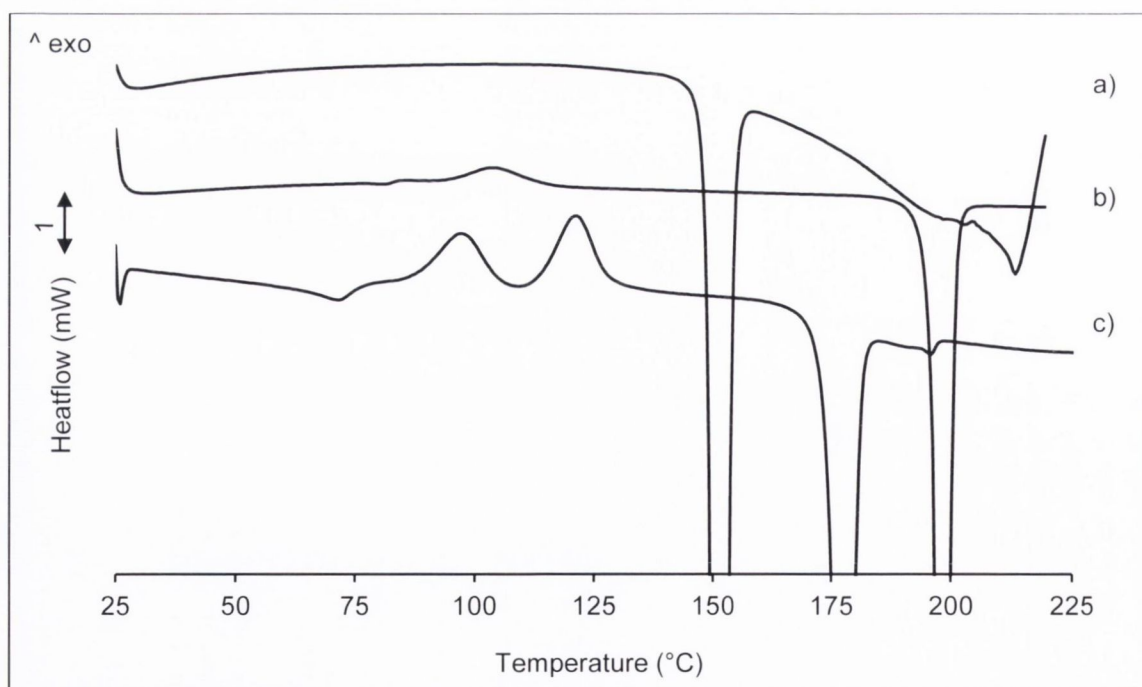
Figure A.2.2: DSC thermograms of a) 4-ASA, spray-dried, b) SD, spray-dried and c) SD:4-ASA 2:1, spray-dried.
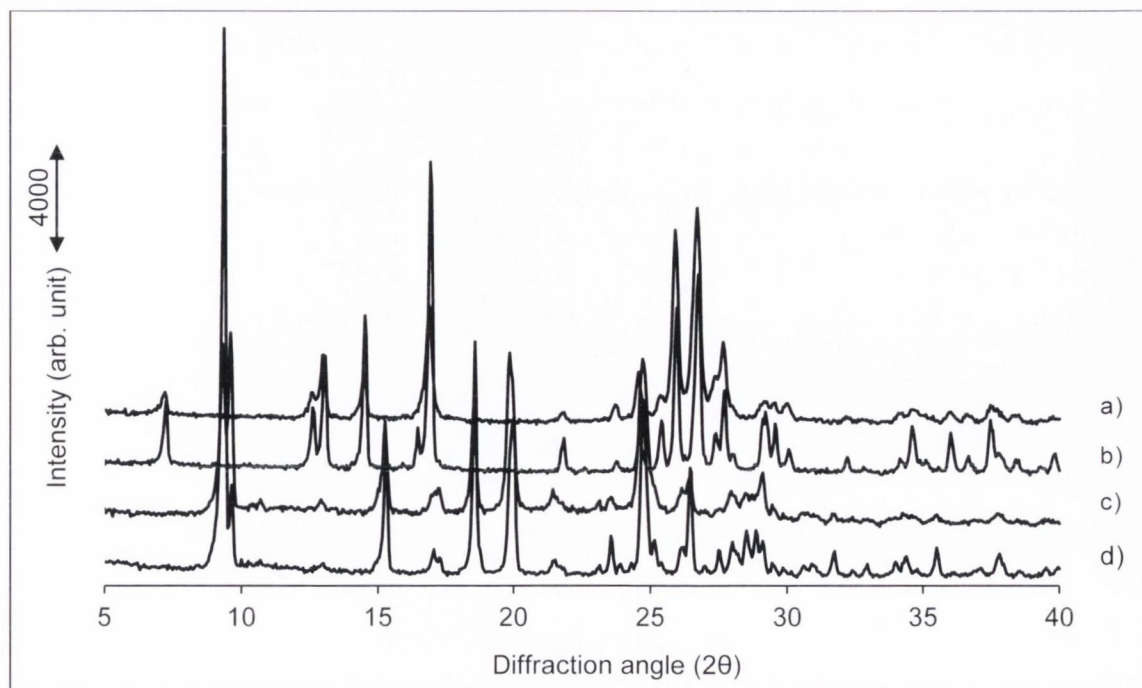
Figure A.2.3: PXRD patterns of a) 4-ASA, spray-dried, b) 4-ASA, raw material, c) SD, spray dried and d) SD, raw material.
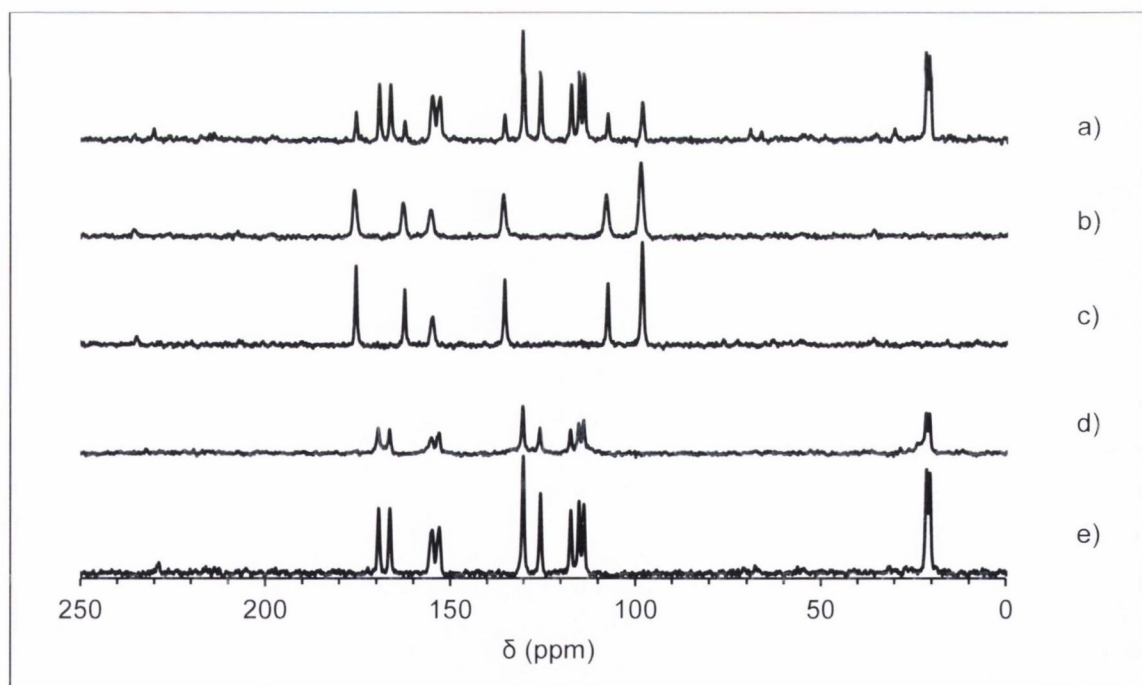
Figure A.2.4: ^{13}C CPMAS spectra of reference samples of a) SD:4-ASA 1:1 physical mixture, b) 4-ASA, spray-dried, c) 4-ASA raw material, d) SD, spray-dried and e) SD, raw material.
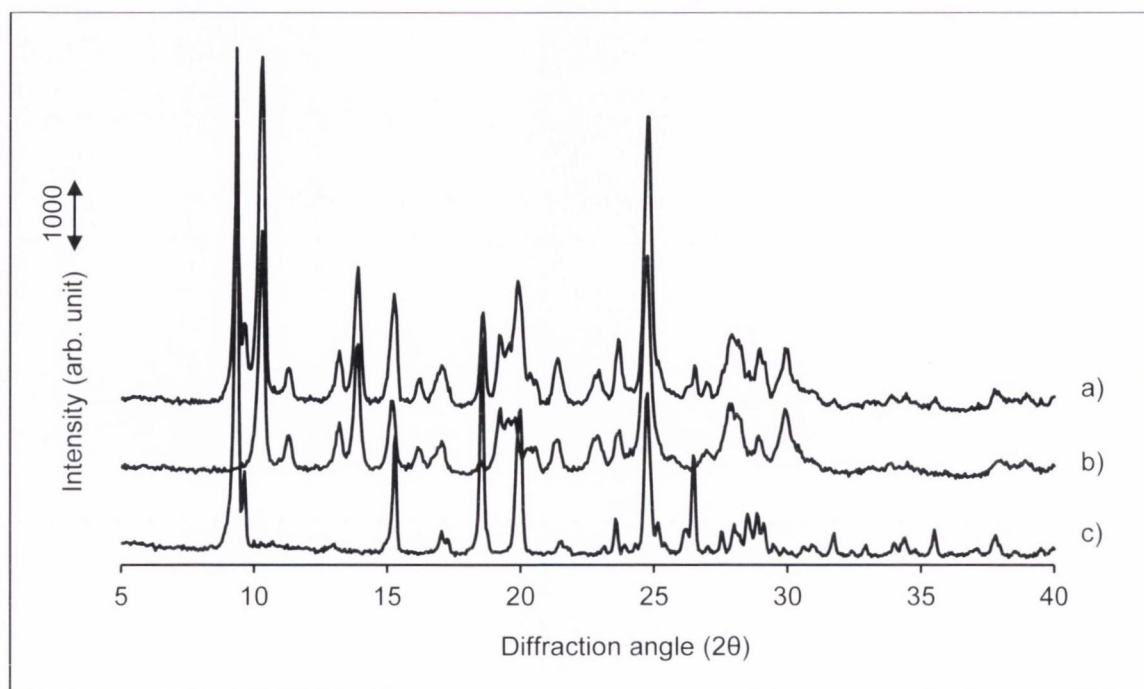
Figure A.2.5: PXRD pattern of a) solid remaining phase at the transition concentration, b) SD:4-ASA 1:1 form I cocrystal and c) SD.
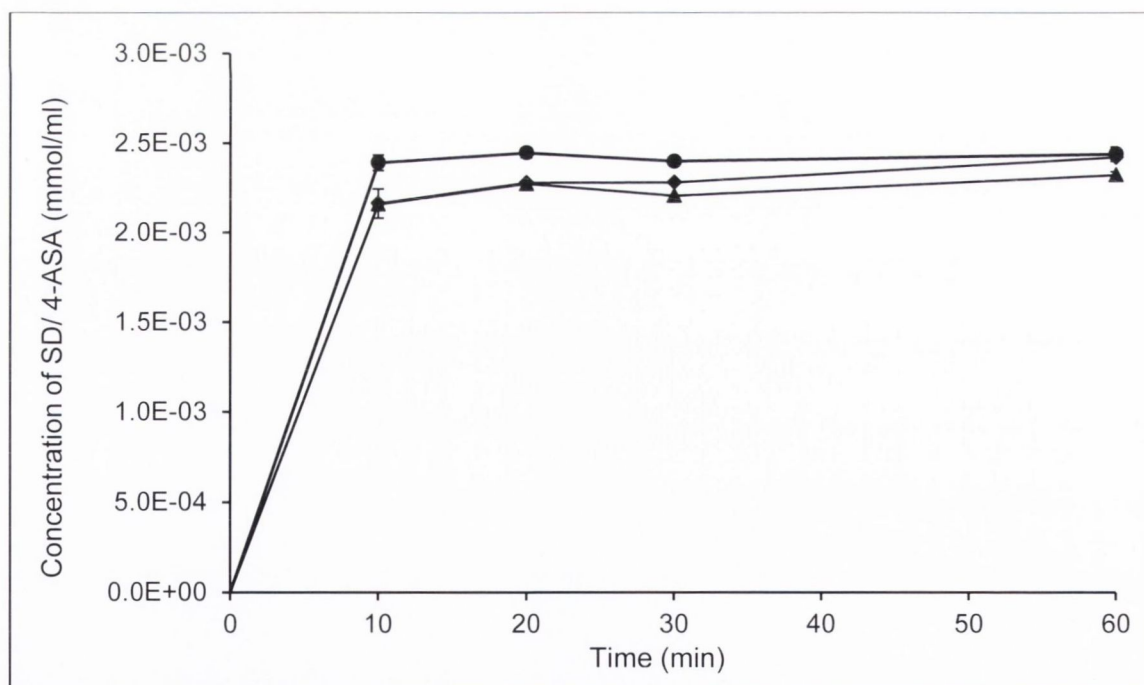
Figure A.2.6: Concentration – time profile of the SD:4-ASA 1:1 form I cocrystal and pure SD in water at 37 °C. Diamonds and triangles symbolise SD and 4-ASA from the cocrystal, circles represent pure SD.
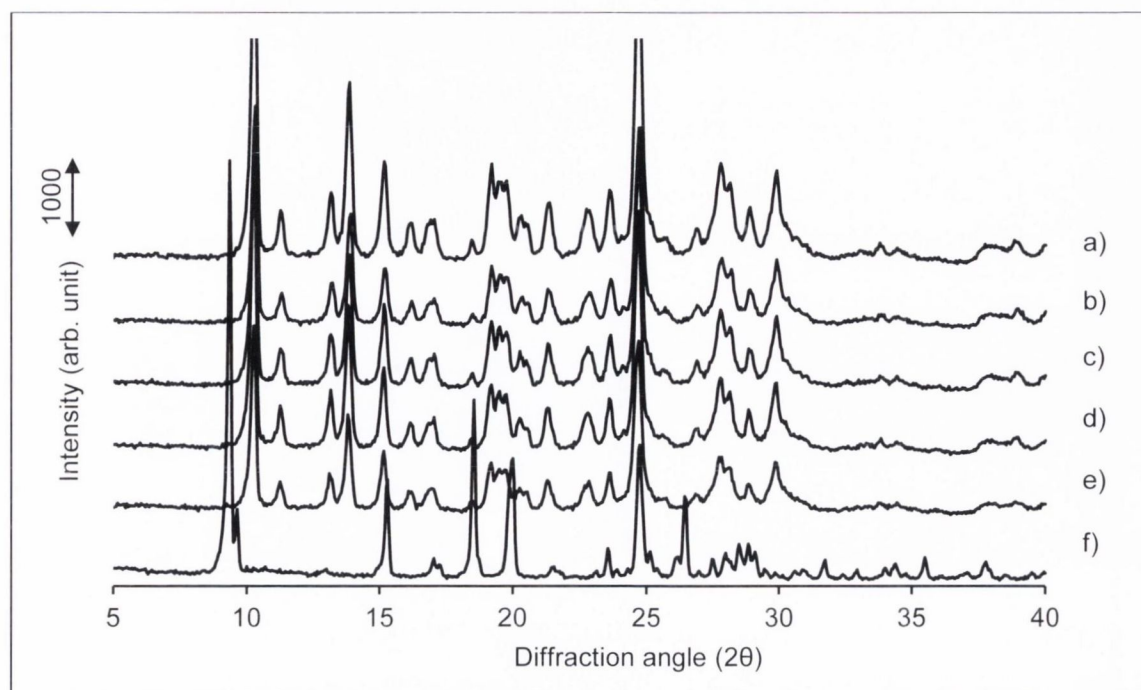
Figure A.2.7: PXRD patterns of the solid phase during dynamic solubility studies in water at 37 °C of the SD:4-ASA 1:1 form I cocrystal: a) at 10 minutes, b) at 20 minutes, c) at 30 minutes, d) at 60 minutes compared to e) SD:4-ASA 1:1 form I cocrystal before subjected to solubility test and f) SD, raw material.
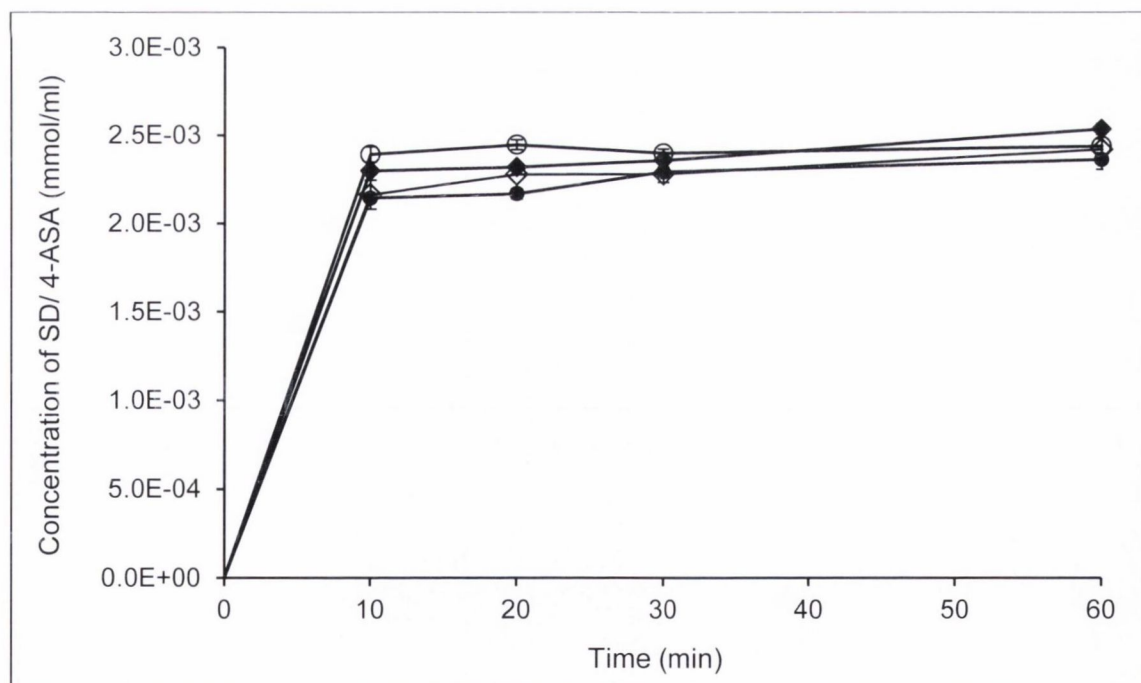
Figure A.2.8: Concentration – time profile of pure SD and SD from the SD:4-ASA 1:1 form I cocrystal in water and in 0.1% (w/v) PVP solution (37 °C). Closed and open circles reppresent SD concentrations of pure SD with and without PVP, respectively. Closed and open diamonds symbolise SD concentrations of the form I cocrystal with and without PVP, respectively.
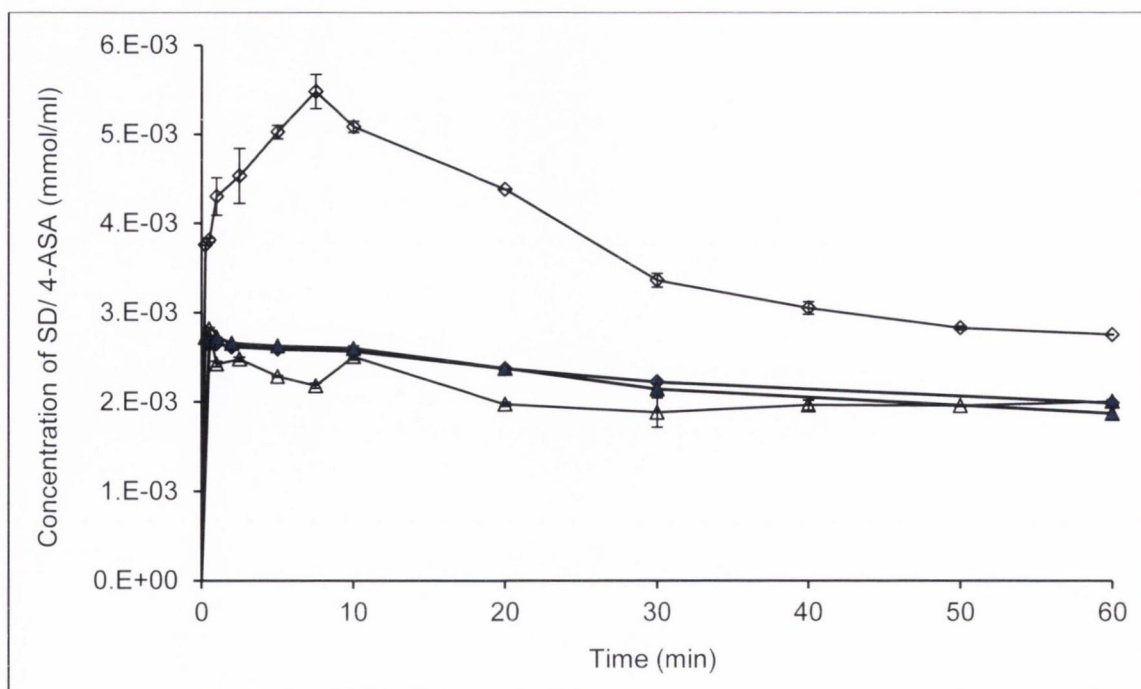
Figure A.2.9: Concentration – time profile of the SD:4-ASA 1:1 form II cocrystal, produced by spray drying and by the solvent evaporation method in water at 37 °C. Open diamonds and triangles symbolise SD and 4-ASA of the spray-dried product, closed diamonds and triangles represent SD and 4-ASA of the crystallised product form solvent evaporation.
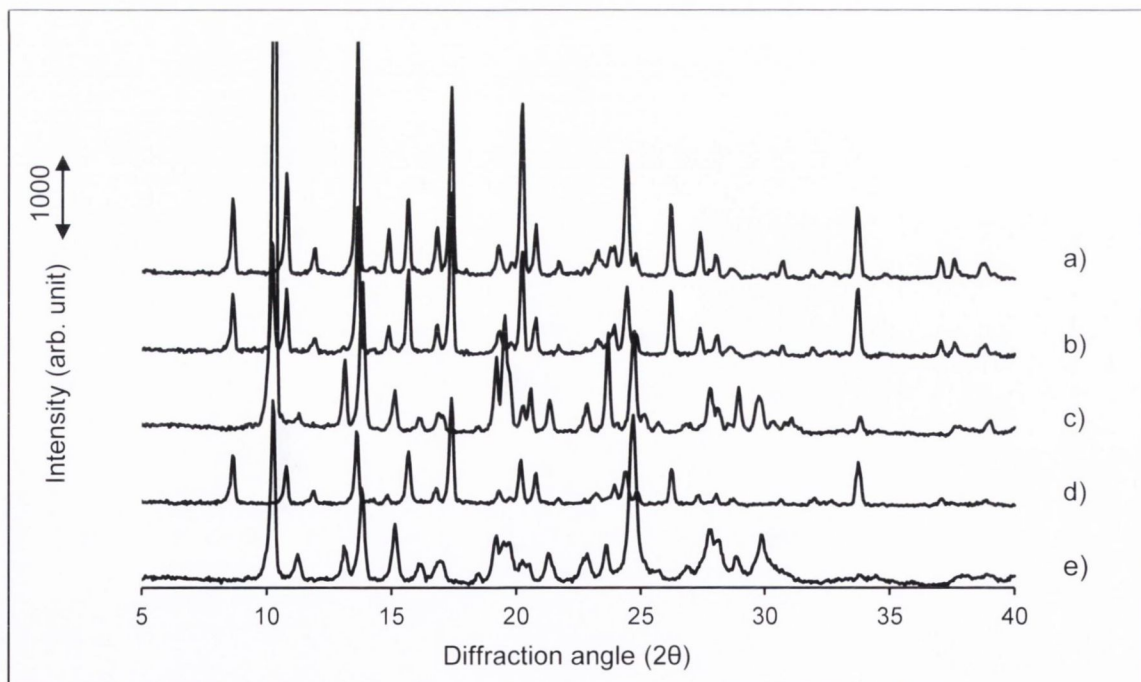
Figure A.2.10: PXRD analysis of the solid phase during dynamic solubility studies in water at 37 °C of the SD:4-ASA 1:1 form II cocrystal produced by solvent evaporation: a) at 5 minutes, b) at 10 minutes, c) at 60 minutes compared to d) SD:4-ASA 1:1 form II cocrystal before subjected to solubility test and e) SD:4-ASA form I cocrystal (reference material).

Table A.2.1: Compression pressure and time applied to prepare compacts for intrinsic dissolution studies.

Sample	Compaction pressure and time
4-ASA	8 tonnes, 1.5 minutes
SD	8 tonnes, 1.5 minutes
SD:4-ASA 1:1 physical mixture	8 tonnes, 1 minute
SD:4-ASA 1:1 form I cocrystal	8 tonnes, 1 minute
SD:4-ASA 1:1 form II cocrystal	8 tonnes, 20 seconds
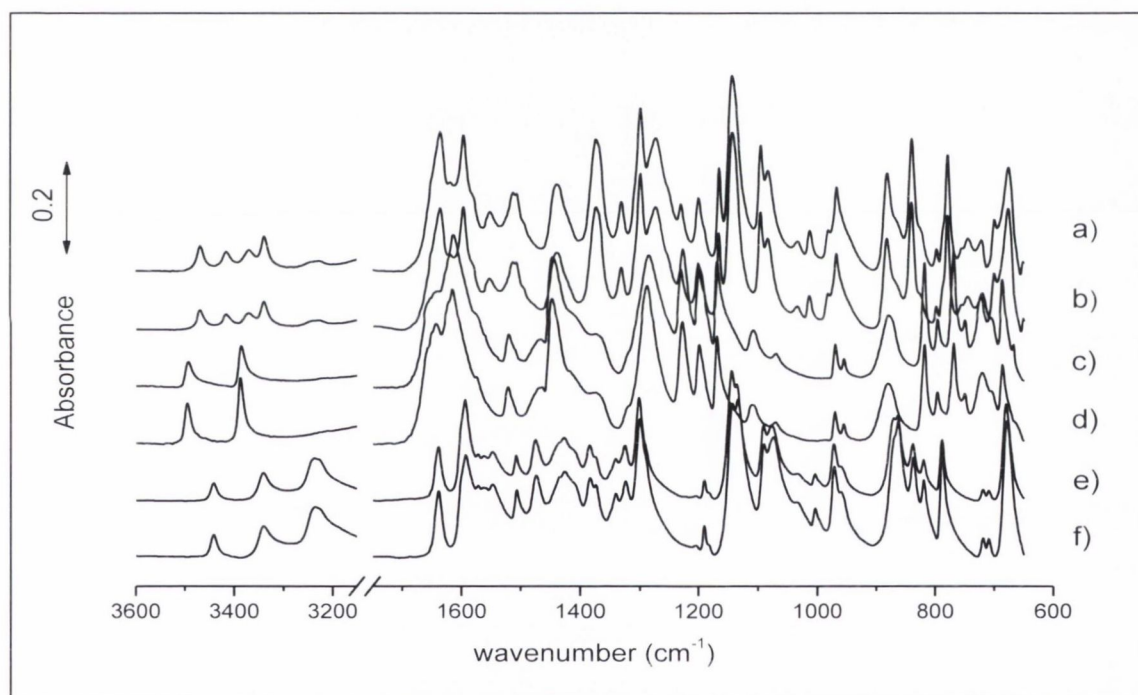
Figure A.2.11: IR spectra of compact surface before and after intrinsic dissolution (ID) studies: a) SD:4-ASA 1:1 form I cocrystal after ID, b) SD:4-ASA 1:1 form I cocrystal before ID, c) 4-ASA after ID, d) 4-ASA before ID, e) SD after ID and f) SD before ID.
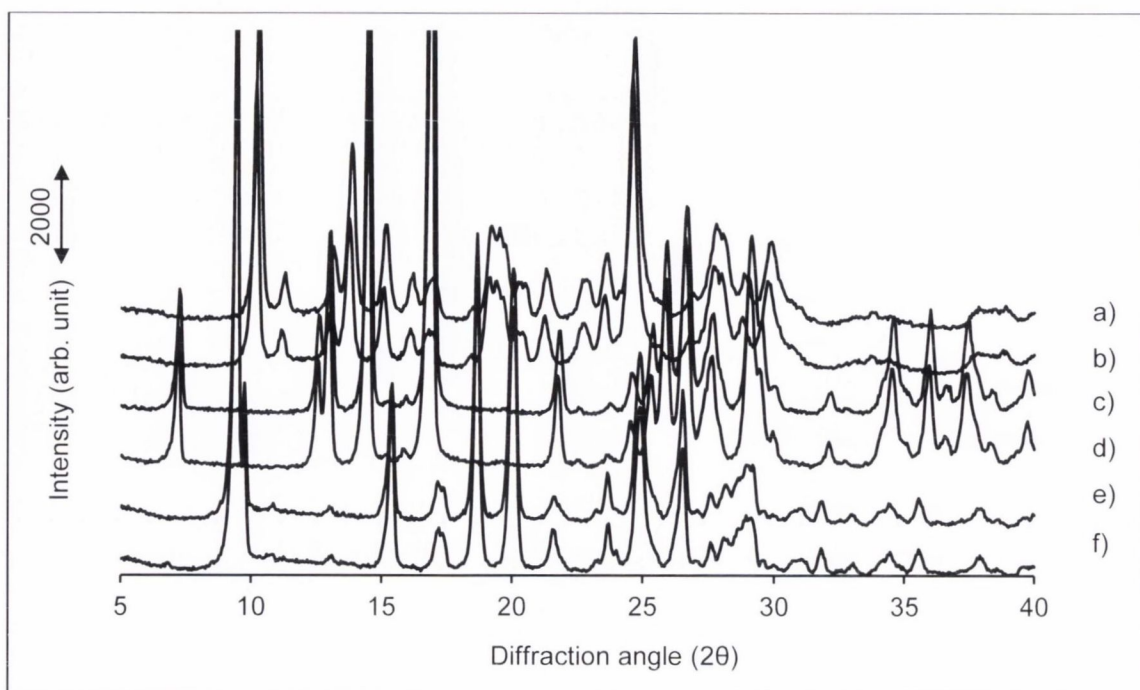
Figure A.2.12: PXRD analysis of compact surface before and after intrinsic dissolution (ID) studies: a) SD:4-ASA 1:1 form I cocrystal after ID, b) SD:4-ASA 1:1 form I cocrystal before ID, c) 4-ASA after ID, d) 4-ASA before ID, e) SD after ID and f) SD before ID.
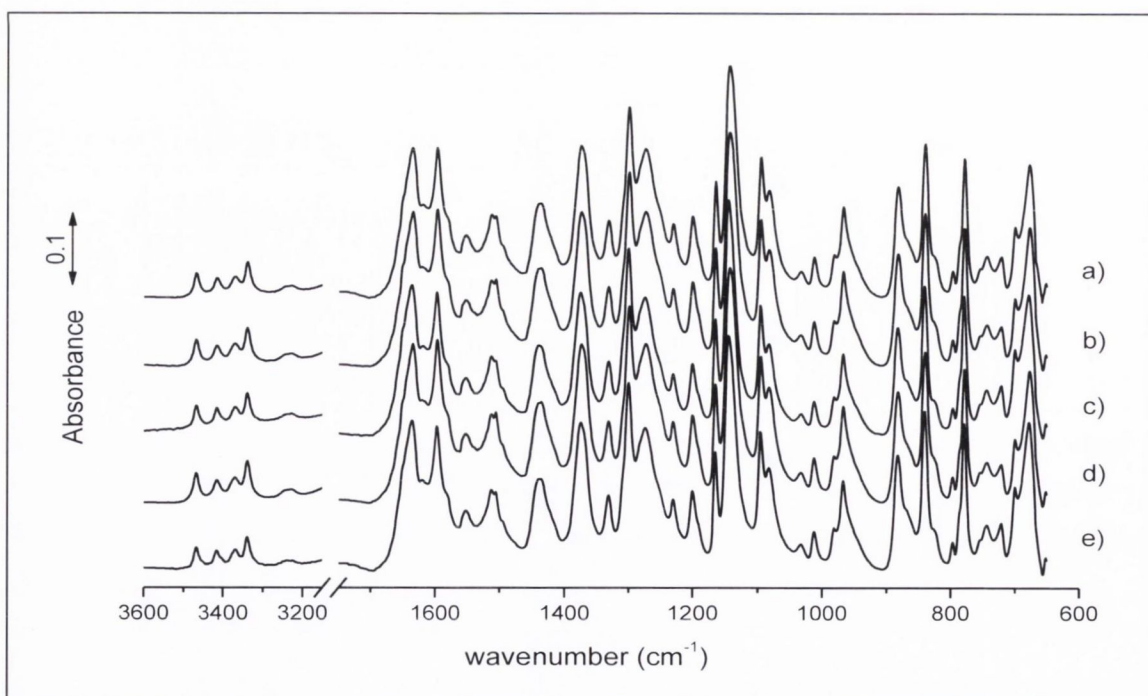
Figure A.2.13: IR spectra of SD:4-ASA 1:1 form I cocrystal. a) Before the study and analysed at different time points during long-term stability test: b) 1 month c) 2 months d) 6 months e) 12 months.
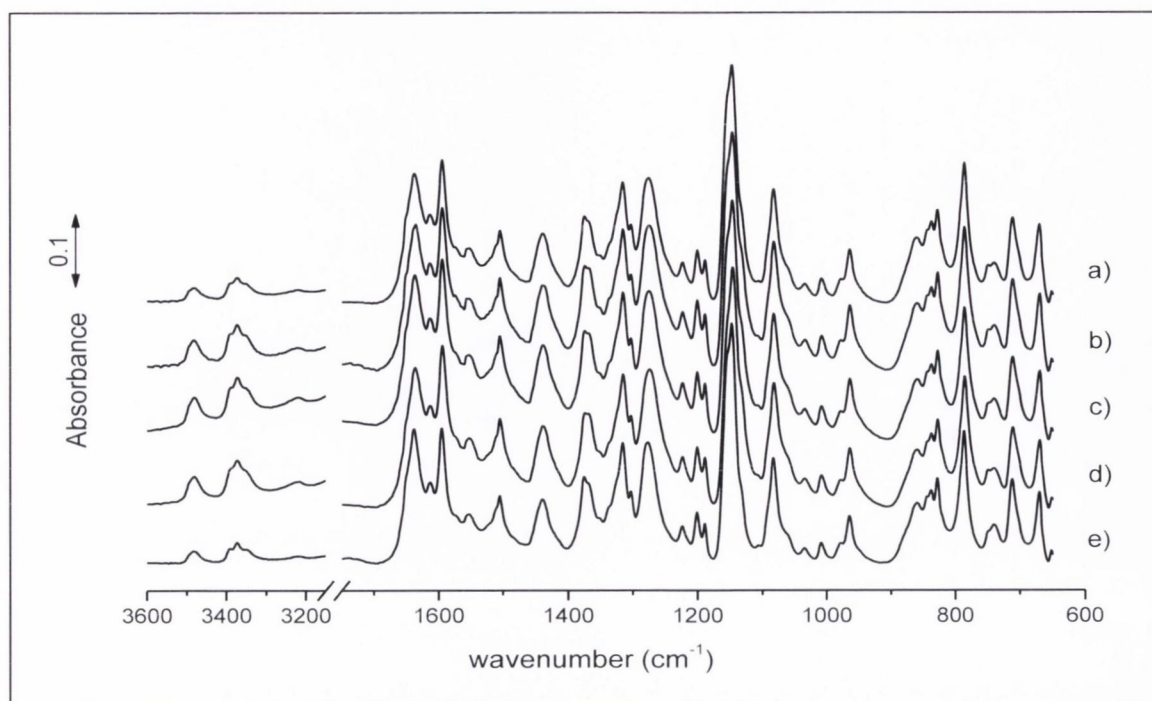
Figure A.2.14: IR spectra of SD:4-ASA 1:1 form II cocrystal. a) Before the study and analysed at different time points during long-term stability test: b) 1 month c) 2 months d) 6 months e) 12 months.
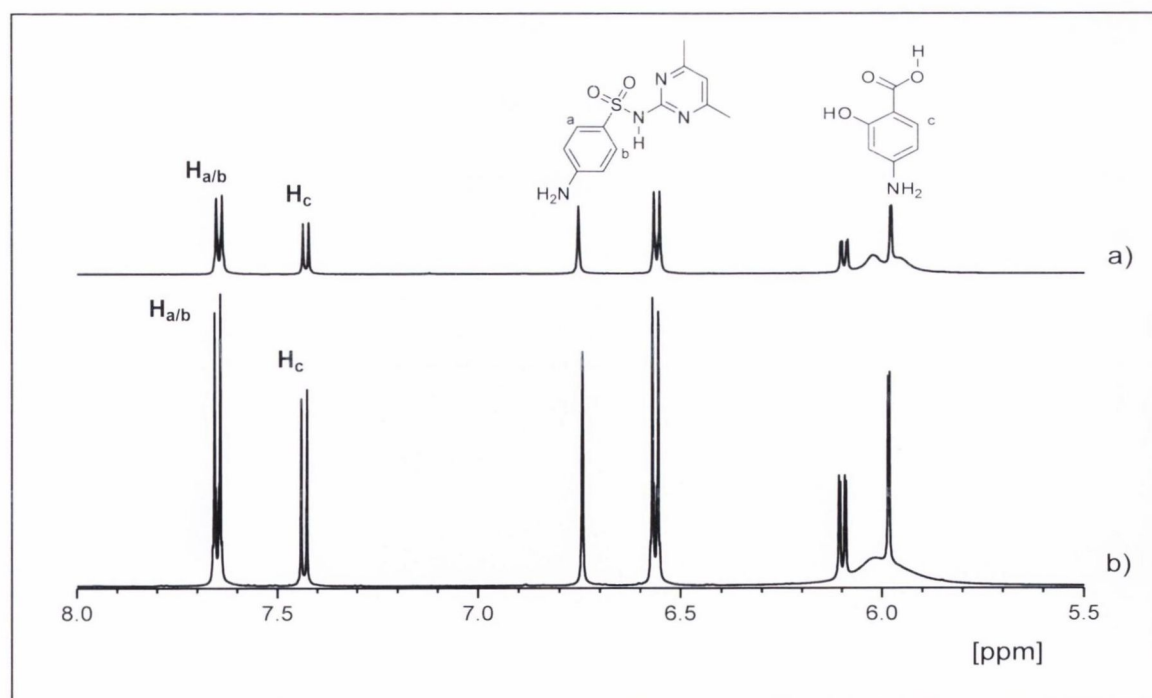
Figure A.2.15: ^{1}H-NMR spectra of the SD:4-ASA 1:1 cocrystal. a) form I (produced by liquid-assisted milling), b) form II (produced by spray drying).

Table A.2.2: A summary of ^{1}H-NMR results of the SD:4-ASA 1:1 form I (produced by liquid-assisted milling) and form II cocrystal (produced by spray drying).

Cocrystal	^{1}H assignment	v(F1) [ppm]	Intensity [abs]	Split	Integral [rel]
form I	$H_{a/b}$ (SD)	7.64	4320609.92	d	2.08
	H_c (4-ASA)	7.42	2072181.14	d	1.00
form II	$H_{a/b}$ (SD)	7.64	12579849.55	d	2.23
	H_c (4-ASA)	7.43	5637360.36	d	1.00
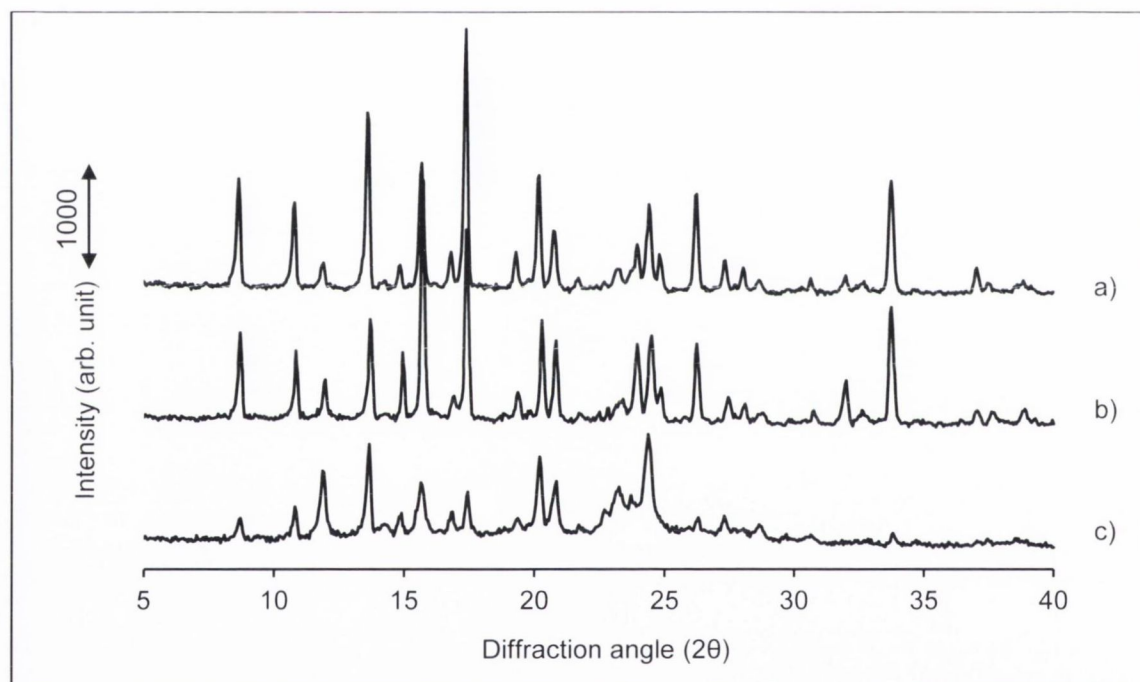
Figure A.2.16: PXRD patterns of the SD:4-ASA 1:1 form II cocrystal. a) crystallised from EtOH by solvent evaporation, b) crystallised from Me_2CO by solvent evaporation and c) spray-dried.
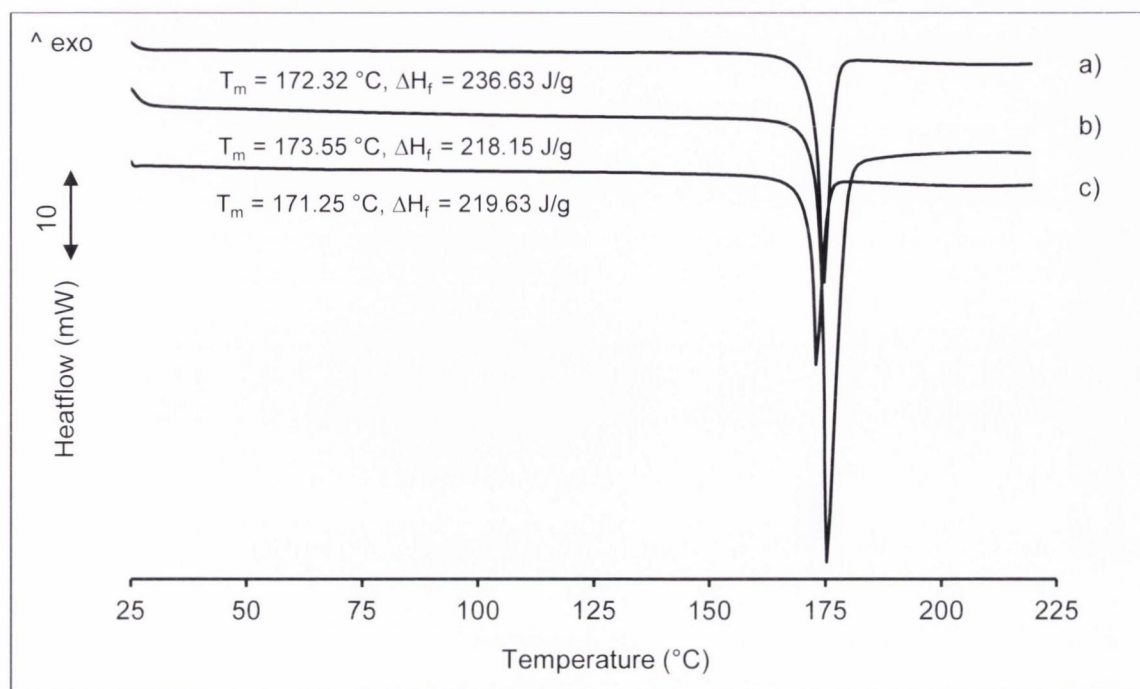
Figure A.2.17: DSC thermograms of the SD:4-ASA 1:1 form II cocrystal. a) crystallised from EtOH by solvent evaporation, b) crystallised from Me_2CO by solvent evaporation and c) spray-dried.

Table A.2.3: Data from structure determination of the SD:4-ASA 1:1 form II cocrystal calculated on basis of PXRD - final coordinates and equivalent isotropic displacement parameters of the non-hydrogen atoms.

Atom	x	y	z	U (eq) Å^2
S27	0.2693(18)	0.558(4)	0.055(4)	0.0127
O218	0.314(4)	0.648(9)	-0.004(8)	0.0127
O219	0.215(3)	0.638(8)	0.064(7)	0.0127
N28	0.287(5)	0.526(11)	0.193(9)	0.0127
N210	0.375(6)	0.402(13)	0.174(11)	0.0127
N214	0.348(4)	0.559(13)	0.348(10)	0.0127
N215	0.238(4)	-0.092(11)	-0.190(8)	0.0127
C21	0.225(6)	0.237(16)	0.032(11)	0.0127
C22	0.262(6)	0.359(14)	-0.014(13)	0.0127
C23	0.289(7)	0.327(16)	-0.120(10)	0.0127
C24	0.286(7)	0.170(17)	-0.173(12)	0.0127
C25	0.246(6)	0.049(16)	-0.132(10)	0.0127
C26	0.218(5)	0.084(15)	-0.025(9)	0.0127
C29	0.340(7)	0.494(16)	0.240(11)	0.0127
C211	0.426(7)	0.369(13)	0.225(12)	0.0127
C212	0.438(6)	0.428(16)	0.336(12)	0.0127
C213	0.399(8)	0.525(16)	0.397(9)	0.0127
C216	0.410(5)	0.598(13)	0.518(9)	0.0127
C217	0.466(6)	0.264(13)	0.154(11)	0.0127
O8	-0.002(4)	0.287(9)	0.312(8)	0.0109
O10	-0.010(4)	0.589(9)	0.287(7)	0.0109
O11	0.021(4)	0.801(9)	0.400(7)	0.0109
N7	0.092(4)	0.070(11)	0.656(7)	0.0109
C1	0.034(6)	0.496(19)	0.446(14)	0.0109
C2	0.025(5)	0.319(16)	0.410(11)	0.0109
C3	0.044(5)	0.185(15)	0.479(14)	0.0109
C4	0.073(5)	0.208(15)	0.587(13)	0.0109
C5	0.083(6)	0.378(16)	0.624(10)	0.0109
C6	0.064(5)	0.514(15)	0.555(12)	0.0109
C9	0.015(6)	0.63(2)	0.376(10)	0.0109

U(eq) = 1/3 of the trace of the orthogonalized U tensor

Table A.2.4: Data from structure determination of the SD:4-ASA 1:1 form II cocrystal calculated on basis of PXRD - hydrogen atom positions and isotropic displacement parameters.

Atom	x	y	z	U (eq) Å^2
*H11	0.0164	0.85703	0.33904	0.019
*H21	0.20497	0.26187	0.10319	0.05
*H212	0.47232	0.40311	0.37072	0.0152
*H21A	0.50013	0.2496	0.19911	0.019
*H21B	0.47447	0.32178	0.08111	0.019
*H21C	0.44992	0.15445	0.13781	0.019
*H21D	0.40788	0.72028	0.51445	0.019
*H21E	0.38291	0.55486	0.57298	0.019
*H21F	0.44711	0.56426	0.54263	0.019
*H21G	0.2553	-0.11057	-0.25558	0.0152
*H21H	0.2139	-0.16578	-0.1641	0.0152
*H23	0.31007	0.41383	-0.15609	0.0152
*H24	0.30499	0.14768	-0.24051	0.05
*H26	0.19414	0.002	0.00663	0.0152
*H28	0.25948	0.529	0.2433	0.0152
*H3	0.03525	0.06975	0.44791	0.05
*H5	0.10382	0.39669	0.69802	0.05
*H6	0.07195	0.62581	0.57958	0.05
*H7A	0.11493	0.00931	0.61461	0.0152
*H7B	0.10886	0.10822	0.71793	0.0152
*H8	-0.00932	0.37677	0.27791	0.0164

The temperature factor has the form of Exp(-T) where $T = 8*(Pi^2)*U*(Sin(Theta)/Lambda)^2$ for isotropic atoms.

Table A.2.5: Data from structure determination of the SD:4-ASA 1:1 form II cocrystal calculated on basis of PXRD - bond distances (Angstrom).

Atom	Atom	Distance (Å)	Atom	Atom	Distance (Å)
C21	C26	1.37(17)	C216	H21D	0.96
C21	C22	1.40(18)	C216	H21E	0.96
C22	C23	1.38(19)	C217	H21A	0.96
C23	C24	1.37(18)	C217	H21B	0.96
C24	C25	1.4(2)	C217	H21C	0.96
N210	C211	1.4(2)	C211	C217	1.49(19)
N210	C29	1.33(19)	C211	C212	1.36(19)
N214	C213	1.4(2)	C212	C213	1.4(2)
N214	C29	1.33(17)	C213	C216	1.50(15)
N215	C25	1.30(15)	C3	H3	0.99
N215	H21H	0.86	C212	H212	0.93
N215	H21G	0.86	C216	H21F	0.96
N28	C29	1.4(2)	C3	C4	1.4(2)
N28	H28	0.87	C4	C5	1.41(17)
N7	C4	1.40(15)	C5	C6	1.39(17)
N7	H7B	0.86	C5	H5	0.98
N7	H7A	0.86	C6	H6	0.94
O10	C9	1.21(15)	C1	C9	1.4(2)
O11	C9	1.37(17)	C1	C2	1.5(2)
O11	H11	0.82	C2	C3	1.38(18)
O8	C2	1.30(15)	C26	H26	0.93
O8	H8	0.82	C1	C6	1.4(2)
S27	O218	1.44(10)	C25	C26	1.40(16)
S27	O219	1.44(8)	C21	H21	0.95
S27	N28	1.63(11)	C23	H23	0.94
S27	C22	1.75(12)	C24	H24	0.9

Table A.2.6: Data from structure determination of the SD:4-ASA 1:1 form II cocrystal calculated on basis of PXRD - bond angles (degrees).

Atom	Atom	Atom	Angle (°)	Atom	Atom	Atom	Angle (°)
C1	C6	H6	117	C211	C217	H21B	110
C2	O8	H8	110	C24	C23	H23	119
C2	C3	H3	115	H21D	C216	H21F	109
C21	C22	C23	119(12)	C4	C5	C6	120(12)
C211	C212	C213	120(14)	C213	C216	H21D	109
C212	C211	C217	123(14)	C213	C216	H21F	109
C212	C213	C216	123(14)	C213	C216	H21E	110
C213	C212	H212	120	C211	C217	H21A	109
C22	C21	C26	120(12)	N7	C4	C3	123(11)
C22	C23	C24	121(13)	C1	C6	C5	125(12)
C23	C24	C25	119(13)	O10	C9	C1	116(13)
C24	C25	C26	118(11)	O10	C9	O11	118(12)
C25	N215	H21G	121	C1	C2	C3	121(12)
C25	N215	H21H	120	C2	C3	C4	123(11)
C29	N28	H28	116	C21	C26	H26	120
C29	N210	C211	115(12)	C25	C26	H26	119
C29	N214	C213	115(11)	C2	C1	C6	114(12)
C4	N7	H7B	109	C6	C1	C9	125(13)
C4	N7	H7A	109	O8	C2	C3	120(11)
C4	C3	H3	122	C211	C217	H21C	110
C4	C5	H5	118	H21A	C217	H21B	109
C5	C6	H6	119	H21A	C217	H21C	109
C6	C5	H5	122	H21B	C217	H21C	110
C9	O11	H11	110	C22	C23	H23	120
H21G	N215	H21H	120	O8	C2	C1	119(11)
H7A	N7	H7B	110	C2	C1	C9	121(13)
N210	C211	C217	117(12)	C211	C212	H212	120
N214	C213	C216	117(12)	H21E	C216	H21F	110
N214	C213	C212	120(11)	H21D	C216	H21E	110
N215	C25	C26	122(12)	O11	C9	C1	126(11)
N215	C25	C24	120(11)	N210	C211	C212	121(13)
N28	S27	C22	108(6)	C26	C21	H21	121
O218	S27	O219	119(5)	C21	C26	C25	121(11)
O218	S27	N28	109(6)	N210	C29	N214	129(14)
O218	S27	C22	108(6)	N28	C29	N214	114(12)
O219	S27	N28	103(6)	N28	C29	N210	117(12)
O219	S27	C22	109(6)	C22	C21	H21	119
S27	N28	C29	129(9)	C25	C24	H24	119
S27	N28	H28	115	C23	C24	H24	121
S27	C22	C21	120(11)	C3	C4	C5	117(11)
S27	C22	C23	120(10)	N7	C4	C5	120(11)

Table A.2.7: Data from structure determination of the SD:4-ASA 1:1 form II cocrystal calculated on basis of PXRD - torsion angles (degrees).

Atom	Atom	Atom	Atom	Angle (°)
C2	C1	C9	O10	2(19)
C2	C1	C9	O11	-180(13)
C2	C3	C4	C5	-1(19)
C2	C3	C4	N7	180(12)
C211	N210	C29	N28	-178(10)
C211	C212	C213	C216	-178(12)
C211	C212	C213	N214	2(19)
C213	N214	C29	N28	178(11)
C217	C211	C212	C213	180(12)
C22	S27	N28	C29	83(11)
C23	C24	C25	N215	172(13)
C24	C25	C26	C21	6(19)
C26	C21	C22	S27	178(10)
C29	N210	C211	C212	0(18)
C29	N210	C211	C217	179(11)
C29	N214	C213	C212	-1(17)
C29	N214	C213	C216	179(11)
C3	C4	C5	C6	1(18)
C6	C1	C2	O8	180(11)
C6	C1	C2	C3	1(19)
C6	C1	C9	O10	-180(13)
C9	C1	C2	C3	180(13)
C9	C1	C6	C5	-180(14)
C9	C1	C2	O8	-1(19)
N210	C211	C212	C213	-1(19)
N215	C25	C26	C21	-177(12)
N28	S27	C22	C21	56(13)
N28	S27	C22	C23	-129(12)
N7	C4	C5	C6	-180(12)
O218	S27	N28	C29	-34(11)
O218	S27	C22	C21	174(11)
O218	S27	C22	C23	-12(14)
O219	S27	N28	C29	-162(10)
O219	S27	C22	C21	-56(13)
O219	S27	C22	C23	119(12)
O8	C2	C3	C4	-179(12)
S27	N28	C29	N210	-35(16)
S27	N28	C29	N214	147(10)
S27	C22	C23	C24	177(12)

Appendix 3

Table A.3.1: Spray drying conditions (Concentration of feed solution: Conc. % (w/v), inlet temperature:IT, outlet temperature :OT).

Sample	Solvent	Conc. % (w/v)	IT (°C)	OT (°C)
SD:BA 1:1	EtOH	1	78	55
	MeOH	1	70	49
	Me$_2$CO	2	70	54
	MeCN	0.5	82	60
SD:SA 1:1	EtOH	2	78	53
	MeOH	2	70	47
	Me$_2$CO	2	70	52
	MeCN	1	82	57
SD:4-ASA 1:1	EtOH	1	78	57
	Me$_2$CO	2	70	53
SD:NA 1:1	EtOH	1	78	55
	MeOH	2	70	43
SD:PCA 1:1	EtOH	1	78	55
	MeOH	2	70	49
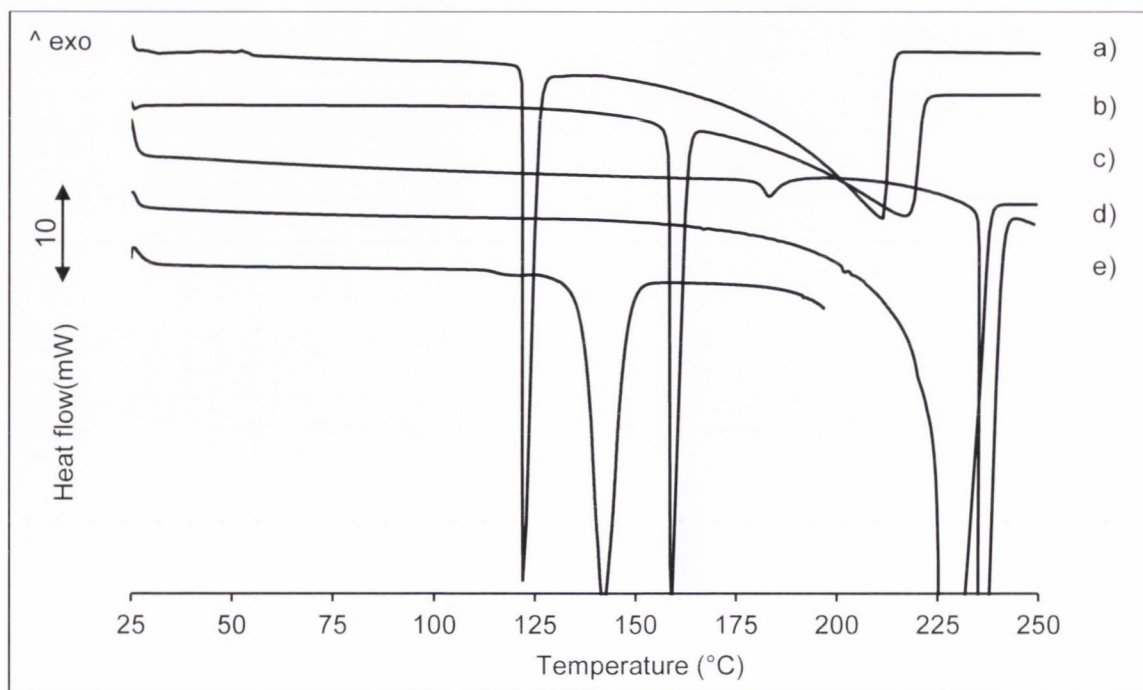
Figure A.3.1: DSC thermograms of a) BA, b) SA, c) NA, d) PCA and e) PA.
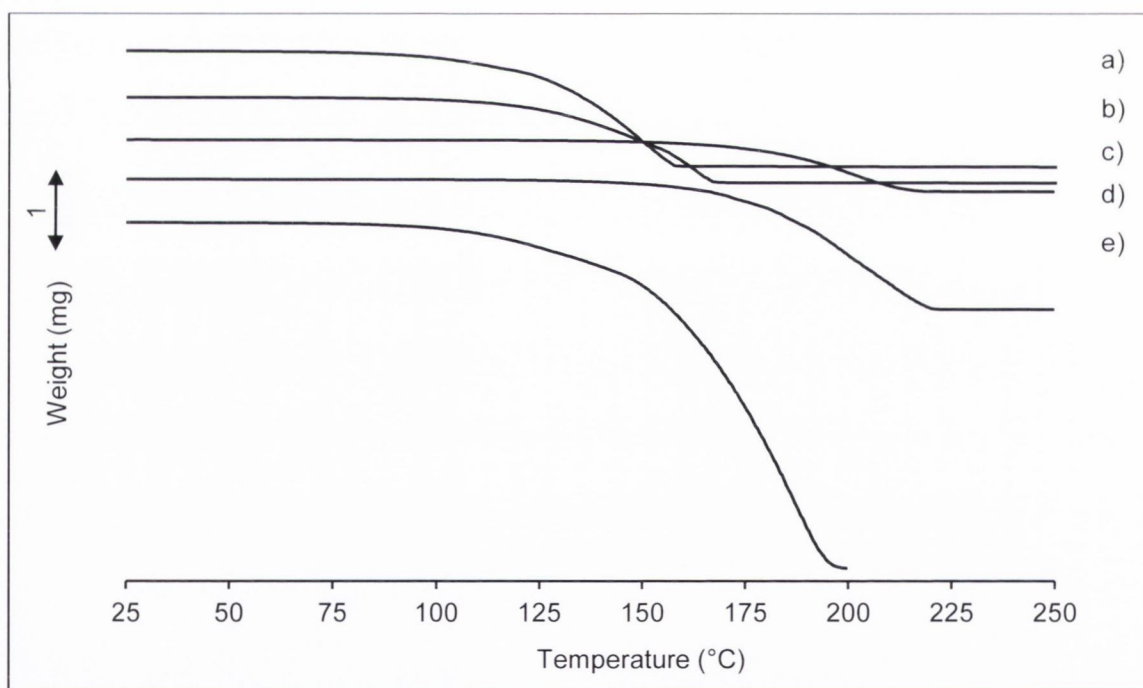
Figure A.3.2: TGA thermograms of a) BA, b) SA, c) NA, d) PCA and e) PA.

Table A.3.2: Determined exothermic (T_{exo}) and endothermic melting (T_m) temperatures and the corresponding enthalpies shown in brackets of SD:aromatic carboxylic acids produced by spray drying (SPD), liquid-assisted milling (LAM), solvent evaporation (SEV) and cooling crystallisation (CCR) using different solvents. Presented values refer to an average of 2 results, if not otherwise specified.

Product	Molar ratio	Method	Solvent	Exotherm	Endotherm 1	Endotherm 2
SD:BA	1:1	SPD	EtOH	–	186.38 ± 4.64 (99.45 ± 10.44)*	189.66 ± 1.25 (170.97 ± 5.98)
	1:1		MeOH	–	185.9 ± 1.30 (7.50 ± 1.59)	208.59 ± 4.82(174.17 ± 17.35)
	1:1		MeCN	–	184.56 ± 1.89 (181.51 ± 10.91)*	188.51 ± 0.46 (113.86 ± 11.93)
	1:1		Me$_2$CO	–	184.1 ± 5.64 (109.53 ± 11.50)*	166.04 ± 0.68 (173.34 ± 22.64)
	1:1.3		Me$_2$CO	–	218.39 ± 2.23 (157.20 ± 0.98)	–
SD:BA	1:1	LAM	EtOH	–	212.02 ± 5.48 (206.56 ± 4.85)	–
	1:1		MeOH	–	216.94 ± 1.23 (205.06 ± 4.81) (n=3)	–
	1:1		MeCN	–	212.56 ± 0.14 (301.68 ± 18.80)	–
	1:1		Me$_2$CO	–	208.00 ± 0.36 (284.00 ± 20.53)	–
SD:BA	1:1	SEV	EtOH	–	118.55 (12.92) ± n.a	212.69 (225.56) ± n.a.
	1:1		MeOH	–	120.76 ± 1.26 (6.18 ± 0.75)	213.32 ± 10.55 (209.65 ± 18.05)
	1:1		MeCN	–	189.76 (23.24) ± n.a	204.99 (276.13) ± n.a.
	1:1		Me$_2$CO	–	186.79 ± 0.13 (7.04 ± 1.01)	210.23 ± 11.85 (157.24 ± 14.62)
SD:BA	1:1	CCR	EtOH	–	190.46 ± 1.35(42.05 ± 6.45)*	207.04 ± 13.88 (112.28 ± 12.65)
	1:1		MeOH	–	191.91 ± 0.13 (57.99 ± 5.21)*	208.15 ± 5.21 (79.15 ± 10.85)
	1:1		MeCN	–	191.58 ± 0.79 (0.9 ± 0.01)	219.13 ± 1.43 (182.25 ± 3.46)
	1:1		Me$_2$CO	–	190.08 ± 1.52 (0.40 ± 0.03)	219.48 ± 1.55 (170.60 ± 12.30)
SD:SA	1:1	SPD	EtOH	–	179.62 ± 0.03 (4.02 ± 0.11)*	193.92 ± 5.72 (119.40 ± 1.69)
	1:1		MeOH	–	183.24 (19.02) ± n.a *	191.82 (97.19) ± n.a
	1:1		MeCN	–	181.50 ± 0.19 (47.97 ± 4.15)*	187.47 ± 0.04 (121.62 ± 5.69)
	1:1.2		MeCN	–	197.01 ± 1.87 (139.78 ±7.47)	–
	1:1		Me$_2$CO	–	181.40 ± 0.48 (12.84 ± 1.39)*	196.69 ± 0.29 (105.30 ± 5.79)
SD:SA	1:1	LAM	EtOH	–	196.84 ± 1.81 (137.45 ± 5.16)	–
	1:1		MeOH	–	196.23 (144.21) ± n.a	–
	1:1		MeCN	–	196.92 ± 1.85 (144.68 ± 9.58) (n=3)	–
	1:1		Me$_2$CO	–	196.64 ± 1.97 (142.12 ± 2.72)	–

Table A.3.2: continued

Product	Molar ratio	Method	Solvent	Exotherm	Endotherm 1	Endotherm 2
SD:SA	1:1	SEV	EtOH	–	149.35 ± 3.27 (8.67 ± 1.75)	195.3 ± 4.00 (127.20 ± 12.45)
	1:1		MeOH	–	153.00 ± 1.42 (58.13 ± 5.96)	185.77 ± 6.97 ± 104.41 ± 10.79)
	1:1		MeCN	–	149.30 ± 3.74 (12.10 ± 5.36)	193.12 ± 1.56 (112.22 ± 11.20)
	1:1		Me₂CO	–	141.66 ± 7.46 (6.61 ± 1.64)	195.47 ± 0.16 (128.28 ± 7.04)
SD:SA	1:1	CCR	EtOH	–	185.51 ± 4.65 (40.02 ± 5.13)*	190.62 ± 1.03 (125.31 ± 4.11)
	1:1		MeOH	–	184.00 ± 0.27 (42.95 ± 6.15)*	194.14 ± 3.06 (130.89 ± 14.28)
	1:1		MeCN	–	184.62 ± 0.38 (1.30 ± 0.14)	198.61 ± 0.27 (142.61 ± 8.07)
	1:1		Me₂CO	–	183.95 ± 0.52 (0.99 ± 0.01)	198.62 ± 1.01 (146.48 ± 4.49)
SD:4-ASA	1:1	SPD	EtOH	–	170.22 ± 1.011 (200.06 ± 0.78)	–
	1:1		Me₂CO	–	167.34 ± 3.13 (201.31 ± 7.79)	–
SD:4-ASA	1:1	LAM	EtOH	–	169.99 ± 0.84 (225.19 ± 20.90)	–
	1:1		Me₂CO	–	166.74 ± 1.01 (207.36 ± 2.91)	–
SD:4-ASA	1:1	SEV	EtOH	–	145.95 (214.14) ± n.a	–
	1:1		Me₂CO	–	157.94 (226.55) ± n.a	–
SD:4-ASA	1:1	CCR	EtOH	–	171.29 ± 1.88 (170.30 ± 8.97)	–
	1:1		Me₂CO	–	159.96 ± 0.69 (235.06 ± 17.62)	–
SD:NA	1:1	SPD	EtOH	–	204.29 ± 1.91 (150.94 ± 18.49)	–
	1:1		MeOH	–	204.70 ± 1.17 (150.99 ± 0.76)	–
SD:NA	1:1	LAM	EtOH	–	204.72 ± 1.58 (156.01 ± 5.45)	–
	1:1		MeOH	–	205.18 ± 0.71 (167.54 ± 6.13) (n=3)	–
SD:NA	1:1	SEV	EtOH	–	206.77 ± 0.88 (166.71 ± 5.52)	–
	1:1		MeOH	–	205.42 ± 1.38 (161.53 ± 7.33) (n=3)	–
SD:NA	1:1	CCR	EtOH	–	189.24 ± 1.27 (3.23 ± 0.12)	205.56 ± 2.00 (147.72 ± 5.62)
			MeOH	–	190.26 ± 0.26 (2.75 ± 0.21)	206.55 ± 0.56 (161.77 ± 3.63)

Table A.3.2: continued

Product	Molar ratio	Method	Solvent	Exotherm	Endotherm 1	Endotherm 2
SD:PCA	1:1	SPD	EtOH	87.51 ± 2.63 (16.47 ± 12.89**)	173.27 ± 0.69 (150.73 ± 1.64)	–
	1:1		MeOH	–	173.25 (148.21) ± n.a.	–
SD:PCA	1:1	LAM	EtOH	–	172.90 ± 1.54 (161.00 ± 1.83)	–
	1:1		MeOH	–	173.68 (159.92) ± n.a.	–
SD:PCA	1:1	SEV	EtOH	–	175.04 ± 0.44 (91.26 ± 5.35)	–
	1:1		MeOH	–	174.01 ± 1.13 (148.28 ± 1.85)	–
SD:PCA	1:1	CCR	EtOH	–	174.78 ± 1.86 (143.50 ± 4.80)	–
	1:1		MeOH	–	175.93 ± 1.46 (152.63 ± 7.40)	–
SD:PCA	1:1	PM	–	–	175.31 ± 0.99 (158.87 ± 18.77)	–
SD:PA	1:1	LAM	EtOH	–	121.19 ± 1.18 (65.38 ± 0.91)	–
	1:1		MeOH	–	122.22 ± 0.07 (71.21 ± 3.01)	–
	1:1		MeCN	–	122.56 ± 0.01 (64.78 ± 5.74)	–
	1:1		Me$_2$CO	–	121.92 ± 0.08 (69.23 ± 0.36)	–
SD:PA	1:1	PM	–	–	125.15 ± 1.96 (93.76 ± 4.91)	–

n.a.: not available

* endotherm 1 and endotherm 2 are merged

** error high, attributed to storage time of 2 months between 1st and 2nd analysis
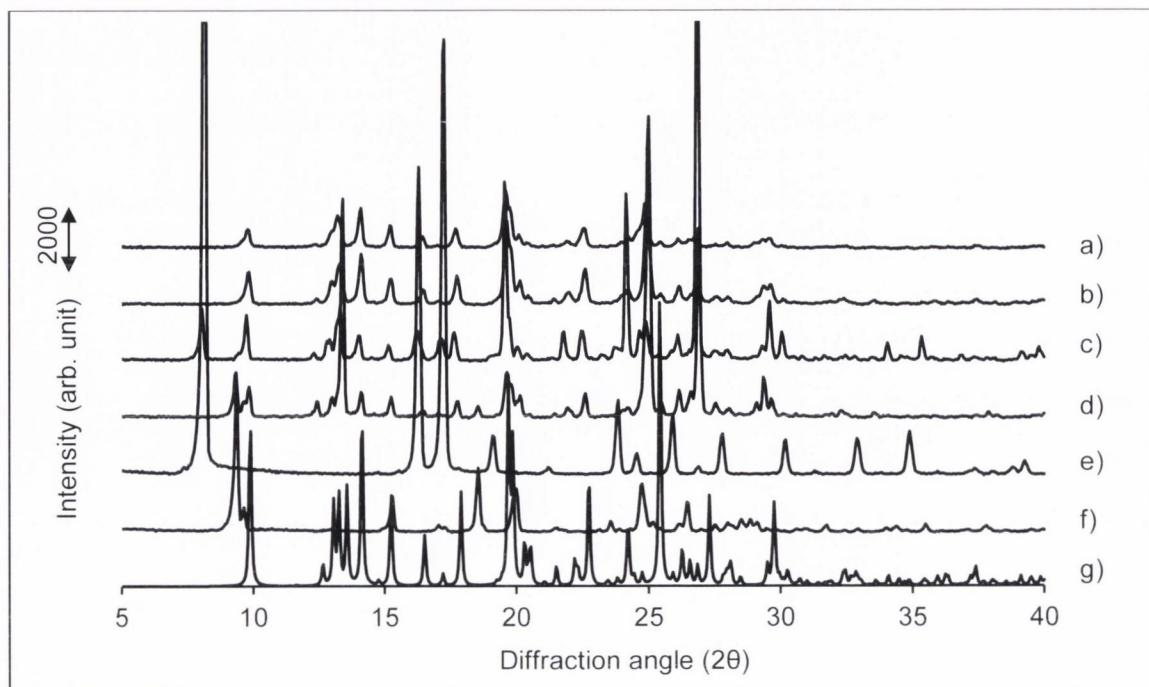
Figure A.3.3: PXRD patterns of SD:BA 1:1 products obtained by a) SPD, b) LAM , c) SEV and d) CCR using EtOH as solvent compared to e) BA, f) SD and g) the theoretical PXRD pattern of SD:BA 1:1 cocrystal obtained from solution, calculated on the basis of single crystal data (Arman et al., 2010).
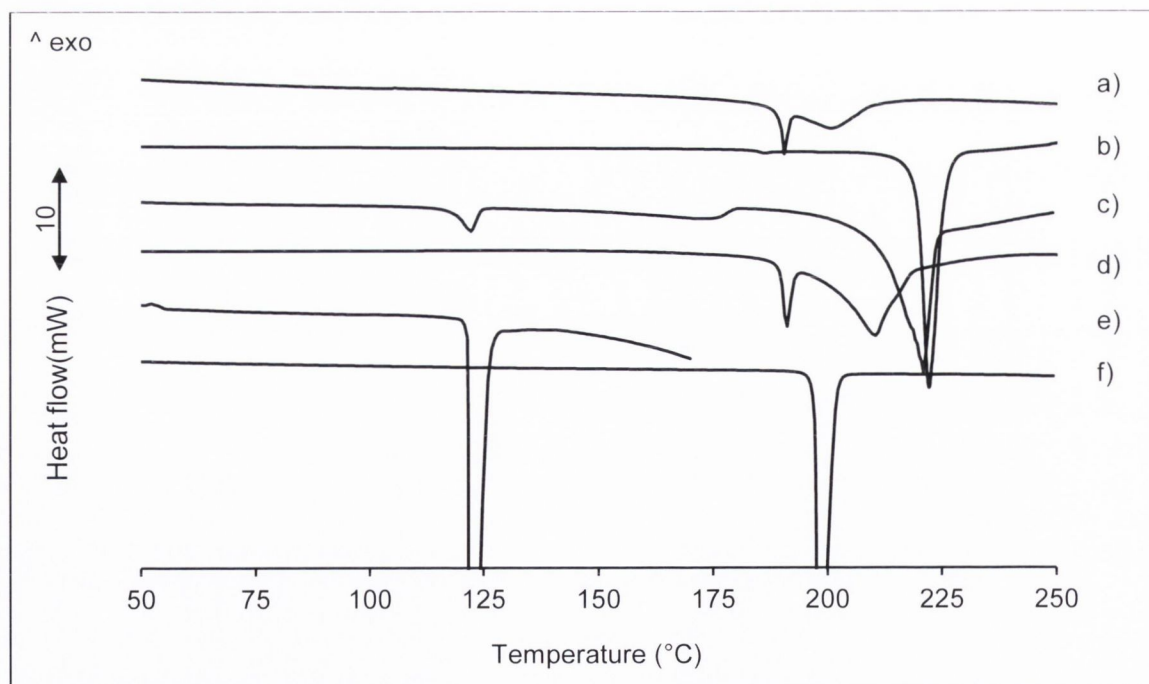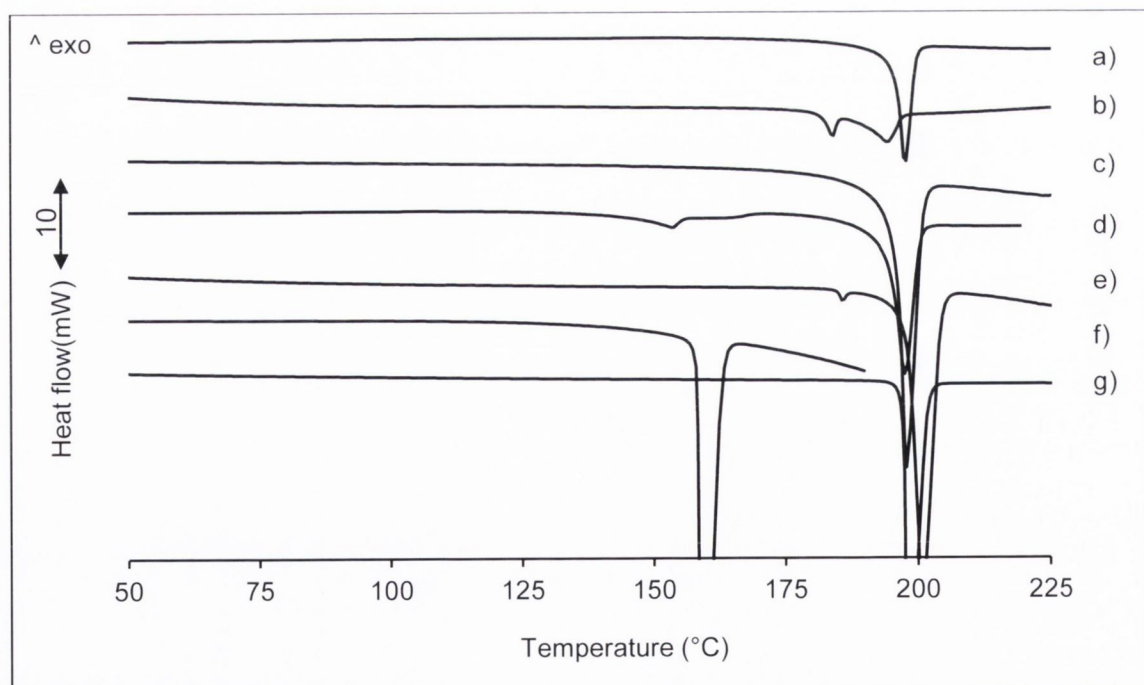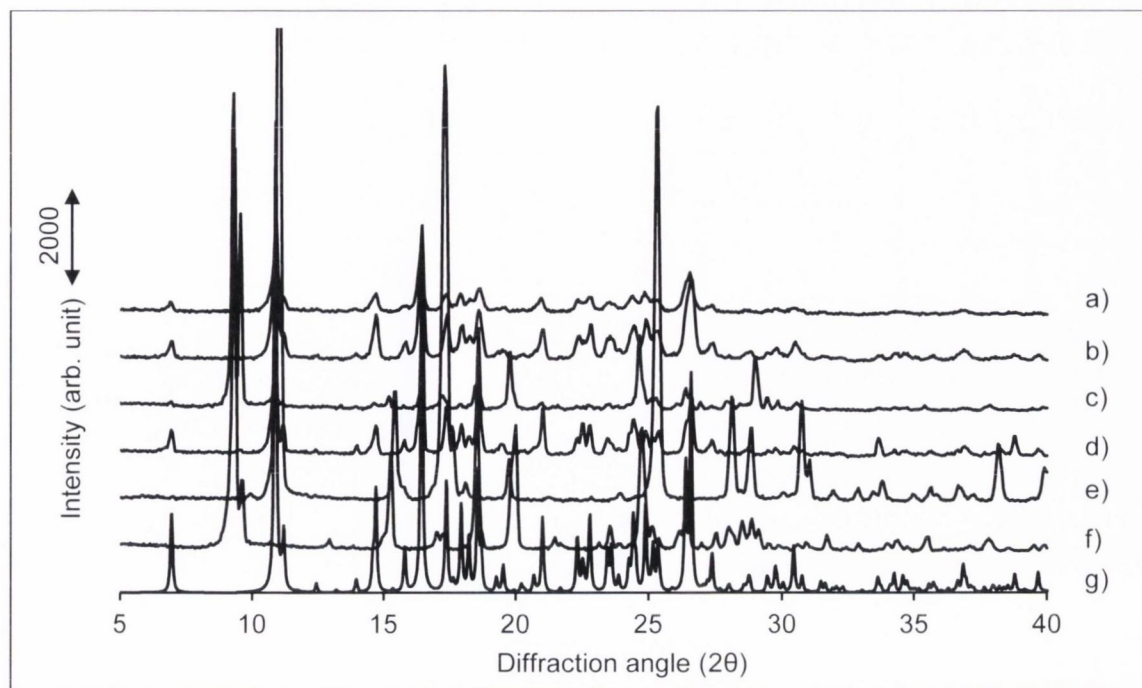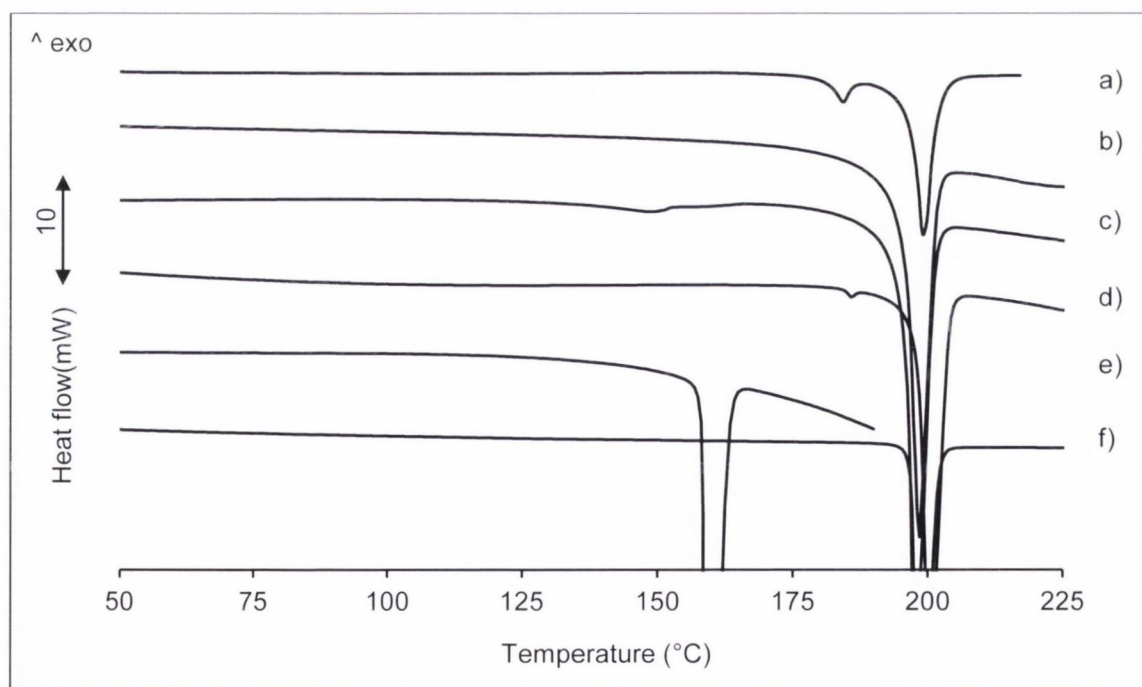

Figure A.3.4: DSC thermograms of SD:BA 1:1 products obtained by a) SPD, b) LAM , c) SEV and d) CCR using EtOH as solvent compared to e) BA and f) SD.
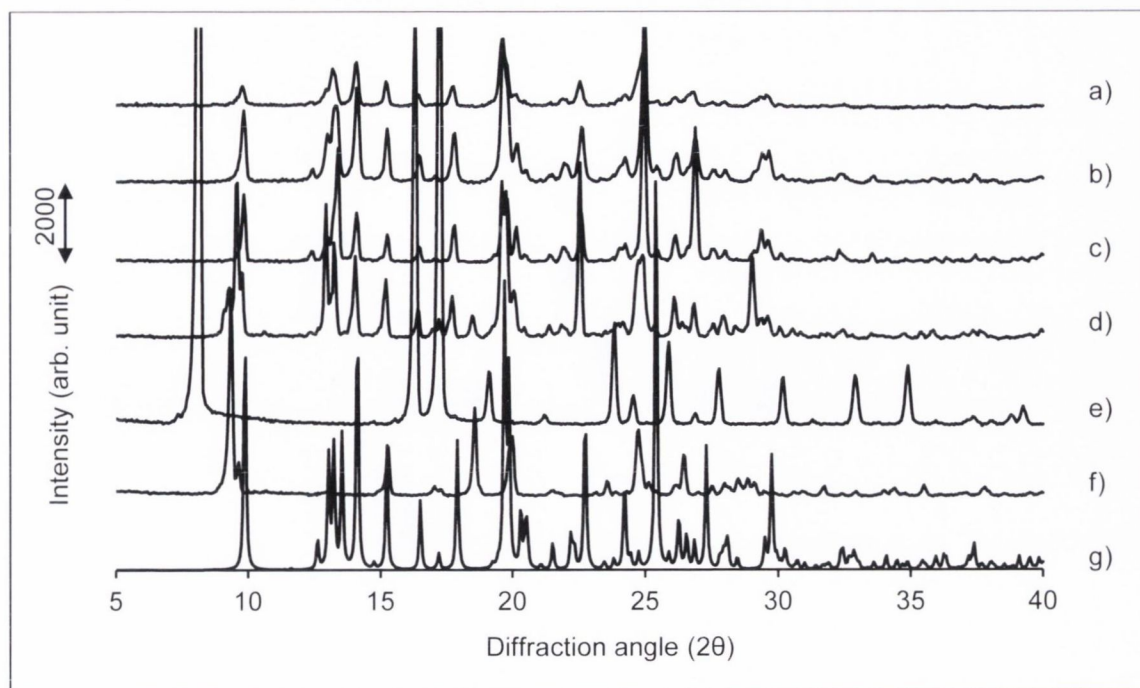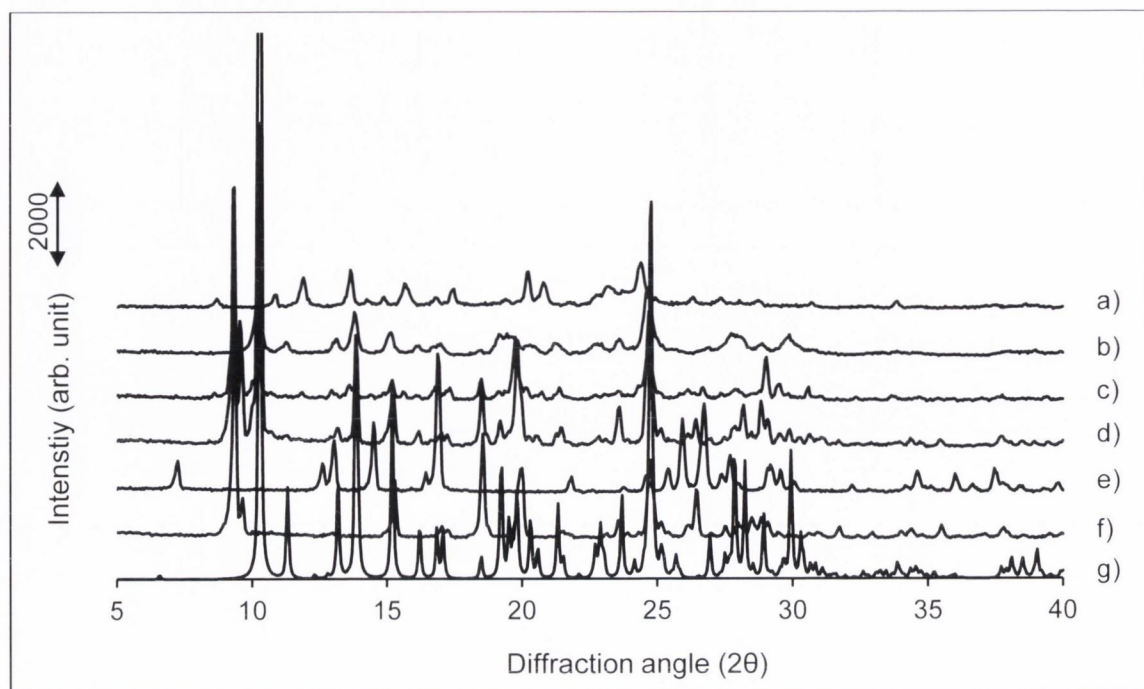
Figure A.3.5: PXRD patterns of SD:BA 1:1 products obtained by a) SPD, b) LAM , c) SEV and d) CCR using MeOH as solvent compared to e) BA, f) SD and g) the theoretical PXRD pattern of SD:BA 1:1 cocrystal obtained from solution, calculated on the basis of single crystal data (Arman et al., 2010).
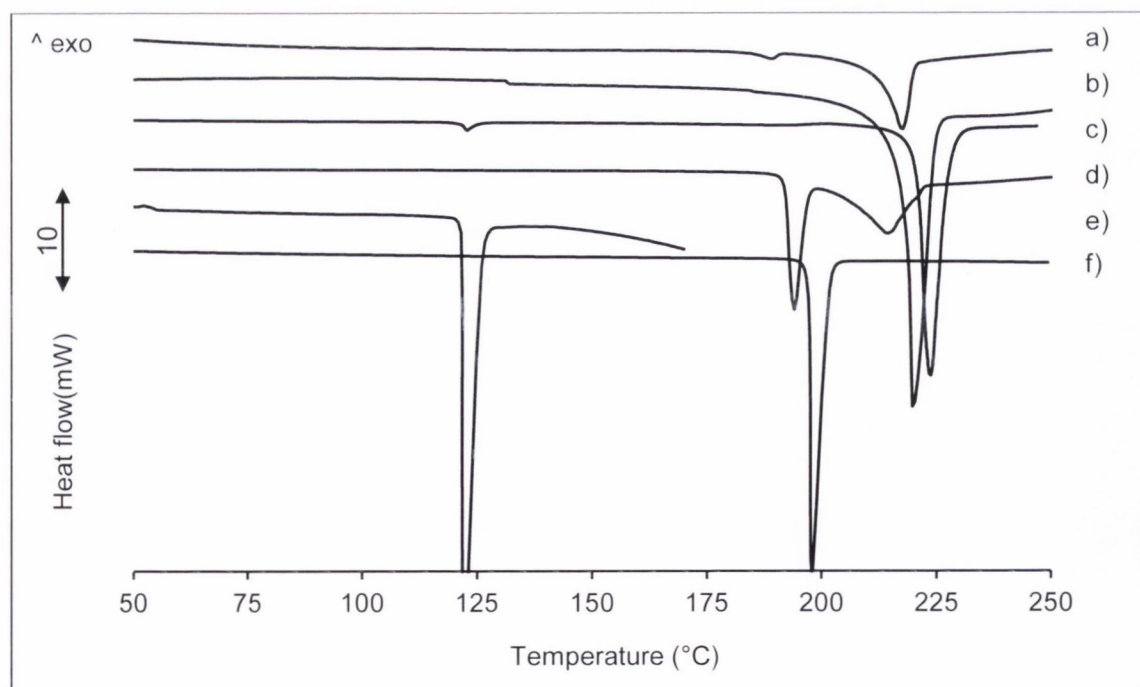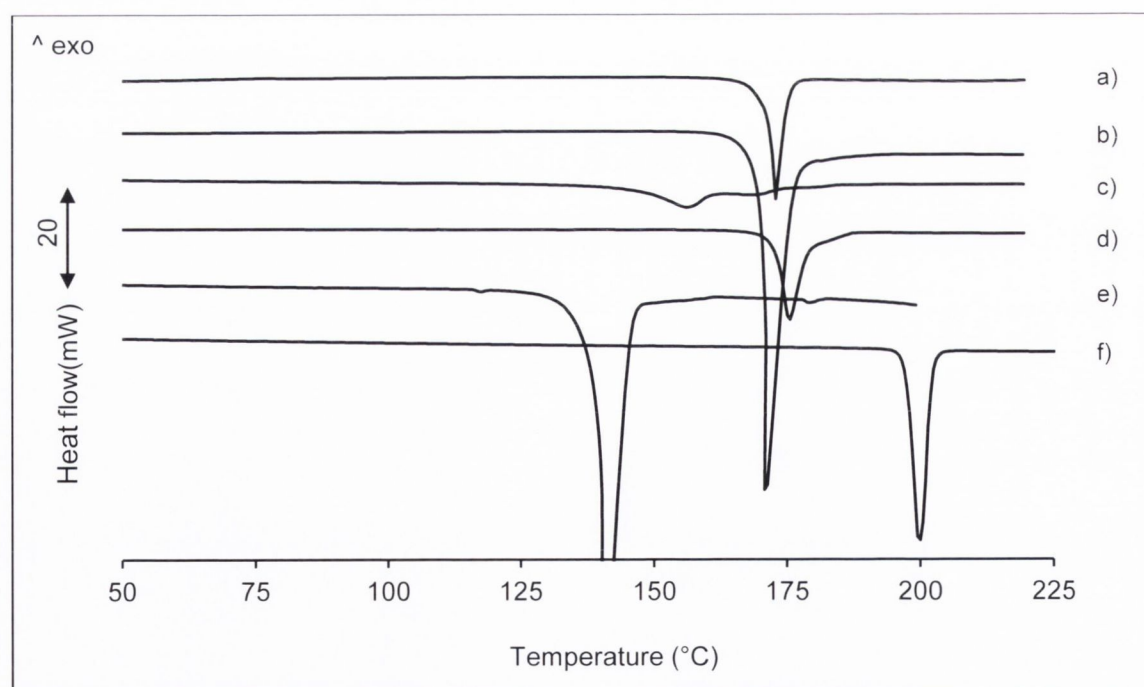

Figure A.3.6: DSC thermograms of SD:BA 1:1 products obtained by a) SPD, b) LAM , c) SEV and d) CCR using MeOH as solvent compared to e) BA and f) SD.
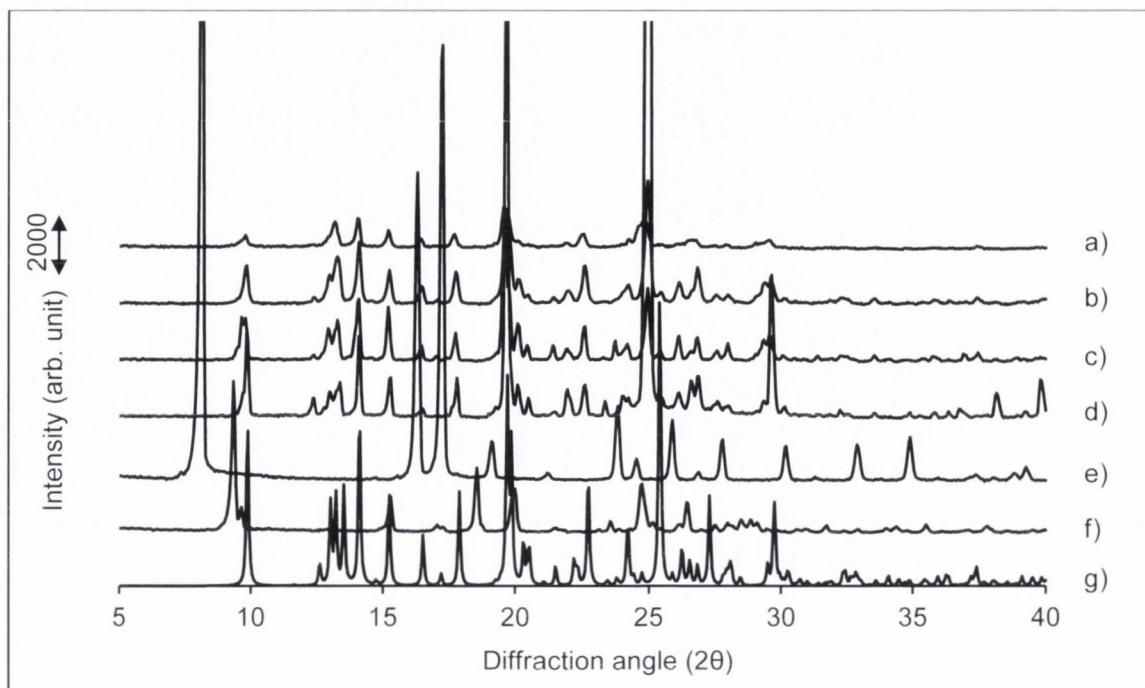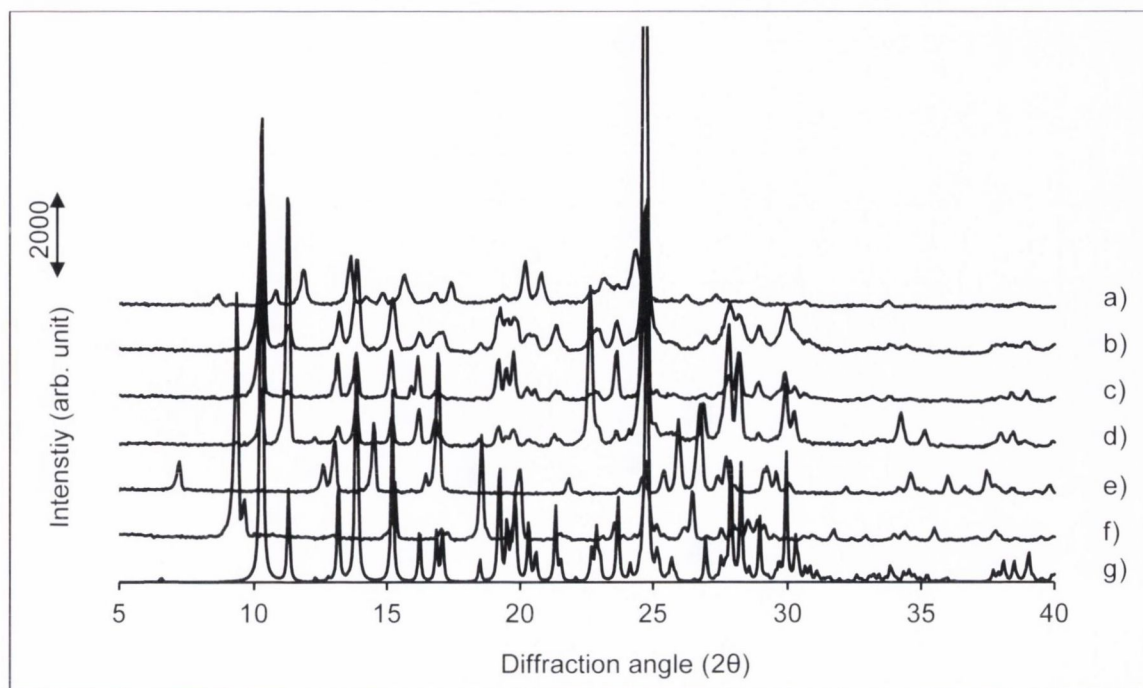
Figure A.3.7: PXRD patterns of SD:BA 1:1 products obtained by a) SPD, b) LAM , c) SEV and d) CCR using MeCN as solvent compared to e) BA, f) SD and g) the theoretical PXRD pattern of SD:BA 1:1 cocrystal obtained from solution, calculated on the basis of single crystal data (Arman et al., 2010).
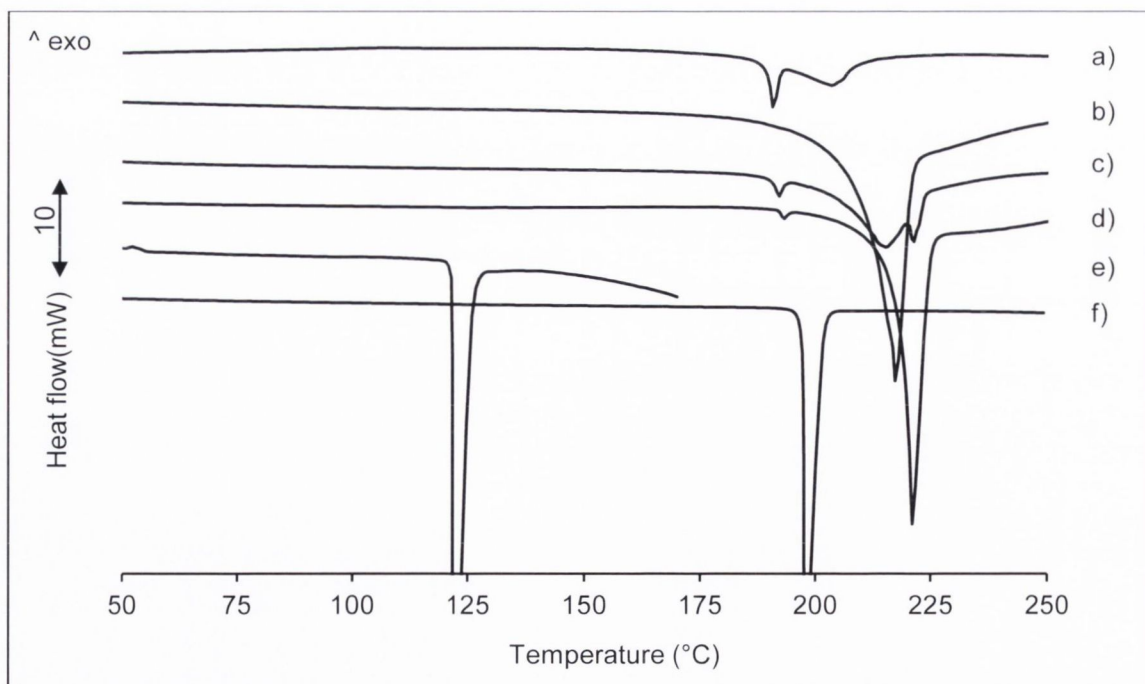
Figure A.3.8: DSC thermograms of SD:BA 1:1 products obtained by a) SPD, b) LAM , c) SEV and d) CCR using MeCN as solvent compared to e) BA and f) SD.
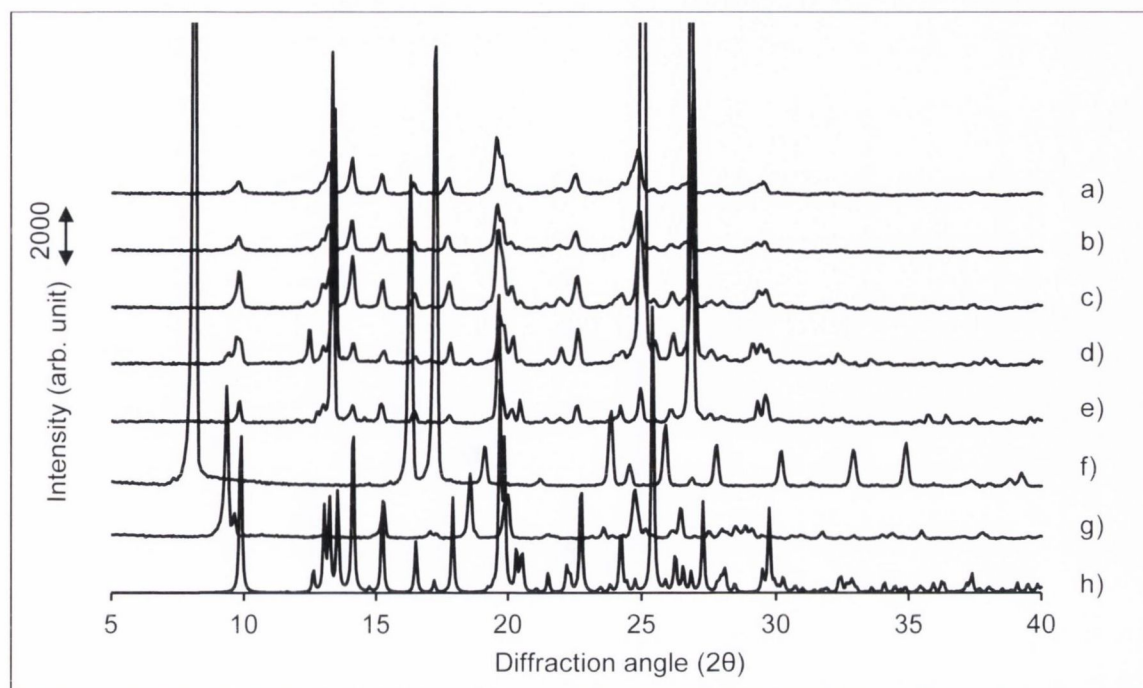
Figure A.3.9: PXRD patterns of a) SD:BA 1:1.3 SPD product and SD:BA 1:1 products obtained by b) SPD, c) LAM , d) SEV and e) CCR using Me$_2$CO as solvent compared to f) BA, g) SD and h) the theoretical PXRD pattern of SD:BA 1:1 cocrystal obtained from solution, calculated on the basis of single crystal data (Arman et al., 2010).
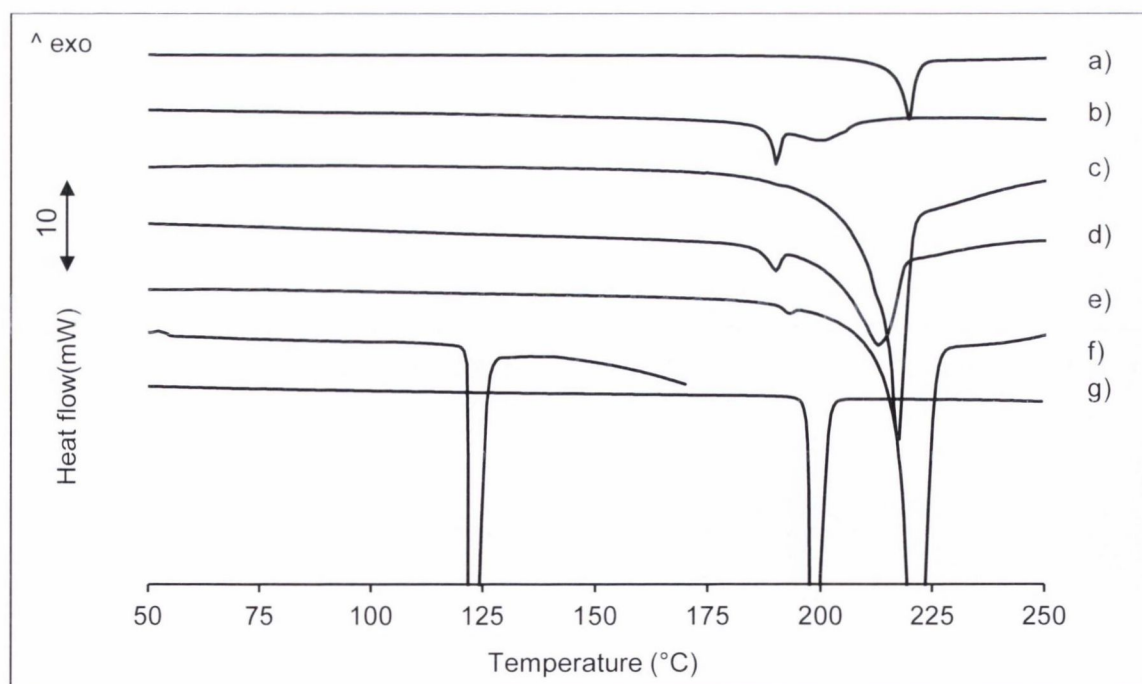

Figure A.3.10: DSC thermograms of a) SD:BA 1:1.3 SPD and SD:BA 1:1 obtained by b) SPD, c) LAM , d) SEV and e) CCR using Me$_2$CO as solvent compared to f) BA and g) SD.
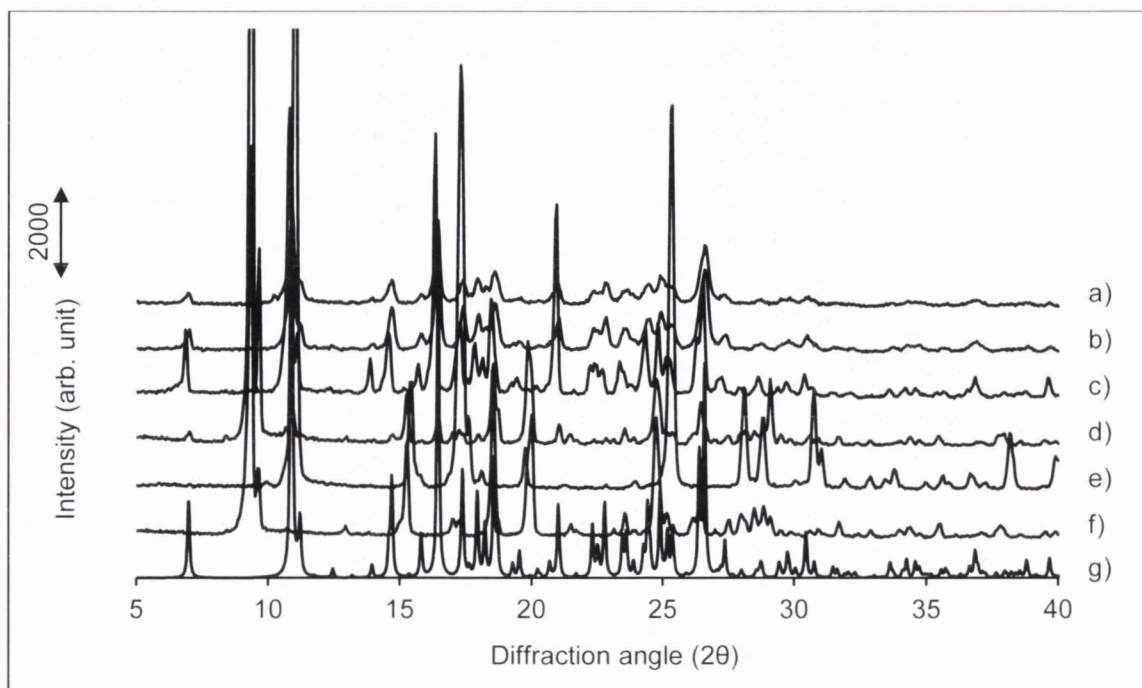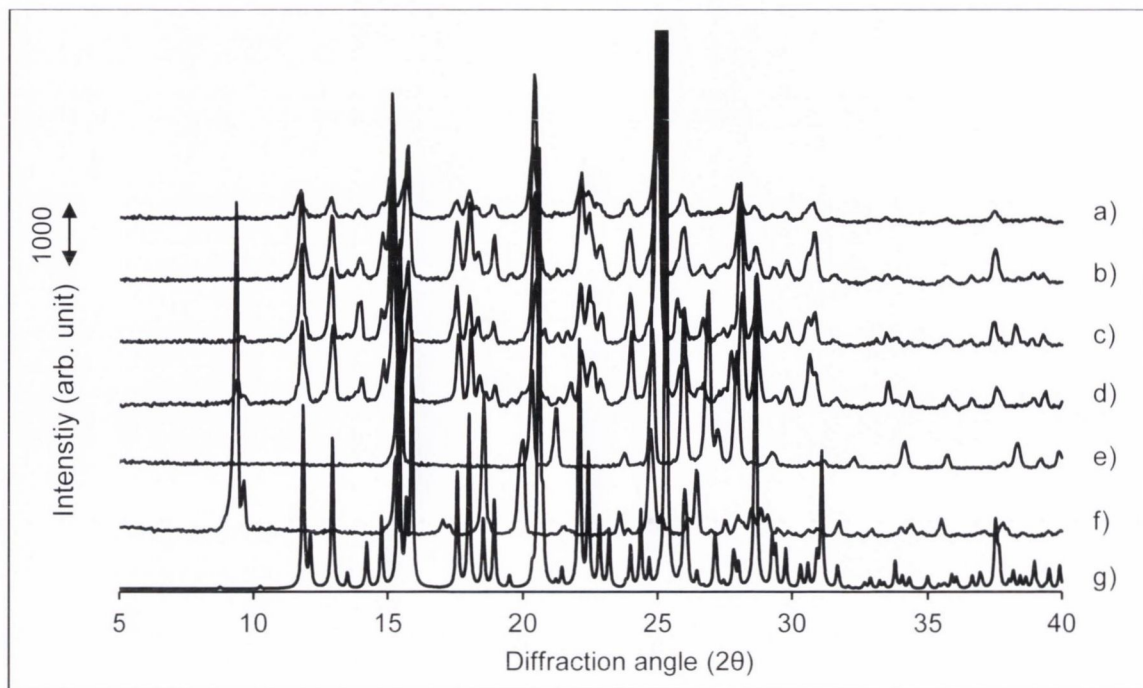
Figure A.3.11: PXRD patterns of SD:SA 1:1 products obtained by a) SPD, b) LAM , c) SEV and d) CCR using EtOH as solvent compared to e) SA, f) SD and g) the theoretical PXRD pattern of SD:SA 1:1 cocrystal obtained from solution, calculated on the basis of single crystal data (Patel et al., 1988).
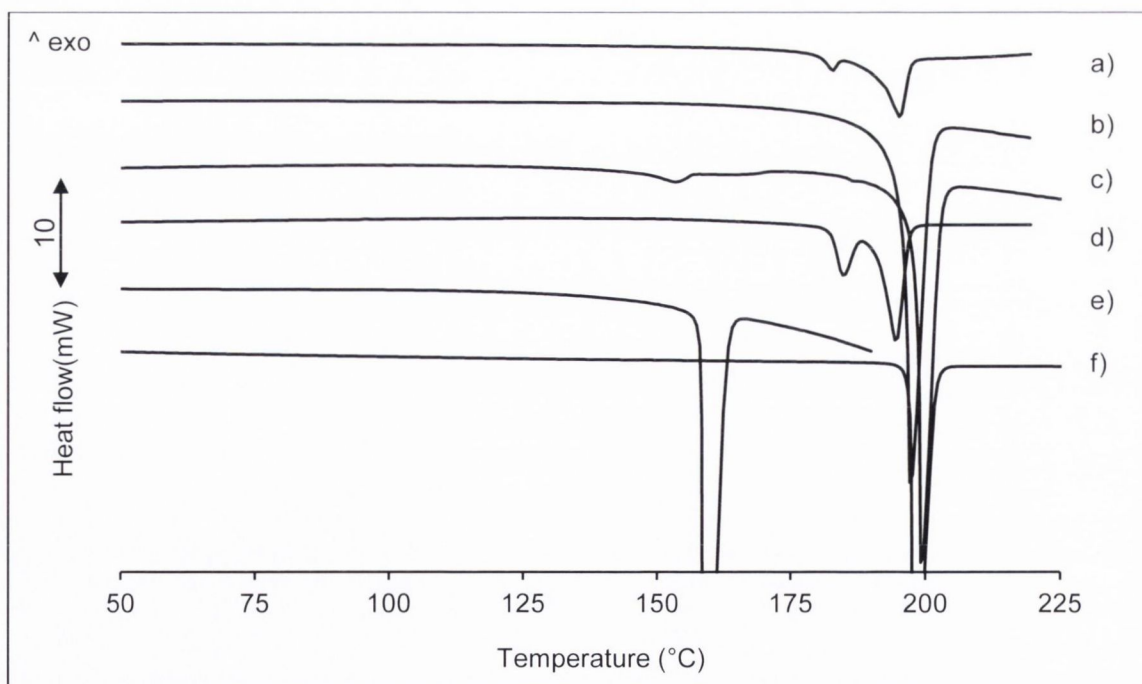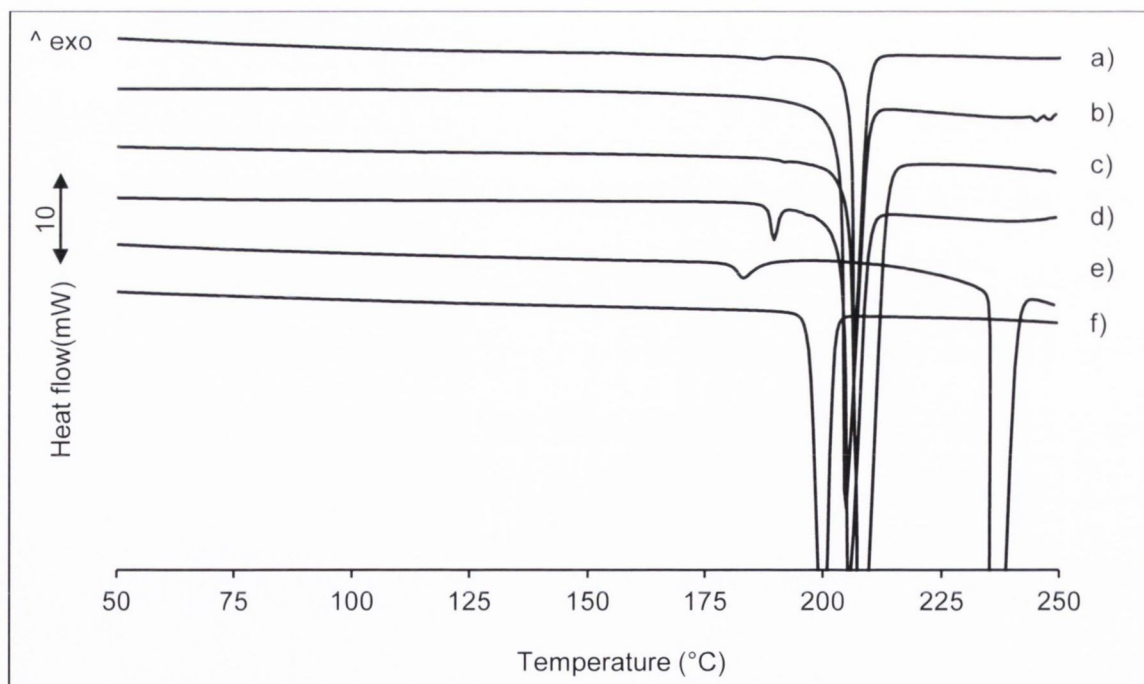

Figure A.3.12: DSC thermograms of SD:SA 1:1 products obtained by a) SPD, b) LAM , c) SEV and d) CCR using EtOH as solvent compared to e) SA and f) SD.
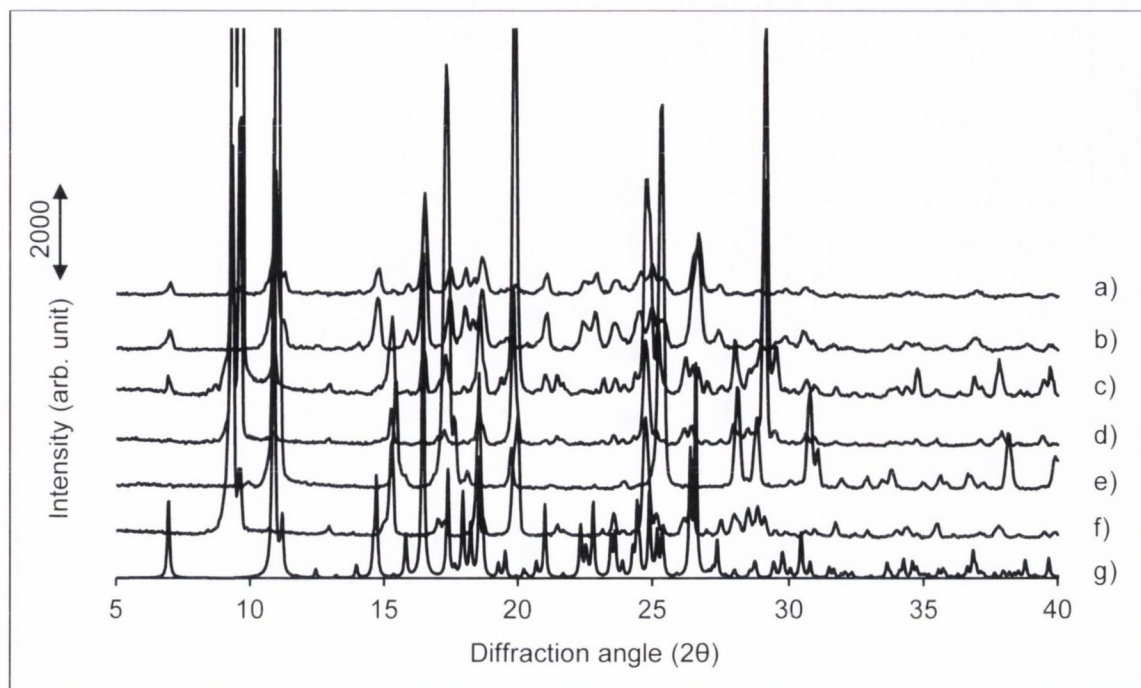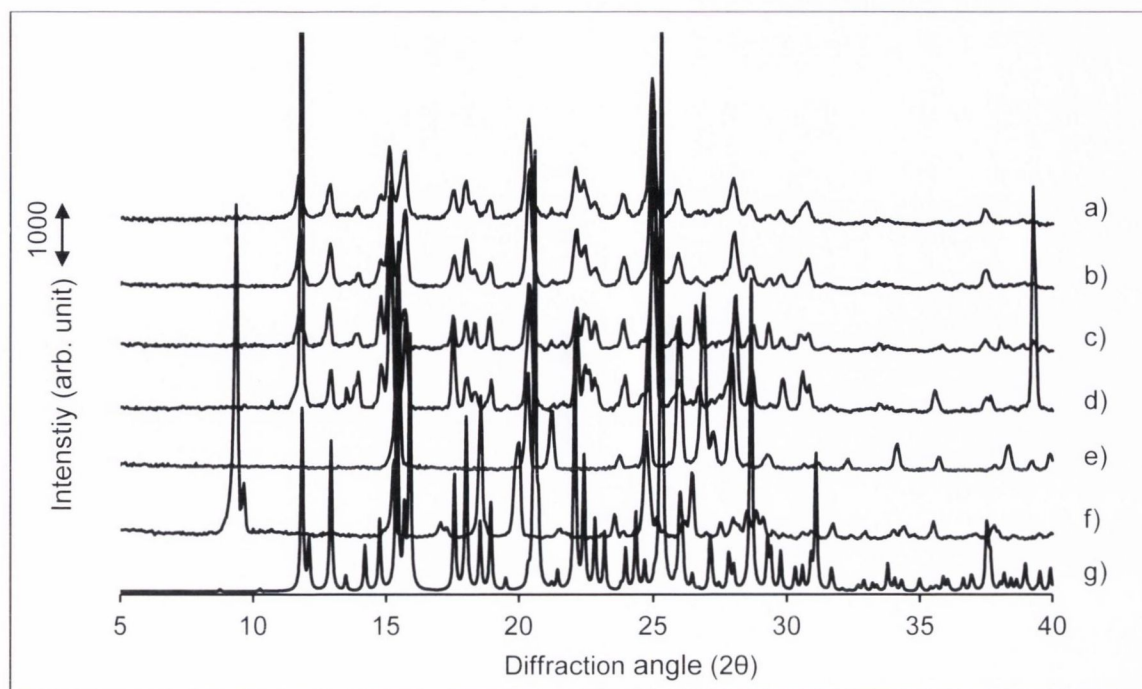
Figure A.3.13: PXRD patterns of SD:SA 1:1 products obtained by a) SPD, b) LAM , c) SEV and d) CCR using MeOH as solvent compared to e) SA, f) SD and g) the theoretical PXRD pattern of SD:SA 1:1 cocrystal obtained from solution, calculated on the basis of single crystal data (Patel et al., 1988).
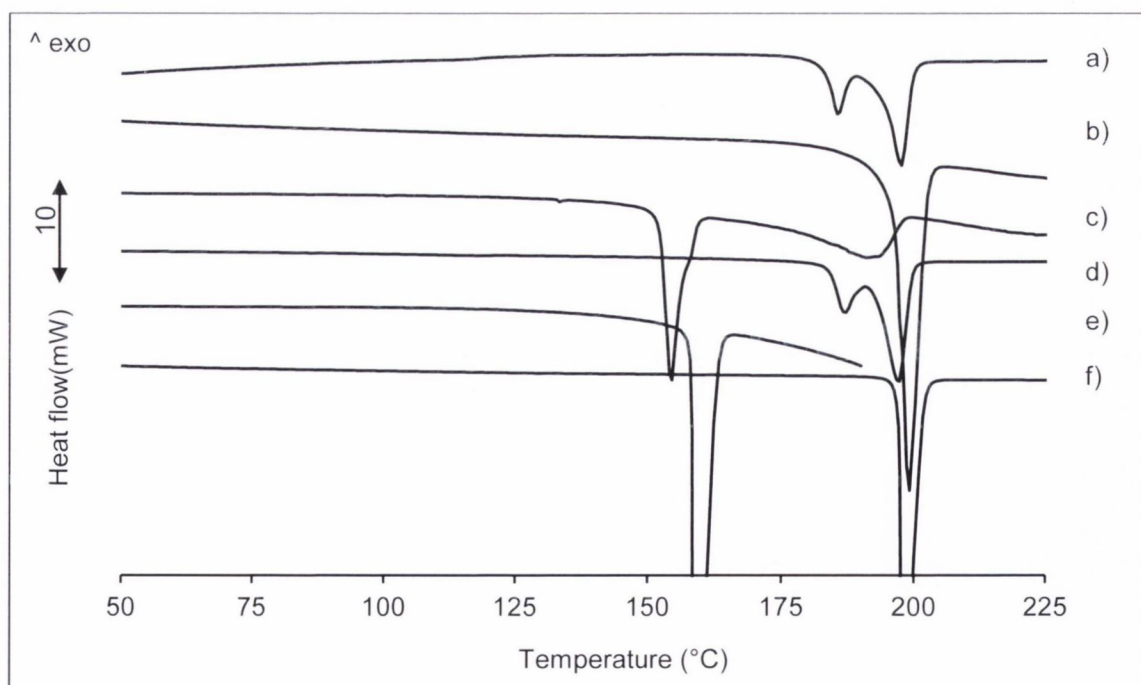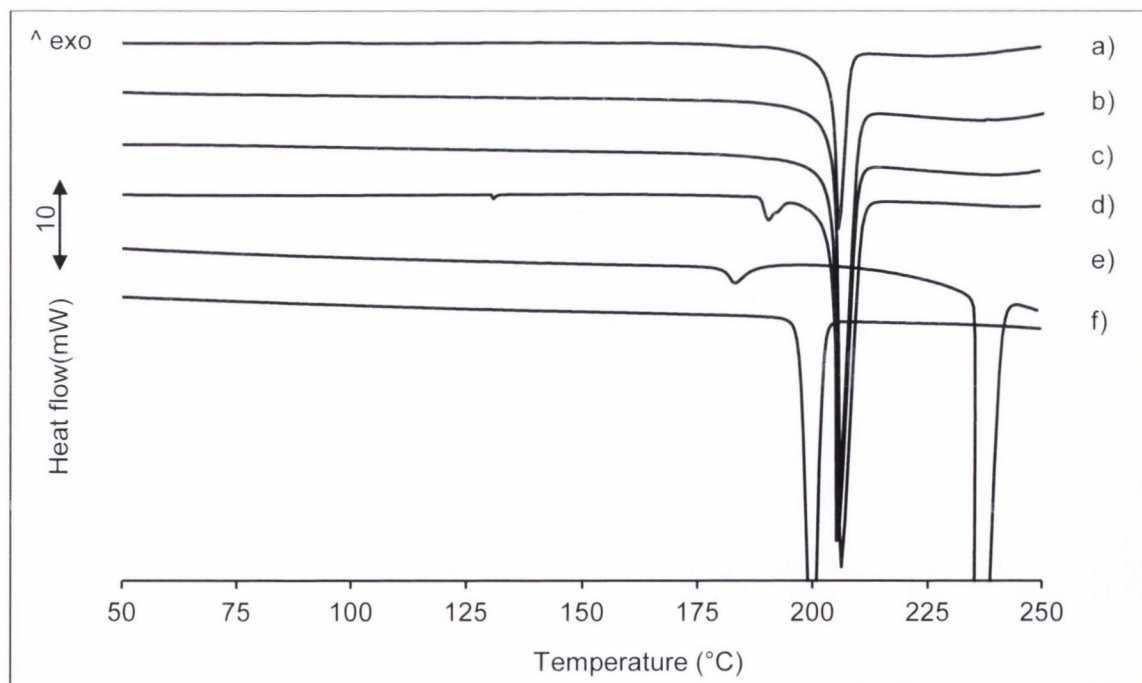

Figure A.3.14: DSC thermograms of SD:SA 1:1 products obtained by a) SPD, b) LAM , c) SEV and d) CCR using MeOH as solvent compared to e) SA and f) SD.
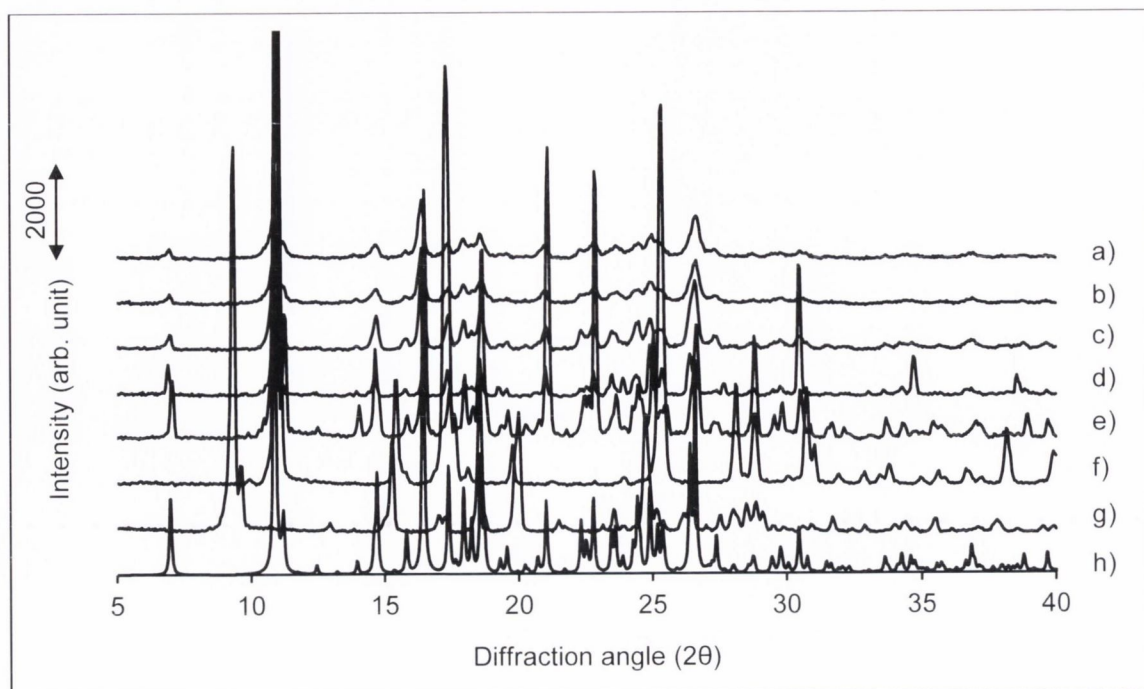
Figure A.3.15: PXRD patterns of a) SD:SA 1:1.2 SPD product and SD:SA 1:1 products obtained by b) SPD, c) LAM , d) SEV and e) CCR using MeCN as solvent compared to f) SA, g) SD and h) the theoretical PXRD pattern of SD:SA 1:1 cocrystal obtained from solution, calculated on the basis of single crystal data (Patel et al., 1988).

Figure A.3.16: DSC thermograms of a) SD:SA 1:1.2 SPD product and SD:SA 1:1 products obtained by b) SPD, c) LAM , d) SEV and e) CCR using MeCN as solvent compared to f) SA and g) SD.

Figure A.3.17: PXRD patterns of SD:SA 1:1 products obtained by a) SPD, b) LAM , c) SEV and d) CCR using Me₂CO as solvent compared to e) SA, f) SD and g) the theoretical PXRD pattern of SD:SA 1:1 cocrystal obtained from solution, calculated on the basis of single crystal data (Patel et al., 1988).

Figure A.3.18: DSC thermograms of SD:SA 1:1 products obtained by a) SPD, b) LAM , c) SEV and d) CCR using Me₂CO as solvent compared to e) SA and f) SD.
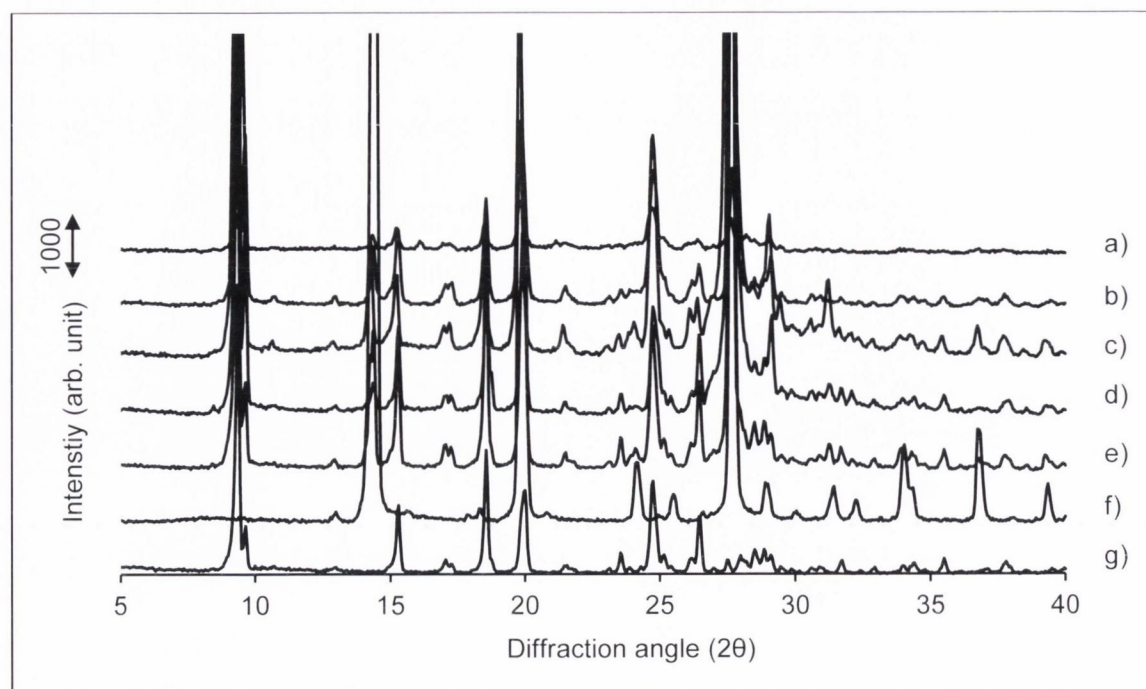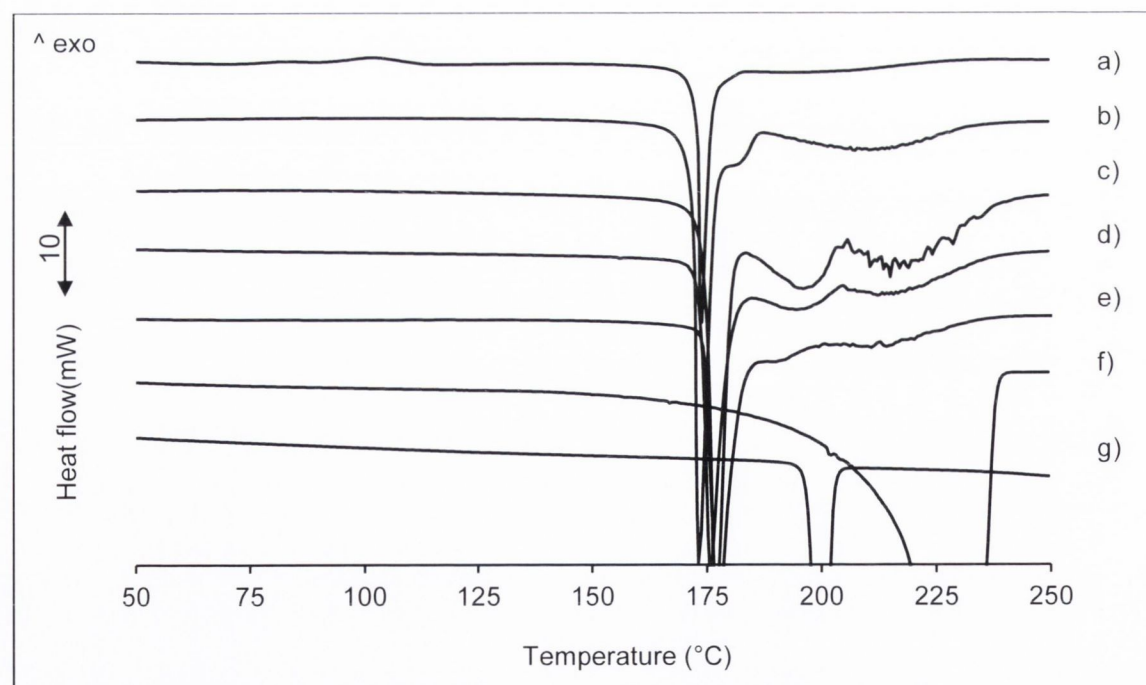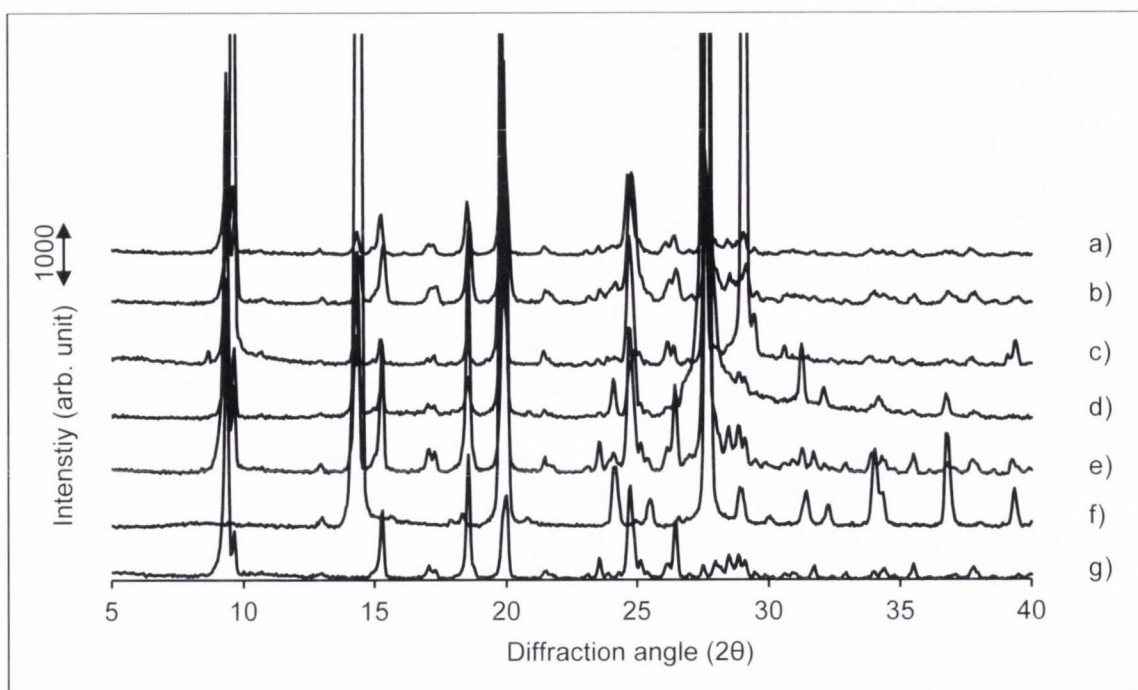
Figure A.3.19: PXRD patterns of SD:4-ASA 1:1 products obtained by a) SPD, b) LAM , c) SEV and d) CCR using EtOH as solvent compared to e) 4-ASA, f) SD and g) the theoretical PXRD pattern of SD:4-ASA 1:1 cocrystal obtained from solution, calculated on the basis of single crystal data (Caira, 1992).
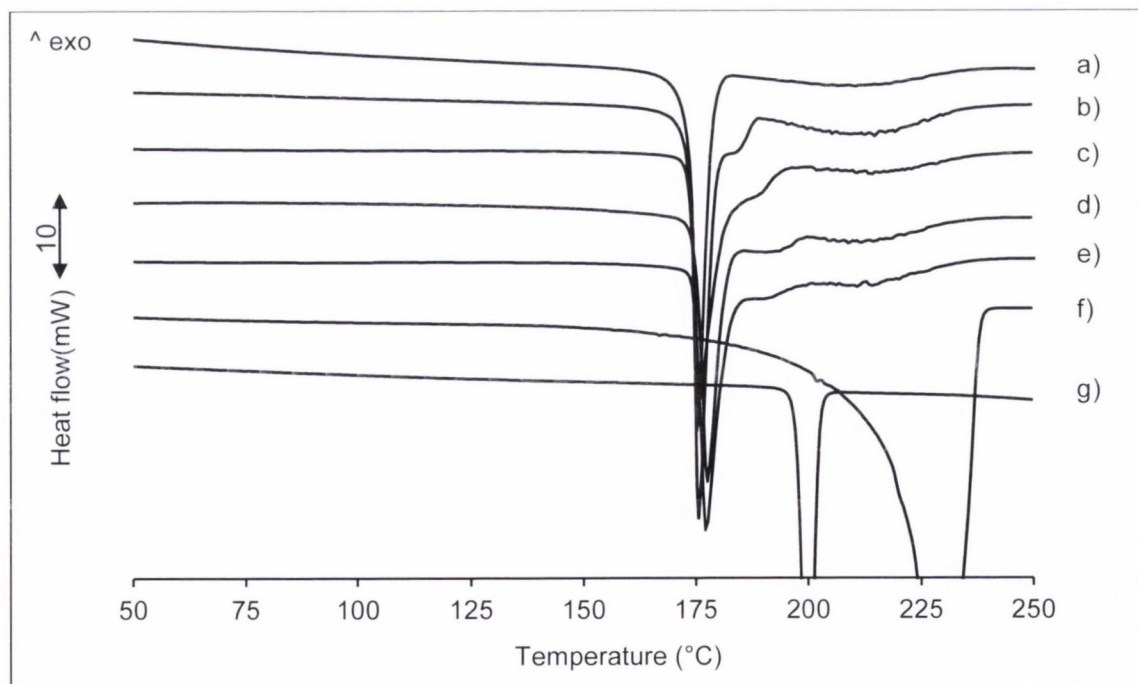

**Figure A.3.20:** DSC thermograms of SD:4-ASA 1:1 products obtained by a) SPD, b) LAM , c) SEV and d) CCR using EtOH as solvent compared to e) 4-ASA and f) SD.

Figure A.3.21: PXRD patterns of SD:4-ASA 1:1 products obtained by a) SPD, b) LAM , c) SEV and d) CCR using Me₂CO as solvent compared to e) 4-ASA, f) SD and g) the theoretical PXRD pattern of SD:4-ASA 1:1 cocrystal obtained from solution, calculated on the basis of single crystal data (Caira, 1992).
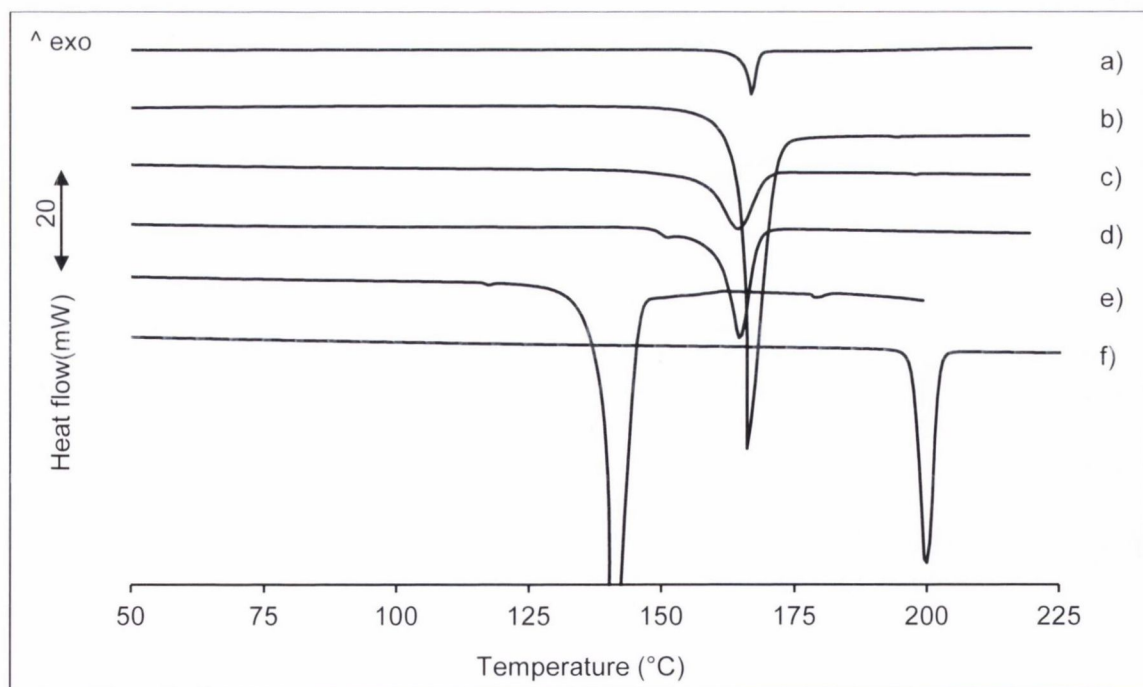
Figure A.3.22: DSC thermograms of SD:4-ASA 1:1 products obtained by a) SPD, b) LAM , c) SEV and d) CCR using Me₂CO as solvent compared to e) 4-ASA and f) SD.

Figure A.3.23: PXRD patterns of SD:NA 1:1 products obtained by a) SPD, b) LAM , c) SEV and d) CCR using EtOH as solvent compared to e) NA, f) SD and g) the calculated PXRD pattern based on single crystal data of the SD:NA 1:1 cocrystal.

Figure A.3.24: DSC thermograms of SD:NA 1:1 products obtained by a) SPD, b) LAM , c) SEV and d) CCR using EtOH as solvent compared to e) NA and f) SD.

Figure A.3.25: PXRD patterns of SD:NA 1:1 products obtained by a) SPD, b) LAM , c) SEV and d) CCR using MeOH as solvent compared to e) NA, f) SD and g) the calculated PXRD pattern based on single crystal data of the SD:NA 1:1 cocrystal.

Figure A.3.26: DSC thermograms of SD:NA 1:1 products obtained by a) SPD, b) LAM , c) SEV and d) CCR using MeOH as solvent compared to e) NA and f) SD.

Figure A.3.27: PXRD patterns of SD:PCA 1:1 products obtained by a) SPD, b) LAM , c) SEV and d) CCR using EtOH as solvent compared to e) SD:PCA 1:1 physical mixture, f) PCA and g) SD.

Figure A.3.28: DSC thermograms of SD:PCA 1:1 products obtained by a) SPD, b) LAM , c) SEV and d) CCR using EtOH as solvent compared to e) SD:PCA 1:1 physical mixture, f) PCA and g) SD.

Figure A.3.29: PXRD patterns of SD:PCA 1:1 products obtained by a) SPD, b) LAM , c) SEV and d) CCR using MeOH as solvent compared to e) SD:PCA 1:1 physical mixture, f) PCA and g) SD.

Figure A.3.30: DSC thermograms of SD:PCA 1:1 products obtained by a) SPD, b) LAM , c) SEV and d) CCR using MeOH as solvent compared to e) SD:PCA 1:1 physical mixture, f) PCA and g) SD.

Appendix 4

Table A.4.1: pH changes during equilibrium solubility study of the SD:BA 1:1 , SD:SA 1:1 and SD:NA 1:1 cocrystal (CC) in water at 37 °C.

Time (h)	SD:BA CC	SD:SA CC	SD:NA CC
12	3.61 ± 0.02	3.18 ± 0.01	3.61 ± 0.01
24	3.60 ± 0.01	3.19 ± 0.02	3.59 ± 0.01
48	3.62 ± 0.06	3.20 ± 0.00	3.60 ± 0.00
72	3.60 ± 0.03	3.24 ± 0.01	3.60 ± 0.01
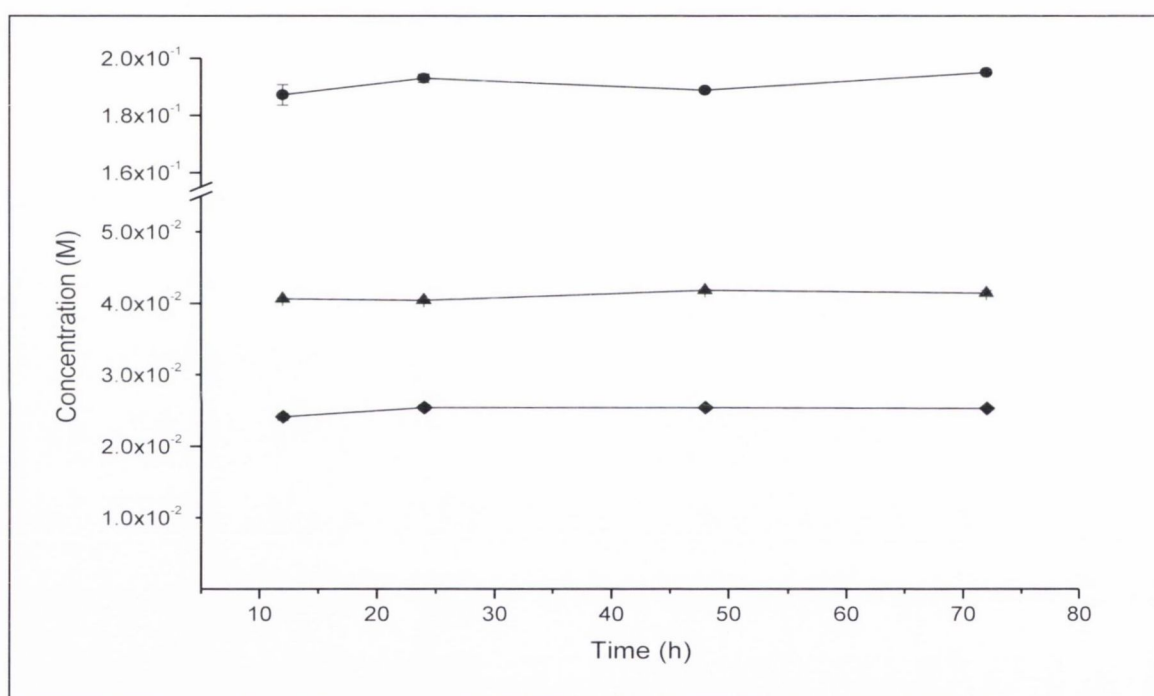
Figure A.4.1: Equilibrium solubility determination of BA (triangles), SA (diamonds) and NA (circles) in water at 37 °C.

Table A.4.2: pH changes during equilibrium solubility study of BA, SA and NA in water at 37 °C.

Time (h)	BA	SA	NA
12	3.07 ± 0.01	2.85 ± 0.05	3.48 ± 0.01
24	3.10 ± 0.02	2.82 ± 0.01	3.47 ± 0.01
48	3.07 ± 0.03	2.80 ± 0.01	3.47 ± 0.00
72	3.08 ± 0.01	2.79 ± 0.03	3.48 ± 0.01

The derivations of equations 5.1 and 5.2 described in Chapter 5.

This model was derived based on the equilibrium reactions for a 1:1 cocrystal with amphoteric drug and monoprotic acidic coformer (Bethune et al., 2009). For the SD:BA 1:1 cocrystal the following equations can be established:

$$SD{:}BA_{solid} \rightleftharpoons SD_{soln} + BA_{soln} \qquad (A.4.1)$$
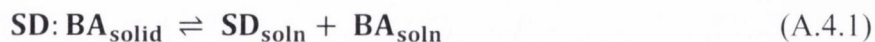
$$K_{sp} = [SD][BA] \qquad (A.4.2)$$

For SD the equilibrium reactions and the thereof derived mass constants can be described by:

$$SDH^+ \rightleftharpoons SD + H^+ \qquad (A.4.3)$$

$$K_{a1,SD} = \frac{[SD][H^+]}{[SDH^+]} \qquad (A.4.4)$$

$$SD \rightleftharpoons SD^- + H^+ \qquad (A.4.5)$$

$$K_{a2,SD} = \frac{[SD^-][H^+]}{[SD]} \qquad (A.4.6)$$

For BA the equilibrium reactions and the thereof derived mass constants can be described by:

$$BA \rightleftharpoons BA^- + H^+ \qquad (A.4.7)$$

$$K_{a,BA} = \frac{[BA^-][H^+]}{[BA]} \qquad (A.4.8)$$

The total SD and BA concentrations (SD_t and BA_t) are then calculated by the sum of the ionized and nonionised species as described below:

$$[SD]_t = [SDH^+] + [SD] + [SD^-] \qquad (A.4.9)$$

$$[BA]_t = [BA] + [BA^-] \qquad (A.4.10)$$

The equilibrium constants (K_{sp} and K_a) can be used to substitute equations A.4.9 and A.4.10:

$$[SD]_t = \frac{K_{sp}}{[BA]}\left(1 + \frac{[H^+]}{K_{a1,SD}} + \frac{K_{a2,SD}}{[H^+]}\right) \tag{A.4.11}$$

$$[BA]_t = [BA]\left(1 + \frac{K_{a,BA}}{[H^+]}\right) \tag{A.4.12}$$

$$[BA] = \frac{[BA]_t}{\left(1 + \frac{K_{a,BA}}{[H^+]}\right)} \tag{A.4.13}$$

Substituting equation A.4.13 into equation A.4.11:

$$[SD]_t = \frac{K_{sp}}{[BA]_t}\left(1 + \frac{K_{a,BA}}{[H^+]}\right)\left(1 + \frac{[H^+]}{K_{a1,SD}} + \frac{K_{a2,SD}}{[H^+]}\right) \tag{A.4.14}$$

For a 1:1 cocrystal considering stoichiometric conditions, $S_{cocrystal} = [SD]_t = [BA]_t$ and thus equation A.4.14 can be rewritten as:

$$S_{cocrystal} = \sqrt{K_{sp}\left(1 + \frac{K_{a,BA}}{[H^+]}\right)\left(1 + \frac{[H^+]}{K_{a1,SD}} + \frac{K_{a2,SD}}{[H^+]}\right)} \tag{A.4.15}$$

At the transition (tr) point equation A.4.14 can be rewritten as:

$$[SD]_{tr} = \frac{K_{sp}}{[BA]_{tr}}\left(1 + \frac{K_{a,BA}}{[H^+]}\right)\left(1 + \frac{[H^+]}{K_{a1,SD}} + \frac{K_{a2,SD}}{[H^+]}\right) \tag{A.4.16}$$

Hence, the solubility product (K_{sp}) can be determined by:

$$K_{sp} = \frac{[SA]_{tr}[BA]_{tr}}{\left(1 + \frac{K_{a,BA}}{[H^+]}\right)\left(1 + \frac{[H^+]}{K_{a1,SD}} + \frac{K_{a2,SD}}{[H^+]}\right)} \tag{A.4.17}$$

The derivations of equations 5.3 and 5.4 described in Chapter 5.

This model was derived based on the equilibrium reactions for a 1:1 cocrystal with amphoteric drug and diprotic acidic coformer (Reddy et al., 2009). For the SD:SA 1:1 cocrystal the following equations can be established:

$$SD:SA_{solid} \rightleftharpoons SD_{soln} + SA_{soln} \tag{A.4.18}$$

$$K_{sp} = [SD][SA] \tag{A.4.19}$$

For SD the equilibrium reactions and the thereof derived mass constants can be described as shown by the equations A.4.3 to A.4.6.

For SA the equilibrium reactions and the thereof derived mass constants can be described by:

$$SA \rightleftharpoons SA^- + H^+ \tag{A.4.20}$$

$$K_{a1,SA} = \frac{[SA^-][H^+]}{[SA]} \tag{A.4.21}$$

$$SA^- \rightleftharpoons SA^{2-} + H^+ \tag{A.4.22}$$

$$K_{a2,SA} = \frac{[SA^{2-}][H^+]}{[SA^-]} \tag{A.4.23}$$

The total SD and SA concentrations (SD_t and SA_t) are then calculated by the sum of the ionized and nonionised species as described below:

$$[SD]_t = [SDH^+] + [SD] + [SD^-] \tag{A.4.24}$$

$$[SA]_t = [SA] + [SA^-] + [SA^{2-}] \tag{A.4.25}$$

The equilibrium constants (K_{sp} and K_a) can be used to substitute equations A.4.24 and A.4.25:

$$[SD]_t = \frac{K_{sp}}{[SA]}\left(1 + \frac{[H^+]}{K_{a1,SD}} + \frac{K_{a2,SD}}{[H^+]}\right) \tag{A.4.26}$$

$$[SA]_t = [SA]\left(1 + \frac{K_{a1,SA}}{[H^+]} + \frac{K_{a1,SA}K_{a2,SA}}{[H^+]^2}\right) \tag{A.4.27}$$

$$[SA] = \frac{[SA]_t}{\left(1 + \frac{K_{a1,SA}}{[H^+]} + \frac{K_{a1,SA}K_{a2,SA}}{[H^+]^2}\right)} \tag{A.4.28}$$

Substituting equation A.4.28 into equation A.4.26 gives:

$$[SD]_t = \frac{K_{sp}}{[SA]_t}\left(1 + \frac{K_{a1,SA}}{[H^+]} + \frac{K_{a1,SA}K_{a2,SA}}{[H^+]^2}\right)\left(1 + \frac{[H^+]}{K_{a1,SD}} + \frac{K_{a2,SD}}{[H^+]}\right) \qquad (A.4.29)$$

For a 1:1 cocrystal considering stoichiometric conditions, $S_{cocrystal} = [SD]_t = [SA]_t$ and thus equation A.4.29 can be rewritten as:

$$S_{cocrystal} = \sqrt{K_{sp}\left(1 + \frac{K_{a1,SA}}{[H^+]} + \frac{K_{a1,SA}K_{a2,SA}}{[H^+]^2}\right)\left(1 + \frac{[H^+]}{K_{a1,SD}} + \frac{K_{a2,SD}}{[H^+]}\right)} \qquad (A.4.30)$$

At the transition (tr) point equation A.4.30 can be rewritten as:

$$[SD]_{tr} = \frac{K_{sp}}{[SA]_{tr}}\left(1 + \frac{K_{a1,SA}}{[H^+]} + \frac{K_{a1,SA}K_{a2,SA}}{[H^+]^2}\right)\left(1 + \frac{[H^+]}{K_{a1,SD}} + \frac{K_{a2,SD}}{[H^+]}\right) \qquad (A.4.31)$$

Hence, the solubility product (K_{sp}) can be determined by:

$$K_{sp} = \frac{[SD]_{tr}\,[SA]_{tr}}{\left(1 + \frac{K_{a1,SA}}{[H^+]} + \frac{K_{a1,SA}K_{a2,SA}}{[H^+]^2}\right)\left(1 + \frac{[H^+]}{K_{a1,SD}} + \frac{K_{a2,SD}}{[H^+]}\right)} \qquad (A.4.32)$$

Table A.4.3: Compression pressure and time applied to prepare compacts for intrinsic dissolution studies.

Sample	Compaction pressure and time
BA	6 tonnes, 30 seconds
SD:BA 1:1 physical mixture	6 tonnes, 30 seconds
SD:BA 1:1 cocrystal	6 tonnes, 30 seconds
SA	8 tonnes, 2 minutes
SD:SA 1:1 physical mixture	8 tonnes, 2 minutes
SD:SA 1:1 cocrystal	8 tonnes, 2 minutes
NA	8tonnes, 30 seconds
SD:NA 1:1 physical mixture	6 tonnes, 30 seconds
SD:NA 1:1 cocrystal	6 tonnes, 30 seconds
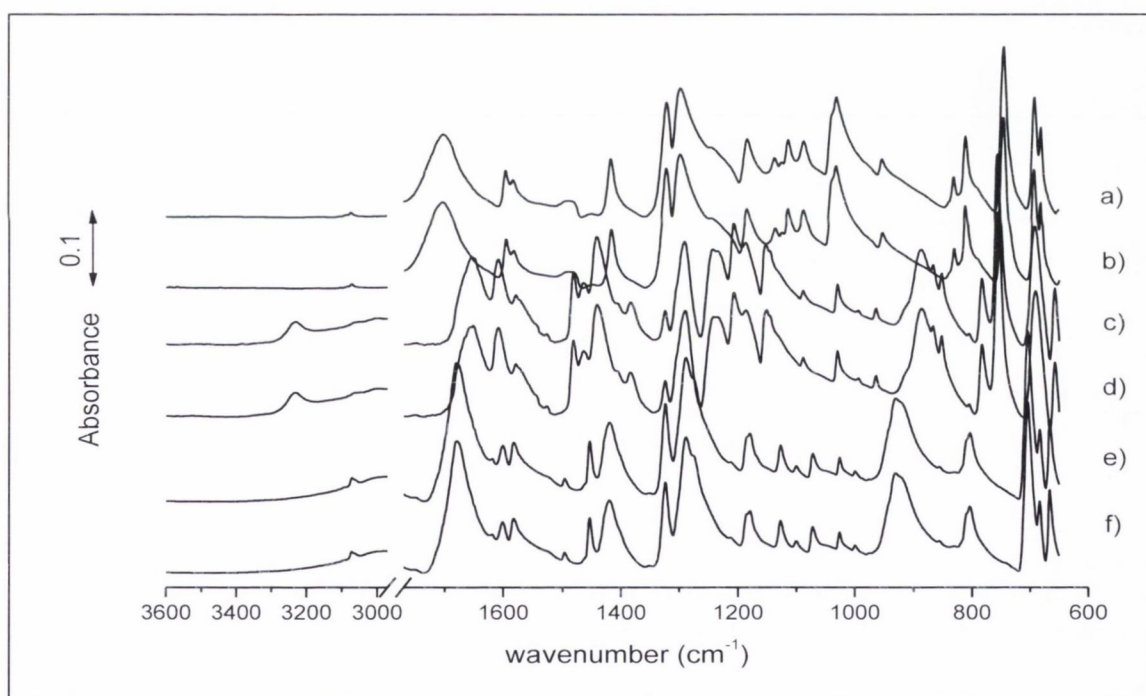
Figure A.4.2: IR spectra of a) NA after ID, b) NA before ID, c) SA after ID, d) SA before ID, e) BA after ID and f) BA before ID.

Appendix 5

Table A.5.1: Chemical structure, molecular weight, pK_a value(s) and melting point of all drug and coformer components. The melting temperatures (T_m) and corresponding enthalpies of fusion (ΔH_f) refer to experimental data shown in Chapter 2 (for BAM and DBSO), in Chapter 3 (for SD and 4-ASA) and in Appendix 3 (for all other components).
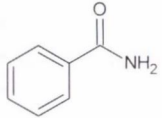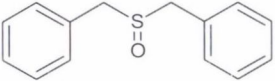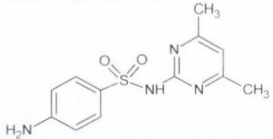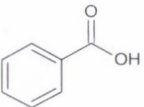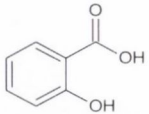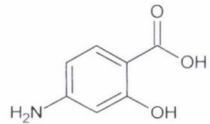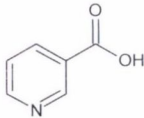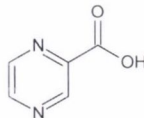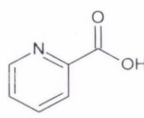
Cocrystal compound	Structure	Molecular weight (g/mol)	pK$_a$ values	T$_m$, °C (ΔH_f, J/g)
Benzamide (BAM)		121.14	$pK_a = 13$[a]	126.90 ± 0.31 (188.05 ± 3.79)
Dibenzyl sulfoxide (DBSO)		230.32	$pK_a = 19.25$[b]	134.23 ± 0.53 (131.90 ± 1.24)
Sulfadimidine (SD)		278.33	$pK_{a1} = 2.79$[c] $pK_{a2} = 7.4$[c]	197.16 ± 0.43 (130.45 ± 6.60)
Benzoic acid (BA)		122.12	$pK_a = 4.21$[d]	121.14 ± 0.69 (139.43 ± 0.32)
Salicylic acid (SA)		138.12	$pK_{a1} = 3.00$[e] $pK_{a2} = 13.4$[e]	158.07 ± 0.68 (170.06 ± 5.99)

Table A.5.1: continued

Cocrystal compound	Structure	Molecular weight (g/mol)	pK$_a$ values	T$_m$, °C (ΔH$_f$, J/g)
4-aminosalicylic acid (4-ASA)		153.14	pK$_{a1}$ = 2.0[f] pK$_{a2}$ = 3.56[f]	139.07 ± 0.93 (392.80 ± 7.33)
Nicotinic acid (NA)		123.11	pK$_{a1}$ = 2.14[g] pK$_{a2}$ = 4.82[g]	235.65 ± 0.59 (205.67 ± 7.43)
Pyrazine-2-carboxylic acid (PCA)		124.10	pK$_a$ = 2.90[h]	224.74 ± 0.37 (798.72 ± 32.11)
Pyridine-2-carboxylic acid (PA)		123.11	pK$_{a1}$ = 1.01[i] pK$_{a2}$ = 5.39[i]	136.60 ± 1.03 (177.35 5.02)

a) Perrin, 1965

b) ChemBase (ID: 75258); Matthews et al., 1975

c) Sukul and Spiteller, 2006

d) Harris, 2010

e) Kolthoff and Stenger, 1942

f) Newton and Kluza, 1978

g) Nagy and Takács-Novák, 1997

h) Zhang et al., 2003

i) Abdullah and Tofiq, 2010